THERMAL DESIGN AND ANALYSIS OF A RADIANT FURNACE FOR UNIFORM THERMAL CONDITIONS

A Thesis

Submitted By

RAMCHANDRA P. CHOPADE

For the Award of the Degree

of

DOCTOR OF PHILOSOPHY

DEPARTMENT OF MECHANICAL ENGINEERING

INDIAN INSTITUTE OF TECHNOLOGY GUWAHATI

GUWAHATI - 781039, INDIA

MAY 2012

CERTIFICATE

It is certified that the work contained in the thesis entitled **Thermal Design and Analysis of a Radiant Furnace for Uniform Thermal Conditions** by Ramchandra P. Chopade, a PhD student in the Department of Mechanical Engineering, Indian Institute of Technology Guwahati for the award of the degree of the Doctor of Philosophy has been carried out under our supervision, and this work has not been submitted elsewhere for a degree.

Dr. Subhash C. Mishra
Professor
Department of Mechanical Engineering
Indian Institute of Technology Guwahati
Guwahati – 781039, India

Dr. P. Mahanta
Professor
Department of Mechanical Engineering
Indian Institute of Technology Guwahati
Guwahati – 781039, India

ACKNOWLEDGEMENTS

First of all, I express my deepest gratitude to my supervisors, Prof. Subhash C. Mishra and Prof. P. Mahanta for their invaluable guidance, encouragement, inspiration and support throughout my PhD work. I can never forget the vigor and attention bestowed by them in taking my research ahead. Their innovative ideas and acumen helped me in truly understanding what research means, and how with a focused mind, with patience and perseverance, an unsolved problem can be solved and its results physically interpreted and analyzed. Their personal character combined with professional ethics will remain a source of inspiration for the rest of my life.

I am thankful to my Doctoral Committee members, Prof. U. K. Saha, Dr. P. Muthukumar and Dr. C. Somayaji for their insightful comments and valuable suggestions during my progress seminars, and on other occasions too.

I would like to express my sincere thanks to Prof. D. Chakraborty and all other faculty members of the Department of Mechanical Engineering for their encouragement and support. I am thankful to the other faculty members especially Dr. R. Uppaluri, of Department of Chemical Engineering, and staff of IIT Guwahati who directly or indirectly motivated me to complete my thesis work. I express my thanks to all the staff members of the Department of Mechanical Engineering for their kind help.

I am extremely grateful to Prof. Shegenao Maruyama and Dr. Astushi Komiya of Institute of Fluid Sciences, Tohoku University, Sendai, Japan for their support and guidance to carry out a part of my research work. I spent five very productive months in their laboratory. In a short time, I could experience what a Japanese research culture is, with what great enthusiasm the researchers work, and how Professors truly support their students. I express my sincere thanks to all the members and staff of Maruyama-Komiya Lab and the Global COE office, Tohoku University, Sendai, Japan for their kind cooperation and help during my stay.

Last but not the least, the patience and forbearance of my parents and my wife need special mention. Leaving rest other things aside, their continued moral support and blessings, allowed me to concentrate on my work for long hours. It is their trust and confidence in me that I am in a position to write this acknowledgement.

The company of my friends at IIT Guwahati made my four years of stay enjoyable. Here, I learned not only the academics and research, but many other things which are needed in personal and professional lives. They indeed made me realize, what the life is. Each of them deserves special thanks.

May 2012 **Ramchandra P. Chopade**

IIT Guwahati

List of Publications form this Thesis Work

International Journals:

1. R. P. Chopade, S. C. Mishra, P. Mahanta, S. Maruyama, Numerical Analysis of an Inverse Boundary Design Problem of 3-D Radiant Furnace with a 3-D Design Object, *Numerical heat Transfer, Part A*, Vol. 60, 2011, pp. 25–49.

2. R. P. Chopade, S. C. Mishra, P. Mahanta, Effects of Locations of a 3-D Design Object in a 3-D Radiant Furnace for Prescribed Uniform Thermal Conditions, *Applied Thermal Engineering*, Vol. 31, 2011, pp. 3262–3274.

3. R. P. Chopade, S. C. Mishra, P. Mahanta, S. Maruyama, A. Komiya, Uniform Thermal Conditions on 3-D Object: Optimal Power Estimation of Panel Heaters in a 3-D Radiant Enclosure, *International Journal of Thermal Sciences*, Vol. 51, 2012, pp. 63–76.

4. R. P. Chopade, S. C. Mishra, P. Mahanta, S. Maruyama, Power Estimation of Radiant Heaters for Uniform Thermal Conditions on 3-D Irregular Shaped Objects, *International Journal of Heat and Mass Transfer, IN PRESS, http://dx.doi.org/10.1016/j.ijheatmasstrasfer.2012.03.083*, 2012.

5. R. P. Chopade, S. C. Mishra, P. Mahanta, S. Maruyama, On Configuration of Load in Radiant Furnace for Uniform Thermal Conditions, revised manuscript submitted to *Heat Transfer Engineering*.

International Conferences:

1. R. P. Chopade, S. C. Mishra, P. Mahanta, S. Maruyama, A. Komiya, On Location of Load in Radiant Furnace for Uniform Thermal Conditions using REM^2 and Micro-genetic Algorithm, Proc. 7th Int. Conf. on Flow Dynamics, November 1-3, 2010, Sendai, Japan.

2. R. P. Chopade, S. C. Mishra, P Mahanta, S. Maruyama, For Uniform Thermal Conditions: Radiant Boundary Design for Irregular Shape Design Surface, Proc. Int. Conf. on Thermal Energy and Environment, 2011, Kalasalingam University, Shrivilliputhur, India, pp. 552-559.

ABSTRACT

Furnaces play an important role in manufacturing industries. Various types of furnaces are available for numerous heating applications, and also several problems associated with their operations. Non uniform thermal conditions on the load, ineffective heat transfer from heat sources to the load, difficulty in controlling atmosphere inside the furnace, high energy losses, etc., are some of the important problems in furnace operations. Among these problems, difficulty in controlling the thermal conditions (temperature and heat flux distributions) is the most prevalent in many furnaces. Additionally, in solid and liquid fuel combustion furnaces, the major concern is maintaining the controlled environment inside the furnace. For a better thermal control and maintaining a controlled environment, radiant furnaces are the best suited ones. Because of the inherent advantages of the radiant furnaces over the conventional ones, over last two decades the radiant furnaces are gaining popularity in various industrial applications. These applications are not limited to precise heating in laboratories but several industrial heating processes, etc.

For the desired post processing results, many industrial heating processes require specific thermal conditions over the region/ part of the system where the heating takes place. In several material heating applications, the uniform thermal conditions are needed. Such cases are found in rapid thermal processing, drying or curing of paints, curing of powder coating, chemical vapor deposition, food processing, material heating for precision heat treatment processes/hot working processes, manufacturing of electronic components, etc. The spatially uniform thermal conditions on the products prevent thermal stresses which avoid structural damage of the products, such as cracking, bending, etc. Furthermore, the desired uniform heating is very much advantageous to achieve the specific metallurgical properties such as the desired microstructure, surface conditions, etc. The non-uniform heating always results in poor quality products.

For a given specific application, furnace geometry, properties of the furnace materials, participating medium, location and powers of the heaters, and position of the design object (products) (DO) inside the furnace, are to be properly accounted. For the desired thermal conditions over the specific region (design surfaces) of the system, estimation of thermal boundary conditions in a radiant furnace falls under the purview of inverse boundary design problems. It is well known that, in inverse formulation the computational expense is considerably lower than that of the trial-and-error methods. However, the system of equations defining the inverse problems is ill-posed, and their solution requires a special treatment. Finding the optimal solution for such problems is a challenging task. Apart from the methodologies used for the direct problem, solution of the inverse problem necessitate the use of either regularization or optimization techniques.

Due to the increasing relevance in the precision thermal processing, a good number of inverse furnace boundary design problems have been investigated by many researchers. To handle the ill-posed nature of such problems, several regularization and optimization techniques have been proposed. In spite of the inherent advantages such as ease in handing the design constraints, literature on application of the evolutionary optimization methods such as the genetic algorithm, to the furnace boundary design problems is scarce. The available literature mostly deals with the analyses of 2-D furnace with 2-D DO. Such studies have of only academic relevance and cannot apply in practical applications. Thus, in this area, there is a need to carry out the analyses for general situation like 3-D furnace geometry with 3-D DOs. The present work, therefore, aims at the numerical analysis of inverse boundary design problem of a 3-D radiant furnace that yield uniform thermal conditions on 3-D DO placed inside it.

With the furnace geometry specified, the work in this thesis focus on estimation of optimal heater power settings along the furnace walls of a 3-D radiant furnace that produce desired uniform thermal conditions (temperature and heat flux distributions) on 3-D DOs. The study is made for a wide range of cases such as multiple 3-D DOs, their sizes and locations. To generalize the study, the case of 3-D irregular shaped DOs have

also been taken up. Further, towards the ease in thermal control, fabrication and operation of the radiant furnace, a new approach of grouping the panel heaters has been introduced.

The dissertation is divided into seven chapters. Chapter 1 starts with the introduction to the problems in furnace operations, importance of thermal uniformity and factors affecting it. The motivation, detail literature review and objectives of the present work are presented in sequence. Reviews of various solution methods for inverse problems are given in Chapter 2. Their merits and demerits for furnace boundary design problems are also been discussed. For uniform thermal conditions on 3-D DOs, formulation and algorithm to estimate the optimal heater power settings in a 3-D radiant furnace using radiation element method by ray emission model (REM^2) and micro-genetic algorithm (MGA) are discussed in Chapter 3. Different types of problems and for a given problem, the effects of various parameters on estimated uniform thermal conditions are given in Chapters 4-6. Conclusions and scope for future work are given in Chapter 7. In following paragraphs the contents of the each chapter are briefly described.

Chapter 1 entitled Introduction starts with a brief discussion of furnace applications and importance of the furnaces in industries. The basic requirement of the furnaces, importance of thermal uniformity in the furnace and the factors affecting it are elaborated. After stating the motivation of the present work, detailed literature review is given. This includes the discussion on previous studies dealing with furnace boundary design problems for uniform thermal conditions and the various methodologies used for them. Based on the literature review, the objectives of the present work are outlined.

Chapter 2 is devoted for reviewing the solution methods for inverse furnace design problems. In this chapter, several inverse and optimization methods are reviewed, and their merit and demerit in radiant furnace design problems are discussed. Use of the regularization techniques, especially for furnace boundary design problems may result in negative heat flux on heater surfaces. It is difficult to impose the design constraints using the regularization techniques and this limit its applicability for practical situations. However, optimization methods handle the design constraints very well. For the present

boundary design problem, this aspect is handled by the MGA which is an improved form of the genetic algorithm. The advantages of the MGA in the furnace design problems are elaborated. In the last section of this chapter, the working procedure of the MGA is discussed through a flowchart.

In Chapter 3, formulation of the direct and the inverse radiative transfer problems are given. In both direct and inverse problems, radiative information is computed using the REM^2. In the inverse analysis the MGA has been used as an optimization tool. Before going for actual computation, the solution methodologies by REM^2 for the direct problem and REM^2 + MGA for the inverse problem are validated. For the direct problem, the results of grid and ray independent test are given. The present algorithm (REM^2 + MGA) is implemented for basic furnace boundary design problem. For the desired uniform thermal conditions on the 3-D DO, the optimal configurations and powers of the panel heaters along the walls of the 3-D radiant furnace are estimated. The uniformity in the estimated heat flux distribution on the surfaces of the 3-D DO is found accurate within the maximum deviation < 3%. It is found that the mere placement of panel heaters along the top wall does not provide uniform thermal conditions on the surface of the 3-D DO. This necessitates consideration of panel heaters along the four vertical walls of the furnace too. Having found the need of panel heaters along the five walls of the furnace, next the effects of aspect ratios of the furnace enclosure and the design constraints (heater power ranges) on the estimated heat flux distribution on the DO are calculated. The results are found better for aspect ratios 0.5 and higher. In the last section of the chapter, for every case, the optimal heater power settings are plotted and results are analyzed. It is found that for the uniform thermal condition, not all the heaters along the furnace walls need to be placed.

In Chapter 4, estimation of desired uniform thermal conditions in the radiant furnace is done for three different situations in material heating processes. In this chapter, the first study deals with finding the constraints on the size of a centrally located 3-D DO. To cover a wide range of dimensions, 29 DO models are considered. The suitability of the DO models is decided on the basis of maximum deviation in estimated heat flux

distribution. Out of 29 DO models considered, only 16 are found suitable to yield the uniform heat flux distribution with the maximum deviation <3%. In the second study, for uniform thermal conditions, the effect of the locations of 3-D DO on the bottom of the furnace enclosure is investigated. For 3 DO models, 22 possible locations are evaluated. From a comparative study of the 22 cases it has been found that the height of 3-D DO impose more restrictions on suitable locations than that of the length and the width. In these cases also the criteria of suitability was maximum deviation < 3%.

To have an idea of implementation of the present numerical results in practical application, the simple experiments have been conducted using the model of 3-D radiant furnace with 3-D DO. The difference between the numerically computed heat flux distribution and that of from calculated from experimental results have been analyzed. Due to the differences in the numerical and experimental parameters such as, the material properties, working environment and energy losses, the experimental results are found deviating from the numerical results. The average difference is found 30%. On the positive side the trends of experimental values are matching with the numerical results. Since the experimental study is not the main aim of the thesis, it goes as additional information in Annexure-1. The exact simulation of the experiments can be a scope for future work. The detail of the experiments, fabrication of experimental setup, experiment procedure, and the results analysis is given in Annexture-1. The calibration of thermocouples and the error analysis are given in Appendix I and II, respectively.

Towards the furnace design for mass production, the third study deals with the heater powers design in which multiple DOs are accommodated. A total of 19 different configurations with 2, 3, 4, 5, 6, 8 and 9 DOs are considered. The inverse analysis is done to estimate the heat flux distributions on the DOs and thus the suitable configurations of the DOs are decided. In every study, the estimated heat flux distributions on the surfaces of the 3-D DO(s), and for a sample cases the optimal heater power settings along the walls of the furnace enclosure are estimated. With other parameters fixed, the distances among the DOs are found to have a significant effect. More the distances, better the estimation of the uniform thermal conditions. For the

present furnace dimensions, for particular configurations, the maximum 4 numbers of DOs are found suitable to achieve the uniform thermal conditions.

For desired uniform thermal conditions on a 3-D DOs, in Chapter 5, towards the ease in implementation, operation and control of the heater power settings, the concept of grouping of discrete heaters is introduced. In this the panel heaters are grouped together in a appropriate manner, and thus total numbers of heaters are reduced.The implementation of this concept is exemplified in 3-D furnace design problem with 2-D and 3-D DOs, and in these savings in CPU time are 32.24 and 52.24 %, respectively. This study is useful in radiant boundary design problems and implementing the solution for practical applications.

Having analyzed several situations of regular 3-D DOs, in chapter 6, results are presented for the estimation of optimal heater power settings in a 3-D radiant furnace with 2-D and 3-D irregular shaped DOs. In this study, hemispherical, conical, cylindrical and combinations of these irregular shaped DOs are considered. In all these cases, deviation in estimated heat flux was within ± 1%. In every case, the effect of size of the DOs and the corresponding heater powers setting are given. In the last section of this Chapter, the optimal heater power design is given for a complex case. Here, a replica of a car body is considered as DO. In this, from the knowledge of earlier discrete heater power settings, heaters are grouped into only 6 heaters along the 5 walls of the furnace. This concept is found to give satisfactory results. The maximum deviation in estimated heat flux distribution is found to be 5.8%. In this way the optimal boundary heaters design of a radiant furnace is achieved for yielding the desired uniform thermal conditions on the 3-D regular and irregular shaped DO(s).

The detail conclusions from the present research work are presented in Chapter 7. Scope for future work and recommendations are also given in this chapter.

CONTENTS

Nomenclature

A_i	-	area of surface element "i" (m^2)
dA_i	-	differential surface element on A_i
$F_{i,j}$	-	view factor from surface element "i" to "j"
$F_{i,j}^{A}$	-	absorption view factor
$F_{i,j}^{D}$	-	diffuse reflection view factor
F	-	view factor matrix
G_i	-	irradiance ($W.m^{-2}$)
J_{Di}	-	diffuse radiosity ($W.m^{-2}$)
N	-	total number of surface elements
N_R	-	number of rays
N_P	-	number of population in the micro genetic algorithm
Q_G		heat transfer rate of irradiation ($W.m^{-2}.s^{-1}$)
Q_J		heat transfer rate of diffuse radiosity ($W.m^{-2}.s^{-1}$)
Q_T	-	heat transfer rate of thermal emission ($W.m^{-2}.s^{-1}$)
Q_X	-	net heat loss ($W.m^{-2}$)
Q	-	heat transfer vector
q_i	-	heat flux at element A_i ($W.m^{-2}$)
T_i	-	temperature of surface element "i" (K)

Greek Symbols

α	-	absorptivity
θ	-	polar angle measured from normal of a surface (rad)
ϕ	-	circumferential angle (rad).
ρ^D	-	diffuse reflectivity
ρ^S	-	specular reflectivity
σ	-	Stefan-Boltzmann constant = 5.669×10^{-8} (W. $m^{-2}.K^{-4}$)
ω	-	solid angle (rad)

Subscripts

DO	-	design object
G	-	values due to irradiation
H	-	heater
J	-	value due to diffuse radiosity
i, j	-	value son surfaces A_i and A_j
R	-	reference
T, X	-	values due to thermal emission and net heat generation

Superscripts

A	-	absorption
D	-	diffuse
S	-	diffuse specular
*	-	dimensionless quantity

Abbreviations

2-D/ 3-D	Two/Three- dimensional
CFD	Computational fluid dynamics
Dia.	Diameter
DO	Deign object
GA	Genetic algorithm
IHTP	Inverse heat transfer problem
MCM	Monte Carlo Method
MGA	Micro-genetic algorithm
REM^2	Radiation element method by ray emission model
RTE	Radiative transfer equation
TSVD	Truncated singular value decomposition
SGA	Simple genetic algorithm

List of Figures

List of Tables

CHAPTER 1

INTRODUCTION

1.1 Motivation

In industrial and domestic applications, almost every product comes across the heating process directly or indirectly. Various kinds of heating are used in numerous applications, such as space heating, manufacturing, various heat treatment processes, drying, chemical processing, food processing, etc. All the heating processes are carried out inside an insulated enclosure called the furnace. By definition, furnaces are insulated enclosures designed to deliver the heat energy to the load (material). The heating operations encompass a wide range of temperatures, the purpose of the heating process, which depend on the material being heated, and subsequent operations. Owing to the importance of furnaces, for their efficient utilization, continuous update of heating technology and the analysis of the updated technology remain in demand. This includes addressing the various problems related to furnaces, exploration of new solution methods and their use for different situations in furnace applications.

The furnace should have some of the important basic qualities, such as desirable output corresponding to the available input, effective heat transfer inside the enclosure, no damage of product, easy control, and safe and pollution free operation. Various types of available furnaces can be broadly classified according to the shape (cubical, cylindrical, deep/ shallow type), source of heat generation (combustion of fuels, electric heating, magnetic heating), location of heat sources (direct, indirect fired), method of handling (batch type, continuous), inside environment (vacuum, specified environment), and applications (laboratory, melting, brazing, sintering, etc.).

There are several problems associated with different types of furnaces and their operations. Non uniform thermal conditions on the load, difficulty in controlling inside atmosphere, high energy losses, adverse properties and structural changes of in-process materials are

some of the problems in furnace operations. With time, a great deal of issues related to the thermal design of radiant furnace have been resolved, however, there are yet some problems that need to be addressed.

Among these problems, difficulty in controlling the thermal conditions (temperature and heat flux distributions) is the most prevalent in many furnaces. Additionally, in solid and liquid fuel combustion furnaces, the major concern is maintaining the controlled environment inside the furnace. For better thermal control and controlled environment, electric heating radiant furnaces are the best suited ones. In these, the utilization of energy is the maximum. Because of the inherent advantages over the conventional ones, over last two decades, the radiant heating is emerging as an alternative to the conventional furnaces in various industrial applications. These applications includes, but not limited to precise heating in laboratories and several industrial heating processes.

For desired post processing results, several industrial heating processes require specific thermal conditions over the region of the system where the heating take place. Almost in all the heating processes, uniform heating is desirable. Moreover, in some of the heating applications, the uniform thermal conditions are essential. These applications include but are not limited to the rapid thermal processing (RTP), drying, curing of paints, curing of powder coating, chemical vapor deposition, food processing, material heating for precision heat treatment processes/ hot working processes, manufacturing of electronic components, etc.

The spatially uniform thermal conditions on the products prevent thermal stresses which save the structural damage of the products, such as cracking, bending, etc. Furthermore, the desired uniform heating is very much advantageous to achieve the specific metallurgical properties such as the desired microstructure and surface conditions. The non-uniform heating always results in poor quality products [Mataga *et al*, 1987]. The desired uniform thermal conditions (temperature and /or heat flux distribution) are an important aspect in material heating.

The uniformity of thermal conditions inside the furnace enclosure depends on several factors, such as location, size and power of the heating sources, size, shape and orientation of load (product), effective area for heat transfer, movement of gases inside the enclosure, properties of the medium inside the furnace (absorptivity, reflectivity, transitivity), and properties of the load and furnace wall material (specific heat, conductivity, reflectivity). To achieve the uniform thermal conditions on the specific region of the furnace, the above stated aspects have to be accounted.

Basically, the problems of finding the configuration and optimal powers of the heaters to produce the desired thermal conditions come under the class of inverse design problems. For finding the solution of such problems, traditional procedure is a trial-and-error method, which is extremely monotonous and time consuming. Further, this method does not assure the optimal solution. Using the inverse formulation, computational expense is considerably lower than that of the trial-and-error method. However, the drawback is that the inverse problems are defined in terms of ill-posed set of equations, and finding their solution requires a special treatment(s) / technique(s). Solution procedure for such problems is a challenging one (Howell *et al.,* 2000). Their solution must require either regularization or optimization techniques. From the decade of sixties, the high speed computers offered the great opportunity to develop and use the new solution methodology which gives fast and accurate solutions of the complex problems. Considering the above stated aspects, for the thermal design and analysis of furnaces the computational experiment is one of the reliable solutions.

Having understood the importance of uniform thermal conditions in various material heating applications and advantages of the radiant furnaces, the study involving boundary heaters design of 3-D radiant furnaces to yield desired uniform thermal conditions on the 3-D design objects (product) bears a significant importance. It is useful in material heating applications. Furthermore, the furnace boundary design problems involving other levels of complexities like irregularity in object shape, blockage effects due to different configuration of the objects, and different application based situations are also important. Such problems are of practical importance, and therefore, the work towards their design

and analysis can be a valuable contribution in the field of material heating. In next section, the literature on furnace boundary design problems is reviewed. Next, the aim and objectives of this work are decided.

1.2 Literature Review

In the previous section, the problems associated with the furnace operations, the importance of thermal uniformity and difficulties in achievement of thermal uniformity have been discussed. Finding the solution of inverse problems, like the present one, must need regularization or optimization tool. For the desired improvement in technology, a good number of researchers are engaged in computational and/or experimental investigations. For different kinds of furnace design problems, various solution methods are proposed. In the following pages the literature related to the boundary design of furnaces are discussed in detail.

1.2.1 Inverse methods for furnace design problems

In literature direct solution methodologies for the heat transfer problems including conduction, convection, radiation and also for the conjugate mode heat transfer problems are well established [Hottel and Cohen, 1954; Fleck, 1961; Raithby and Chui, 1990; Mahanta and Mishra, 2002]. To achieve the desired uniform conditions, boundary design of radiant furnaces falls under the categories of inverse design problems. In last three decades, researchers have contributed the good number of works towards the inverse design problems, and various solution techniques are proposed. In this section, literature review of various inverse furnace boundary design problems is given. The application based problems involving the study of uniform thermal conditions are also been discussed.

In early days, Tikhonov (1975) proposed a regularization technique for solving the system of ill-conditioned equations in the inverse conduction problem, later the technique recognized by his name. Nowadays this is well known Tikhonov regularization technique. In the years later, several methods have been proposed for different inverse

heat transfer problems [Yang and Nishi, 1980; Hansen, 1992; Kudo, 1995; Wu and Wu, 1999; Liu, 2000; Park and Jung, 2001c; Erturk *et al.,* 2002a, 2004]. Detailed discussions on mathematical techniques for inverse heat transfer problems are given by Beck *et al.,* 1985; Alifanov *et al.,* 1977; and Ozisik and Orlande, 2000.

For solving the inverse radiative transfer problem in inhomogeneous media Ho and Ozisik (1988) have given the usage of the nonlinear least-squares equations constructed from the measured data and the exact solutions of the direct problem. They estimated the optical thickness and space-dependent single-scattering albedo from the exit radiation intensities. The advantage of the method is that the inverse solutions are computed directly from the measured exit intensities, without the need for integration of the intensities over all solid angles. In addition, this method is flexible in selecting measurement locations, such as either reflected, transmitted, or both reflected and transmitted intensities may be taken as the measured data. From their study they found that if both reflected and transmitted intensities are used, only 2-digit accuracy in the measured data is needed to ensure acceptable accuracy for predictions. Inverse problems that deal with the prediction of the temperature distribution in a medium from radiation measurements have been reported by several researchers. Li and Ozisik (1992), Siewert (1993,1994), and Li (1994) have reconstructed the temperature profiles or source terms in plane-parallel, spherical, and cylindrical media, respectively using inverse analysis from the measurement of exit radiation intensities at the boundaries.

Inverse source estimation in the two-dimensional rectangular enclosure with a radiating enclosure containing absorbing-emitting medium is investigated by Kudo *et al*. (1995). They solved for the optimal locations for the specified power input in the medium to satisfy design conditions along the boundaries. Truncated singular value decomposition method has been used to produce stable and accurate solutions, while radiative heat transfer was calculated using the Monte Carlo method. Using the above said methodology the source location has been retrieved accurately. For estimating the unknown temperature field in 3-D furnace Linhua *et al.* (1999) proposed an inverse method using the conjugate gradient method (CGM). The information of incident heat

flux on the boundaries has been obtained from the computationally experimented values. The radiative properties were known beforehand. The discrete ordinates method has been used to solve radiation problem. The objective function was defined as an error between the calculated incident radiation heat fluxes and the experimental data and minimized using the CGM. Their results showed that using the proposed method, even with noisy data the temperature field can be estimated accurately.

Using an inverse methodology Park and Chung (1999) determined the time-varying strength of a heat source, which was responsible for natural convection in a 2-D cavity. To model the natural convection induced by the heat source, the Boussinesq equation was used. The inverse natural convection problem was posed as a minimization problem, and for solution the CGM has been used. The gradient of the performance function (objective function) needed in the conjugated gradient technique is obtained by solving the adjoint equation which determines the descent direction. For correct estimation of the end point value of the unknown function for unsteady problems, the combination of the modified conjugate gradient method with the regular conjugate gradient method has been suggested. Using this combination of methods, the solution of inverse natural convection problem has been found accurately, even without a priori information about the unknown function to be estimated.

To determine the unknown flux on the active boundary over certain time interval, from temperature measurements taken at the sensor's position, Prudhomme and Nguyen (2001) studied the inverse natural convection problem. The ad-joint equations and the CGM have been used. Using the knowledge of temperatures within the flow, the unknown space and time dependent boundary heat flux on the enclosure walls has been determined. The direct, sensitivity and ad-joint set of equations for a Boussinesq fluid are solved by control volumes approach. Solutions were given for different types of boundary conditions and a wide range of Rayleigh number values for a square enclosure. It has been shown that the accuracy of the solutions strongly depend on the Rayleigh number, the sensor's position and the type of boundary conditions imposed along all the boundaries. They concluded that even without any a priori information, the proposed

method is capable of predicting an arbitrary function from temperatures measured by sensors located within the cavity.

Franca *et al.* (2001) investigated the inverse boundary design for combined mode heat transfer problem in two dimensions. The problem consists of finding the heat flux distribution on the heaters that satisfies both the temperature and the heat flux prescribed on a design surface of an enclosure formed by two finite parallel plates. A gray participating medium flows in laminar regime between the gray parallel plates, diffuse emitters and absorbers. All the thermal properties have been assumed uniform. The solution was obtained by regularizing the system of equations using the truncated singular value decomposition (TSVD), by first decomposing the coefficients into its singular values and then finding the solution vector by iterative back substitution. They calculated the optimal heater length and required power input within the average error of the solution less than 1.0 percent which is highly difficult by using the conventional trial and error method.

Erturk *et al.* (2002a) solved a transient inverse boundary condition estimation problem. In their study the boundary conditions on the heater walls have been estimated. The information from the design surface at each time step has been used for finding the boundary conditions. In 2-D irregular shaped radiating enclosure, along the top wall heaters and on the bottom wall plane design object was considered. To handle specularly reflecting surfaces and the blockage effect, the radiative heat transfer has been modeled using the Monte Carlo method. The problem was solved by first discritizing the time domain, linearising the nonlinear set of equations, and then solving the inverse problem by iterative CGM at each time step. They obtained the accurate results. It is suggested that in order to avoid changes in the resulting profiles, the results of a fixed number of solution steps should be used in all time steps. This yields smooth profiles at the expense of some loss in accuracy in terms of prescribed transient temperature distribution of the design environment. In another work, Erturk *et al.* (2002b) have compared the performance of three regularization solution techniques viz. the CGM, the bi-conjugate gradient method and the TSVD, for the inverse boundary condition estimation problems

in a 3-D radiating enclosure. The design surface in this case was a planer one. In their study, it has been found that the CGM is more economical than TSVD, but the TSVD supposed to be advantageous in analyzing the system and in certain inverse transient problems.

Fan *et al.* (2002) have given an inverse radiation analysis for estimating the temperature and the heat load distributions of heater surface from the knowledge of temperature and the heat flux measurements of the heated object (design surface). The two-dimensional system with non-participating gas was considered and all the solid walls in the system were assumed to be gray. During computation, the numerical solution of the direct radiation problem are adopted as experimental measurements, the effect of noise was also taken into account artificially. The heat flux of the heated surface was taken the sum of measurement errors (1-5%) and exact heat flux calculated numerically. The solution was obtained using the CGM and singular value decomposition method (SVDM). They estimated the heat load distribution of the heating surface accurately for the exact and noisy data. The effects of the measurement errors on the accuracy of the inverse analysis were also given. More accurate estimation has been observed using the CGM than that of using the SVDM. Lin and Chu (2002) presents a finite difference method formulation in the inverse problem algorithms, for uniform temperature tracking of different linear ramp-up rates in rapid thermal processing. A one-dimensional thermal model and temperature dependent thermal properties of silicon wafers were considered. The required incident heat flux profiles for temperature uniformity across silicon wafer (300 mm diameter and 0.775 mm thick) have been evaluated. The temperature over the wafer was obtained within 0.665 °C of the wafer center. In the advanced rapid thermal processing system this temperature non-uniformities could be acceptable.

Colaco and Orlande (2004) used the GCM for the simultaneous estimation of two boundary conditions in inverse natural convection problems in 2-D irregular cavities. The hollow annular cavity has been considered where the position and time-dependent heat fluxes are unknown at the inner and outer surfaces. Irregular physical domain geometries have been transformed into regular geometries by using an elliptic scheme of numerical

grid generation. The unknown boundary conditions were estimated with no a priori information about their functional forms. They observed that the sensors need to be located near each of the surfaces, inside the thermal boundary layer, in order to be sensitive to variations on the boundary heat flux. To satisfy the desired temperature and heat flux distributions over the design surface, Sarvari (2005) has investigated the inverse optimization problem for finding the two-dimensional heat source distribution in an irregular conductive-radiative medium. A concentric circular shaped computational domain has been considered. The participating medium was gray and non-scattering, the walls were diffuse and gray, and all the thermal properties were uniform. Objective function was expressed by the sum of square residuals between estimated and desired heat fluxes over the design surface and minimized using the CGM. A combination of the finite element method with the discrete transfer method was used to solve the direct problem of conductive–radiative heat transfer. The effects of conduction–radiation parameter, initial guess and mesh refinement are investigated by comparing the results with available numerical solution, and the ability of the inverse method for determination of heat source distribution in irregular geometries. The estimated values of heat flux were in good agreement with the desired values in an acceptable range of error.

Pourshaghaghy *et al.* (2006) solved an inverse radiative design problem to determine the spatial distribution of heat source strengths in a 3-D furnace with an absorbing, emitting, and scattering medium, which produces a desired temperature and heat flux distribution on the 2-D design surface. The surfaces of furnace walls were assumed to be diffuse-grey. For inverse design calculations the CGM was used. The function to be minimized was defined as the sum of squares of the differences between the desired and calculated radiative heat fluxes at the design surface. Maximum relative error for the cases considered in their work was 5%, which reported satisfactory for most engineering purposes. Their investigation shows the capability of the presented algorithm to estimate heater strengths accurately. It was also shown that scattering has a significant effect on inverse computation results. An inverse radiant boundary design problems in a 2-D radiative domain has been studied by Rukolaine (2007). He used three methods of regularization, viz. the ad-joint problem method, the Tikhonov iterative method and

parametric regularization methods. In a two dimensional rectangular cavity the heaters were placed along the top wall and a part of the bottom surfaces considered as the design surface. Performances of all three methods were reported satisfactory. The maximum deviation from the net desired heat fluxes was approximately 2.5%.

To estimate the unknown strengths of heaters, Payan *et al.* (2009) have solved the inverse problem in a square cavity with free convection. The conjugate gradient method has been used for minimization of an objective function, which expressed by sum of square of the residuals between estimated and desired heat fluxes over the design surface. The inverse methodology was employed to estimate the unknown strengths of heaters from the knowledge of the desired temperature and heat flux distributions over a design surface. In the direct problem, for solving the natural convection in the square cavities was solved by the finite volume method. For the example problem, the ability was shown for the inverse method to boundary design of a square cavity. They estimated the strength of heaters within the specified accuracy. To achieve uniform temperature and heat flux on the design surface, Hoffmann *et al.* (2010) presented the inverse design methodology to the systems of wavelength dependent emissivities of the surfaces. They determined the required powers of the heaters using the TSVD regularization method. In a 3-D rectangular enclosure formed by non-gray, diffuse surfaces, convective heat transfer was considered negligible, and the interior of the enclosure does not contain a participating medium. The heat transported solely by thermal radiation exchanges between the surfaces. The strip heaters mounted on the top wall and a plane design surface on the bottom surface. The solution involved an iterative approach in which the radiation distribution in the spectrum bands is repeatedly guessed and corrected as the estimation of the heaters temperatures changes. The TSVD found satisfactory for such kind of heat transfer problems.

In case of furnace boundary design problems, the inverse methodology has a drawback. In inverse methodology, imposing the design constraints is difficult. So there may be negative heat flux on the heaters surface, which is not realistic one. Hence it restricts the application of solution in the practical situations. On the other hand, optimization

methods provide a good way to impose the design constraints. In next section, the studies involving use of the optimization methods for furnace design problems are discussed.

1.2.2 Optimization methods for furnace design problems

In furnace boundary design problems, for estimation of optimal heater power settings to produce desired uniform thermal conditions, the optimization methods have inherent advantages over the regularization methods. Use of the optimization techniques can be traced from the time of Newton and Cauchy. These techniques are vigorously used for numerous problems not only in the field of engineering and science but several others fields, like scheduling [Khouja *et al.*, 1998], transport [Levine, 1996], etc. In the area of inverse heat transfer, use of optimization techniques for inverse parameter retrieval has successfully demonstrated by several researchers [Kim *et al.*, 2004; Christophe and Frederic, 2004; Deiveegan *et al.*, 2006; Verma and Balaji, 2007; Das *et al.*, 2008; Chopade *et al.*, 2011]. However, the uses of optimization techniques for furnace boundary design problems are recent.

Norman (1992) proposed a technique based on linear programming for minimization, in a model of an axis-symmetric circular multi-lamp RTP system. In this independently controlled lamp zone was mounted on the top wall that provide temperature uniformity for specified process trajectories on the wafer of 4 inch diameter. The wafer and chamber surfaces are modeled as gray and diffuse. He used minimax error approximation methods. He has studied the trajectory a ramp-down of wafer temperature from 1100 °C to 800 °C at 40 °C/s and second example of trajectory studied was ramp-up from 600 °C to 1100 °C at 100 °C/s, in both the cases the minimal non-uniformity predicted by the linear programming solution was 3 °C and that obtained from nonlinear simulation was 3.1 ºC, indicating that the error in the linear programming formulation due to linearization of the model was indeed small. From the results it is suggested that, the designed model has delivered excellent temperature uniformity both during transient and steady state hold. To produce the desired thermal conditions on a 2-D surface, Fedorov *et al.* (1998) developed a thermal model of transient three-dimensional industrial oven. In a transient, quasi-three-

dimensional model of heat transfer in which a continuous load considered to be moving inside an oven on a conveyor belt at a constant speed. An array of radiant heaters/burners was placed on the top wall inside the furnace enclosure. The model accounts for radiative exchange between the heaters and the load, heat conduction in the load, and convective heat transfer between the moving load and oven environment. The Levenberg-Marquardt nonlinear least squares optimization algorithm has been used to obtain the optimal temperatures of the heaters/burners that needs to be specified to achieve a prescribed temperature distribution of the surface of a load. Using the proposed solution technique the temperature uniformity on the design surfaces has been achieved within the acceptable range.

Park and Yoo (2001) have studied an inverse problem for estimation of time-varying strength of the heat source, from temperature measurements data in three-dimensional conduction- radiation with participating media. The inverse radiation problem was posed as a minimization problem of the least-squares criterion, and solved using the CGM employing the adjoint equation to determine the descent direction. The performance of the proposed technique was evaluated by several numerical experiments. It has been found that the technique works to solve the inverse radiation problem accurately without a priori information about the unknown function to be estimated. Park and Jung (2001a) demonstrated the usage of Karhunen-Loeve Galerkin method to determine the time-varying strength of a heat source from temperature measurement in 2-D natural convection domain. The Karhunen-Loeve Galerkin procedure can reduce the Boussinesq equation to a set of minimal number of ordinary differential equations by limiting the solution space to the smallest linear subspace that is sufficient to describe the observed phenomena. The performance of this technique was compared with the traditional technique of employing the Boussinesq equation. The proposed method was found to be very accurate and efficient. For RTP Park and Jung (2001b) have developed an efficient recursive method to solve the inverse heat transfer problem that estimate the wall heat flux from the measurements of wafer surface temperature. In this study also, they used the method based on the Kalman filtering technique and the Karhunen–Loeve Galerkin procedure.

To estimate the unknown boundary conditions over the surface of 2-D enclosures and shields in radiation equilibrium from the knowledge of the boundary condition over the surface of an enclosure surrounding them, Sarvari *et al*. (2003a) have given an optimization analysis. The discrete transfer method has been employed to solve the radiative transfer equation. The conjugate gradient method is used for minimization of a objective function which was represented by the sum of square values of net heat flux through the shields. The performance of the present technique was evaluated by several numerical experiments on two- and three-dimensional enclosure shield systems. In another work, to satisfy the desired temperature and heat flux distributions over the design surface, the same methodology was later extended (Sarvari *et al.*, 2003b.) for finding the heat source distribution in a 2-D irregular conductive-radiative medium. In this work a combination of the finite-element method with the discrete transfer method was used to solve the conductive-radiative heat transfer equation. The objective function was expressed as the sum of square residuals between estimated and desired heat fluxes over the design surface. The performance and accuracy of the method for solving inverse conduction-radiation heat transfer problems were demonstrated by comparing the results with a benchmark problem. Also for a 2-D annular shaped domain the results were demonstrated.

Daun *et al.* (2003a) proposed an optimization methodology for designing the radiant enclosures containing specularly reflecting surfaces. The radiant enclosure was analyzed using a Monte Carlo technique based on exchange factors, and the design was optimized using the Kiefer-Wolfowitz method. This stochastic optimization design methodology has been demonstrated by solving two dimensional design problems. The objective function was expressed as the sum residuals between estimated and desired heat fluxes over the design surface. The optimization design methodology has been demonstrated by solving two industrially-relevant design problems, involving 2-D enclosures that contain specular surfaces. In another work, Daun *et al.* (2003b) introduced a methodology for geometry design of diffuse-walled radiant enclosures through nonlinear programming. In this study, the enclosure was represented parametrically using B-spline curves, while the

radiosity distribution was solved by infinitesimal-area analysis. The enclosure geometry was repeatedly adjusted with a gradient-based minimization algorithm until a near-optimum solution was found. With the objective of obtaining a desired radiosity distribution over a portion of the enclosure surface, the methodology was demonstrated by optimizing the geometry of the 2-D radiant enclosures.

Later, Daun *et al.* (2004) presented an optimization methodology for finding the heater settings that provide spatially uniform transient heating in manufacturing processes involving radiant heating. Equations governing the transient temperature and temperature sensitivity distributions over the design surface were derived using an infinitesimal-area technique and then solved numerically to calculate the objective function and gradient vector. The objective function was expressed as the sum of square residuals between estimated and desired heat fluxes over the design surface. Minimization has been done using a quasi-Newton algorithm that incorporates an active set method to enforce design constraints. This methodology was demonstrated by finding the optimal transient heater settings of a two-dimensional annealing furnace. The design surface was located on the bottom surface and was irradiated by 10 heaters on the top wall. The density, specific heat, and thickness, was assumed to be uniform over the design surface. Using this method fast and accurate performance was reported and the intended temperature profile was achieved.

To solve design problems involving radiative transfer, Daun and Howell (2005) demonstrated the use of optimization and inverse methodologies, the TSVD regularization, Newton's method, and conjugate gradient method. The estimation of optimal heater settings in 2-D radiant enclosure design problem was considered. An objective function was defined as the variance between the heat flux distribution obtained with a given set of design parameters and the desired heat flux distribution, evaluated at discrete locations over the design surface. The optimization and inverse design methodologies were demonstrated by applying them to solve a design problem involving the 2-D diffuse-walled enclosure. In the inverse design methodology, both thermal boundary conditions were specified over the design surface, while no boundary

condition was specified over the heater surface. They concluded that, to solve the design problem the optimization methodology requires more iteration compared to the inverse methodology. However, the major advantage of the optimization design methodology is that the design constraints can be imposed easily that ensure the solution applicability in a practical use.

For 2-D design surface placed in three-dimensional radiant enclosure, Porter *et al.* (2006) proposed the use of two metaheuristic optimization approaches viz. simulated annealing and tabu search. Both approaches were demonstrated for radiant enclosure design problem. The difference between the calculated and desired heat flux distributions on the design surface was used in the objective function. Tabu search shown better performance and faster than the simulated annealing approach. Safavinejad *et al.* (2008) estimated the desired thermal conditions on a centrally located planer design surface placed on the bottom of the cubical radiant enclosure and 50 panel heaters considered along the top wall only. The effect of aspect ratio of furnace enclosure was given. The radiation element method by ray emission model has been employed to calculate the radiative heat flux on the design surface. Micro-genetic algorithm was used as an optimization tool. In another work, Safavinejad *et al.* (2009) presented the solution for optimal number and location of equally powered heaters that produce desired thermal conditions over a design surface in 2-D radiant enclosure with a transparent medium. In this study they kept the total power of heaters constant but floating the number of heaters and their locations. The effect of refractory surface characteristics on optimal number and location of heaters was reported significant. For different cases the optimum numbers and locations of the heaters was demonstrated. The objective function was expressed as the sum of square of differences between estimated and desired heat fluxes over the design surfaces.

Jaluria (2009) proposed the general aspects on the design and optimization of thermal systems on the basis of the mathematical and numerical modeling. A multi-objective optimization was suggested, since most thermal systems involve several important objective functions, such as heat transfer rate and pressure in electronic cooling systems, property variations, complicated regions, combined transport mechanisms, chemical

reactions, and intricate boundary conditions. To illustrate these approaches, the design and optimization results for few practical thermal systems, such as optical fiber drawing system, an impingement type chemical vapor deposition system, multiple heat sources in a channel with a vortex promoter, approximating an electronic system, were demonstrated through simulations. The objective function was taken as the square root of the sum of the squares of these three quantities (fiber quality, taking the tension, defect concentration and velocity difference across the fiber) and was minimized. Several search methods, such as golden-section for single variable and univariate for mutivariable cases, were employed. He successfully demonstrated the general aspects on the design and optimization of thermal system. Tan and Liu (2009) proposed a mesh less method in inverse geometry design in two-dimensional radiating enclosure filled with participating media that provide the pre-specified radiative heat flux distribution on a designed boundary wall. The direct collocation mesh less method was adopted to solve the radiative transfer problem. Two-dimensional enclosure composed of a high temperature heating surface on top wall, three cold surfaces (part of the bottom surface and conveyor belt), and two diffuse reflection surfaces (side vertical walls). The temperature and geometry shape of top wall high temperature surface were given and the upside of a conveyer belt (cold surface, design surface) and the geometry shape of this cold surface was unknown. In the design process, the geometry shape of the designed surface (belt) has been adjusted to meet the uniform distribution of radiative heat flux on the belt surface. The geometry shape design problem was transformed to the position design problem of discrete geometry points. The geometry shape of the design surface was optimized using the conjugate gradient method.

Recently, with the objective of achieving the uniform heat flux distribution over a diffuse-spectral temperature specified design surface, Bayat *et al.* (2010) have proposed the application of optimization procedure through the CGM. They estimated the temperatures over reflector and heater surfaces placed along the boundaries of a 2-D radiant enclosure. The variation of emissivity with respect to the wavelength was approximated by considering a set of spectral bands with constant emissivities and then the radiative transfer equation was solved by the net radiation method for each band. An

iterative method based on the conjugate gradient method has been used for estimation of temperatures over reflector and heater surfaces. The inverse problem was formulated as an optimization problem for minimizing the square deviations between desired and estimated heat fluxes over the design surface. The maximum relative error and the root mean square error in estimating the total heat flux on the design surface were compared for two cases with diffuse-spectral design surface and diffuse-gray design surface. The results show that the uniform heat flux distribution over the design surface was recovered; however the assumption of diffuse-gray design surface may generate errors in estimating the heater powers. To determine the unknown heat flux profile through the active constraints in radiative boundary design problem, Rahmani *et al.* (2010) developed a combined approach which includes utilizing a new search optimization technique merged with the maximum entropy method (MEM). A generalized computational grid based on finite-volume scheme was devised to solve the radiative transfer equation. It was shown that use of the merged MEM algorithm minimizes both the occurrence of negative values and the oscillatory profile of heat flux. Numerical simulations were demonstrated to evaluate the performance and accuracy of the present approach.

1.2.3 Other numerical studies related to furnace design problems

In the previous sections, the studies involving the use of inverse and optimization techniques in various types of inverse furnace boundary design problems have been discussed. Other than these, some other numerical studies related to the thermal uniformity inside the systems are available in literature. In this section, the numerical studies related to the thermal uniformity in the furnace/ thermal systems are given.

Abraham and Sparrow (2003) proposed the numerical simulation of 3-D natural convection in an enclosure containing the discrete thermal load using FLUENT 6.0. The model includes the rod-like discrete heat sources placed at the bottom of enclosure, to simulate electrically heated oven used in the baking mode and the thermal load mimicking the foodstuff. Their particular interest was to study the variation in the flow field above the upper surface of the load as a function of the temperature difference between the enclosure walls and the load surface. All simulations were carried out for the

steady-state situation. They obtained the convective heat transfer rates at the surface of thermal load as a function of enclosure-to-load temperature difference. It was given that, for the blackened thermal load, radiation accounted for about 72% of the total heat transfer rate, while for a highly reflecting thermal load, the corresponding percentage was about 8%. Passive cooling of electronic components by natural convection heat transfer is the least expensive, quick and most reliable method of heat rejection. Addressing to this important issue, Dias and Milanez (2006) carried out the optimization of the natural convection heat transfer for a two-dimensional vertical square cavity. The micro genetic algorithm was used as an optimization tool. Four cases were studied: one heat source, two heat sources with same dissipation rate, and two heat sources with different dissipation rates on an adiabatic vertical wall. For the case 1 and 2, good agreements were observed between the obtained results and those presented in literature. For the first case about 50 numerical simulations were performed. In the third configuration two cases with two heat sources with different dissipation rates were considered. In the third case, in first case larger heat dissipation was in the upper heat source and another where the higher dissipation was in the lower heat source. These cases show that the optimization software was able to find the better heat source configuration and location according to the heat dissipation rate, independently of the initial configurations provided to the software. From the results they suggested that the genetic algorithm is computationally feasible optimization methodology for finding the optimal location of heat sources along the vertical wall

Malhotra *et al.* (2006) proposed a model of temperature uniformity during the vacuum deposition process for the production of stable thin-film photovoltaic cells. With target of achieving the temperature uniformity of 1 °C, a finite element thermal model of a commercial-scale deposition station has been developed and optimized. For performance improvements, they have studied the effects radiation shielding, addition of radiation spreader, contouring of radiation spreader and optimizing power distribution among the radiation lamps. In their model, to simulate heating from the infra red lamps, a surface flux was applied to the outer surface of the lamp shells. The steady-state solver in ABAQUS was invoked and the solution was assumed to be converged when the

maximum residual heat flux in the model was below 0.5%. Each calculation took approximately 3 h. While mesh refined by approximately 1.5 times, the maximum difference in temperature at points of interest in the source and substrate changed by only 0.3% and the computational time increased to 15 h. For further applications the earlier mesh was suggested. A new configuration of lamps has also been proposed for attaining the desired temperature uniformity levels. A hybrid method based numerical simulation has been given by Kang and Rong (2006), studying the heat transfer in heat treatment processes. The effects of load pattern and work piece quantity on the temperature behavior were evaluated. Two cases, the furnace with round shaped and rectangular shaped work pieces was considered. In the radiation model view factor between the furnace and workpieces, among workpieces were calculated by the exposed surface area over the total surface area. In the conduction model workpieces were classified into lumped capacitance and massive objects. The flowchart used for this gas-fired furnaces, they proposed the same for electric furnaces. The optimization of work piece loading and the thermal schedule was proposed.

Zashkova (2008) developed the algorithm for determination of the shortest baking system for ceramic articles in chamber furnaces. It enables the determination of the most suitable thermal regime in view of the production quality, furnace possibility and its efficiency. The shortest baking time means that, at which the temperature gradients in the ceramic bodies are smaller with 50% than the boundary value for the material. He studied the gas fired furnace model using ANSYS 9.0. The baking processes were implemented in furnaces with high energy consumption at the temperatures from 1000 to 1700°C. Verboven *et al.* (2009) have given the application of computational fluid dynamics (CFD) to calculate the 3-D isothermal air flow in an industrial electrical forced-convection oven. The governing fluid flow equations were expanded with a fan model and a turbulence model. The standard and the re-normalization group version of the k-ε turbulence model produced comparable results. The performance of the CFD model was assessed by point measurements of the velocity with a directionally calibrated hot-film velocity sensor. From the validation it has been found that important aspects of the model are the fan head-capacity relationship, the fan swirl and the oven geometry. The

calculation error was on an average 22% of the actual velocity. This could be attributed to the limitations in turbulence modeling and numerical grid density. In overall conclusion, good approximation of the 3D flow pattern in a forced convection oven was seen using the CFD modeling technique.

1.2.4 Experimental studies related to furnace design problems

Several experimental studies are available in literature towards the furnace operations [Taberlet and Fautrelle, 1985], combustion [Fan *et al.*, 1999; Suda *et al.* 2002], heat transfer [Zhou *et al.*, 2005; Banan *et al.*, 1991], and several other related issues. For uniform thermal conditions inside the furnaces, very few experimental studies are available. Among the available studies, most of were done for yielding the uniform thermal conditions on a silicon wafers placed inside the rapid thermal processing furnace [Campbell *et al.*, 1991; Hodul and Morda, 1991; Apte and Saraswat, 1992; Theodoropoulou, 1998, 1999]. The silicon wafer in the RTP is similar to 2-D surface. The results from these experiments may not be implemented to produce uniform thermal conditions on the general products, i.e. 3-D objects. In the following paragraphs some of the experimental studies related to the uniform thermal conditions in the furnaces are discussed.

White and Probert (1991) investigated the indirect heating furnace for finding the optimal arrangement of the stacked cylindrical aluminum billets, in order to minimize the required heating period in a particular heat treatment process. They studied the forced convection heat transfer ignoring the radiation. According to the results, for maximum effectiveness of thermal energy transfer from the forced convecting air to the billets, the optimal horizontal pitch-to-diameter ratio for the billets should be 1.33 ± 0.05. Knutson *et al.* (1994) developed a 3-D steady-state model of the 4108 Heatpulse rapid thermal processing system for the study of thermal uniformity across 8 inch wafers. The situations with various lamp-array configurations and tilted wafer with respect to the plane of the lamps have been investigated. They found that changing the power of one lamp by 25% can lead to temperatures changes of up to 7°C at various points on the wafer. Also, they have shown that a subtle tilt of the wafer can lead to relative

temperature changes of up to 5°C at various points on the wafer. For Predicting 3-D spatial temperature uniformity in food storage systems from inlet temperature distribution, Ozcan *et al.* (2005) investigated the relation between the 2-D inlet temperature distribution measured by the airflow pattern sensor and 3-D uniformity index in the room, for different ventilation rates. Regression analysis was used to model the uniformity index from the temperature measurements by airflow pattern sensor. Their results show that 2-D inlet temperature measurements can be used to predict 3-D uniformity of temperature in a mechanically ventilated space.

The indirect resistance heating cylindrical furnace was built by Khlevnoy *et al.* (2008) for high temperature metallurgical experiments. The investigation shows that the temperature uniformity of a pyrographite furnace strongly depends on the position of pyrographite heater rings, and resistance. The temperature uniformity optimized for high temperature fixed point application by arranging the rings in such a way that the lowest resistance in the center of the heater and increases towards the ends. Finally the temperature of the central part of the furnace was achieved uniform within 2°C over a length of 40 mm at a temperature of 2500°C. Recently, Erturk *et al.* (2008) have experimentally validated the results of an inverse boundary design analysis used in the design of an axis-symmetric vacuum chamber which can be characterize as a semiconductor rapid thermal processing furnace. The radiative heat transfer was a dominant mode of energy transfer. The experimental apparatus was an axisymmetric vacuum chamber designed to reproduce the main features of RTP equipment used for silicon wafer processing. In numerical model the radiative transfer was calculated using the Monte Carlo Method. The vacuum chamber with heaters composed a thermometry test bed, and temperature distribution along the silicon wafer (200 mm) was measured. The target wafer temperatures 600 °C was achieved within the error of 3% and the difference between the maximum and minimum measured temperatures 2.6 °C was reported.

1.2.5 Summary of literature review and scope of research

Indeed the uniform thermal conditions are important aspect in any furnace applications and it is of paramount importance in material heating. Uniform thermal conditions are

essential within the required accuracy in several heating applications such as material heating in precision heat treatment processes, hot working processes, electronic component manufacturing, drying, curing of paints, etc.

For various types of boundary design problems, use of different regularization and optimization techniques have been discussed in the literature review section separately. Despite the large interest expressed in inverse design problems, most of the analyses are demonstrated with two-dimensional furnace enclosure and for two-dimensional design object, which has a limited use in the practical applications. The studies involving the radiant furnace boundary design problems in 3-D furnaces with 3-D design object (DO) have not been found. Also in the boundary design problems various aspects in material heating applications, such as design limitation for the maximum size and numbers of the DO(s), locations of DO, irregular shapes of the DO, etc. have not found in literature. In spite of inherent advantages of optimization methods, specifically the metaheuristic and evolutionary algorithms like genetic algorithm, very few studies show the applications of these methods in furnace design problems. Yet the use of evolutionary methods not fully developed in furnace boundary design problems.

In the literature, good numbers of experimental studies on the furnace operations, applications, efficiency improvement, safety aspects, etc, are available. However, the experimental studies on yielding the uniform thermal conditions over a specified region in the furnace are scanty. From the available literature it is observed that most of the experimental studies on thermal uniformity were done for RTP type furnaces and very limited cases are analyzed.

Despite the large amount of literature available on furnace boundary design problems and related issues, the more generalized design and analysis in this field can be explored.

1.3 Aim and Objectives

Based on the literature review, the present work is aimed at the thermal design and analysis of a radiant furnace for uniform thermal conditions. For the chosen aim, following are the objectives:

1. Develop an algorithm for optimal design of boundary heaters along the walls of a 3-D radiant furnace that produce the uniform thermal conditions on a 3-D object(s) placed inside the furnace enclosure.
2. Thermal design and analysis of the radiant furnace that produce uniform thermal conditions for different situations in material heating applications.
3. Develop the solution for design of 3-D radiant furnace for uniform thermal conditions on 3-D irregular shaped design objects placed inside the furnace enclosure.
4. Model a furnace for easy thermal control and operation.
5. Compare the sample numerical results of present problems with that of experimental work.

1.4 Organization of the Thesis

The studies in this thesis focus on the optimal boundary design of a 3-D radiant furnace (estimating the optimal configuration and power of the panel heaters) that produces the desired uniform thermal conditions (temperature and heat flux distribution) on 3-D DOs. Furthermore, the thermal analysis of furnace boundary design problems for different situations in material heating is given.

This dissertation is divided into seven chapters. Chapter 1 starts with the motivation of work, which include the introduction to the problems in furnace operations, importance of thermal uniformity and factors affecting it. The literature review and objectives of the present work are presented in sequence. Reviews of various solution methods for inverse heat transfer problems are given in Chapter 2. Their merits and demerits for furnace boundary design problems are discussed. For uniform thermal conditions on 3-D DOs, in

Chapter 3, formulation of the algorithm to estimate optimal heater power settings in a 3-D radiant furnace is given. Different types of problems and for a given problem, the effects of various parameters on estimated uniform thermal conditions are given in Chapters 4-6. Conclusions and scope for future work are given in Chapter 7. In following paragraphs, the contents of the each chapter are briefly described.

Chapter 1 entitled Introduction starts with the motivation of the present work, which include a brief discussion of furnace applications and importance of the furnaces in industries. The basic requirement of the furnaces, importance of thermal uniformity and the factors affecting it, are elaborated. After stating the motivation of the present work, detailed literature review is given. This includes the discussion on previous studies dealing with furnace boundary design problems for uniform thermal conditions and the various methodologies used for them. Based on the literature review, the objectives of the present work are outlined.

Chapter 2 is devoted for reviewing the solution methods for inverse furnace boundary design problems. In this chapter, several inverse and optimization methods are reviewed, and their merit and demerit in radiant furnace design problems are discussed. For the present boundary design problem, this aspect is handled by the micro genetic algorithm (MGA) which is an improved form of the genetic algorithm. The advantages of the MGA in the furnace design problems are elaborated. In the last section of this chapter, the working procedure of the MGA is given in detail.

In Chapter 3, formulation of the direct and the inverse radiative transfer problems are given. In both direct and inverse problems, radiative information is computed using the radiation element method by ray emission model (REM^2). The MGA is used as an optimization tool in the inverse analysis. Before going for actual computation, the solution methodologies by REM^2 for the direct problem and REM^2 + MGA for the inverse problem are validated. For the direct problem, the results of grid and ray independent tests are given. The algorithm (REM^2 + MGA) is implemented for basic furnace boundary design problem. For the desired uniform thermal conditions on the 3-D

DO, the optimal configurations and powers of the panel heaters along the walls of the 3-D radiant furnace are estimated. The effects of aspect ratios of the furnace enclosure and the design constraints (heater power ranges) on the estimated heat flux distribution on the DO are given. In the last section of this chapter, for every case, the optimal heater power settings are plotted and results are analyzed.

In Chapter 4, estimation of desired uniform thermal conditions in the radiant furnace is done for three different situations in material heating processes. In this chapter, the first study deals with finding the constraints on the size of a centrally located 3-D DO. To cover a wide range of dimensions, 29 DO models are considered. Next, the present numerical results are compared with a sample experimental study. The fabrication of experimental setup and experiment procedure are described in detail in Annexure 1. Calibration of thermocouples and the error analysis are given in Appendix I and II respectively. In the second study, for uniform thermal conditions, the effect of the locations of 3-D DO on the bottom of the furnace enclosure is investigated. Towards the furnace design for mass production, the third study deals with the furnace heaters design in which multiple DOs are accommodated. For the desired uniform thermal conditions, the inverse analysis is done to estimate the heat flux distributions on the DOs and thus the suitable configurations of the DOs are decided. In every study, the estimated heat flux distributions on the surfaces of the 3-D DO(s), and for a sample cases, the optimal heater power settings along the walls of the furnace enclosure are estimated.

For desired uniform thermal conditions on 3-D DOs, in Chapter 5, towards the ease in implementation and control of the heater power settings, the concept of grouping of discrete heaters is introduced. The implementation of this concept is exemplified in 3-D furnace design problem with 2-D and 3-D DOs.

Having analyzed several situations of regular 3-D DOs, in Chapter 6, results are presented for the estimation of optimal heater power settings in a 3-D radiant furnace with 2-D and 3-D irregular shaped DOs. In this study, hemispherical, conical, cylindrical and combinations of these irregular shaped DOs are considered. In every case, the effect

of size of the DOs and the corresponding heater powers setting are given. In the last section of this Chapter, for the desired uniform thermal conditions, the optimal heater power design is given for a complex case. Here, a replica of a car body is considered as DO. In this way, for yielding the desired uniform thermal conditions on the 3-D regular and irregular shaped DO(s), the estimation of the optimal boundary heaters design for a radiant furnace is done.

The conclusions from the present research work are presented in Chapter 7. Scope for future work and recommendations are also given in this chapter.

CHAPTER 2

SOLUTION METHODS IN INVERSE HEAT TRANSFER PROBLEMS

2.1 Introduction to Inverse Problems in Heat Transfer

In science and engineering, physical phenomena are cast in terms of mathematical equations. When it comes to thermal problems, in most of the situations, for the known geometrical configurations, thermo-physical properties and initial and boundary conditions are known. In these cases, the objective remains the determination of thermal field such as temperature and or heat flux distributions in the solution space. On the contrary, there are plenty of cases, in which temperature and/or heat flux distributions are known, and one or more of the thermo-physical properties and/or initial and boundary conditions are unknown. If the former belongs to the class of direct problems, the latter one falls under the class of inverse problems (Modest, 2002). In a simple language, contradictory to the direct problems, from the knowledge of effect(s), the determination of the cause(s), viz., boundary and initial conditions, thermo-physical properties, etc., remain subject of the inverse heat transfer problems. The determination/estimation of desired quantity may be different in different problems, such as the surface conditions (Alifanov, 1974), energy generation (Christophe and Frederic, 2004), thermo-physical properties (Huang and Ozisik, 1999; Huang and Yan, 1995), desired thermal conditions (Fedorov *et al.*, 1998), shape of boundaries (Huang *et al.*, 1999), etc. An extensive review of the inverse problems has been given in a series of papers by McCormic (1984, 1986, and 1992).

It is seen that the inverse problems plays an important role in almost every field, from the medical to engineering sciences, in electrodynamics, geophysics, astrophysics, engineering designs and many other fields. Particularly in the thermal engineering,

inverse optimization problems have several applications. These applications include but are not limited to:

- Optimum designing of the heat transfer systems,
- Design of boundary fluxes in melting and solidification processes,
- Determination of outer surface temperature during re-entry of a space vehicle,
- Estimation of surface conditions at the exhaust of rocket or jet engine,
- Remote sensing for the atmospheric properties,
- Temperature measurement in glass manufacturing.

Inverse problems can be broadly categorized as

- Inverse boundary estimation problems (IBEP): estimation of the surface heat flux mostly along the boundary of system from measured/ desired temperature/flux/pressure along one or more interior location [Fedorov *et al.*, 1998; Franca *et al.*, 2001; Howell *et al.*, 2002; Erturk *et al.*, 2004; Daun *et al.*, 2005; Pourshaghaghy *et al.* 2006; Rukolaine, 2007; Sarvari, 2007; Payan *et al.*, 2009; Hoffmann *et al.*, 2010].

- Parameter estimation (PE): evaluation of certain parameters describing physical properties from measured /desired temperature history at interior locations. In this, unlike to the IBEP the number of unknowns are less [Garcia and Scott, 1998; Garcia *et al.*, 1998; Fan *et al.*, 2002; Kim *et al.*, 2004; Das *et al.*, 2008].

- Inverse geometry problem (IGP): estimating the system geometry to produce specific condition(s) inside the domain is termed as geometry optimization [Huang and Hsiung, 1999; Daun *et al.*, 2003; Sarvari, 2007].

- Initial inverse problems (IIP): determining the initial condition(s) from the temperature/ flux/ velocity, distribution inside a domain. The IIPs are not of much

importance in engineering problems, because the initial condition(s) influences the thermal conditions inside a domain, only for a limited time interval.

- Other inverse problems: estimation of the location or strength of internal heat sources for specific conditions.

The studies in this thesis involve estimation of optimal power of heaters placed along the boundaries of radiant furnace that produce the desired uniform thermal conditions on a 3-D design objects. This kind of problems falls in the category of inverse boundary design problems.

Owing to the wide scope and the importance of the inverse problems in heat transfer, the study of their solution methodologies also becomes equally important. In next section, the solution techniques for inverse heat transfer problems are briefly discussed.

2.2 Solution Techniques for Inverse Problems in Heat Transfer

It is found from literature (refer section 1.2) that different solution techniques are used for variety of inverse heat transfer problems. Since no single technique is competent for finding the solution of all the inverse problems efficiently, the solutions techniques can be different for different problems and for specific applications. Some of the methods may prove best for specific problems, at the same time, others may not work well.

Since the inverse problems are mathematically defined in terms of ill posed system of equations, the conventional linear algebraic solutions methods fail. These types of systems of equations need to be treated before the conventional linear algebraic methods are used. The solution techniques for inverse heat transfer problems are broadly categorized in two classes, viz., inverse (regularization) techniques and optimization techniques. Some of the known solution techniques for the solution of inverse problems in heat transfer are listed below. Such techniques generally require the solution of the

coupled direct problem, and its solution accuracy also depends on the combination of the direct method and inverse technique.

2.2.1 Regularization techniques

For inverse methodology the known regularization techniques for boundary design problems are:

- Tikhnov regularization (Tikhonov, 1975)
- Truncated singular value decomposition (Franca *et al.*, 2001, 2002b)
- Conjugate gradient regularization (Park and Chung, 1999)
- Least-square QR decomposition (Wang *et al.*, 2008),
- Levenberg-Marquardt method (Levenberg, 1944; Neto and Ozisik, 1995; Deiveegan *et al.*, 2006)

An extensive review of the IHTP has been given by Mc Cormic (1984, 1986, and 1992). Also several texts are dedicated to IHTP (Kurpisz and Nowak 1995; Ozisik and Orlande, 2000).

2.2.2 Optimization techniques

In order to achieve desirable outcomes, researchers are often faced with the challenges of making tradeoffs between different factors. For achieving desirable effect(s), optimization is an act of choosing the best possible tradeoffs under given circumstances. Applications of optimization are wide spread in the fields of engineering, sciences, medicine, finance, transport, planning, construction, maintenance, manufacturing, etc. Even the evolution process in nature reveals that, it follows the optimization. The ultimate goal of all such decisions is to either minimize the effort required or maximize the desired benefit. There is no single method available for solving all optimization problems efficiently. Hence several optimization methods have been developed by researchers /mathematicians for solving different types of optimization problems.

In fact optimization methods can be traced to the days of Newton, Lagrange and Cauchy (Rao, 1990). In spite of the early contributions, a very little progress was made until the middle of the twentieth century. The availability of digital computers in the decade of sixties made the implementations of the optimization procedures possible for solving complex problems encountered in science and technology, and in this way further research stimulated. This advancement also resulted in the emergence of the several well-defined new areas and new optimization techniques. In that days many of the new methods were put forward, like simplex method for linear programming problems, stochastic programming, and later on the multi-objective programming (1961).

Several optimization techniques are available for different types of problems, some of the known optimization techniques in ITHP are listed below.

- Downhill simplex method (Nelder and Mead, 1965),
- Gradient descent method (Park and Yoo, 2001a; Li, 2001),
- Successive approximation method (Wu and Wu, 1999),
- Least square approximation (Su and Chen, 2007),
- Newton-type iteration algorithm (Zhou *et al.*, 2002),
- Karhunen Loeeve Galerkin procedure (Park and Yoo, 2001b),
- Genetic algorithms (Holland, 1975; Goldberg, 1989),
- Simulated annealing (Kirkpatrick *et al.*, 1983),
- Tabu search (Glover,1986),
- Ant colony optimization (Dorigo and Maria,1992) ,
- Particle swarm optimization (Kennedy and Eberhart, 1995, Mossi *et al.*, 2008),
- Differential evolution (Storn and Price, 1997).

A good introduction to a various optimization techniques is given by Onwubolu and Babu (2004). Development of the optimization techniques like genetic algorithm, ant colony algorithm and differential evolution are recent. In next sections, for the present problem of thermal design of radiant furnace, the merit, demerit, and limitations of available methods are discussed.

2.3 Selection of Optimization Method

For IHTP, various regularization and optimization techniques are given in section 2.2.1 and 2.2.2, respectively. The selection of solution methodology for the particular problem depends on nature of the problem, number of unknown parameters to be estimated, required accuracy and the available resources (computational capacity), etc.

The present problems falls in the category of boundary design problem, in which the objective is to estimate the optimal heater power settings along the walls of the 3-D radiant furnace that produce the desired uniform thermal conditions on the surfaces of 3-D DO. In present studies the numbers of unknown parameters are in the range of 300-500.

For the solution of the boundary design problems, in literature several regularization and the optimization techniques are proposed, and demonstrated their applications for various inverse heat transfer problems. The literature review on use of inverse and the optimization techniques for the boundary design problems is given in section 1.2.1 and 1.2.2, respectively. The optimization methodology solves the inverse problems implicitly in its original form while in the inverse methodology solves the problem explicitly using regularization techniques.

Using inverse and the optimization methodologies, especially in case of furnace boundary design problems, the key difference lies in the quality and usefulness of the solutions. The solution obtained using inverse methods is generally mathematically accurate. However, in inverse methodologies imposing the design constraints is difficult and so the solutions may provide negative heat flux on some of heaters. It is impractical to operate the radiant heaters with negative heat flux conditions. On the other hand, the optimization methodologies handle the design constraints easily, this ensures the realistic solution. In the problems of this thesis, we ensure the positive heater power and within the specified limit. The capability to accommodate design constraints in the optimization methods is one of the prominent characteristics.

In section 2.2.2, some of the known optimization methods are listed. However most of them suffer from one major drawback, they may get trapped in the local optima. Recently, evolutionary based algorithms such as genetic algorithms (Holland, 1975; Goldberg, 1989), simulated annealing (Kirkpatrick *et al.*, 1983), tabu search (Glover, 1986), ant colony optimization (Dorigo and Maria,1992), particle swarm optimization (Kennedy and Eberhart, 1995), and differential evolution (Storn and Price,1997), etc., have an emerging trend for the optimization problems in various fields of engineering and sciences. The genetic algorithm has some of the inherent advantages over the conventional search methods. The detail methodology of genetic algorithms is discussed in next section.

2.4 Concept of the Genetic Algorithm

Genetic algorithms (GAs) are computational techniques for searching the minimum or maximum of complex objective/ fitness functions based on the principles of genetics. The procedure of the GA simulates Darwin's nature evolution theory (1859) "survival-of-the-fittest".

Evolutionary computation techniques have drawn much attention as an optimization tool in the last three decades, and became possible for solving real-world problems on desktop computers. In 1975, Holland built the first genetic algorithm based on the principles of natural evolution to optimization problems. Since then, extensive research has been carried out on the GA theories, and its applications in variety of scientific fields. GAs possess some of the inherent characteristics such as feasible for parallelism, robust, wider solution space, ability to handle very complex objective functions, ability to handle noisy functions, robust response to changing circumstances, easy to discover global optimum, only uses the function evaluations, easy modification, no requirement of gradient information and resistant to trapping in local optima. Also, the GAs are able to solve non-smooth, non-continuous, and non-differentiable objective functions. The GA concept works well to problems where heuristic (computing to a solution by trial and error or by rules that are only loosely defined) solutions lead to unsatisfactory results [Sivanandam

and Deepa, 2008]. The ability of the GAs have proved through the successful applications to real-world problems, and recognized as a powerful, robust optimization tool. Several researchers have successfully used the GA in different engineering fields such as software engineering [Asllani and Lari, 2007], electrical engineering [Osman *et al.*, 2004], civil engineering [Yong *et al.*, 2008], mechanical processing [Kaya, 2006], including heat transfer problems [Li, 1997; Kim *et al.*, 2004; Kim and Baek, 2007; Das *et al.*, 2008a].

The GA is working on the evolutionary principles applied in genetics. GA is an iterative procedure. Instead of working with a single solution, the GA works with a number of solutions (collectively known as a population) in each of the iterations. Figure 2.1 shows a flowchart of the GA. The coded parameters look as a DNA-like linear data structure forming a vector or a string. A set of parameters is called population. The working of the GA starts with the random generation of an initial population, the values of different parameters generated using a random number generator. Typical population size in the GA can be from few dozens to thousands.

The GA chooses the best set of solutions on the basis of different operators such as reproduction, crossover and mutation. Optimization using the GAs needs an objective function (also known as cost function or fitness function). The genetic algorithm loops over an iteration process to make the population evolve. After generation of population, each iteration consists of four basic steps, viz. selection of individuals to form mating pool, reproduction (crossover), evaluation of fitness and replacement of old population to the newly produced offspring. The first step consists in selecting individuals for reproduction. This selection is done randomly with a probability depending on the relative fitness of the individuals so that best ones are often chosen for reproduction than poor ones. In the second step of reproduction, offspring are produced by the selected individuals. For generating new chromosomes, the algorithm can use both recombination/crossover and mutation. In the crossover process, to produce new offspring, the pairs form new strings mate by exchanging the genes systematically. The crossover is then followed by the mutation operation. In this, through an assigned

probability, the mutation operator randomly changes the genes in the strings. After evaluating the fitness of the new chromosomes, the parents are replaced by the newly produced offspring. In this way, the generation completes.

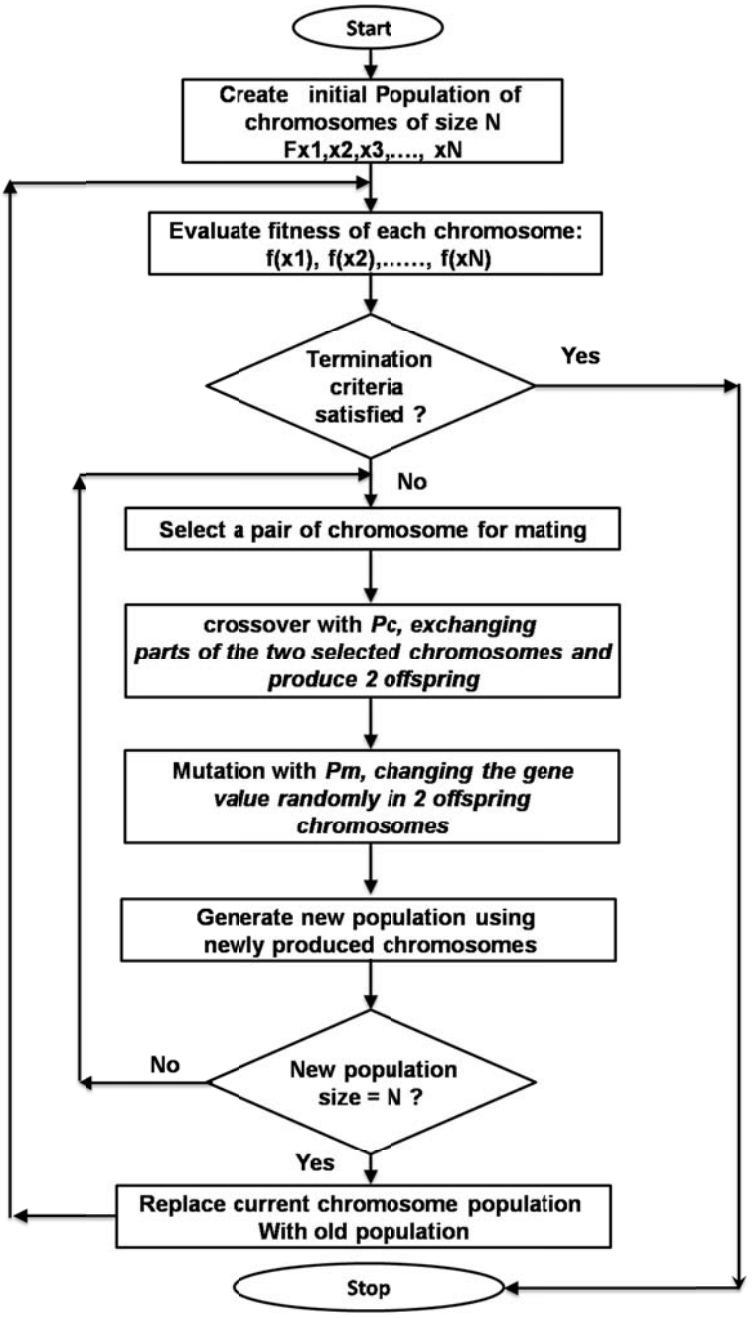

Figure 2.1. Flowchart showing basic procedure of genetic algorithm.

Next, the production of new offspring takes place. In the GA terminology, one iteration of these three operators is known as a generation. This process continues till either a satisfactory value of the fitness function is attained or a certain maximum number of generations are exceeded. After the convergence of objective function, the GA gives the final set of the solution corresponding to the minimum value of the objective function. Since the representation of the solution in a GA is similar to natural chromosomes and GA operators are similar to genetic operators, the above procedure is named as GA, it is also known as traditional GA or simple GA (SGA).

It is well known that, the GA provides a better solution with a bigger population size. The population size requirement in the GA depends on the length of the chromosomes, and the length of chromosomes is proportional to the number of unknown parameters. If the numbers of parameters are large, the length of chromosome will be big and this needed a large population size. However, a bigger population size requires more computational time to find the optimum solution (Goldberg, 1989). In the present design problems the number of unknown parameters (i.e. power of heaters) is ranging from 300 to 500. In such situations, the traditional GA requires a huge computational effort and time. To overcome such problems, several versions of the GAs have proposed (Goldberg, 1989; Deep, *et al.*, 2009). To address the drawback of an appetite for the computational time of the SGA, Krishnakumar (1989) proposed the GA which is able to provide accurate results with a very small population size, and is termed as micro genetic algorithm (MGA). Since in this work the numbers of unknown parameters are large, MGA is the best option. For all the studies in this thesis, the MGA has been used as an optimization tool. In next section, the detail working procedure of the MGA is given.

2.5 The Micro-Genetic Algorithm

To address the drawback of an appetite for the computational time of the SGA, in 1989, Krishnakumar (1989) proposed the MGA which has been able to provide accurate results with very small population size. In this, premature convergence was absent and also required less number of iterations (generations). This version of the GA became very

handy particularly when the numbers of unknown variables are large. The MGA works with a small population size and is computationally less demanding. Owing to its improved characteristics, especially very fast operation due to small population size and the ability to attain the global optimum, many researchers have successfully implemented the MGA for solving different kinds of optimization problems (Carroll, 1996; Roy *et al*., 1997; Yang *et al.*, 1998; Tse and Chan, 1999; Karim *et al.*, 2004; Madadi and Balaji, 2008; Safavinejad *et al.*, 2008, 2009; Szollos *et al.*, 2009).

Except elitism and start-restart processes, like the SGA, in the MGA, the procedure consists of generation of population, selection, reproduction, crossover, elitism and convergence checking and re-starts. To maintain the genetic diversity in the population, the MGA uses a restart strategy, not the conventional mutation operation. That is, once the current generation converges, a new generation will be generated that has the same population size and consists of the best individual from the previously converged generation and other new randomly generated individuals from the entire space. This evolutionary process continues until the global optimum is found. The elitism strategy ensures the best individuals in next generation while the start-restart procedure helps in avoiding the premature convergence and the search continues for better strings. The MGA code has been written by the candidate in FORTRAN and it is coupled to the code of REM^2. The flowchart showing the sequential steps involved in the working procedure of MGA is given in Fig. 2.2. In the following paragraphs, working procedure of the MGA is given in detail.

2.5.1 Generation of population and encoding-decoding of the variables

Working of the MGA starts with random generation of an initial population. With the help of random number the population is generated within the predefined higher and lower values of the variable constraints. Next step is coding the every design variables in fixed length binary strings to form a chromosome. Each chromosome encodes a binary (bit) string. Thus, a total strings (chromosomes) represents a complete solution, specifying all N unknown variables. Several methods can be adopted for coding of variables or even one can also use the real numbers for the same. Using the later method

it is called the real coded GA. In the present work, the binary coding system has been used. Binary encoding gives many possible chromosomes with a smaller number of Alleles (feature value). The length of substring is generally decided by the precision needed on variable. Precision of a variable depend on design constraints and numbers of

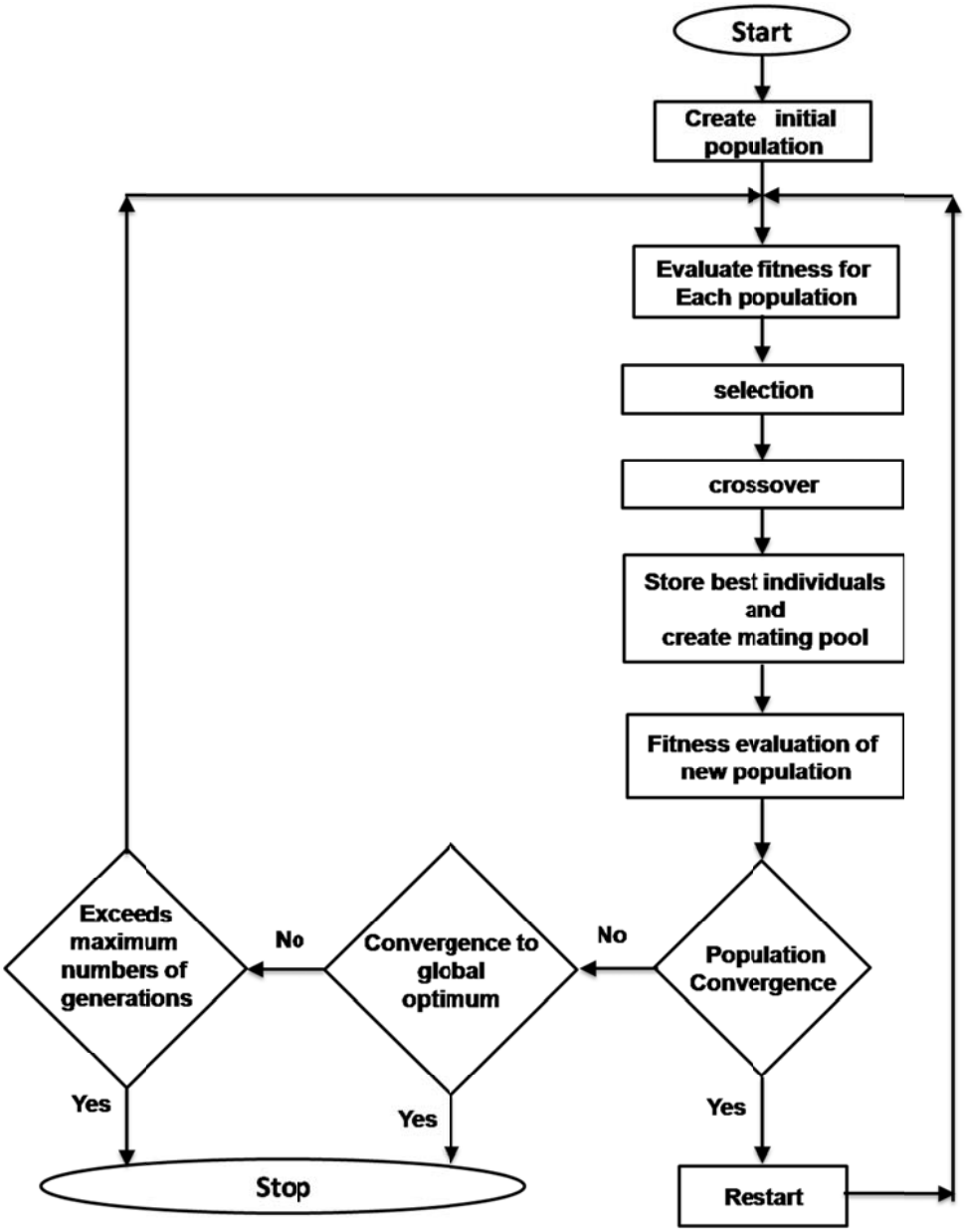

Figure 2.2. Flowchart of micro-genetic algorithm used in present work

bits allotted for the variable. Since in the present studies, different constraints are studied, to achieve the 4 digits precision, 16 bits for each variable are used. Precision of the design variable is calculated using the relation from Homaifar *et al.*, (1994).

$$\pi = \frac{X_{\max} - X_{\min}}{2^{\lambda} - 1} \tag{2.1}$$

where λ is the numbers of bits used to code the design parameter.

In the present work, with the difference between upper and lower constraint values of the design variable (8.0 - 0.0001, non-dimensional powers of the heaters) and using 16 bits, from Eq. (2.1) the precision of the design variables becomes 1.220×10^{-4}. This precision is sufficient for the boundary design problems.

1 0 1 0	1 1 1 0	1 1 1 1	0 1 0 1
Gene 1	Gene 2	Gene 3	Gene 4

.

Figure 2.3. Representation of a gene in the MGA

Chromosome	1 0 1 0 1 1 1 0 1 1 1 1 0 1 0 1

Figure 2.4. Representation of a chromosome in the MGA

.

population	Chromosome 1	1 1 1 0 0 0 1 0
	Chromosome 2	0 1 1 1 1 0 1 1
	Chromosome 3	1 0 1 0 1 0 1 0
	Chromosome 4	1 1 0 0 1 1 0 0
	Chromosome 5	0 1 0 1 1 1 0 1

Figure 2.5. Representation of the Population in the MGA

Figure 2.3 shows the representation of the gene in binary form. Combination of these genes forms a chromosome, the chromosome encoded by bit strings are is shown in Fig. 2.4. All the chromosomes together constitutes the population, the representation of the population in terms of chromosomes is shown in Fig. 2.5.

2.5.2 Evaluation of objective function

In the MGA, each string created either in an initial population or in the subsequent generation, must be assigned a fitness value which is related to the objective function. The algorithm selects the best set of solutions on the basis of fitness function value.

2.5.3 Selection and reproduction

In the selection process, like SGA, in the MGA, a mating pool of individual chromosomes of the current generation is chosen for reproduction in the next generation, and this is done according to the fitness values of the chromosomes. According to the principle of the GA, survival-of-the-fittest, chromosomes with the higher fitness value are discarded and selecting the chromosomes with the lower fitness value (since the present problem is of minimization type). This process is intended to improve the average quality of the population by giving individuals of higher fitness a higher probability to produce the new individuals in the next generation.

In reproduction process, good strings in a population are selected to form a mating pool. The essential idea is that above average strings are picked from the current population and duplicates of them inserted in the mating pool. Numbers of selection schemes are popular in GAs, such as proportionate selection, ranking selection, tournament selection, etc. In the present study, to ensure the better diversity in the small populations of individuals, the tournament selection strategy has been used. In this, on the basis of their fitness value, initially $\left(N_P/2\right)$ groups of individuals are selected from the total population $\left(N_P\right)$. These groups are allowed take part in a tournament where the winning individuals of each tournament (in the present study, individuals with lower objective

function value) will form the $\left(N_P/2\right)$ mating pool. To form the mating pool $\left(N_P\right)$ this process is repeated twice. In this way the mating pool is ready to undergo the GA operators. The mating pool comprising of the tournament winner has higher average population fitness. The fitness difference provides the selection pressure, which drives GA to improve the fitness of the succeeding genes.

2.5.4 The crossover

After selection of the individuals completed and the mating pool is formed, to create new individuals for the next generation, the crossover starts. In crossover, in the mating pool, some portion of the parent strings (chromosomes) is exchanged to form a new offspring.

Parent 1	1 0 1 1 0 0 1 0
Parent 2	1 0 1 0 1 1 1 1
Child 1	1 0 1 1 0 1 1 1
Child 2	1 0 1 0 1 0 1 0

Figure 2.6. Representation of single point crossover in the MGA

Parent 1	A B C D E F G H	A B C D E F G H
Parent 2	I J K L M N O P	I J K L M N O P
Mask	1 0 1 0 1 0 1 0	0 1 0 1 0 1 0 1
Child 1	A J C L E N G P	I B K D M F O H
Child 2	I B K D M F O H	A J C L E N G P

Figure 2.7. Representation of uniform crossover with mask in the MGA

Parent	1 0 1 1 0 0 1 0
Mutation chromosome	1 0 0 0 1 0 0 1
Child	0 0 1 0 1 0 1 1

Figure 2.8. Representation of the mutation in the MGA

In the GA, three types of crossovers, viz., one-point, two-point and uniform crossover schemes are used. The working of the single point crossover is shown in Fig. 2.6. In the present work the uniform crossover has been used. The uniform crossover operator, which was developed by Syswerda in 1989, generally works better than the one-point and two-point crossovers. This allows the parent chromosomes to be mixed at the gene bit level rather than at the gene segment level (as in the one- and multi-point crossover schemes). Following the reproduction process, in which pairs of chromosomes have been chosen for mating and stored in the mating pool, the uniform crossover operator proceeds. Representation of uniform crossover with mask is shown in Fig. 2.7.

In uniform crossover, for each bit at the same position of two mated chromosomes, a random number is generated and compared with a preset crossover possibility; if the random number is larger than the crossover possibility, the crossover operator swaps the two bits of the mated chromosomes. On the other hand, if the random number is smaller, the two chromosomes remain unchanged and the crossover operation on this bit is finished. This crossover operation is performed to every bit of the mated chromosomes in sequence. Apart from that we can use the masking to have a control over the crossover. When the crossover operation completes, two new chromosomes are created for the next GA operation. In the present study, the well known uniform crossover scheme has been used. In the uniform crossover for binary strings, each bit from either parent is selected with a probability of 0.5. After the crossover, the individuals are decoded and the fitness is evaluated. Next to this the elitism proceeds.

2.6.5 The elitism strategy

In the SGA, the mutation process is followed by crossover. The goal of mutation in the SGA is to prevent the genetic population from converging to a local minimum and to introduce some new possible solutions in the generation. The mutation process is shown in Fig. 2.8. Here, in the MGA, this operator is replaced by elitism. In this, the first best chromosome or the few best chromosomes i.e. of better fitness function value are copied to the new population. The rest is done in a classical way (crossover and mutation). Such individuals can be lost if they are not selected to reproduce or if crossover or mutation destroys them. Elitism ensures the best individual survives in every successive generation. One can also use the mutation with a very small probability and the elitism together.

2.5.6 Convergence checking and population re-start

In MGA, the convergence is evaluated in two ways, namely population convergence and the algorithm convergence. Due to the small population maintaining the diversity in consecutive generations is difficult. Hence whenever diversity lost, the population needs to be restart with keeping the very best individuals (elitism) for next generations. Like mutation process in the SGA, in MGA, for preventing premature convergence, restarting the population several times during the algorithm has added benefits.

In the present work, with the following way, the population convergence and population re-restart takes place. According to Kazarlis *et al.*, (2001), population convergence is the progression towards chromosome uniformity. For the GA operators described above, a gene can be considered to be converged, when 95% of that particular gene in the entire population gives the same value, and then a population is said to be converged when all of the genes are converged. When a population gets converged, the best individuals are stored and the rest are re-started.

After performing all these operations, a generation is said to have completed, and thus the production of new offspring takes place. This process continues until the satisfactory

value of fitness function is attained, or a certain maximum number of generations are completed, this is an algorithm convergence. When the entire process is continued for every set of solutions, the MGA gives the final set of solutions corresponding to the minimum value of objective function.

2.6 Summary

For different types of inverse problems, several solution methodologies are available in the literature. In the inverse furnace boundary design problem, like the present one, use of inverse methodologies with regularization techniques have a major drawback. In these problems, in the inverse methodologies, enforcing the constraints on the design variables is difficult, and in this, occurrence of negative heat flux condition on the heaters is common. Unlike the inverse methods, the optimization methods handle the design constraints very well. Among the optimization techniques, the evolutionary methods like the GA have some added advantages. Since, in the problems considered in this thesis, the numbers of unknown parameters (power of the panel heaters) are large (300-500), the SGA is not suitable. Therefore, for the present studies, the improved version of the SGA, the MGA is selected as an optimization tool.

CHAPTER 3

BOUNDARY DESIGN OF RADIANT FURNACE FOR DESIRED UNIFORM THERMAL CONDITIONS ON A 3-D DESIGN OBJECT: A BASIC APPROACH

3.1 Introduction

For numerous heating applications in industries, various types of furnaces are used. Proper design and analysis of these thermal systems is of paramount importance. For precise control of thermal conditions inside a system the radiant furnaces are well suited. Radiant furnaces find extensive applications in industries such as space heating, material heating for heat treatment processes, drying processes, rapid thermal processing of semiconductor wafers, and so on. In most of the cases, the products placed inside the radiant furnace are irradiated by the heaters placed along one or more walls of the enclosure. Several material heating applications require the desired uniform thermal conditions over the specific region of the system, where the heating take place. In some applications the uniform thermal conditions are not only desirable but essential. These applications includes but not limited to the rapid thermal processing (RTP), drying, curing of paint, curing of powder coating, chemical vapor deposition, food processing, material heating for precision heat treatment processes/ hot working processes, manufacturing of electronic components, etc. The importance of the uniform thermal conditions is discussed in chapter 1. To obtain the uniform thermal conditions on the design object (DO), the enclosure geometry, arrangement of heaters, power of heaters, location of the DO, etc. need to be properly accounted. If these factors are not optimized properly, in the heating processes occurrence of non-uniform thermal conditions is a normal phenomenon.

For desired thermal conditions on the DO, estimation of configuration and power of heaters, these types of inverse problems falls in the category of inverse boundary design problems. To handle the ill-posed conditions associated with the boundary design problems, use of either the regularization or the optimization methods is an essential step. In the present problems improved version of the GA, the MGA (Krishnakumar, 1989) has been used. The motive behind choosing this particular optimization tool is discussed in detail in Chapter 2, section 2.3. In the inverse analysis the radiative information is computed using the radiation element method by ray emission model (REM^2) (Maruyama, 1993).

In the present boundary design of a 3-D radiant furnace, the aim is to estimate the optimal configuration and power of the panel heaters placed along the walls of furnace that produce desired uniform thermal conditions on the surfaces of a 3-D DO, placed inside furnace enclosure. In this chapter, formulation of the algorithm (REM^2 + MGA) is given and is implemented with the basic furnace design problem. In the inverse analysis, various aspects in the present boundary design problems are studied. In the following pages, problem has been defined in Section 3.2, formulations of the REM^2 and development of the objective function has been given. Next, the results and discussion are provided in Section 3.3, and summary is given in section 3.4.

3.2 Formulation

The study in this chapter deals with estimation of optimal power settings of the panel heaters placed along the walls of a 3-D radiant furnace that produce desired uniform heat flux and temperature distribution on the surfaces of a 3-D DO.

A schematic of the radiant enclosure dimensions: $L = 2.0$ m, $W = 2.0$ m, $H = 1.0$ m containing a centrally $(1.0, 1.0, 0.0)$ located 3-D DO, having dimensions: $l = 1.0$ m, $w = 1.0$ m, $h = 0.3$ m, is shown in Fig. 3.1a. Except the bottom surface (X-Y plane), the DO is considered to be irradiated by the panel heaters placed along one or more of the remaining 5 walls of the enclosure. The bottom surface of the

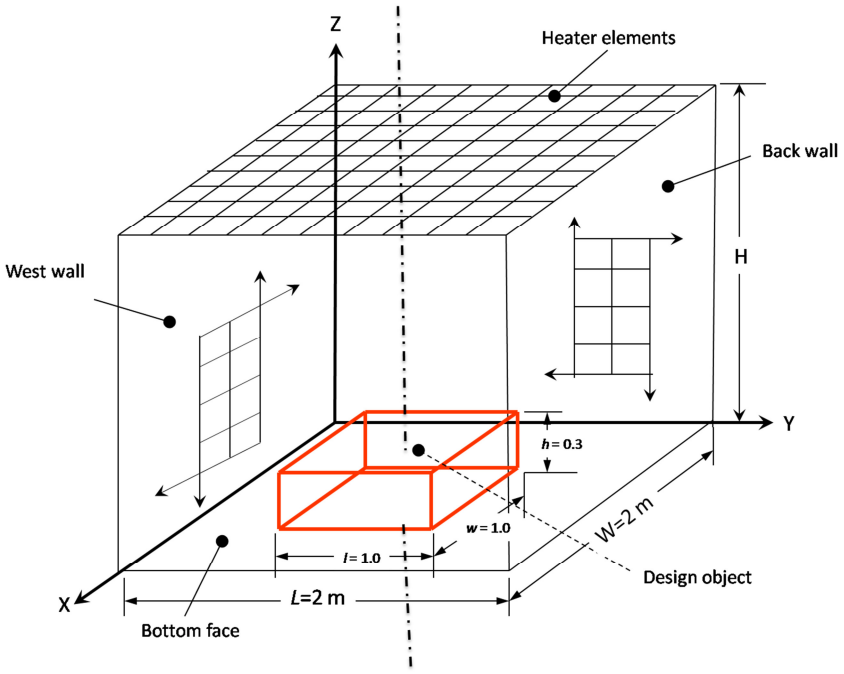

(a)

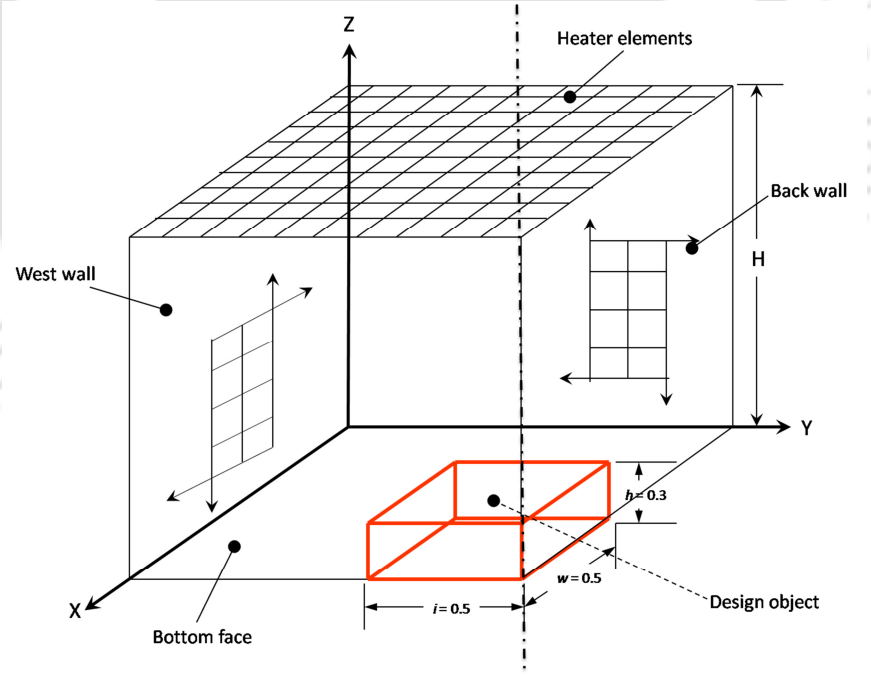

(b)

Figure 3.1. Schematic of (a) the radiant furnace enclosure showing heater elements along 5 walls with centrally located 3-D design object on the bottom face, and (b) the computational domain.

.

56	66	76	86	96	106	107	108	109	110
57	67	77	87	97	111	112	113	114	115
58	68	78	88	98	116	117	118	119	120
59	69	79	89	99	121	122	123	124	125
60	70	80	90	100	126	127	128	129	130
61	71	81	91	101	**1**	**2**	**3**	**4**	**5**
62	72	82	92	102	**6**	**7**	**8**	**9**	**10**
63	73	83	93	103	**11**	**12**	**13**	**14**	**15**
64	74	84	94	104	**16**	**17**	**18**	**19**	**20**
65	75	85	95	105	**21**	**22**	**23**	**24**	**25**

(a) bottom surface with top wall of design object

131	132	133	134	135	136	137	138	139	140
141	142	143	144	145	146	147	148	149	150
151	152	153	154	155	156	157	158	159	160
161	162	163	164	165	166	167	168	169	170
171	172	173	174	175	176	177	178	179	180
181	182	183	184	185	186	187	188	189	190
191	192	193	194	195	196	197	198	199	200
201	202	203	204	205	206	207	208	209	210
211	212	213	214	215	216	217	218	219	220
221	222	223	224	225	226	227	228	229	230

(b) Top wall

240	250	260	270	280	290	300	310	320	330
239	249	259	269	279	289	299	309	319	329
238	248	258	268	278	288	298	308	318	328
237	247	257	267	277	287	297	307	317	327
236	246	256	266	276	286	296	306	316	326
235	245	255	265	275	285	295	305	315	325
234	244	254	264	274	284	294	304	314	324
233	243	253	263	273	283	293	303	313	323
232	242	252	262	272	282	292	302	312	322
231	241	251	261	271	281	291	301	311	321

(c) Back wall

430	429	428	427	426	425	424	423	422	421
420	419	418	417	416	415	414	413	412	411
410	409	408	407	406	405	404	403	402	401
400	399	398	397	396	395	394	393	392	391
390	389	388	387	386	385	384	383	382	381
380	379	378	377	376	375	374	373	372	371
370	369	368	367	366	365	364	363	362	361
360	359	358	357	356	355	354	353	352	351
350	349	348	347	346	345	344	343	342	341
340	339	338	337	336	335	334	333	332	331

(d) West wall

28	**31**	**34**	**37**	**40**
27	**30**	**33**	**36**	**39**
26	**29**	**32**	**35**	**38**

(e) back wall of design object

55	**54**	**53**	**52**	**51**
50	**49**	**48**	**47**	**46**
45	**44**	**43**	**42**	**41**

(f) west wall of design object

Figure 3.2. Designation of the surface elements of the (a) bottom surface of the radiant enclosure and the top surface of the DO, (b) top wall, (c) back wall and (d) west wall of the radiant enclosure, (e) back wall, and (f) west wall of the DO.

radiant enclosure not covered by the DO is insulated. There is no energy interaction with the surroundings, the furnace is assumed to be externally thermally insulated. Since the DO is centrally located on X-Y plane (bottom surface) of the radiant enclosure, the system becomes symmetric about the two axes, viz., X and Y (Fig. 3.1a). Thus in an effort to save the computational time, subject to a proper consideration of the radiative boundary conditions, one-fourth of the domain (Fig. 3.1b) becomes good enough for the computation. The two symmetric planes, viz., Z-Y and Z-X that serve as two boundaries of the computational domain are considered fully specular. The three boundaries (top, west and back) containing heaters can be diffuse or diffuse specular. Temperature, heat flux and emissivity of a given surface element are constant over the area, and they are different for different surface elements. To calculate the radiative information using REM^2, the inside surfaces of the radiant enclosure and the surface areas of the DO are divided into equal size $(0.1\text{m}\times 0.1\text{m})$ surface elements. The numerical designations of the surface elements along furnace walls and along the surfaces of the DO are shown in Fig. 3.2.

The surface elements along the furnace walls (top, back, and west wall) are considered as the panel heaters. With panel heaters of size $0.1\text{m}\times 0.1\text{m}$ and the surface elements on the surfaces of DO also of same size, we have a total of 432 surface elements in the enclosure (Fig. 3.1b). The surfaces of DO has 55 elements (1-55), the three walls of the radiant enclosure which form the part of the computational domain contain 300 elements (Top wall: 131-230; back wall: 231-330, west wall: 331-430) (refer Fig. 3.2). The insulated portion of the bottom surface not covered by DO has 75 elements (56-130). Thus, the net radiative heat flux on any element will be the cumulative effects of the radiative exchanges from remaining 431 elements. The sequence of the surface elements can be different and it does not affect the final solution. Since the objective is to estimate the power of the panel heaters not only for the enclosure dimensions $(L=1.0\text{ m},\ W=1.0\text{ m},\ H=1.0\text{ m})$ but also for the effect of increasing the enclosure height H, the number of panel heaters will further increase.

To produce the uniform heat flux and temperature distribution on the surfaces of the DO, the estimation of optimal power settings is accomplished by first specifying the desired temperature distribution on the DO and then calculating heat flux on the surfaces of DO using the optimization algorithm, in which the REM^2 is used for radiative calculation and the MGA as an optimization tool. In the following sections (section 3.2.1 – 3.2.3), the formulations for the algorithm is given.

3.2.1 Radiation element method

In this study, we consider a 3-D radiant furnace with the panel heaters embedded along its five walls except the bottom wall on which the DO is placed (refer Fig. 3.1). The portion of the bottom wall not covered by the DO is insulated. The furnace walls and the heater surfaces are diffuse and/or diffuse specular. In the calculation of radiative information with specular surfaces, the REM^2 (Maruyama, 1993) is a reliable method. REM^2 has been developed by Maruyama (1993), and its efficacy and benefits have been demonstrated by Maruyama and coworkers [Guo *et al.*, 1997; Maruyama and Aihara, 1997; Guo and Maruyama, 2001; Maruyama *et al.* 2002]. Since in optimization methodology, the direct problem needs to be repeatedly solved, for the sake of computational time, selection of an efficient method for radiative calculations is important. Unlike the other radiative transfer methods [Fiveland, 1988; Raithby and Chui, 1990; Mishra and Prasad, 2002; Mahanta and Mishra, 2002], REM^2 is suitable to couple with the optimization methodology. Without changing configuration factors matrix many repetitive radiative transfer calculations can be done rapidly using the REM^2. Hence, in the present work, for calculation of radiative information in a 3-D enclosure the REM^2 has been used. In this method, most of the calculation time consumed by determination of absorption and diffuse reflection configuration factors, and about only 3-5% of calculation time required for solving radiation heat transfer [Maruyama *et al.*, 2002].

First let us understand what is REM^2? Consider a system of closed space comprised of N numbers of gray diffuse surface elements of area $A_i \left(i = 1, ..., N\right)$, as shown in Fig. 3.3a. Each surface is assumed to be isothermal, and the space between the surfaces does not

emit, absorb or scatter any radiation. The radiative energy calculated at each surface element is the collective effect of all other surface elements. Fig. 3.3b shows the energy conversion of radiative energy from diffuse specular surface element. In the present problems the surface elements along the walls of the furnace indicate the panel heaters and to that of along the surfaces of the DO are design elements.

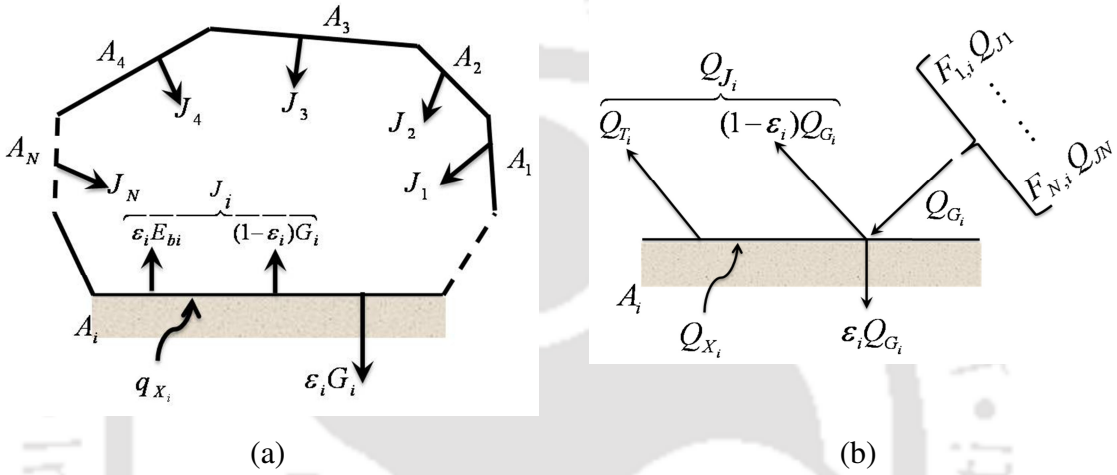

Figure 3.3. (a) Relation between spectral irradiation and radiosity of a system composed of *N* surface elements, (b) energy conversion of radiative energy from diffuse surface.

As mentioned before and shown in Figs. 3.1, on the walls of radiant enclosure the panel heaters $(0.1\text{ m}\times 0.1\text{ m})$ are placed and they are designated as surface elements. The surfaces of DO are also divided into surface elements having the same dimensions $(0.1\text{ m}\times 0.1\text{ m})$ as that of the panel heaters. To handle the specularity effects, reflectivity ρ of any particular element *i* has two components, viz., diffuse ρ^S and specular ρ^D and the same can be written as

$$\rho_i = \rho_i^S + \rho_i^D = 1-\alpha_i = 1-\varepsilon_i \tag{3.1}$$

where α_i is the absorptivity and ε_i is the emissivity of element *i*.

As shown in Fig. 3.3a, consider the amount of total radiation energy per unit area that is radiated from surface A_i, that is the radiosity J_i (W/m^2) which is sum of reflection component of the irradiation $\rho_i G_i$ (W/m^2), and emission component per unit area $\varepsilon_i E_{b,i}(T_i)$ (W/m^2). Assuming the emissivity and the absorptivity of the gray diffuse surface are independent of temperature of the surface element, for analyzing the radiation heat transfer between specular and diffuse surfaces, using Eq. (3.1), the diffuse radiosity J_{Di} is defined as

$$J_{Di} = \varepsilon_i \sigma T_i^4 + \rho_i^D G_i = E_{b,i} + (1-\varepsilon_i) G_i \tag{3.2}$$

Where σ is the Stefan-Boltzmann constant and G_i is the irradiance on surface *i*.

So the diffuse radiation heat transfer Q_{Ji} is expressed as

$$Q_{Ji} = A_i J_{Di} = A_i(\varepsilon_i \sigma T_i^4 + \rho_i^D G_i) \tag{3.3}$$

Consider q_{Xi}, as a net heat flux that supplied form the backside of the surface *i*, then using energy balance on a surface area A_i can be expressed as

$$q_{Xi} = \varepsilon_i \sigma T_i^4 - \varepsilon_i G_i \tag{3.4}$$

The net heat supplied Q_{Xi} to the element *i*

$$Q_{Xi} = A_i \varepsilon_i (\sigma T_i^4 - G_i) \tag{3.5}$$

To consider the effect of the specular surfaces, the REM^2 (Maruyama, 1993) utilizes the concept of absorption configuration factor $F_{i,j}^A$ and the diffuse reflection configuration

factor $F_{i,j}^{D}$. The absorption configuration factor $F_{i,j}^{A}$ is defined as the fraction of the radiation leaving the surface element *i*, that is absorbed by the surface element *j*. The diffuse reflection configuration factor $F_{i,j}^{D}$ is the fraction of the radiation leaving the surface *i*, that is diffusely reflected by surface element *j*. Mathematically, the absorption configuration factor $F_{i,j}^{A}$ and the diffuse reflection configuration factor $F_{i,j}^{D}$ can be expressed as

$$F_{i,j}^{A} = \frac{1}{\pi A_i} \int_{A_i} \int_{2\pi} f_i^{\,j}(\theta,\phi)\varepsilon_j \cos\theta \, d\omega \, dA_i \tag{3.6}$$

$$F_{i,j}^{D} = \frac{1}{\pi A_i} \int_{A_i} \int_{2\pi} f_i^{\,j}(\theta,\phi)\rho_j^{D} \cos\theta \, d\omega \, dA_i \tag{3.7}$$

where A_i is the surface area of element i, $f_i^{\,j}$ is the configuration factor of the elemental surface j with respect to the elemental surface i, θ is the polar angle, ϕ is the azimuthal angle and $d\omega$ is the solid angle.

Defining the irradiation and the emissive power on an element *i* as $Q_{Gi} \equiv A_i G_i$ and $Q_{Ti} \equiv A_i \varepsilon_i \sigma T_i^4$, from Eqs. (3.2) - (3.5), irradiation and absorption energy can be expressed in terms of absorption configuration factor $F_{i,j}^{A}$ and diffuse reflection configuration factor as follows:

$$\rho_i^{D} Q_{Gi} = \sum_{j=1}^{N} F_{j,i}^{D} Q_{Jj} \tag{3.8}$$

$$A_i \varepsilon_i G_i = \sum_{j=1}^{N} F_{j,i}^{A} Q_{Jj} \tag{3.9}$$

Hence, Eqs. (3.3) and (3.5) can be written as

$$Q_{Ji} = Q_{Ti} + \sum_{j=1}^{N} F_{j,i}^{D} Q_{Jj} \tag{3.10}$$

$$Q_{Xi} = Q_{Ti} - \sum_{j=1}^{N} F_{j,i}^{A} Q_{Jj} \tag{3.11}$$

In Eqs. (3.8) – (3.11), N is the total number of surface elements. It is to be noted that for a cubical radiant enclosure having dimensions $(L = W = H = 1.0\ \text{m})$, there will be total of 100 heaters/surface elements on each of the five walls (top, back, front, east and west). For different DO models having different dimensions, the number of surface elements on the bottom surface will be different.

Denoting $F_{j,i}$ as a matrix F and Q_i as a column vector Q, and then Q_J can be eliminate from Eqs. (3.10) and (3.11), we get

$$F_X Q_T = I Q_X \tag{3.12}$$

where

$$F_X = I - F^A (I - F^D)^{-1} \tag{3.13}$$

and I represent a unit matrix, and $(\ )^{-1}$ denote the inverse of matrix. It is to be noted that in Eq. (3.13), F_X is function of configuration factors $F_{i,j}^A$ and $F_{i,j}^D$, only.

The system has a total of N number surface elements, out of which n_1 surfaces have known temperature T_i, and remaining $n_2 = N - n_1$ surfaces with known heat flux. For the insulated surfaces $q_{xi} = 0$. We express the heat transfer vector components that give specified temperature and known heat flux as Q_T^0 and Q_X^0, and corresponding coefficient as F_X^0 and I^0 respectively. For the unknown components of Q_X and Q_T as

$Q_T^{'}$ and $Q_X^{'}$, and corresponding coefficient as $F_X^{'}$ and $I^{'}$, respectively. With this, Eq. (3.12) can be written as

$$\underbrace{F_X^0 Q_T^0}_{\text{known}} + \overbrace{F_X^{'} Q_T^{'}}^{\text{unknown}} = \overbrace{I^{'} Q_X^{'}}^{\text{unknown}} + \underbrace{I^0 Q_X^0}_{\text{known}} \tag{3.14}$$

Rearranging the terms in Eq. (3.14), we get

$$\left[F_X^0 - I^0\right]\begin{pmatrix} Q_T^0 \\ Q_X^0 \end{pmatrix} = \left[I^{'} - F_X^{'}\right]\begin{pmatrix} Q_X^{'} \\ Q_T^{'} \end{pmatrix} \tag{3.15}$$

$$\begin{pmatrix} Q_X^{'} \\ Q_T^{'} \end{pmatrix} = \left(I^{'} - F_X^{'}\right)^{-1}\left[F_X^0 - I^0\right]\begin{pmatrix} Q_T^0 \\ Q_X^0 \end{pmatrix} \tag{3.16}$$

Now the right hand side of Eq. (3.16) is a known quantity. After solving the matrix for known and unknown values of the heat flux and the surface temperature, in the REM^2 the unknown heat flux and surface temperature are obtained using

$$q_{Xi} = \frac{Q_{Xi}}{A_i} \tag{3.17a}$$

$$T_i = \left(\frac{Q_{Ti}}{A_i \sigma \varepsilon_i}\right)^{1/4} \tag{3.17b}$$

3.2.2 Ray tracing and the ray emission model

In the computation of radiative information, calculation of absorption configuration factor $F_{i,j}^A$ and diffuse reflection configuration factor $F_{i,j}^D$ of the surface elements is carried out by ray tracing, using the radiation emission model by Guo *et al*. (1997). For this study 8081 (90×90) rays are used (ray independence test is given in section 3.3.3). In this ray emission model, the ray directions are given as

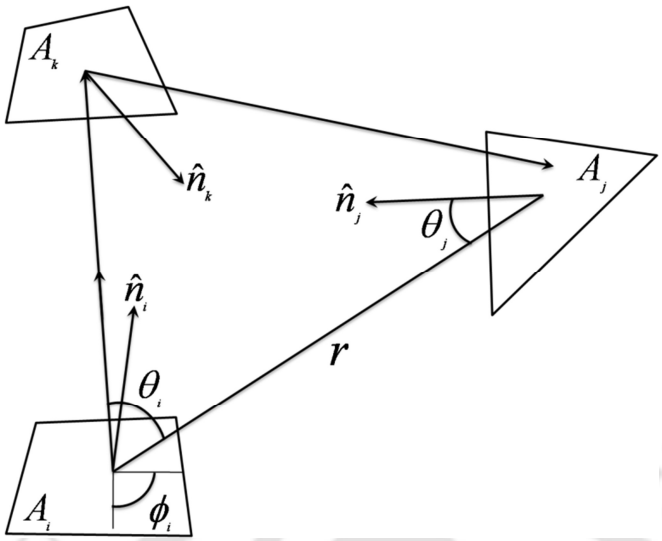

Figure 3.4. Ray emission model for specular surfaces.

$$\theta_0 = \phi_0 = 0 \tag{3.18}$$

$$\theta_m = \sin^{-1}\left[\sin^2\psi_{m-1} + 2/N_R\right]^{0.5}, \quad (m = 1,2,3,.....,n^2) \tag{3.19}$$

.

$$\phi_{i\times n+j+1} = \left((i+nj)\pi/2n^2\right), \quad \text{where} \quad (i = 0,1,....,n-1; \quad j = 0,1,.....,n-1) \tag{3.20}$$

and

$$n = \left(\sqrt{N_R - 1}/2\right) \tag{3.21}$$

$$\psi_0 = \sin^{-1}\left(1/N_R\right)^{0.5} \tag{3.22}$$

$$\psi_m = \sin^{-1}\left[4/N_R + \sin^2\left(\psi_{m-1}\right)\right]^{0.5}, \quad (m = 1,2,.....,n^2) \tag{3.23}$$

In the above equations N_R is the total number of rays and the initial intensity of each ray is $1/N_R$ and θ and ϕ are the zenith and azimuthal angle respectively, based on the normal of the surface element.

Each ray that weigh $\left(1/N_R\right)$ is emitted in the direction of the hemisphere from the surface element *i*. When a ray reaches *j* (refer Fig. 3.4) the energy of the ray splits according to Eq. (3.1), and the absorbing component and diffuse reflecting component is accumulated to $F_{i,j}^{A}$ and $F_{i,j}^{D}$, respectively. The specular reflection component will continue to travel the ray until it is absorbed or diffusely reflected by either surface completely or until the ray is attenuated to less than 1% of its initial intensity. After tracing the rays from all the surface elements, the configuration factors in Eq. 3.6 and 3.7 can be obtained automatically.

3.2.3 Objective function

For desired uniform thermal conditions on a 3-D DO, objective of the present study is to estimate the optimal configuration and power of the panel heaters embedded along the five walls of radiant furnace. In this, first the desired initial temperature distribution over the DO have been specified, then using the present algorithm (REM^2 + MGA), the desired heat flux distribution is estimated on the surfaces of the DO. To accomplish this task, the objective function is defined as the sum of the squares of the differences between the desired and estimated values of heat flux on the surfaces of DO, mathematically expressed as:

$$F(\boldsymbol{q}_H) = \sum_{i=1}^{N_{DO}} (q_{desired,i} - q_{estimated,i})^2 \tag{3.24}$$

where N_{DO} is the number of surface elements on the DO, $q_{desired,i}$ is the desired fixed value of the heat flux and $q_{estimated,i}$ is the estimated heat flux obtained using the MGA and the REM^2.

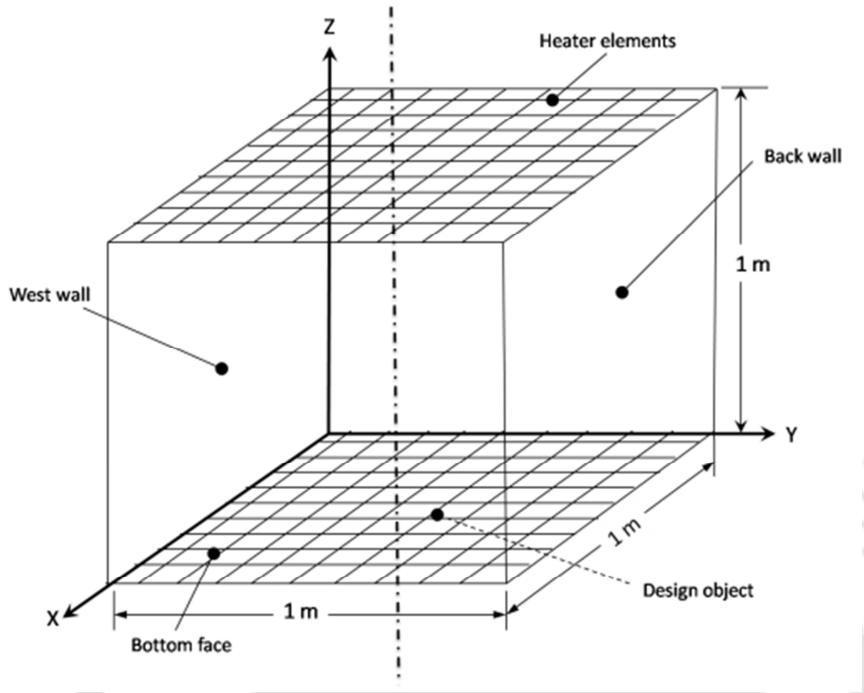

(a)

1	11	21	31	41	51	61	71	81	91
2	12	22	32	42	52	62	72	82	92
3	13	23	33	43	53	63	73	83	93
4	14	24	34	44	54	64	74	84	94
5	15	25	35	45	55	65	75	85	95
6	16	26	36	46	56	66	76	86	96
7	17	27	37	47	57	67	77	87	97
8	18	28	38	48	58	68	78	88	98
9	19	29	39	49	59	69	79	89	99
10	20	30	40	50	60	70	80	90	100

(b)

Fig. 3.5. (a) The computational domain for numerical tests, (b) Designation of surface elements on the bottom surface of the radiant enclosure.

For all studies in this thesis the MGA is used as an optimization tool. The detail working procedure of the MGA is described in section 2.5. In the following pages, the results of numerical tests for the direct and inverse methodologies are given. Next results and discussions are presented.

3.3 Numerical Tests for the Methodology

To verify the accuracy of the numerical calculations, three tests are conducted, viz. grid independency test, ray independency test and validation of the direct and inverse problem. The computational domain used for these numerical tests is a cubical enclosure $\left(L=W=H=1.0\ \mathrm{m}\right)$. The schematic is shown in Fig. 3.5a. The top wall is set to provide a dimensionless heat flux $q_H^* = 1.0$ and the bottom surface is maintained at the dimensionless temperature $T^* = 1.0$. All the remaining surfaces of the enclosure are externally insulated. In both REM^2 and in the analytic solution, the whole domain is divided into equal size $\left(0.1\ \mathrm{m}\times 0.1\ \mathrm{m}\right)$ square elements. The designation of the surface elements on the bottom surface of the radiant enclosure is shown in Fig. 3.5b.

3.3.1 Grid independence test for REM^2

Before using the REM^2 for radiative calculation, the grid independence test has been conducted. A sample case of radiant enclosure (dimensions: $L = W = H = 1\ \mathrm{m}$) is considered (refer Fig. 3.5a). In this study, the dimensionless temperature $\left(T^* = 1.0\right)$ on the bottom surface and the dimensionless heat flux $\left(q_H^* = 1.0\right)$ on the heater elements along the top wall were considered. Remaining vertical walls of the radiant enclosures were assumed to be insulated. To calculate the radiative information using the REM^2, surfaces of the computational domain has to be divided to form the surface elements. The distribution of dimensionless heat flux on the bottom surface has been calculated using REM^2. For grid independence test the element size $0.05\ \mathrm{m}\times 0.05\ \mathrm{m},\ 0.1\ \mathrm{m}\times 0.1\ \mathrm{m},$ and

$0.2\,\mathrm{m} \times 0.2\,\mathrm{m}$, are used. Thus the number of total surface elements in the computational domain are 2400, 600 and 150 respectively.

The distribution of dimensionless heat flux $\left(q_H^*\right)$ on the bottom surface is shown in Fig. 3.6. The heat flux distribution obtained using the given grid sizes is compared with that of calculated using the analytical approach (Siegel and Howell, 2002). For better understanding, in Fig. 3.7, the results are shown for 10 surface elements on the design surface (a) 1-10, (b) 11-20, (c) 21-30, (d) 31-40, and (e) 41-50. In the grid independence study, maximum deviation and the average deviation for grid size 0.05×0.05, 0.1×0.1, and 0.2×0.2, is found to be 0.24%, 1.25%, 4.4%, and 0.084%, 0.6%, 2.037%, respectively. In the numerical study the differences are considerable, more than the multiple of 3 for increasing the grid sizes.

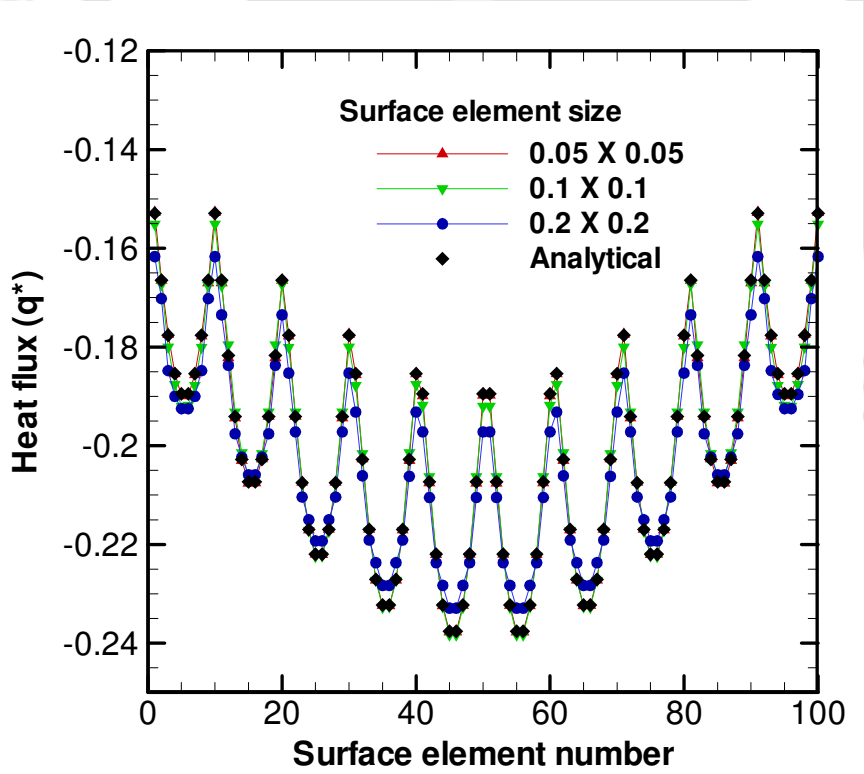

Figure 3.6. Grid independence test for direct problem using the REM^2 shown for all 100 surface elements on the design surface.

It is observed from Fig. 3.6 - 3.7 that the computed heat fluxes using the grid size $0.2\,\mathrm{m} \times 0.2\,\mathrm{m}$ is not matching well with that of calculated using the analytical method, while the heat fluxes calculated using the grid size $0.05\,\mathrm{m} \times 0.05\,\mathrm{m},\ 0.1\,\mathrm{m} \times 0.1\,\mathrm{m},$ are found in good agreement. Thus the grid sizes $0.05\,\mathrm{m} \times 0.05\,\mathrm{m}, \text{and } 0.1\,\mathrm{m} \times 0.1\,\mathrm{m},$ are found appropriate to obtain the accurate heat flux distribution. Since the present problem is a boundary design problem, in which the unknown power of the heaters has to be estimated using the suitable optimization method, so the less number of unknown parameters are desired. In this study, for all the cases inner surface of radiant enclosure including the heater surface and the surfaces of the DO are divided into the surface elements of the size $0.1\,\mathrm{m} \times 0.1\,\mathrm{m}$.

Table 3.1: Computational time for radiative calculation using REM^2 with different grid size.

Grid size	CPU time (S)
0.05×0.05	500.95
0.1×0.1	45.54
0.2×0.2	5.56

The CPU time for the radiative calculation using three grid sizes is given in Table 3.1. From Table 3.1, it is observed that reducing the grid size to half the CPU time increases about 10 times. In all the studies in this thesis including the present one, the computations are performed with the system "Intel core2, duo CPU system having 2.0 GHz and 1.99 GB RAM", the CPU time mentioned above is with respect to the given system configuration.

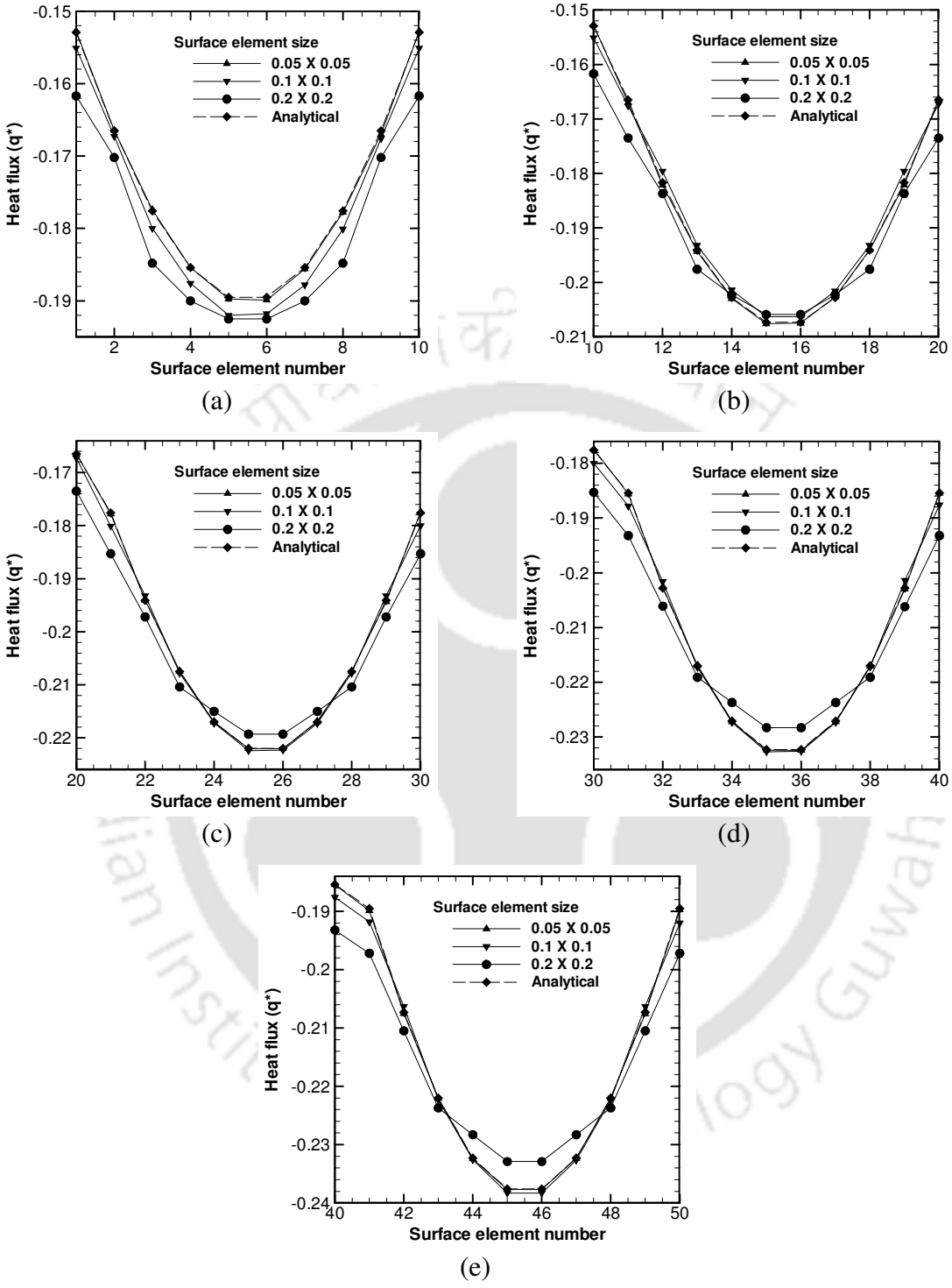

Figure 3.7. Grid independence test shown for surface elements on the design surface (a) 1-10, (b) 11-20, (c) 21-30, (d) 31-40, and (e) 41-50, (refer Fig. 3.6)

3.3.2 Ray independence test for REM^2

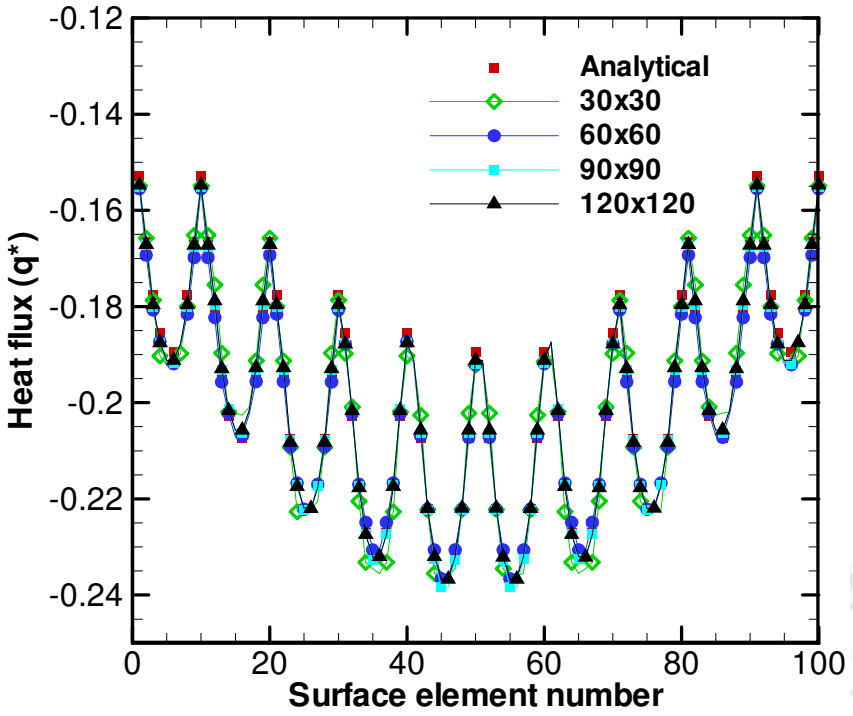

Figure 3.8. Ray independence test for direct problem using the REM^2 shown for all 100 surface elements on the design surface.

In the present radiant boundary design problem radiative information is computed using the REM^2. In the REM^2 the radiative calculation is carried out through the ray tracing, therefore choosing the correct numbers of the rays is an important criterion. For ray independence test, same radiant enclosure $(L=W=H=1\text{m})$ (refer Fig. 3.5) and same boundary conditions as used for grid independence (section 3.3.1) test have been considered.

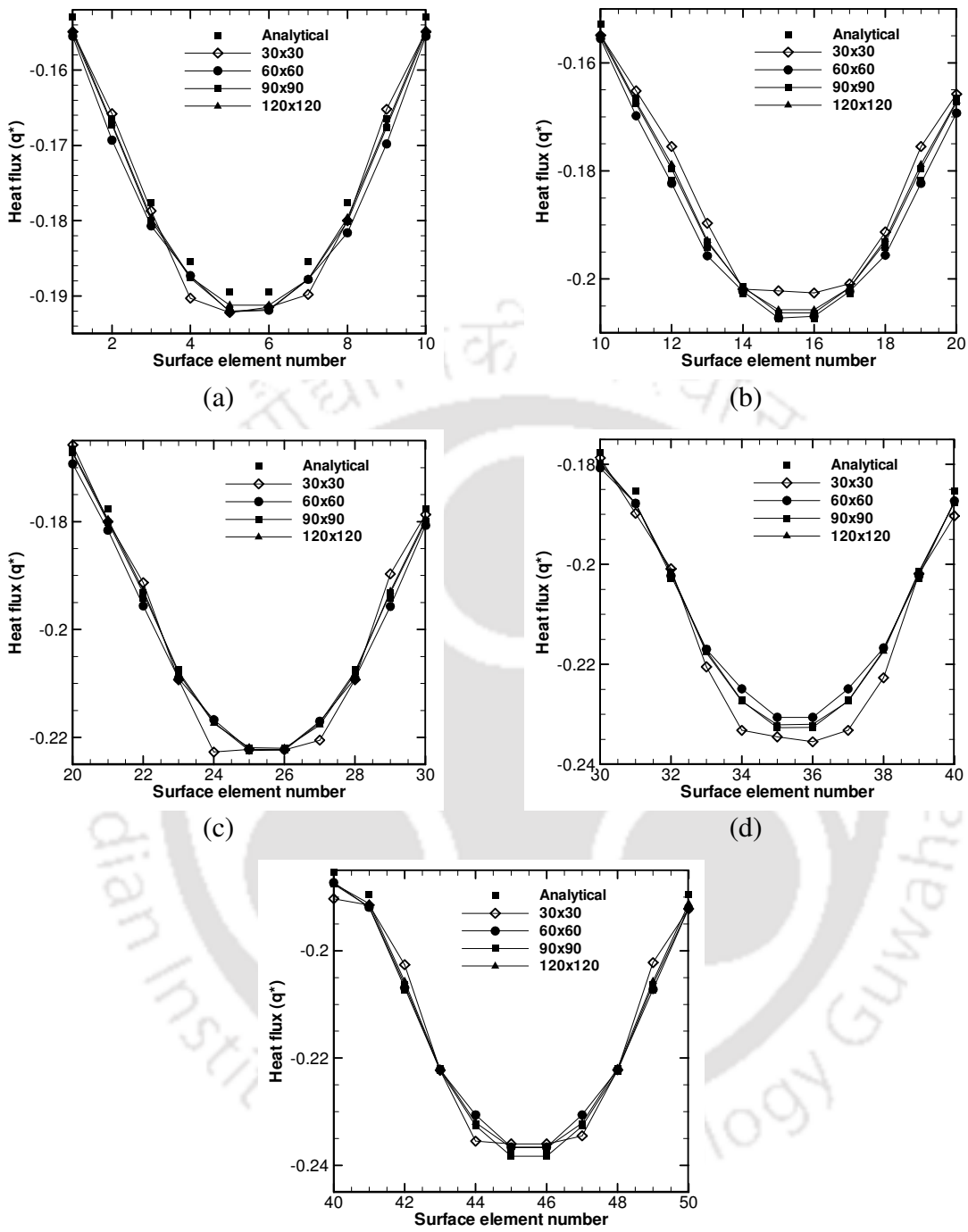

Figure 3.9. Ray independence test shown for surface elements on the design surface (a) 1-10, (b) 11-20, (c) 21-30, (d) 31-40, and (e) 41-50, (refer Fig. 3.8).

Being known from the grid independence test, the suitable grid size taken as $0.1\,\mathrm{m}\times 0.1\,\mathrm{m}$. Using this grid size total numbers of the surface elements along the surfaces of the considered domain become 600.

For the ray independence test, the chosen model is tested for four different numbers of rays viz. 30×30, 60×60, 90×90 and 120×120. With the given numbers of rays, using the REM^2 the radiative heat flux distribution is calculated on the bottom surface of the enclosure, and then compared with that of calculated using the analytical approach. The comparison is shown in Fig. 3.8. For better understanding Fig. 3.9 shows magnified view of Fig. 3.8 for 10 surface elements separately, (a) 1-10, (b) 11-20, (c) 21-30, (d) 31-40, and (e) 41-50. In the ray independence study, maximum deviation and the average deviation for 30, 60, 90 and 120 number of rays are found to be 3.1%, 2.0%, 1.25%, 1.45%, and 1.4584%, 0.7960%, 0.6064%, 0.6024%, respectively. From the comparison, it is seen that 30×30, 60×60 rays are not adequate to get the accurate results. While 90×90 and 120×120 rays are found appropriate to get the accurate heat flux distribution.

Table 3.2: CPU time for radiative calculation using REM^2 with different numbers of rays.

Numbers of rays	CPU time (S)
30×30	7.84
60×60	22.18
90×90	45.84
120×120	79.20

It can be seen from the formulation section, the numbers of elements are directly responsible for computational time. Total numbers of rays per surface element and the corresponding computational time for radiative calculation in each of the case of numbers of rays are given in Table 3.2. Being found suitable the numbers of rays are 90×90 and 120×120, for smaller computational time, for all studies in this work 90×90 rays are adopted.

3.3.3 Validation of the direct (REM^2) and inverse method (REM^2 + MGA)

To verify the accuracy of the calculations, a test case is considered. The accuracy of the REM^2 results are compared with that of against the calculated analytical solution using the standard configuration factors approach (Siegel and Howell, 2002). For this validation study, a cubical enclosure $(L=W=H=1.0\ \mathrm{m})$ is considered (refer Fig. 3.5). With the objective of estimating the heat flux distribution on the bottom surface, the top wall is set to provide a dimensionless heat flux $q_H^* = 1.0$ and the bottom surface is maintained at the dimensionless temperature $T^* = 1.0$. In both REM^2 and in the analytic solution, the whole domain is divided into equal size $(0.1\ \mathrm{m} \times 0.1\ \mathrm{m})$ square elements. The emissivity of all surfaces is set to unity. Fig. 3.10a shows the comparison of the dimensionless heat flux q^* calculated on the bottom surface, using REM^2 and that of calculated using analytical approach. At three locations, viz., $y = 0.05, 0.25$ and $0.45,$ comparisons of heat flux variations along the X-axis are shown. An excellent comparison is observed.

Having verified the accuracy of the direct problem, it is equally important to validate the accuracy of the optimization algorithm (REM^2+MGA). The analysis of an inverse problem involves both direct and inverse/optimization techniques. The inverse methodology is said to be accurate if by imposing the solution of the direct problem as an input conditions to the inverse methodology, and verify whether the initial/ boundary conditions of the direct problem can be recovered.

The accuracy of present optimization algorithm is verified considering the same test case as taken for validation of the direct method (REM^2). The direct problem is solved to get the heat flux distribution on the design surface. Here the entire bottom surface is a design surface. The inverse methodology is verified by providing the solution of the direct problem i.e. heat flux distribution on the design surface as an input and keeping all the properties same as the direct problem along with the same constraints as a known conditions.

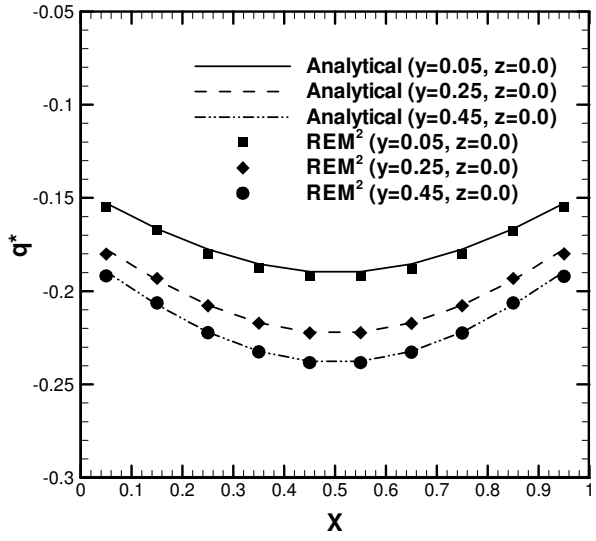

(a)

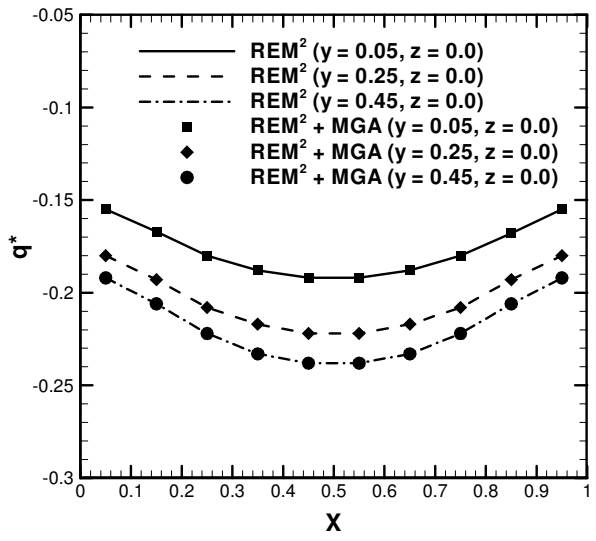

(b)

Figure 3.10. Comparison of the heat flux distribution using (a) REM^2 and analytical method, (b) direct (REM^2) and inverse method (REM^2 + MGA).

Now the aim is to recover the heat flux distribution on the boundary (panel heaters) of direct problem. The inverse methodology using MGA in conjunction with REM^2 is allowed to run for 1000 generations. Within 500 generation the objective function value minimized to as low as 10^{-4} and so the heat flux distribution on the heater surface

recovered uniquely. Fig. 3.10b shows the comparison of the heat flux distribution obtained using the direct method (REM^2) and the inverse method (REM^2 + MGA). With the present optimization algorithm all the panel heater values are retrieved uniquely. The corresponding maximum error in the heat flux distribution on design surface is less than 0.1%. This accuracy is good for the practical design point of view. This implies that the present algorithm is capable to obtain the accurate solution of the inverse boundary design problems.

Having proved the accuracy of both the methods used in the present analysis viz., REM^2 and MGA, in the following pages the results of estimations of optimal heater power settings that yield desired uniform thermal conditions on 3-D DO for various cases are provided and analyzed.

3.4 Results and Discussion

The present study deals with estimation of optimal power of the panel heaters placed along the walls of a 3-D radiant enclosure (dimensions: L = 2.0 m, W = 2.0 m, H = 2.0 m) that produce a uniform thermal conditions $\left(q^*_{DO} = {q_{DO}}/{\sigma T_R^4} = -2, \text{and } T^* = 1.0 \right)$ over a 3-D DO (dimensions: l = 1.0 m, w = 1.0 m, h = 0.3 m). The schematic of the full domain with centrally located $(1.0, 1.0, 0.0)$ DO on the bottom surface of radiant enclosure is shown in Fig. 3.1a. REM^2 has been used to calculate the radiative information and the minimization of the objective function has been achieved using the MGA.

To obtain the radiative information using the REM^2, surfaces of the enclosure including the surfaces of the design object are divided into equal size $(0.1\text{m} \times 0.1\text{m})$ square elements (grid independence test is given in section 3.3.1). Fig. 3.1b shows the schematic of the computational domain. To keep the computational domain unaffected, both the section surfaces (Z-Y and Z-X) passing through the center $(1.0, 1.0, 0.0)$ of the enclosure are considered fully specular $(\rho^S = 1.0)$. The heater elements are considered good

emitters having emissivity 0.95 and the remaining elements on the bottom surface not covered by the design object are insulated, and their emissivity is 0.3. Since most of the products (metals) to be heated have emissivity close to 0.5, the emissivity of the design elements is taken as 0.5. The emissivity is mainly depends upon the surface conditions. One can take any suitable value for the calculation. Table 3.3 shows the values of optical properties considered on the heater, DO and the refractory walls.

Table 3.3: Optical properties of the inner surface of the furnace enclosure, heater surface, and design object.

Surface	Emissivity	Diffuse reflectivity	Specular reflectivity
Heater	0.95	0.05	0.0
Design object	0.5	0.5	0.0
Other surfaces	0.3	0.2	0.5

Fig. 3.2 shows the designation of the heater elements on the enclosure walls and on the surfaces of the design object. These numerical designations of the elements are important for a better understanding and physical interpretation of the results, estimated power of the panel heaters placed along the enclosure walls.

3.4.1 Estimation of heater power settings for uniform thermal conditions

With the objective of having uniform heat flux $q^*_{DO} = -2.0$ on the surfaces of the DO, in the following pages, estimation of optimal power of the panel heaters is done. This estimation is done by considering 100 panel heaters on each of the one or three walls (top, back and west wall) of radiant enclosure. 100 panel heaters, each of the size $0.1\ \text{m} \times 0.1\ \text{m}$, cover the entire surface area of a wall (1.0 m × 1.0 m). With a population size of 10 and uniform crossover probability of 0.5, the MGA was allowed to run for a maximum of 5000 generations or the process was terminated when the objective function value attained the minimum to $O\left(1.0\times10^{-10}\right)$.

For yielding the uniform thermal conditions on a 3-D DO, in the present algorithm requirement of numbers of panel heaters is checked. This study is conducted using the actual computational domain shown in Fig. 3.1b. Except the bottom surface of the enclosure on which the DO is located, 100 panel heaters along each of the 3 walls viz. top, back and west wall have been considered. Initially only the heaters along top wall are considered active for the computation, they are set to deliver the flux $q_H^* = 1.0$. Rest all surfaces are treated as insulated. Fig. 3.11 shows the estimated heat flux distribution on the surfaces of a DO obtained using the present algorithm (REM^2+MGA) and the heat flux distribution without optimization (direct method only, i.e. REM^2). The purpose of this comparison is to show the effect of optimization algorithm and without optimization algorithm on the estimated heat flux distribution on the surfaces of the DO. In Fig. 3.11, heat flux distributions are plotted for all the surface elements ranging from 1-55 (shaded regions in Fig. 3.2a, 3.2e and 3.2f) of the three surfaces of the DO in the computational domain. It is observed from Fig. 3.11 that considering 100 panel heaters along the top wall only, although using the optimization algorithm, desired uniform heat flux distribution on the DO $q_{DO}^* = -2.0$ is not achieved.

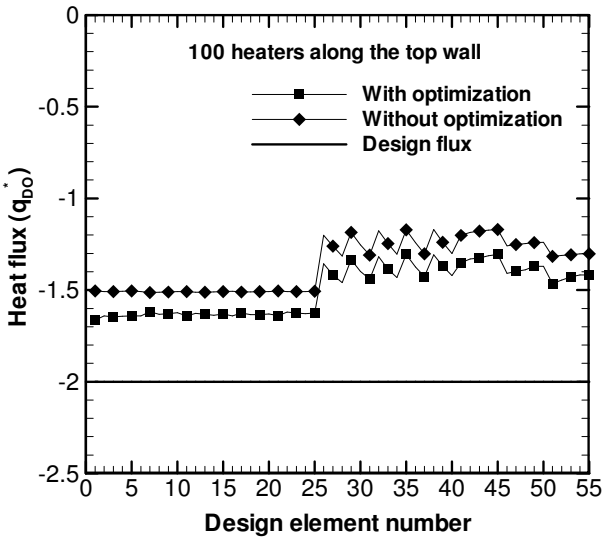

Figure 3.11. Heat flux distribution on design object, with and without optimization using 100 heaters along top wall.

.

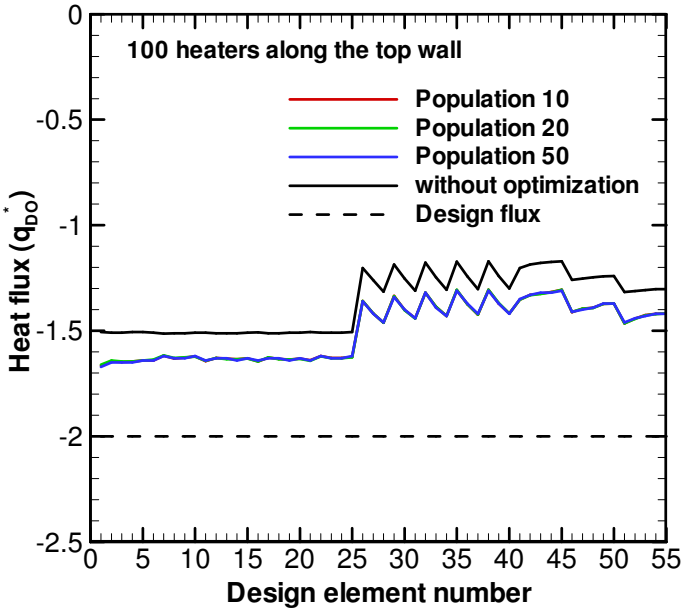

(a)

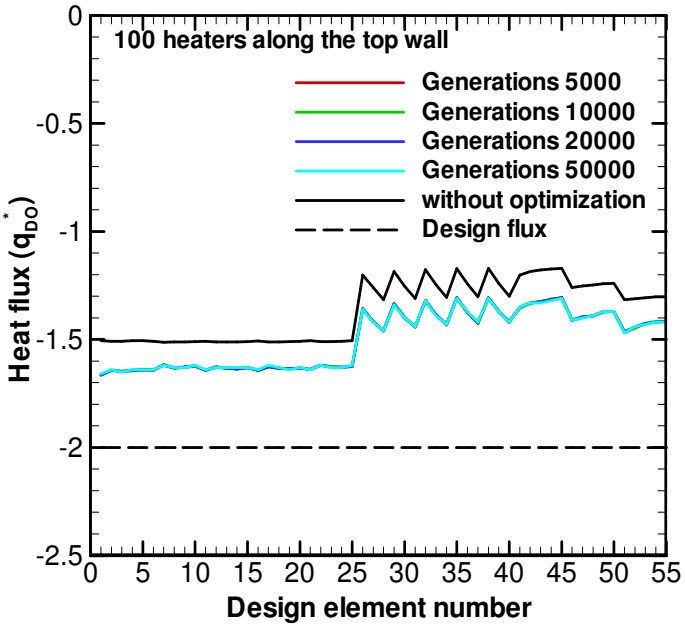

(b)

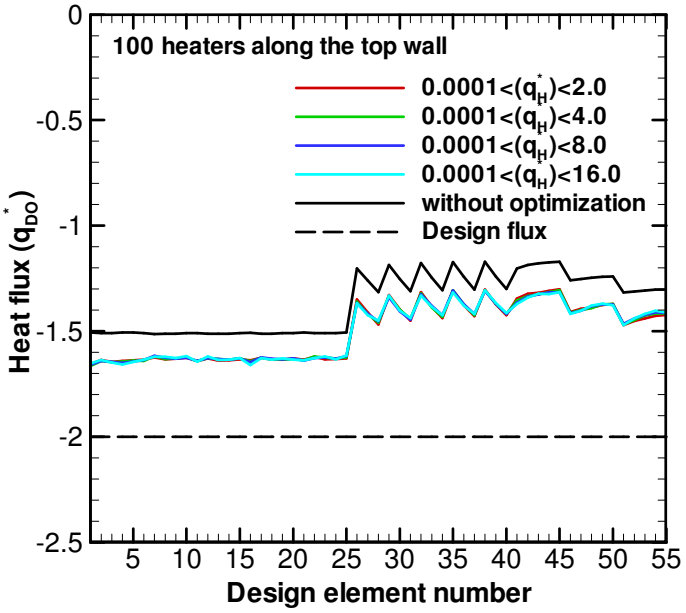

(c)

Figure 3.12. Comparisons of estimated heat fluxes on the design object using 100 heaters along the top wall of furnace for (a) for different population size, number of generations 20000, (b) for different numbers of generations, population size 10, (c) different ranges of heater power, number of generations 10000, population size 10.

.

The heat flux along the top surface (elements: 1-25) of the DO is uniform, but both with and without optimization they are different than the desired one. However, the heat flux distribution along the vertical surfaces (elements: 26-40, and 41-55) of the design object, is found non-uniform. This non-uniformity is owing to the poor radiative visibility among the heater elements along the top surface and the surface elements along vertical surfaces of the DO. For this computation 5000 generations with 10 populations are used.

Further, the same case i.e. yielding uniform thermal conditions on the DO using 100 heaters along the top wall (Fig. 3.11) has been worked out for different aspects, (a) for 3 different population sizes, (population size 10, 20, 50) (b) for 4 different numbers of generations (generations 5000, 10000, 20000, 50000), and (c) for 4 different ranges of heaters power

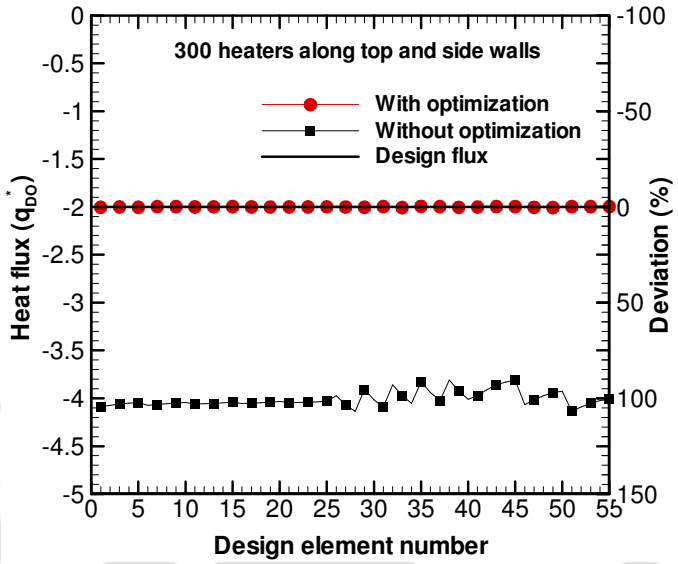

(a)

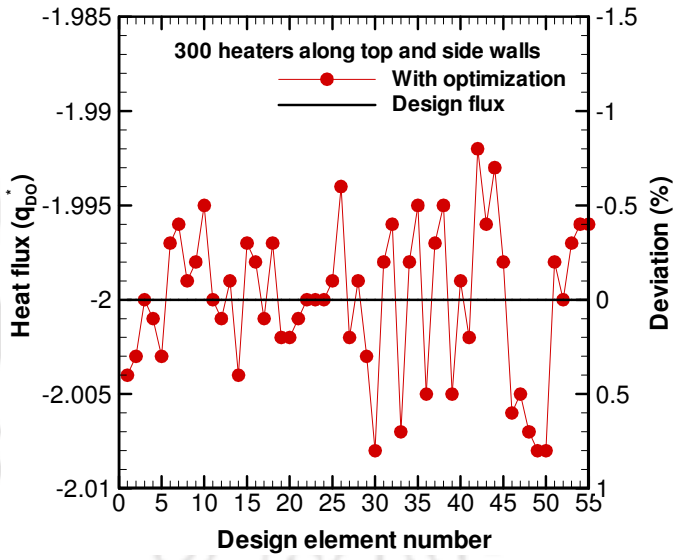

(b)

Figure 3.13. (a) Heat flux distribution on design object with and without optimization using 300 heaters along on top, back and west walls. (b) Magnified view of Fig. 3.13a showing the deviation in the estimated heat flux on the design object with optimization.

.

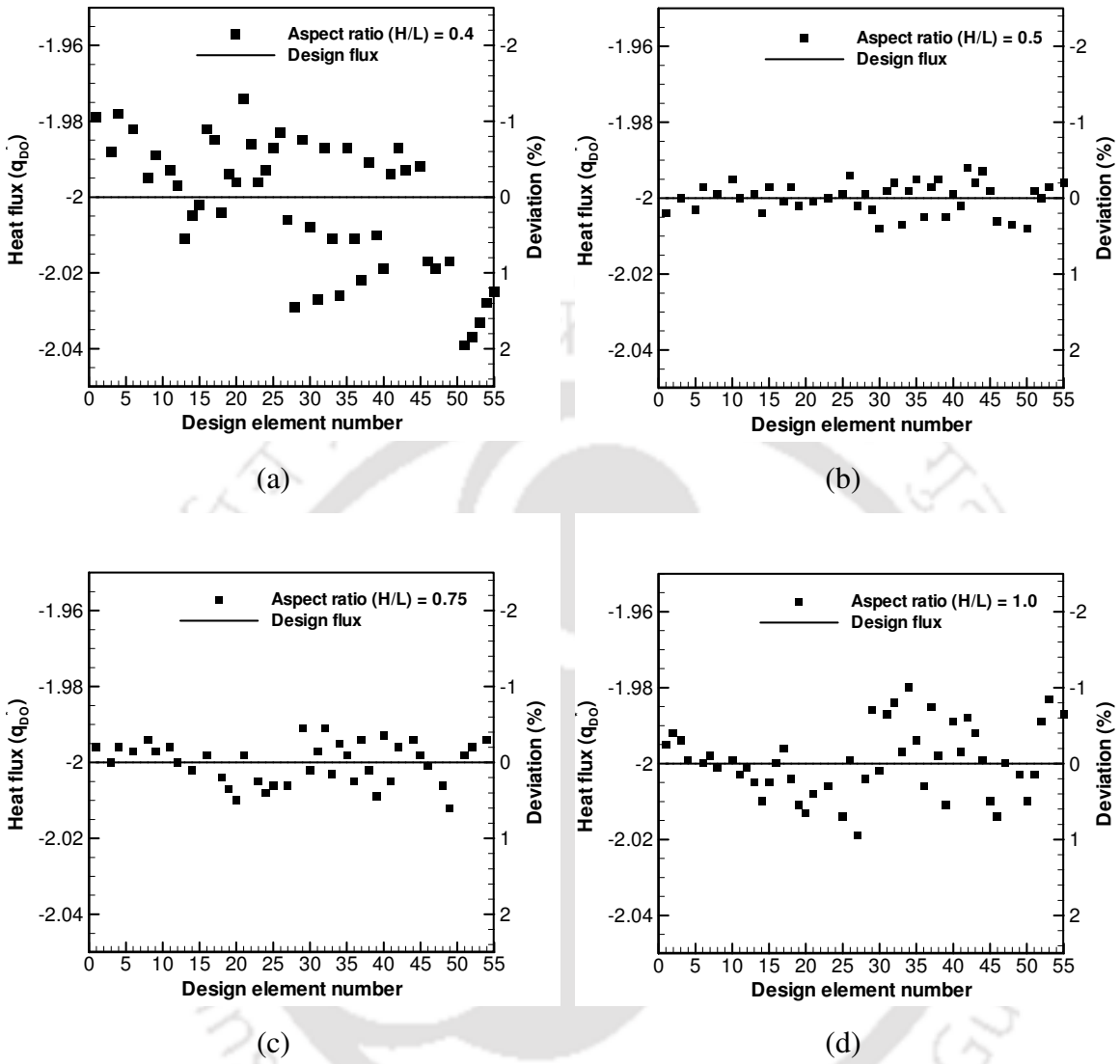

Figure 3.14. Estimated heat flux distribution on the surfaces of a 3-D DO using different aspect ratio (*H/L*) of the radiant enclosure.

$\left(0.0001 \le q_H^* \le 2.0,\ 0.0001 \le q_H^* \le 4.0,\ \ 0.0001 \le q_H^* \le 8.0,\ \text{and}\ 0.0001 \le q_H^* \le 16.0\right)$. The aim of this study is to check the feasibility of solution with different aspects. For different aspects (a), (b) and (c), the comparisons of the estimated heat fluxes on the design object have been shown in Fig. 12a-c, respectively.

From the Fig. 12a-c, it is observed that even with any above combination of number of generations, heater power ranges, and population size, using 100 heaters along the top wall of the furnace do not yield the uniform thermal conditions on the 3-D DO. The estimated heat fluxes are far from the desired uniform flux. This is not because of population size, number of generations or the ranges of heaters power considered, but the solution may not possible with the heaters along the top wall only. It is to be noted that in the present work the design object is 3-D one.

Next, it proceeds with considering 100 panel heaters along each of the three walls, viz., top, back and west walls (refer Fig. 3.1b). Using direct method (REM^2), and the present optimization algorithm (REM^2 + MGA) the heat flux distribution along the surfaces of the DO have been estimated. In this case also in direct method the heaters along the walls are set to deliver the flux $q_H^* = 1.0$. Fig. 3.13a shows the heat flux distribution on the surfaces of the design object with and without optimization. Considering the panel heaters along three walls and using the present optimization algorithm the desired uniform heat flux distribution $q_{DO}^* = -2.0$ is achieved accurately. The maximum deviation in the estimation is less than $\pm 1.0\,\%$. To have clarity in reading the accuracy of the estimation of heat fluxes on the DO, Fig. 13b shows the magnified view of Fig.13a. Another observation from Figs. 3.13a-b is that, unless the optimization is done, although heaters along all walls are considered, the uniform heat flux distribution on the surfaces of a 3-D DO cannot be obtained. Hence in the present study computations are done considering the panel heaters along the three walls of the radiant enclosure (Fig. 3.1b). Further, it is to be noted that to have desired uniform thermal conditions, considering 300 heaters (100 on each wall) for the computation does not mean that all the heaters required to be placed and activated. In following discussion it is demonstrated that even 300 heater elements are considered for computation, to produce the desired uniform thermal conditions for a particular problem, very few of them are required actually. Using this concept several of heater elements can be neglected, however, it is possible only after having the knowledge of optimal heater power setting.

3.4.2 Effect of aspect ratio of radiant enclosure on heater power settings

In the last section, the desired uniform thermal conditions on the surfaces of a 3-D DO has been estimated accurately. keeping length and width of the enclosure constant (L = 2.0 m, W = 2.0 m), for different aspect ratios H/L = 0.4, 0.5, 0.75 and 1.0, it is interesting to study if the uniform heat flux is achievable accurately, and if so, what is the distribution of power of the panel heaters? For practical applications, it is further desirable to know if all the heaters need to be placed. For this study, the design constraints on the non-dimensional power of the panel heaters have been taken 0.0001 to 4.0. The lower bound for the heaters power is intentionally taken very small, so that in practical use the heaters having very less power can be neglected. The configurations and the optimal power requirement on the panel heaters are estimated using the present algorithm; the results for these cases are shown in Figs. 3.15-3.18.

It is seen from Figs. 3.14a-d that for all the four aspect ratios considered, viz. $H/L = 0.4, 0.5, 0.75$ and 1.0, with the given design constraints $\left(0.0001 \le q_H^* \le 4.0\right)$, the desired uniform heat flux of $q_{DO}^* = -2.0$ on the surfaces of the DO is achievable. Among the four cases studied, the uniformity in the estimated heat flux distribution on DO is best with the aspect ratio 0.5. Also, the estimated heat flux distributions with aspect ratios 0.75 and 1.0 are within the acceptable range (deviation < 3%) of deviation. From these results, it is observed that increasing the aspect ratio beyond 0.5 is not that favorable for achieving the uniform thermal conditions on the DO. It is to be noted that in the problems where the heater are considered along the top wall only and the vertical walls are insulated with refractory material, the statement would be reverse. For the aspect ratio $H/L = 0.5$, 0.75 and 1.0, the uniform heat flux distributions are found within the deviation limit $\pm 1.0\%$ .In Figs. 3.15-3.18, for the aspect ratio H/L = 0.4, 0.5, 0.75 and 1.0, the optimal heater power settings along the top, back and west walls are given, respectively. Keeping the MGA and REM^2 parameters same, in all the cases 5000 generations are performed.

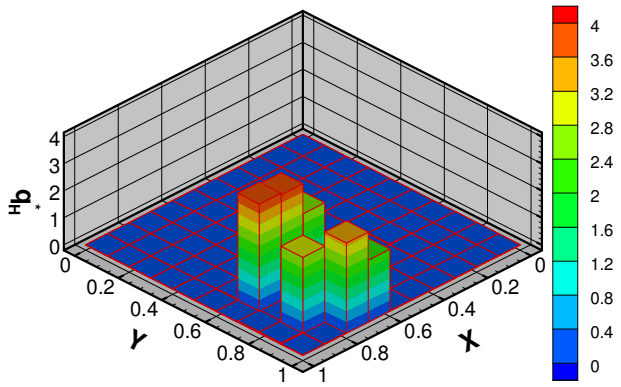

(a) Top wall

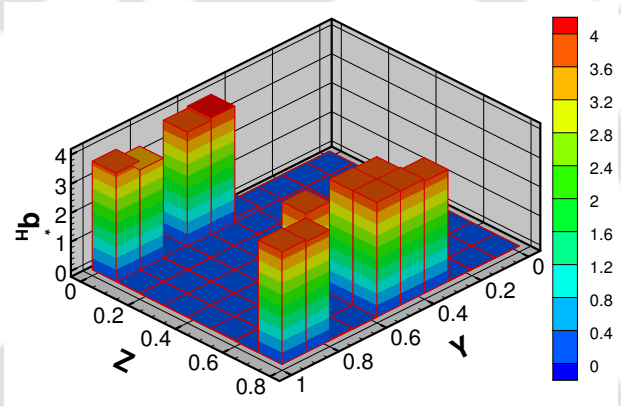

(b) Back wall

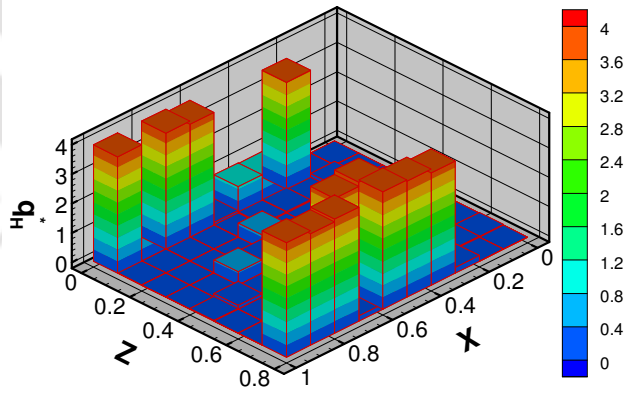

(c) West wall

Figure 3.15. Optimal heater power distribution along the walls of the furnace, with aspect ratio (*H/L*) = 0.4, (a) top wall (b) back wall (c) west wall, $0.0001 < q_H^* < 4.0$.

.

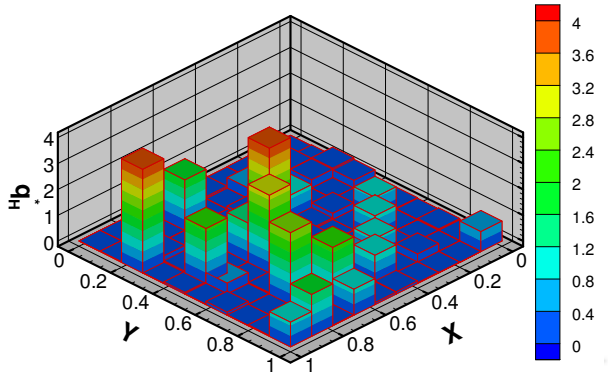

(a) Top wall

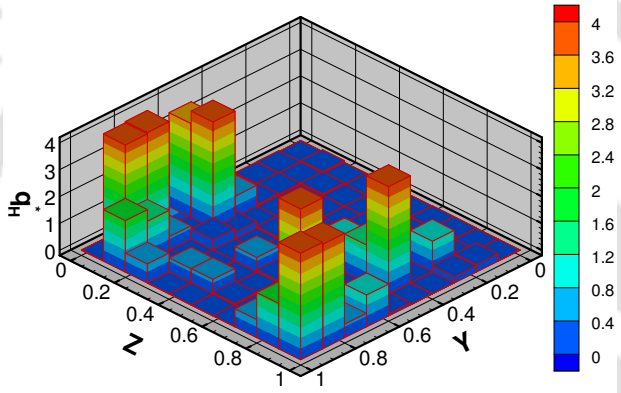

(b) Back wall

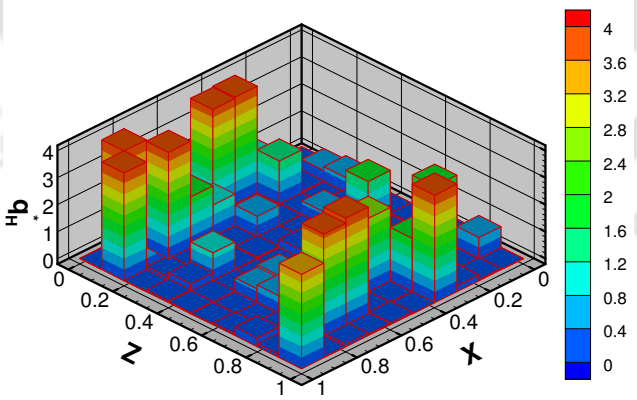

(c) West wall

Figure 3.16. Optimal heater power distribution along the walls of the furnace, with aspect ratio (*H/L*) = 0.5, (a) top wall (b) back wall (c) west wall, $0.0001 < q^*_H < 4.0$.

.

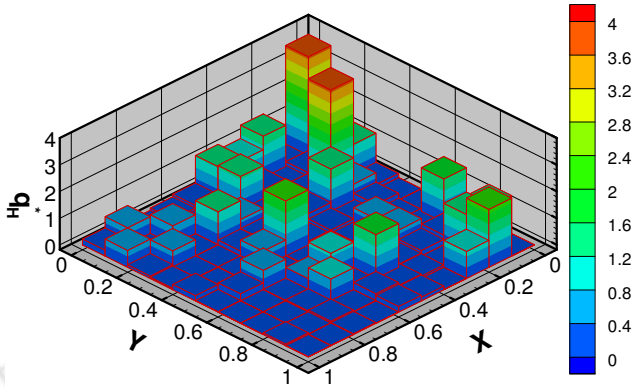

(a) Top wall

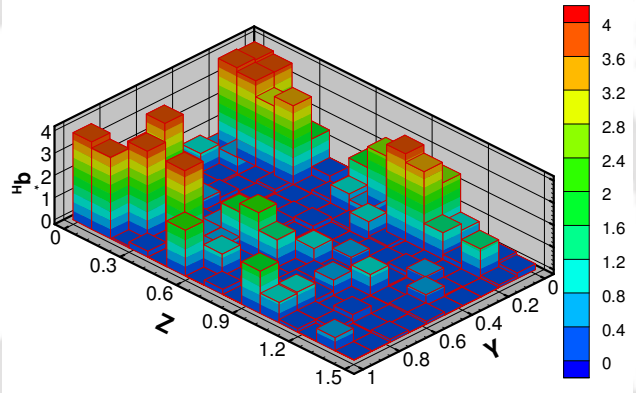

(b) Back wall

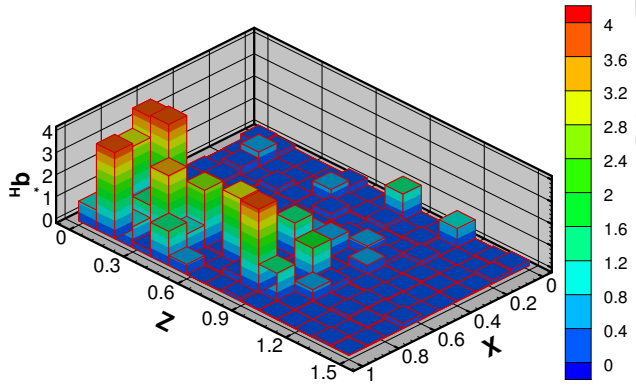

(c) West wall

Figure 3.17. Optimal heater power distribution along the walls of the furnace, with aspect ratio (*H/L*) = 0.75, (a) top wall (b) back wall (c) west wall, $0.0001 < q^*_H < 4.0$.

.

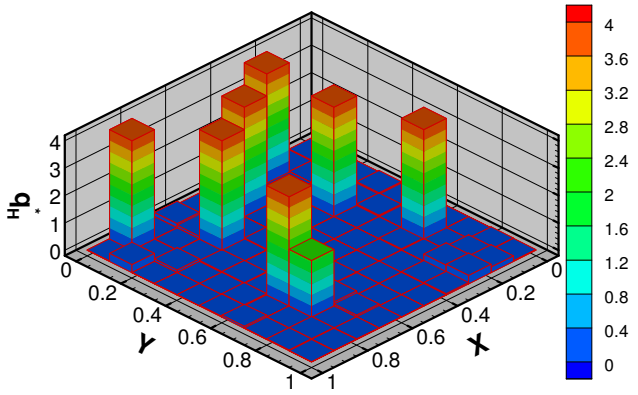

(a) Top wall

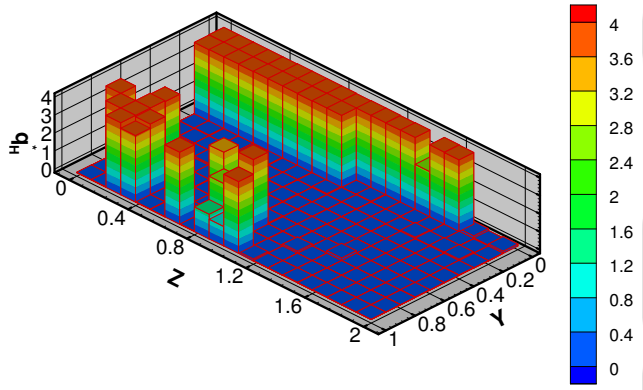

(b) Back wall

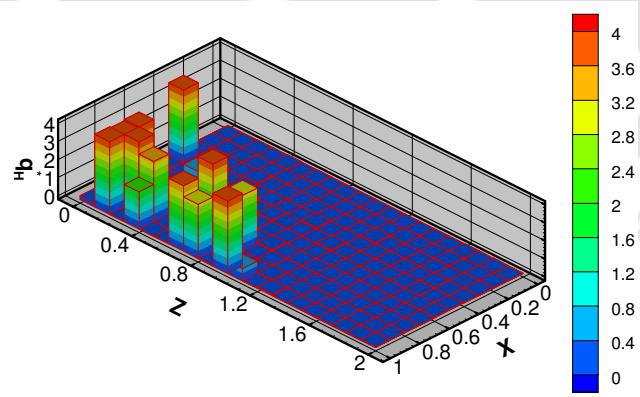

(c) West wall

Figure 3.18. Optimal heater power distribution along the five walls of the furnace, with aspect ratio (*H/L*) = 1.0, (a) top wall (b) back wall (c) west wall, $0.0001 < q_H^* < 4.0$.

.

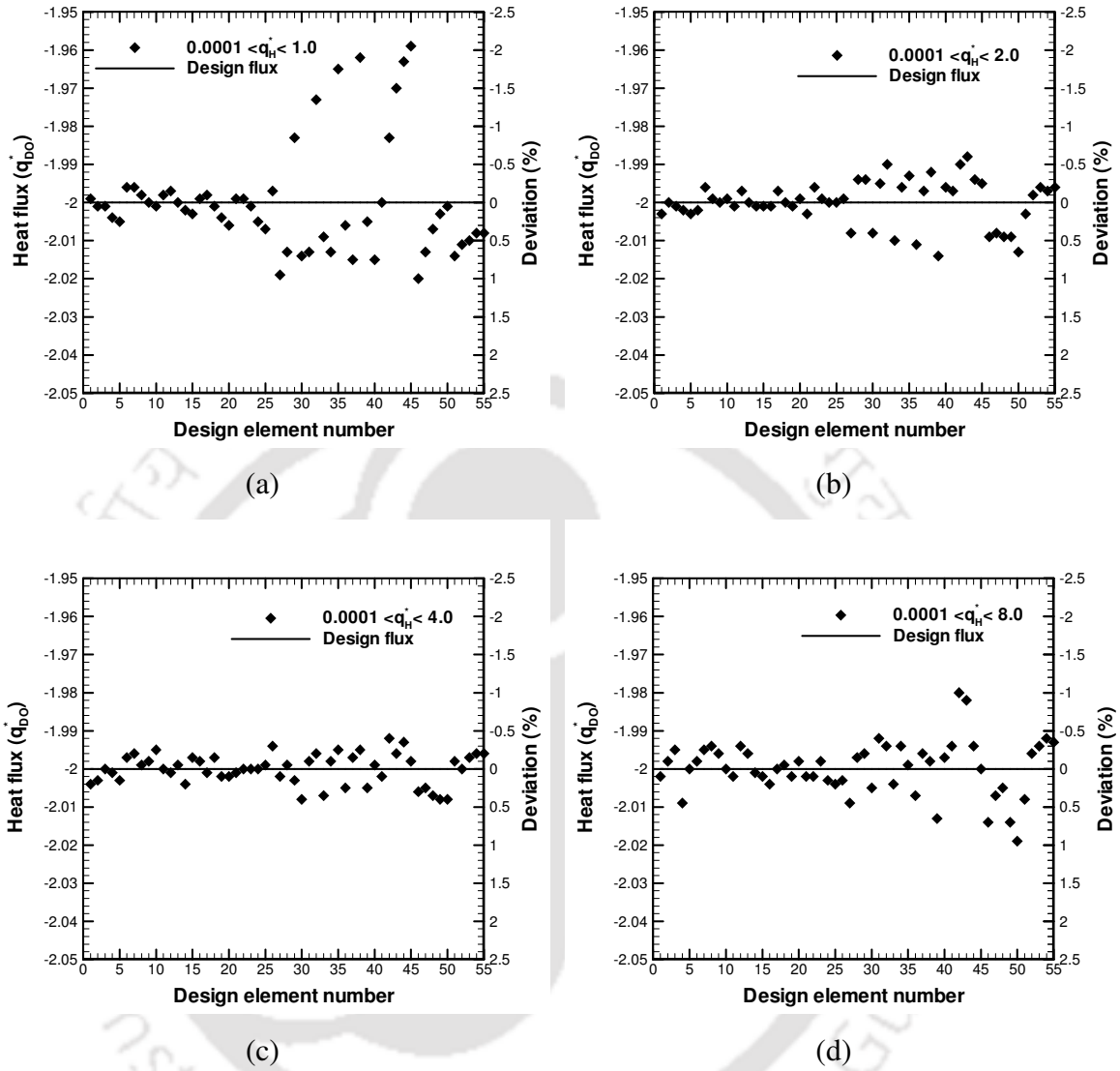

Figure 3.19. Heat flux distribution on the surfaces of a 3-D DO using different design constraints, (a) $0.0001 < q_H^* < 1.0$, (b) $0.0001 < q_H^* < 2.0$, (c) $0.0001 < q_H^* < 4.0$, (d) $0.0001 < q_H^* < 8.0$.

The basic aim of this interpretation of the heaters location and their required power is to show, even though 300 and more heaters have been considered for computation, for the cases with different aspect ratio (Figs. 3.15-3.18), not all the heaters are required to be placed. It is observed from Figs. 3.15-3.18 very few heaters are needed.

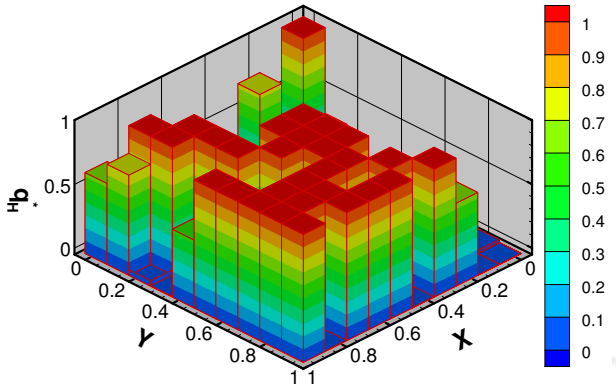

(a) Top wall

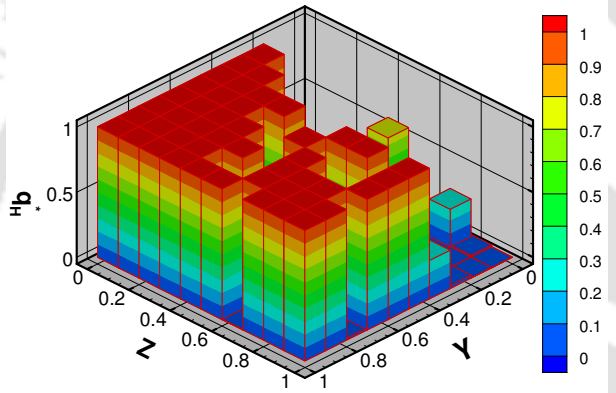

(b) Back wall

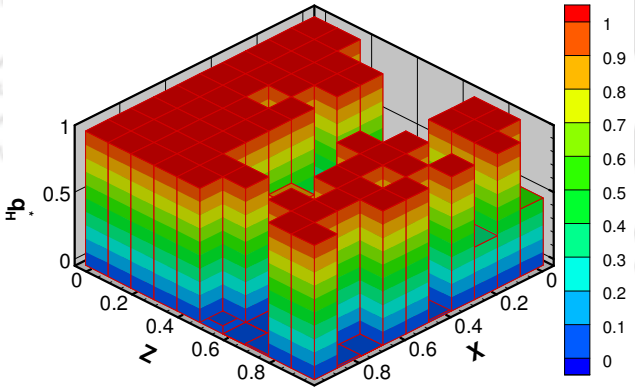

(c) West wall

Figure 3.20. Optimal heater power distribution along the walls of the furnace, with aspect ratio (*H/L*) = 1.0, (a) top wall (b) west wall (c) back wall, $0.0001 < q_H^* < 1.0$.

For practical application, even though the heater power is scattered along the wall of enclosure, either one can go for grouping of heaters, those having virtually same power requirement or can also neglect those heaters which require very less power (<1% of rated power).

A review of results presented above proves that, the present algorithm involving the combination of the REM^2 and the MGA is capable to estimate the optimal heater power setting for 3-D radiant furnace that produce the desired uniform thermal conditions on the 3-D design object.

3.4.3 Effect of design constraints on the estimation of desired thermal conditions

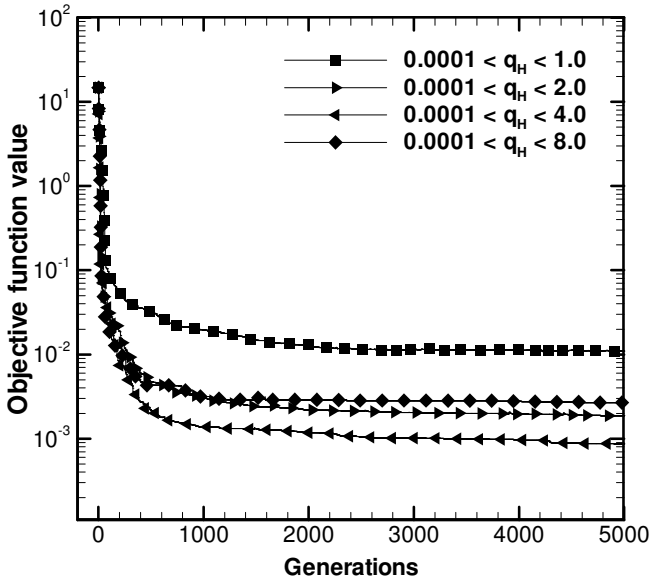

Figure 3.21. Convergence history of objective function using different design constraints (heater power ranges).

Since in the present study the MGA has been used as an optimization tool, it is important to check the effect of design constraints, the range of power of heater. Four values of design constraints, in Fig. 3.21, the convergence histories of objective function for the problems with different design constraints (heater power ranges) are given. The trends of

convergence plots in Fig. 3.21 are supporting to the results shown in Fig. 3.19a-d. In optimization problems wider constraints are desirable, however far wider constraints require more computational efforts to find the optimum solution.

To check the effect of narrow design constraints, Figs. 3.20a-c shows the optimal heater power setting along the three walls of the enclosure using the narrow design constraints as $0.0001 \le q_H^* \le 1.0$. It is observed from Figs. 20a-c that, more numbers of heaters with full rated power are needed. Although such kind of heater power setting is feasible for controlling in practical situations, it does not produce the accurate uniform thermal conditions. The corresponding heat flux distribution is shown in Fig. 3.19a, which do not meet the desired thermal conditions. As shown in Figs. 3.19a-d, in optimization problems the wider range of the design constraints are desirable.

3.4.4 Effects of the MGA parameters

Since in the present study the MGA has been used as an optimization tool, it is important to check the effect of MGA parameters. Towards this aspect, the effects of crossover probabilities $\left(P_c\right)$ are studied. Single point crossover probabilities $\left(P_c\right)$=0.2, 04, 0.6, 0.8, 1.0 and uniform crossover (probability of 0.5) are considered. Fig. 3.21a shows the convergence history of the objective function (Eq. 3.24) against the numbers of generations. It is well known that in minimization problems like present one, as the objective function value approaches to the minimum, simultaneously the accuracy of the optimal solutions approaches to maximum. It is observed from Fig. 3.22 that in case of the single point crossover, increase in the crossover probability gives better convergence and thus better solution. In the present problems the uniform crossovers have shown far better convergence of the objective function than the single point crossover. For the studies in this thesis, the uniform crossover with crossover probability 0.5 has been used. For such kind of problems uniform crossover is recommended.

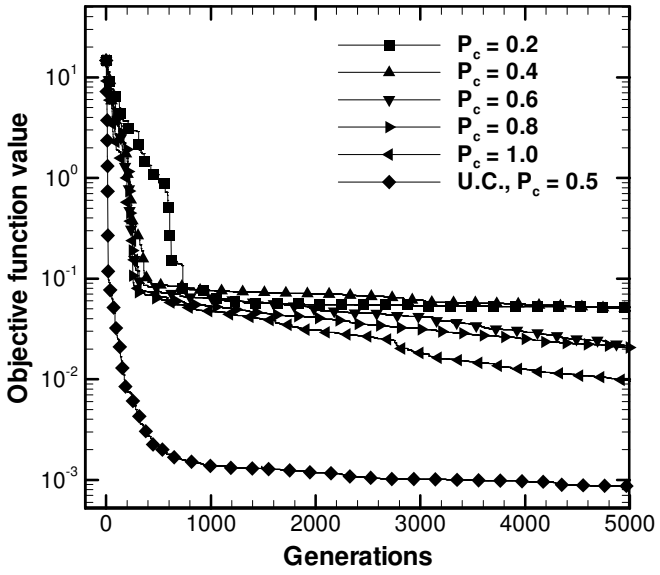

Figure 3.22. Convergence history of objective function with different crossover probabilities.

3.5 Summary

The optimum heater power settings that produces desired uniform thermal conditions on the surfaces of centrally located 3-D object on the bottom of a 3-D rectangular radiant furnace was investigated. Radiative information was computed using the REM^2 and the MGA was used to minimize the objective function. Effect of specular reflections from the heater surfaces and refractory walls was accounted. The desired uniform heat flux distribution on the DO could not be obtained with the consideration of 100 panel heaters along the entire top wall only. However, considering the panel heaters along the top and two vertical walls, the same was achieved within the deviation of ± 1%. The effects of the four aspect ratios of radiant enclosure were studied. Among the four cases studied, the uniformity in the estimated heat flux distribution on DO is best with the aspect ratio 0.5. Also, the estimated heat flux distributions with aspect ratios 0.75 and 1.0 are within the acceptable range (deviation < 3%). From these results, it is observed that increasing the aspect ratio beyond 0.5 is not that favorable for achieving the uniform thermal conditions on the DO. The optimal heater power settings for four aspect ratio of the radiant furnace

were given. Even though 300 and more heaters elements were needed for computation, very few are actually needed to produce uniform thermal conditions on the 3-D DO. For larger aspect ratio better arrangements of the heaters are observed. Further, for a given aspect ratio that provided the uniform heat flux on the surfaces of the design object, the effects of the design constraints on power of the panel heaters were studied. The narrow constraints do not produce the desired conditions accurately. It was found that non-dimensional heater power range 0.0001 to 2.0 and above work well. For such kind of design problems using the genetic algorithm, use of uniform crossover is recommended. This work provides a guideline in the design of a 3-D radiant furnace to produce the uniform thermal conditions on a 3-D object and also establishes the feasibility of the usage of the REM^2 and MGA for complex problems.

CHAPTER 4

RADIANT FURNACE DESIGN FOR UNIFORM THERMAL CONDITIONS – AN APPLICATION BASED APPROACH

4.1 Introduction

For the desired post processing results, in several industrial heating processes, products are needed to be maintained at prescribed thermal conditions (temperature/heat flux distribution), i.e. over the part of system where heating to be take place. Material heating before precision heat treatment processes, hot working processes, drying of paints, drying of powder coating, and manufacturing of electronic components, etc., are some of examples. For better thermal control, the radiant furnaces are best suited one. In the design of radiant furnace, for desired thermal conditions selection of configuration and power of the heaters, geometry of the furnace, properties of the furnace and heater materials are some of the important aspects.

Because of increasing trend of sophisticated heating in manufacturing, heat processing and in laboratory use, to address the different types of furnace boundary design problems several studies are given in literature. Diverse kinds of furnace boundary design problems with different geometry and for specific applications can be found in literature. The detail literature review is given in Chapter 1 section 1.2; it is observed that most of these studies are limited to the 2-D furnace geometries with 2-D design object (DO). The boundary design problems with 3-D geometry are rare. Also the boundary design problem with multiple DOs or the studies related to the location, size, and shape of the DO(s) are not found in literature. Towards the more general case in material heating applications, in Chapter 3, the methodology (REM^2 + MGA) for finding the optimal heater power settings has been given and exemplified with the sample problem, in which a 3-D DO placed inside 3-D radiant furnace. To analyze the real life material heating situations, only a case having centrally located 3-D DO and of fixed dimensions (as given in

Chapter 3), is not enough. Considering the application based situations in material heating, using the present algorithm three studies are given in this chapter. These studies include the situations which frequently encountered in the industrial material heating applications.

With the furnace enclosure dimensions fixed, in first study, for uniform thermal conditions, the constraints on the size of a DO are explored. To cover a wide range of the dimensions, 29 DO models are considered. The results are elaborated in section 4.2.1. In the second study, the effects of the location of 3-D DO have been investigated. In this study the suitability of location of the DO is examined by comparing the estimated heat flux distribution with that of the desired one. For 3 DO models 22 cases are evaluated; results are discussed in section 4.2.2. Next, in section 4.2.3, to address the situation for the mass heating, the possible configurations are explored. In this study, for different numbers of DOs the best possible configurations are explored. In each of these studies, for any sample case, the optimal heaters power settings are given. The results of these 3 studies are summarized in section 4.3.

4.2 Results and Discussion

4.2.1 Study 1- Exploring the constraints on the size of the design objects

With the dimensions $\left(L = W = H = 1.0 \text{ m}\right)$ of the 3-D cubical radiant enclosure fixed, for the uniform thermal conditions, i.e., temperature $\left(T^*_{DO} = {T_{DO}}/{T_R} = 1.0\right)$ and heat flux $\left(q^*_{DO} = {q_{DO}}/{\sigma T_R^4} = -2.0\right)$, chosen size (dimensions) of a 3-D DO are investigated. From the estimated thermal conditions constraints on the size of the DOs are established. The schematic for this study is shown in Fig. 4.1. To cover the possible ranges 29 different dimensions of the DOs are considered. The each case is treated as separate boundary design problem and for each of them it is explored if the desired uniform thermal condition is achievable within the acceptable range (deviation < 3%).

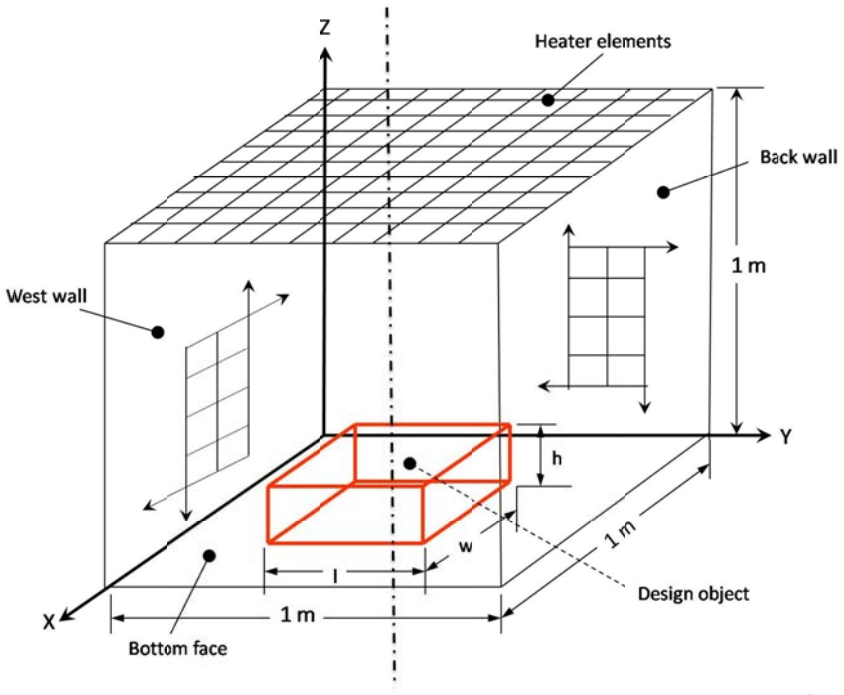

Figure 4.1. Schematic of the radiant furnace enclosure showing heaters along 5 walls, with centrally located 3-D design object on the bottom face.

In this study, since 29 different cases with varying dimensions of the DO are considered, to get an idea of dimensions of the DO with corresponding model number given in Table 4.1, the following nomenclature is used. With the designation of surface elements shown in Fig. 4.2, model number 333 represents a DO having dimensions: $l = 0.3\text{m}, w = 0.3\text{m}$ and $h = 0.3\text{m}$. Similarly, the model 331 represents a DO having dimensions $l = 0.3\text{m}, w = 0.3\text{m}$ and $h = 0.1\text{m}$. For all 29 cases given in Table 4.1, the similar approach of interpretation and designation of surface elements is adopted. As the dimensions of the DO changes the number of surface elements along the surfaces of the DOs changes accordingly. For all these problems the dimensions of the enclosure are fixed, therefore the numbers of surface elements along the five walls of the radiant enclosure, except bottom surface (insulated area) are constant. The surface element distribution is given in Table 4.1.

The configuration and numerical designation of the surface elements as shown in Fig. 4.2 (DO model-333), and model designations as given in Table 4.1 are important for a better understanding and the physical interpretation of results, estimated heat flux distribution on the DOs. It is to be noted that all surface elements, i.e., the panel heaters along the 5 walls of the furnace, the exposed portion of the bottom surface, and 5 surfaces of the DO are of the same size (0.1 m × 0.1 m). Except the bottom wall on which the DO is located, it is assumed that 100 panel heaters (0.1 m × 0.1 m) cover the entire surface of each of the 5 walls. The panel heaters can operate in a set (non-dimensional) power range $\left(q_H^*\right)$: 0.0001 – 4.0.

			Insulated surfaces						
				1	**2**	**3**			
				4	**5**	**6**			
				7	**8**	**9**			
			Insulated surfaces						

(a) Bottom surface of enclosure and the top face of DO (surface elements:1-9)

12	**15**	**18**
11	**14**	**17**
10	**13**	**16**

21	**24**	**27**
20	**23**	**26**
19	**22**	**25**

36	**35**	**34**
33	**32**	**31**
30	**29**	**28**

45	**44**	**43**
42	**41**	**40**
39	**38**	**37**

(b) Back face of DO (c) Front face of DO (d) West face of DO (e) East face of DO

Figure 4.2. Configuration and designation of surface elements on 3-D DO (dimensions: l = 0.3m, w = 0.3m, h = 0.3m) placed inside the furnace enclosure (Refer Fig. 4.1).

In this chapter, for all three studies the heater elements along the five walls of the radiant enclosure are considered good emitters having emissivity 0.95, and the remaining elements on the bottom surface not covered by the DO are considered insulated and their emissivity is 0.3. The emissivity of the surfaces of the DOs is taken as 0.6.

Before going for actual computations, it is necessary to get an idea that, with the objective of having uniform heat flux distribution $q^*_{DO} = -2.0$ on the surfaces of a given 3-D DO, how many heater elements are required for computation? For this study, the given furnace with DO model number 333 (refer Table 4.1) has been considered. There are options for placement of panel heaters. Either consider the heaters along the top wall only, or consider the heaters along all five walls of the furnace, i.e. top wall and four vertical walls. From the literature [Fedorov *et al.*, (1998); Daun and Howell, (2005); Erturk, *et al.*, (2004); Fan *et al.*, (2002)], it is seen that when the DO is 2-D, i.e. only a planer surface, the placement of heaters along the wall opposite to the design surface is enough. However, in the present case the DO is a 3-D one. It is logical that heaters along only on the top wall may not yield uniform thermal conditions on the vertical walls of the DOs, this aspect has been touched in Chapter 3 also.

Using the present algorithm (REM^2 + MGA), the inverse radiant boundary design problem is solved with 4 options of heater placement, viz. (a) 100 heaters along the top wall, (b) 200 heaters along the two opposite walls (east and west wall, refer Fig. 4.1), (c) 400 heaters along each of the four vertical walls (east, west, back and front), and (d) 500 heaters along the five walls i.e. 4 vertical walls and the top wall (refer Fig. 4.1). For the above given arrangement, Figs. 4.3a-d shows the estimated heat flux distributions on DO and the deviation, respectively. In Figs. 4.3a-d, heat flux distributions are plotted for all the surface elements ranging from 1-45 (shaded regions in Fig. 4.2a-e) along the five surfaces of the DO. From Figs. 4.3a-d, it is observed that considering the heaters along the top wall, and on two opposite vertical walls only, the desired heat flux $q^*_{DO} = -2.0$ on the surfaces of DO is not achieved accurately. However, the same is obtained accurately by considering the heaters either along all 4 vertical walls or along the five walls of the enclosure (Figs. 4.3 c-d). The non uniformity in the estimated heat flux distribution on the vertical faces of the DO (elements: 10-45) is owing to poor radiative visibility of the surface elements along the vertical surfaces of DO and the heater elements. It is to be

noted that considering 500 heaters does not mean all the 500 heater elements need to be actually placed, it is merely for computation purpose.

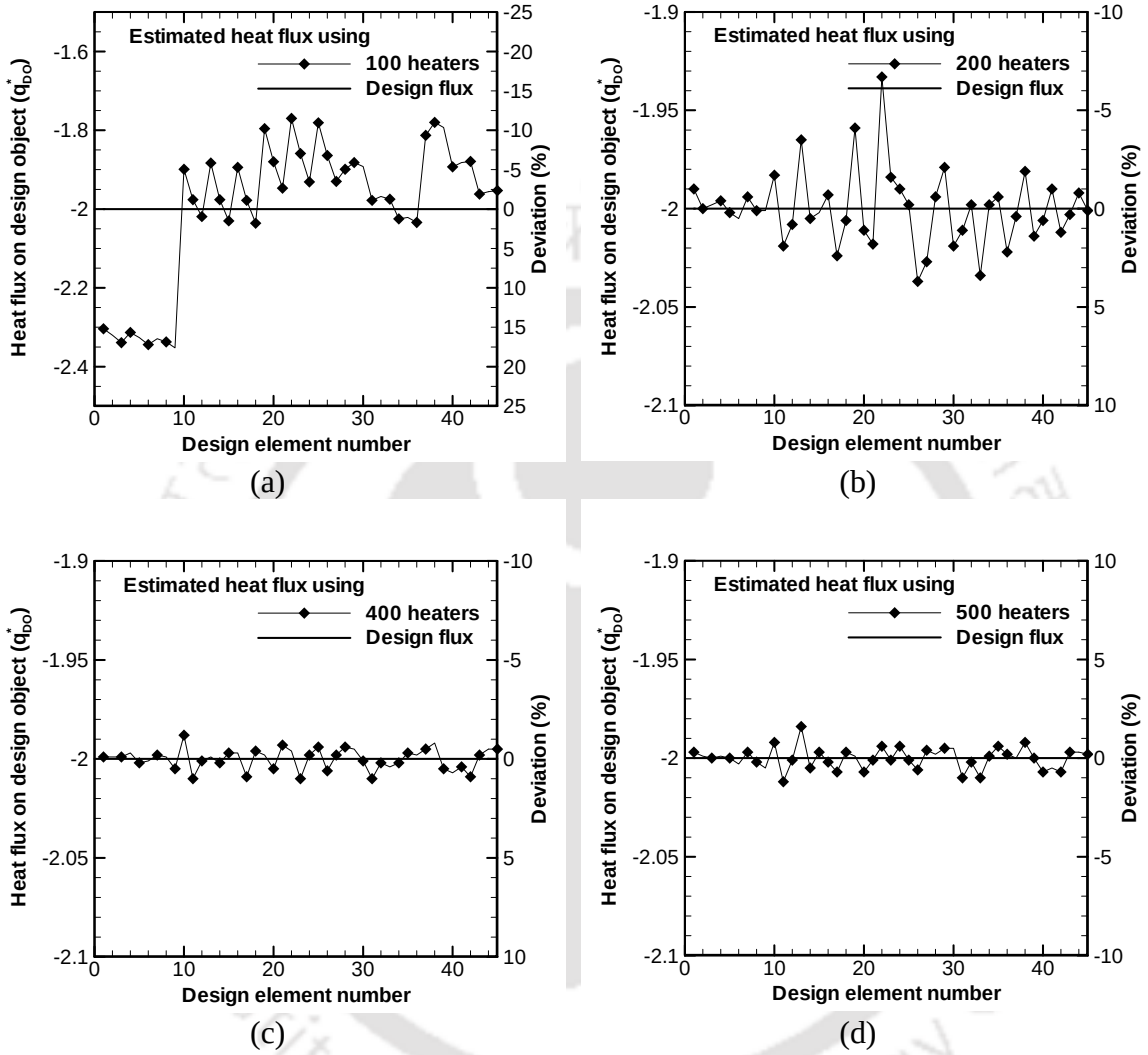

Figure 4.3. Estimated heat flux distribution on a DO model 333 using (a) 100 heaters (along top wall), (b) 200 heaters (along east and west wall), (c) 400 heaters (along four vertical walls) and (d) 500 heaters (along all the walls except bottom), refer Fig.4.1.

For a sample case, it is shown that considering the heaters merely along the one or two walls is not sufficient to yield uniform thermal conditions on a 3-D DO, rather the heaters should be considered along the 5 walls. Next by considering the heaters along all five walls (500 panel heaters) of the radiant furnace, viz., top, east, west, back and front walls, with the given furnace dimensions (L=W=H= 1.0 m), for all 29 cases of the DO, it has

been investigated if the chosen DO size is suitable for achieving the desired uniform thermal conditions.

In each of the 29 cases, the MGA was used to minimize the objective function. With the population size 10, 5000 generations were considered. The design constraints was set as $0.0001 \le q_H^* \le 4.0$. The maximum deviation $(\pm)$ in estimated heat flux on the DO, the minimum value of the objective function, the CPU time for direct and optimization computations are given in Table 4.1. The maximum deviation is calculated with respect to the desired uniform heat flux ($q_{DO}^* = -2.0$). The amount of maximum deviation is an indicative of suitability of size of the DO model for achieving the uniform thermal conditions.

It is seen from Table 4.1 that for model numbers 1-14, 17 and 24, the maximum deviation $(\pm)$ on higher and lower sides of the estimated heat flux for any particular surface elements on the DO is less than 3.0%. It is found in literature that for engineering applications this much deviation is acceptable. For the DO models if the deviations are outside this range, we assume that for desired uniform thermal conditions, for a given dimensions of the furnace, the DO models are not suitable. The maximum deviations on either side of the desired heat flux on the surfaces of DO gives a gross idea about the suitability of the model, it may not reveal the true picture of solution. Hence, the analyses of estimated heat flux distributions on surfaces of the DOs, for 25 DO models are shown in Fig. 4.4-4.8. The aim of this analysis is to show the element wise deviation in estimated heat flux. The desired value of the uniform heat flux is $q_{DO}^* = -2.0$.

In Figs. 4.4a-e, estimated heat flux distribution on the surfaces of DO models number 1-5 having designations 331, 333, 335, 337 and 339, respectively, have been compared. It is to be noted that a model designation like 333 indicates that the dimensions of this DO model are l = 0.3 m, w = 0.3 m, h = 0.3 m. It is to be further noted that for the model 333, with element size $0.1\text{m} \times 0.1\text{m}$, the total number of surface elements on this DO are 45 (refer Figs. 4.2).

Table 4.1. Maximum deviation of estimated heat flux, minimum objective function value, and CPU time (5000 generations) for the problems with different DO models.

Design object model		Total number of elements	Number of elements on a DO	Maximum deviation (%) on a DO		Minimum objective function value	CPU time for	
							direct problem	Optimizati-on
No.	Designati-on			lower side	higher side			
1.	331	612	21	0.15	0.15	0.000022	43.75	288.59
2.	333	636	45	0.60	0.80	0.001331	47.28	547.64
3.	335	660	69	0.70	1.10	0.002781	50.32	578.39
4.	337	684	93	0.95	1.00	0.004287	53.21	603.34
5.	339	708	117	1.35	1.10	0.005543	61.12	640.26
6.	441	616	32	0.15	0.15	0.000053	44.23	516.48
7.	443	648	64	0.65	0.60	0.002380	49.48	558.68
8.	445	680	96	0.80	1.15	0.005238	54.21	599.64
9.	447	712	128	0.90	0.85	0.006910	64.89	647.75
10.	449	744	160	1.45	1.40	0.018965	67.87	692.51
11.	444	664	80	0.75	0.90	0.002614	53.34	593.79
12.	551	620	45	0.50	0.65	0.000667	44.85	290.93
13.	553	660	85	1.05	0.80	0.004894	50.18	575.23
14.	555	700	125	1.45	1.30	0.012978	63.73	636.89
15.	557	740	165	2.15	1.45	0.023737	67.57	705.75
16.	559	780	205	3.60	4.95	0.111869	71.82	763.60
17.	661	624	60	0.35	0.50	0.000518	46.20	534.21
18.	663	672	108	2.01	2.05	0.031488	51.78	622.28
19.	665	720	156	1.75	2.95	0.049839	64.40	669.57
20.	666	744	180	2.10	2.50	0.046581	64.93	696.73
21.	667	768	204	1.95	2.30	0.053124	70.12	745.82
22.	669	816	252	3.15	4.35	0.153612	74.18	810.67
23.	777	796	245	6.00	7.20	0.363744	68.46	773.67
24.	881	632	96	1.00	1.00	0.006659	45.65	571.07
25.	883	760	160	6.20	9.85	0.366106	52.04	627.57
26.	885	760	224	8.05	8.50	0.802519	63.64	714.03
27.	887	824	288	7.10	9.55	1.015151	64.00	796.79
28.	888	856	320	8.75	9.60	1.395303	66.37	852.43
29.	889	888	352	8.80	9.20	1.581945	64.73	897.79

.

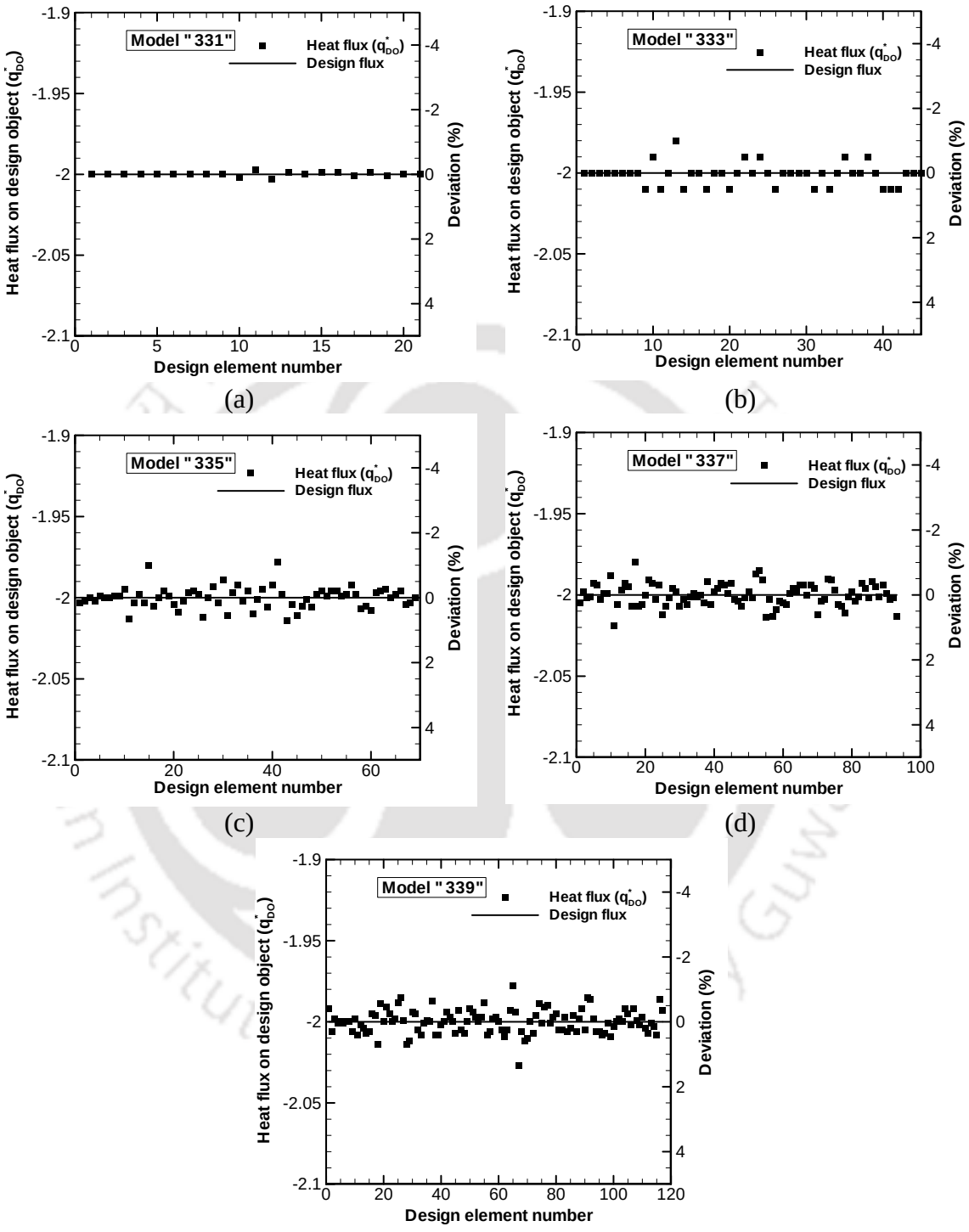

Figure 4.4. Estimated heat flux distribution on the surfaces of DOs, of dimensions $0.3\,\text{m} \times 0.3\,\text{m} \times h$, (a) h = 0.1 m, (b) h = 0.3 m, (c) h = 0.5 m, (d) h = 0.7 m, (e) h = 0.9 m.

.

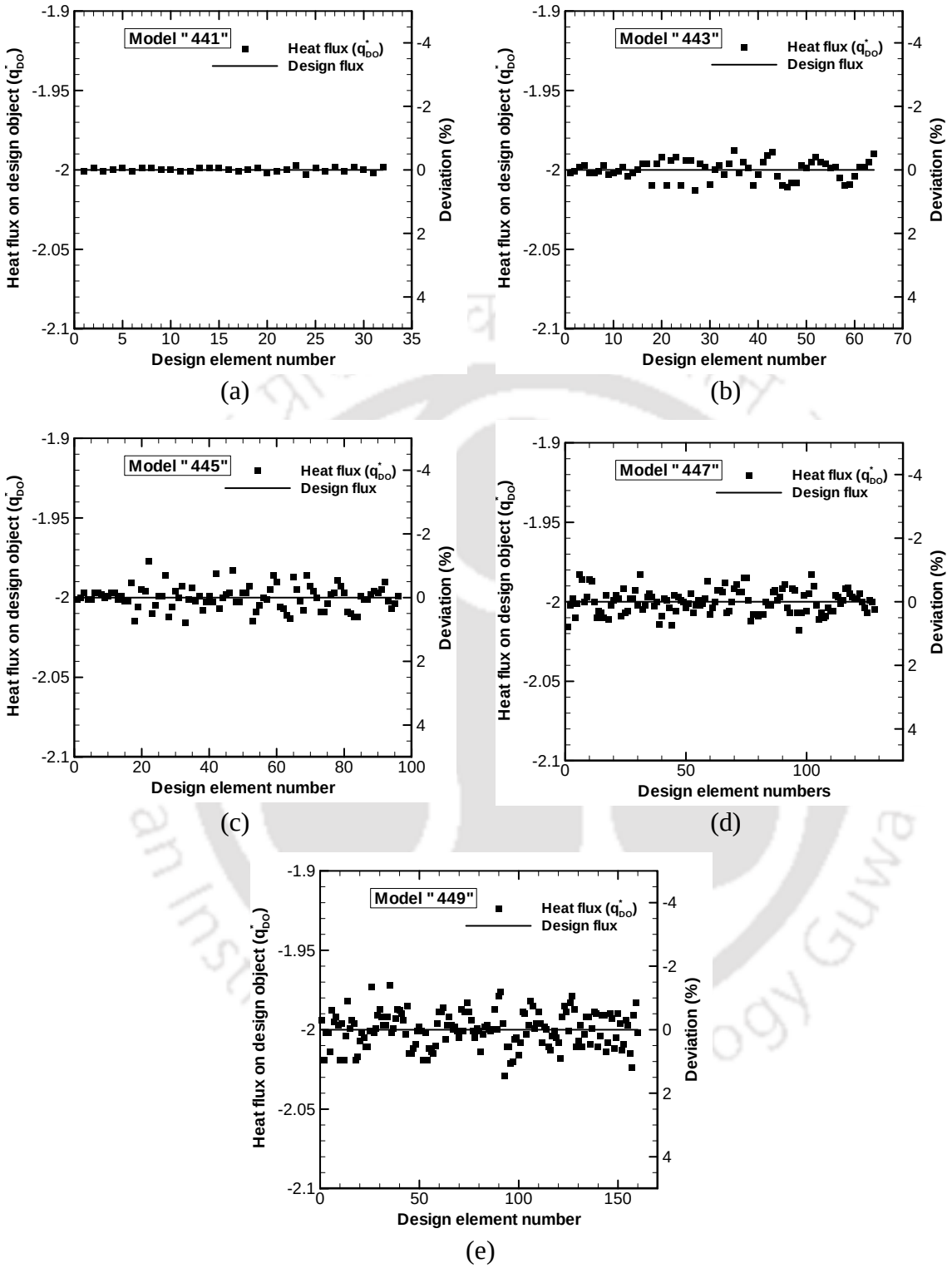

Figure 4.5. Estimated heat flux distribution on the surfaces of DOs, of dimensions $0.4\,\text{m} \times 0.4\,\text{m} \times h$, (a) h = 0.1 m, (b) h = 0.3 m, (c) h = 0.5 m, (d) h = 0.7 m, (e) h = 0.9 m.

.

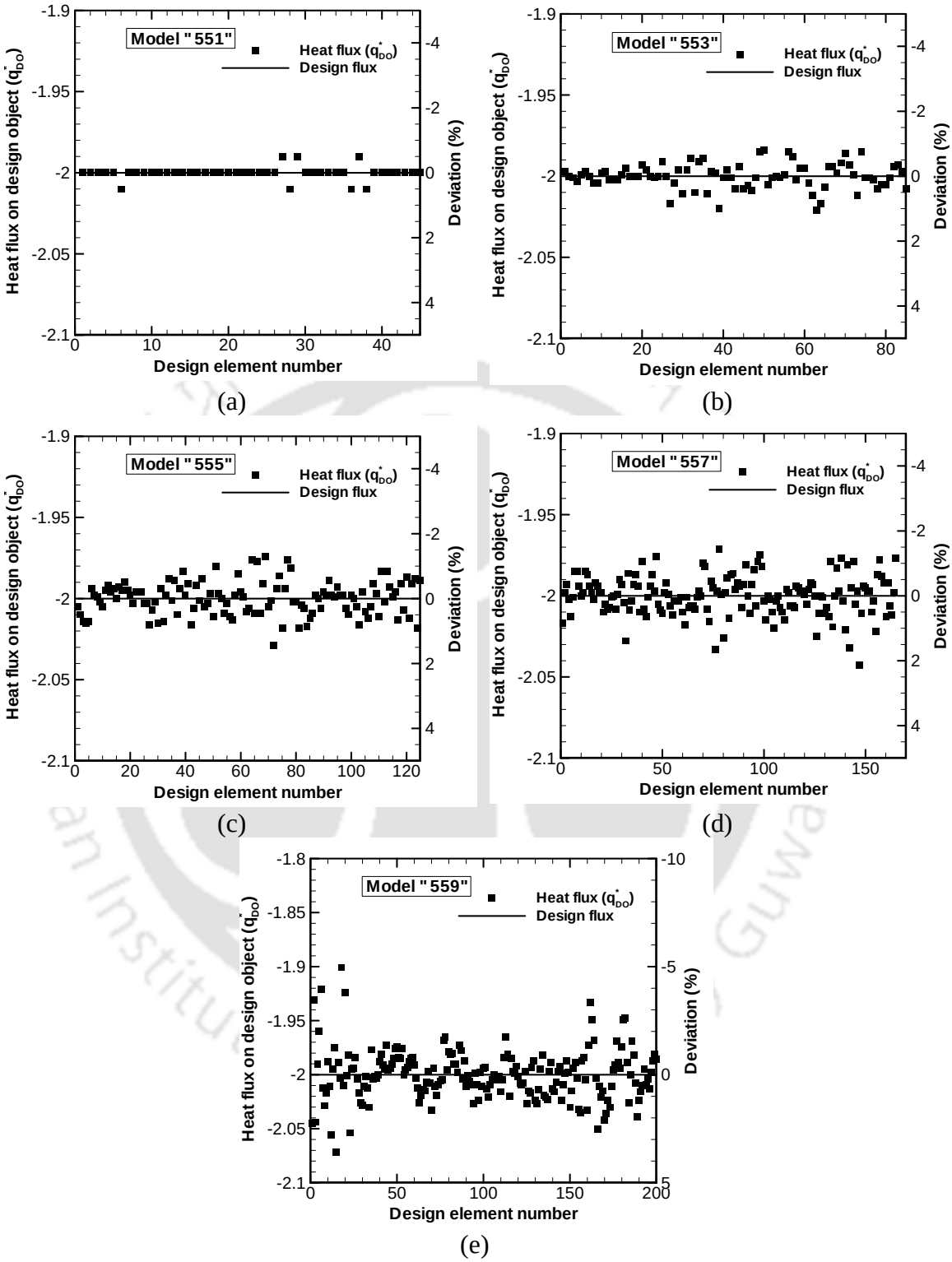

Figure 4.6. Estimated heat flux distribution on the surfaces of DOs, of dimensions $0.5\,\text{m} \times 0.5\,\text{m} \times h$, (a) h = 0.1 m, (b) h = 0.3 m, (c) h = 0.5 m, (d) h = 0.7 m, (e) h = 0.9 m.

.

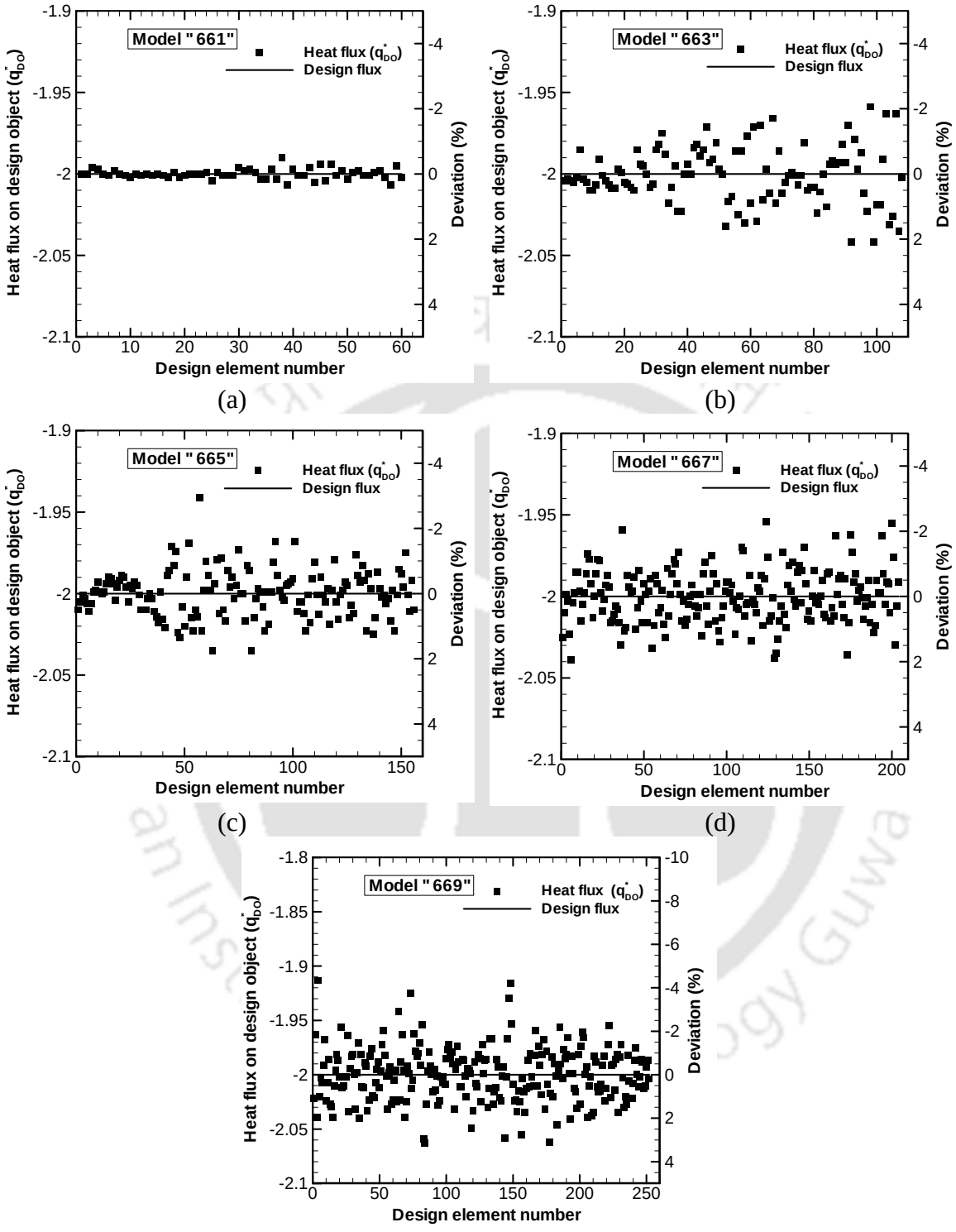

Figure 4.7. Estimated heat flux distribution on the surfaces of DOs, of dimensions $0.6\,\text{m} \times 0.6\,\text{m} \times h$, (a) h = 0.1 m, (b) h = 0.3 m, (c) h = 0.5 m, (d) h = 0.7 m, (e) h = 0.9 m.

.

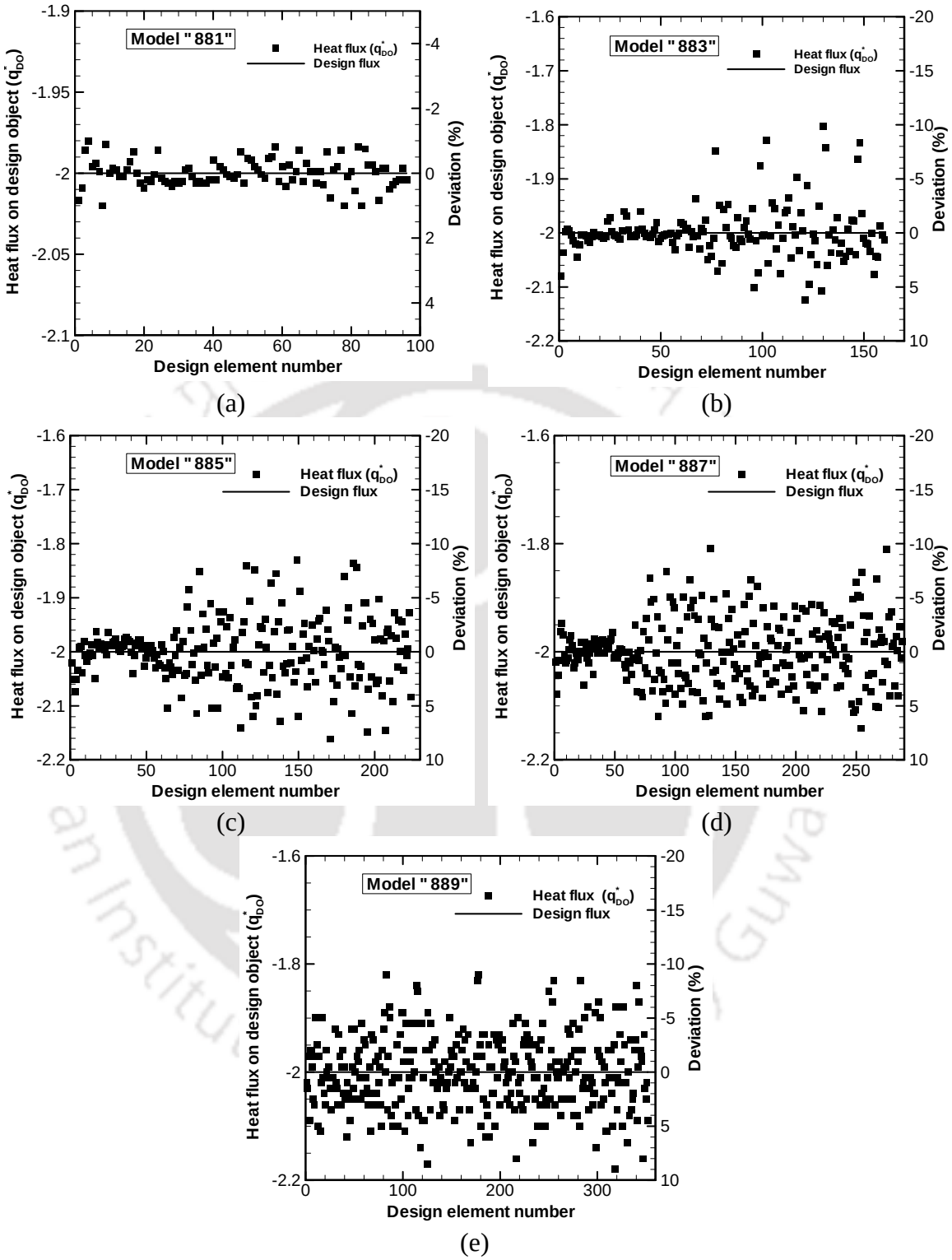

Figure 4.8. Estimated heat flux distribution on the surfaces of DOs, of dimensions $0.8\,\text{m} \times 0.8\,\text{m} \times h$, (a) h = 0.1 m, (b) h = 0.3 m, (c) h = 0.5 m, (d) h = 0.7 m, (e) h = 0.9 m.

For every model against its designation, the total numbers of elements on the DO are given in Table 4.1.

All the plots given in Figs. 4.4 - 4.8 shows the variations in the estimated heat flux on the surfaces of DOs are given against the number of surface elements (design elements). The abscissa show the number of surface elements on corresponding DOs and its maximum range varies according to the number of design elements on the DOs. For the purpose of comparison, ordinates of the plots (range: -2.1 to -1.9) in Figs. 4.4a-e are kept same.

Of the 5 cases considered in Figs. 4.4a-e, for all the cases maximum deviation in estimated heat flux distribution is found within the acceptable range (< 3%). The maximum deviation in estimated heat flux distribution is found 0.3 %, 1.4% , 1.8%, 1.95% and 2.45 % for the DO model 331 (Fig. 4.4a), model 333 (Fig. 4.4b), model 335 (Fig. 4.4c), model 337 (Fig. 4.4d) and model 339 (Fig. 4.4e), respectively, so of the given dimensions, all five DO models are found suitable to yield uniform thermal conditions. From the Figs. 4.4a-e, it is observed that the uniformity in the estimated heat flux distribution is deteriorated with increase in height of a DO.

Next in Figs. 4.5-4.8, the length and width of the DOs has been gradually increased and checked, up to what height of DO the uniform heat flux can be obtained. In Figs. 4.5a-e, the DO model numbers 6-10 with model designations 441, 443, 445, 447 and 449, respectively, have been considered. In this, $l = w = 0.4$ m, with heights of the DOs are $h = 0.1$, 0.3, 0.5, 0.7 and 0.9 m, the estimated heat flux distribution is shown in Figs. 4.5a-e, respectively. For these 5 DO models also, the maximum deviation in estimated heat flux distributions is less than 3.0%, and so they are suitable to yield the uniform thermal conditions.

Figs. 4.6a-e, 4.7a-e, and 4.8a-e, shows the distributions of estimated heat flux on surfaces of the DO models having length and width $0.5\,\text{m} \times 0.5\,\text{m}$, $0.6\,\text{m} \times 0.6\,\text{m}$ and $0.8\,\text{m} \times 0.8\,\text{m}$, respectively, and their corresponding heights are 0.1 m, 0.3 m, 0.5 m, 0.7 m and 0.9 m, respectively. The quantitative details about the maximum deviation in estimated heat flux

on either side of the design heat flux, q^*_{DO}, are given in Table 4.1, while the heat flux distribution trends are shown in Figs. 4.6-4.8. Out of these 15 DO models, only for five models viz., 551, 553, 555, 661 and 881, the maximum deviation is found to be within acceptable range (< 3.0%). Thus the other DO models are not suitable for achieving the uniform thermal conditions.

4.2.1.1 Different uniform heat flux distribution on a 3-D design object

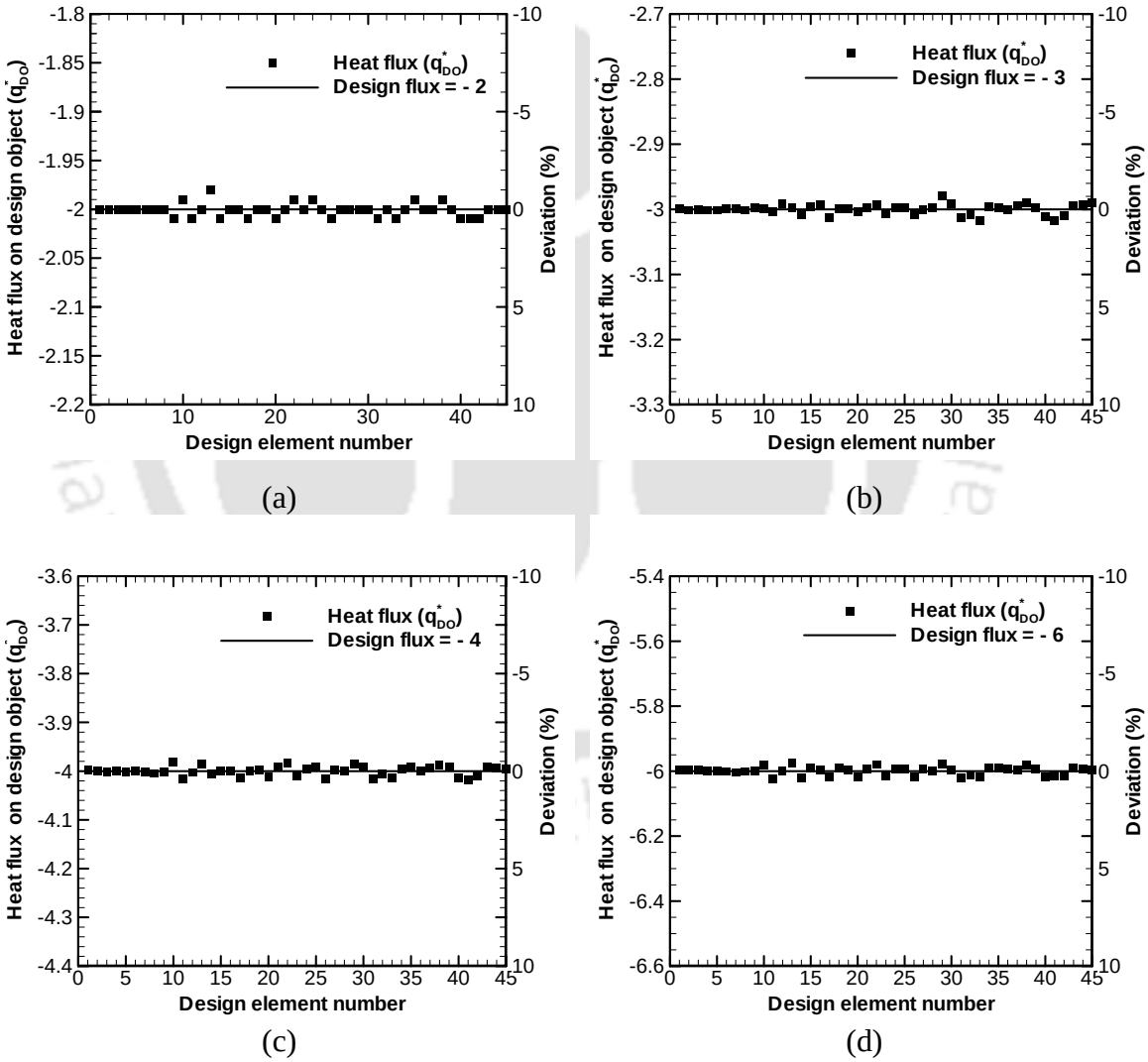

Figure 4.9. Different desired uniform heat flux distribution with fixed heater power range ($0.0001 \le q^*_H \le 4.0$), DO model 333.

For 25 DO models considered in Figs. 4.4-4.8, the suitability of the models was checked for the design uniform heat flux $q^*_{DO} = -2.0$. With the above settings, not all but only for 16 DO models the estimated heat flux distribution was in the acceptable range i.e. the maximum deviation < 3%. Next, keeping the design constraints (range of heater powers) fixed $\left(0.0001 \le q^*_H \le 4.0\right)$, the robustness of the present algorithm is checked through estimating the different values of the desired heat flux $\left(q^*_{DO}\right)$. This study is performed with a sample DO model 333. Four values of the desired uniform heat flux were chosen, viz., $q^*_{DO} = -2.0, -3.0, -4.0$ and -6.0. Results are shown in Figs. 4.9a-d. The maximum deviation for design flux values $q^*_{DO} = -2.0,\ -3.0,\ -4.0$ and -6.0 is found to be 1.4%, 1.3%, 0.9%, 0.81%, respectively. Like before, all the deviations are less than 3%. The results of this sample study are evident that using the present optimization algorithm, one can handle different desired values of uniform thermal conditions on a 3-D DO.

4.2.1.2 Effect of different design constraints (heater power range)

In previous cases, the optimal heater power setting has been estimated with fixed design constraints $\left(0.0001 \le q^*_H \le 4.0\right)$ on the power of the panel heaters. In this study, for a sample DO model 443, the boundary design problems are studied using 4 different design constraints, viz. 0.0001-2.0, 0.0001-4.0, 0.0001-8.0 and 0.0001-16.0. Using the given design constraints, the estimated heat flux distribution on the DO are shown in Figs. 4.10a-d. With the desired heat flux distribution is $q^*_{DO} = -2.0$, for the four cases, the corresponding deviations are found to be 1.05%, 1.25%, 1.6% and 1.30%, respectively. It is seen that for any of the range of the panel heaters the present algorithm works well. This finding is in the expected line of the trend in the optimization problems, relaxing the constraints on the unknown parameters gives the better estimation. This also implies the robustness and applicability of the present algorithm (REM^2 + MGA).

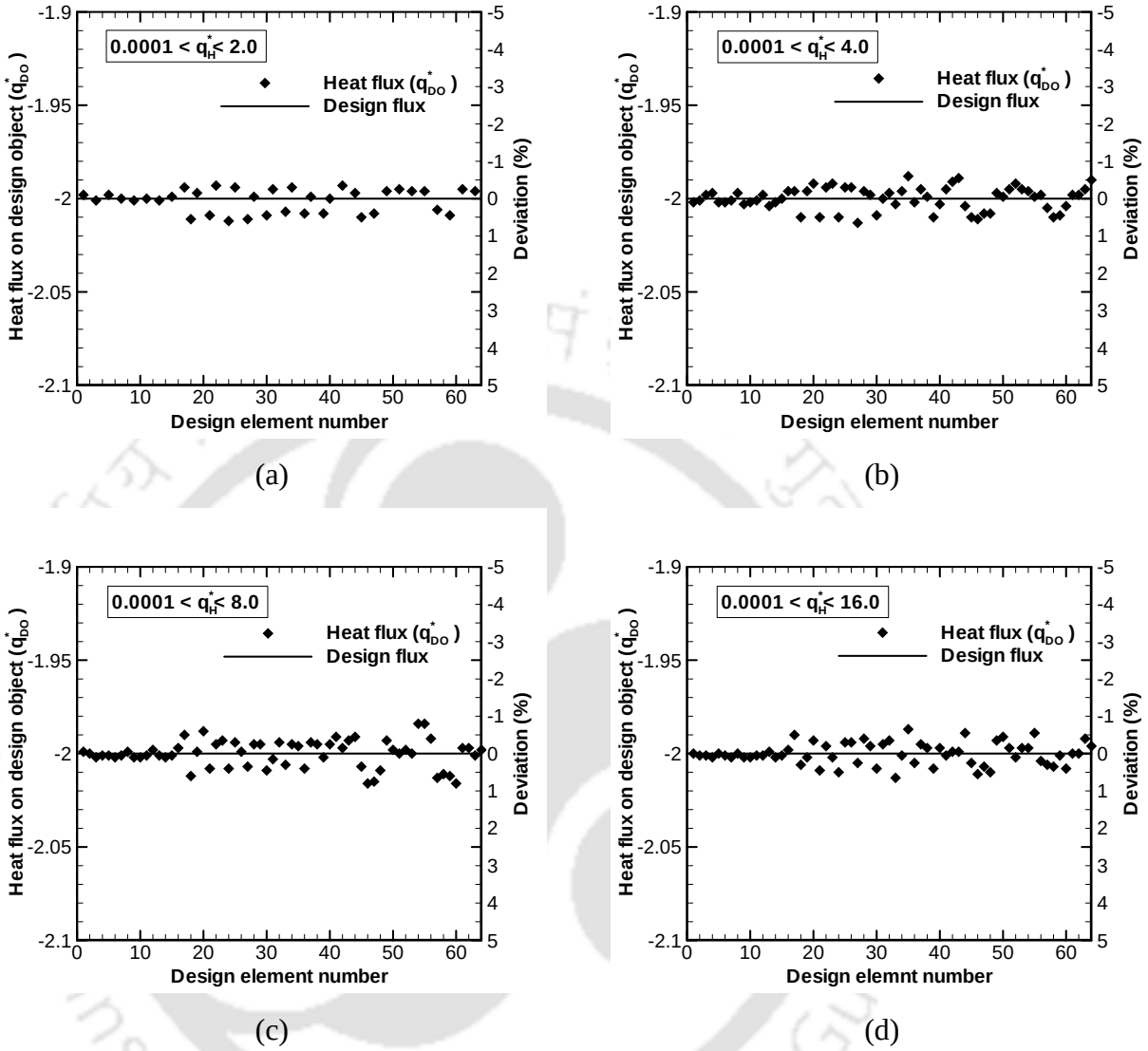

Figure 4.10. Estimated heat flux distribution on the surfaces of DO, model 443, for different ranges of power of the heaters.

.

4.2.1.3 Optimal heater power distribution: A sample results

It has been mentioned before that on each of the 5 walls of the radiant furnace, 100 panel heaters are considered. These panel heaters operate in a given particular power range. For a given model, to achieve the uniform thermal conditions on its surfaces, is that all heaters have to have the power or can some even be neglected? The objective is to get

the uniform heat flux distribution; it would be interesting to see the distributions of power of the panel heaters.

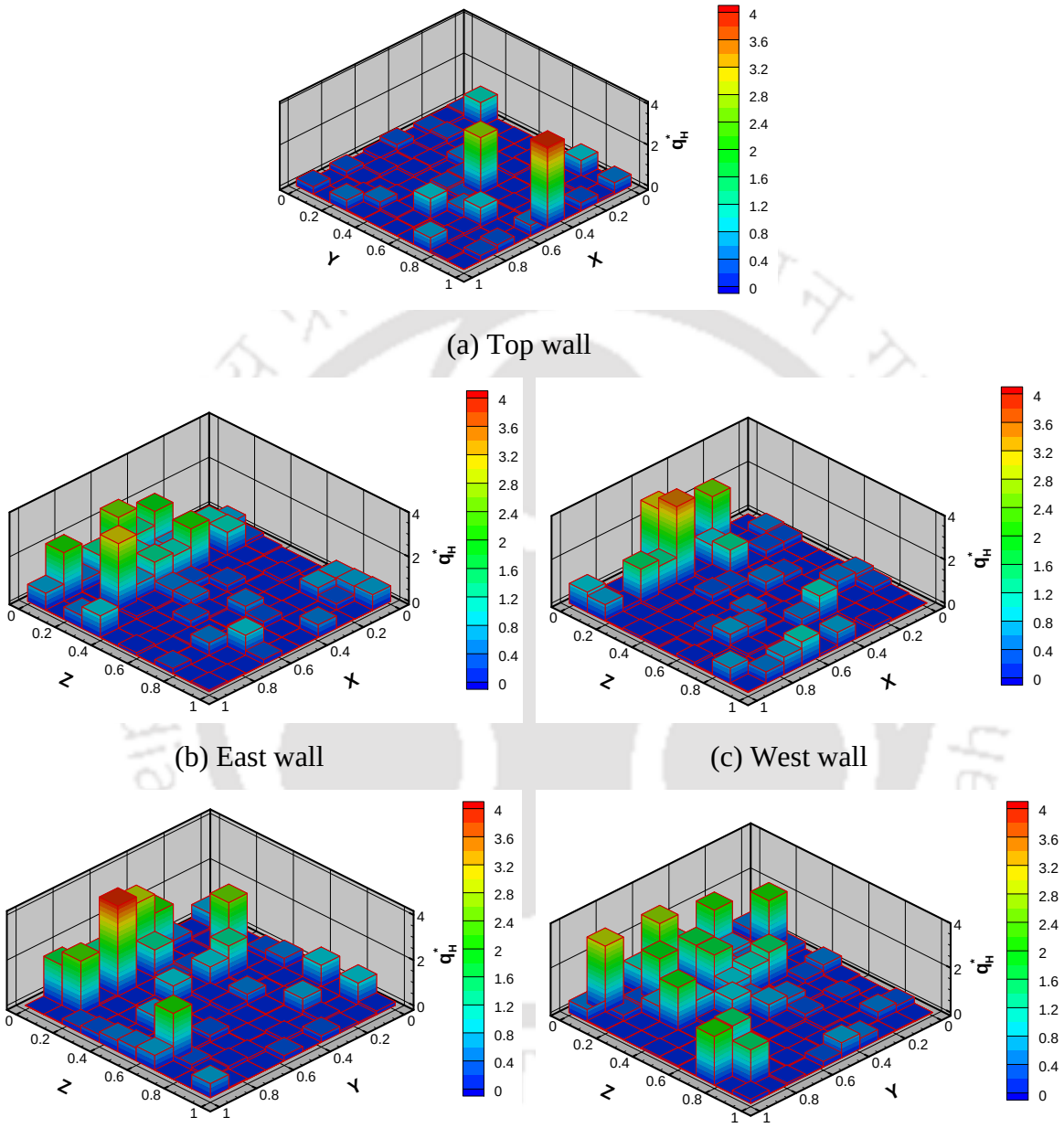

Figure 4.11. Optimal heater power distribution along the enclosure walls for a DO model 553, (a) top wall (b) east wall (c) west wall, (d) back wall, (e) front wall, ($0.0001 \le q^*_H \le 4.0$).

For this a sample study has been taken up with the DO model 553 and with dimensionless heater power range 0.0001 to 4.0 $\left(0.0001 \le q_H^* \le 4.0\right)$. It is to be noted that for the DO model 553, we have obtained the uniform thermal condition (Fig. 4.6b). The distributions of power of the panel heaters on top, east, west, back and front walls are given in Figs. 4.11a-e, respectively. It is seen from Fig. 4.11a-e that on each of the five walls, for only few (5 to 15) heater elements the considerable power is needed. The remaining heaters need very less power (< 1% of the rated power), so in the final design the inactive heater elements need not to be placed. In the present work, even though for the numerical experiments, 500 heater elements were considered, this does not mean that 500 heaters are actually needed. This is what has been demonstrated.

4.2.1.4 An experimental study on the present boundary design problems

To have an idea of implementation of the present numerical results in practical application, the simple experiments have been conducted using the model of 3-D radiant furnace with 3-D DO. In the present experimental work two cases from section 4.2.1, with DO models 553 $(\text{dimensions}: 0.5\,\text{m} \times 0.5\,\text{m} \times 0.3\,\text{m})$, and 333 $(\text{dimensions}: 0.3\,\text{m} \times 0.3\,\text{m} \times 0.3\,\text{m})$ are studied separately. The difference between the numerically computed heat flux distribution and that of from calculated from experimental results have been analyzed. The experimental work is done at the heat transfer laboratory, Institute of Fluid Sciences, Tohoku University, Sendai, Japan. Due to the differences in the numerical and experimental parameters such as, the material properties, working environment and energy losses, the experimental results are found deviating from the numerical results. The average difference is found 30%. On the positive side the trends of experimental values are matching with the numerical results. Since the experimental study is not the main aim of the thesis, it goes as additional information in Annexure-1. The exact simulation of the experiments can be a scope for future work. The detail of the experiments, fabrication of experimental setup, experiment procedure, and the results analysis is given in Annexture-1.

This work provides a guideline for the design of a radiant furnace for producing the desired uniform thermal conditions on 3-D DO, and to ascertain the limitation on the size of the product to be heated with respect to the size of the furnace enclosure. Further, for the given dimensions of radiant furnace, for a given size of the model, in precise control of thermal conditions on the DOs, this study thus gives an exact idea of the configuration and the power settings of the boundary heaters.

4.2.2 Study 2 - On the location of 3-D DO for uniform thermal conditions

In introduction section, it is seen that for yielding the specific thermal conditions on the DO, along with the other parameters locations and power of the panel heaters, location of the DO are need to be properly accounted. It is obvious that in a 3-D radiant furnace, for desired uniform thermal conditions on the DO placed on the bottom of furnace, it cannot be placed anywhere. Thus, with other parameters fixed, it is equally important to know the possible locations where a DO can be placed, and what are the effects of different locations.

In this study, for desired uniform thermal conditions, suitability of the locations for 3-D DOs $\left(\text{dimension: } l \times w \times h\right)$ along the bottom surface of a cubical radiant furnace $\left(\text{dimensions: } L = W = H = 1.0 \text{ m}\right)$ (refer Fig. 4.1) has been investigated. The radiative information is computed using the REM^2 and the objective function Eq. (3.24) is minimized using the MGA. The uniform dimensionless temperature $\left(T^*_{DO} = 1.0\right)$ and heat flux distribution $\left(q^*_{DO} = -2.0\right)$ on the surfaces of DO are the desired thermal conditions.

In this study too, for calculating the radiative information using the REM^2, inner surfaces of the furnace enclosure and the surfaces of the DO are divided into equal size $\left(0.1\text{m} \times 0.1\text{m}\right)$ surface elements. The DO is irradiated by the panel heaters placed along the five walls of the furnace enclosure. The emissivity of heater elements, refractory walls, and surfaces of the DO is 0.9, 0.3 and 0.6, respectively.

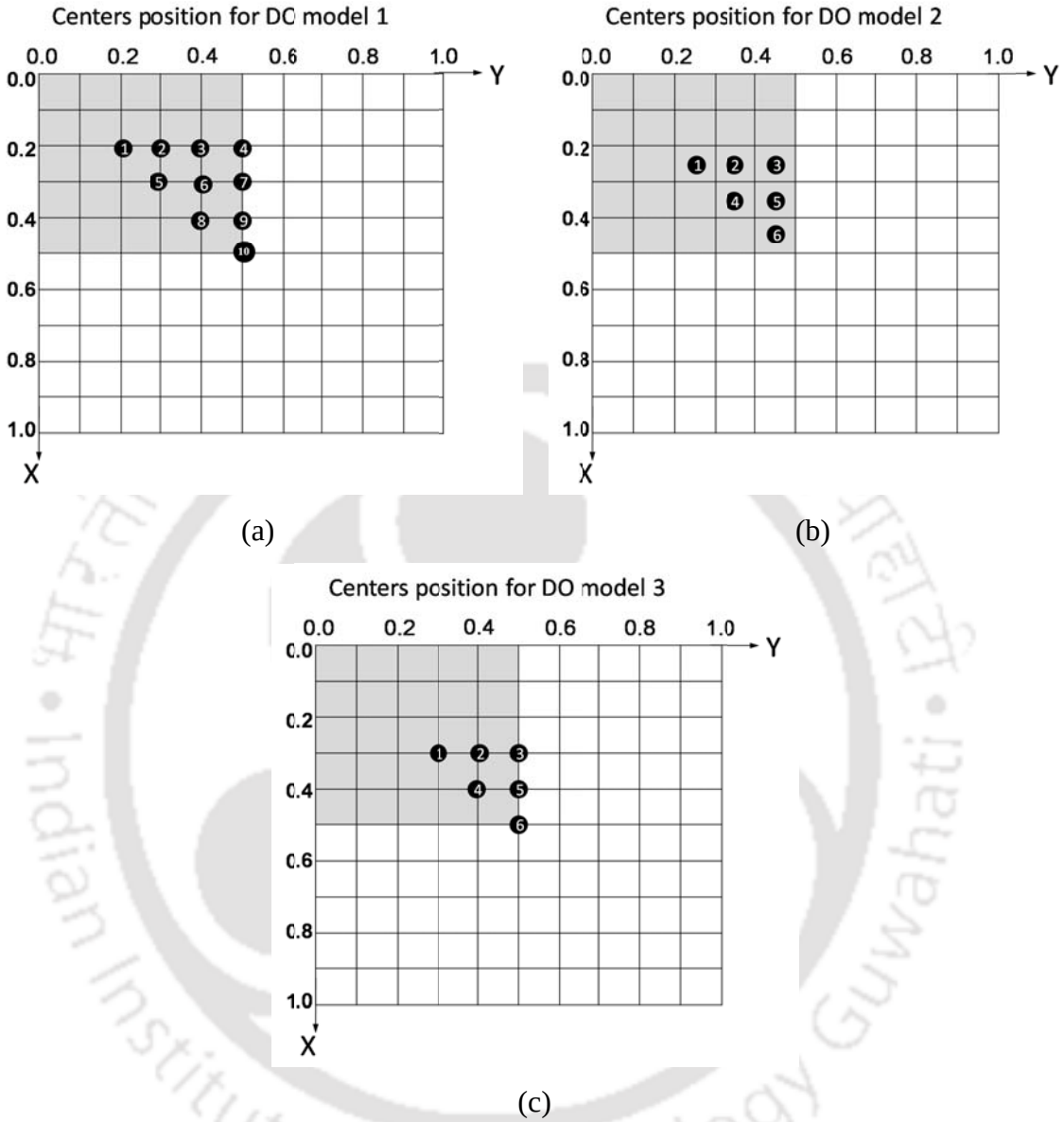

Figure 4.12. Schematic of locations of the DOs in a quadrant of the bottom surface of the radiant enclosure, for three DO models, dimensions: (a) $(l = w = h = 0.2\,\mathrm{m})$, (b) $(l = w = h = 0.3\,\mathrm{m})$, (c) $(l = w = 0.4\ \mathrm{m},\ h = 0.2\,\mathrm{m})$.

With panel heaters considered along the five walls of the furnace, for a given size of the DOs, study has been made for different locations (Fig. 4.12a-c) which cover the maximum possible area on the bottom of the furnace. Since the furnace is cubical, and the same types of panel heaters are placed along the five walls, for the purpose of comparison, $1/4^{th}$ of the area (one quadrant) of the bottom surface is good enough to select the diverse locations. For the 3 DO models, 10 locations for model- 1 $(\text{dimensions: } 0.2\text{ m} \times 0.2\text{ m} \times 0.2\,\text{m})$, and 6 locations each for model- 2 $(\text{dimensions: } 0.3\,\text{m} \times 0.3\,\text{m} \times 0.3\,\text{m})$ and model- 3 $(\text{dimensions: } 0.4\,\text{m} \times 0.4\,\text{m} \times 0.2\,\text{m})$ are considered. The locations are schematically shown in Figs. 4.12a-c. In Table 4.2, for 3 sizes of the DO, 22 cases with different locations of the DOs are listed. For better understanding and to interpret the results, a numerical designation of the surface elements of the DO will be helpful, and for a sample DO (model 3) having dimensions $(0.4\,\text{m} \times 0.4\,\text{m} \times 0.2\,\text{m})$, the same are shown in Fig. 4.13. For all the 22 cases, a similar numerical designation is followed. Since the surfaces of DO are divided into square elements $(0.1\text{m} \times 0.1\text{m})$, as the dimensions of the DO change, the number of surface elements on a DO changes accordingly, while the elements on the five walls of the radiant furnace, except bottom surface (insulated area) is fixed, because the furnace dimensions are fixed.

Being understood from Fig. 4.3 that 100 heaters along the top walls are not sufficient to estimate desired uniform thermal conditions on a 3-D DOs, hence the heaters along the five walls (500 panel heaters) of the radiant furnace, viz., top, back, front, west and east walls are considered.

			Insulated surfaces						
			1	**2**	**3**	**4**			
			5	**6**	**7**	**8**			
			9	**10**	**11**	**12**			
			13	**14**	**15**	**16**			
			Insulated surfaces						

(a) bottom surface of the enclosure with top face of design object

18	**20**	**22**	**24**
17	**19**	**21**	**23**

(b) back face of design object

26	**28**	**30**	**32**
25	**27**	**29**	**31**

(c) front face of design object

40	**39**	**38**	**37**
36	**35**	**34**	**33**

(d) West face of design object

48	**47**	**46**	**45**
44	**43**	**42**	**41**

(e) East face of design object

Figure 4.13. Numerical designation of surface elements on 3-D DO $(l = 0.4 \text{ m},\ w = 0.4 \text{ m},\ h = 0.2 \text{ m})$, located on the bottom of the cubical enclosure (refer Fig. 4.12).

4.2.2.1 Suitability of the locations for 3 DO models

The study has been made for 22 cases (Table 4.2) that represent the maximum possible locations for 3 DO models. Each case is considered an independent inverse boundary design problem. In the optimization process, using the MGA with 10 population size 1000 generations are evaluated. Constraints on the dimensionless heater power was kept as 0.0001 - 4.0.

Table 4.2. Variation in deviation in estimated heat flux and the minimum objective function value for the design objects at different locations.

Design object size $(l \times w \times h)$	Case No.	Center co-ordinates of design object	Minimum objective function value	Maximum deviation in estimated heat flux (%) on	
				lower side	upper side
0.2×0.2×0.2	1	(0.2, 0.2, 0.0)	0.00241	1.150	1.100
	2	(0.2, 0.3, 0.0)	0.00204	1.200	1.150
Model- 1	3	(0.2, 0.4, 0.0)	0.00127	0.800	0.750
	4	(0.2, 0.5, 0.0)	0.00126	0.800	0.700
	5	(0.3, 0.3, 0.0)	0.00096	0.600	0.650
	6	(0.3, 0.4, 0.0)	0.00130	0.650	0.700
	7	(0.3, 0.5, 0.0)	0.00070	0.550	0.650
	8	(0.4, 0.4, 0.0)	0.00085	0.550	0.550
	9	(0.4, 0.5, 0.0)	0.00078	0.550	0.500
	10	(0.5, 0.5, 0.0)	0.00039	0.500	0.400
0.3×0.3×0.3	11	(0.25,0.25 0.0)	0.02642	2.150	3.900
	12	(0.25,0.35 0.0)	0.02095	1.650	2.800
Model- 2	13	(0.25,0.45 0.0)	0.00535	1.000	1.350
	14	(0.35,0.35 0.0)	0.00430	0.900	1.400
	15	(0.35,0.45 0.0)	0.00321	0.900	1.200
	16	(0.45,0.45 0.0)	0.00187	0.700	0.750
0.4×0.4×0.2	17	(0.3, 0.3, 0.0)	0.00914	1.700	1.150
	18	(0.3, 0.4, 0.0)	0.00513	1.050	1.150
Model- 3	19	(0.3, 0.5, 0.0)	0.00445	1.050	1.050
	20	(0.4, 0.4, 0.0)	0.00466	1.150	1.100
	21	(0.4, 0.5, 0.0)	0.00167	0.850	0.750
	22	(0.5, 0.5, 0.0)	0.00188	0.650	0.600

.

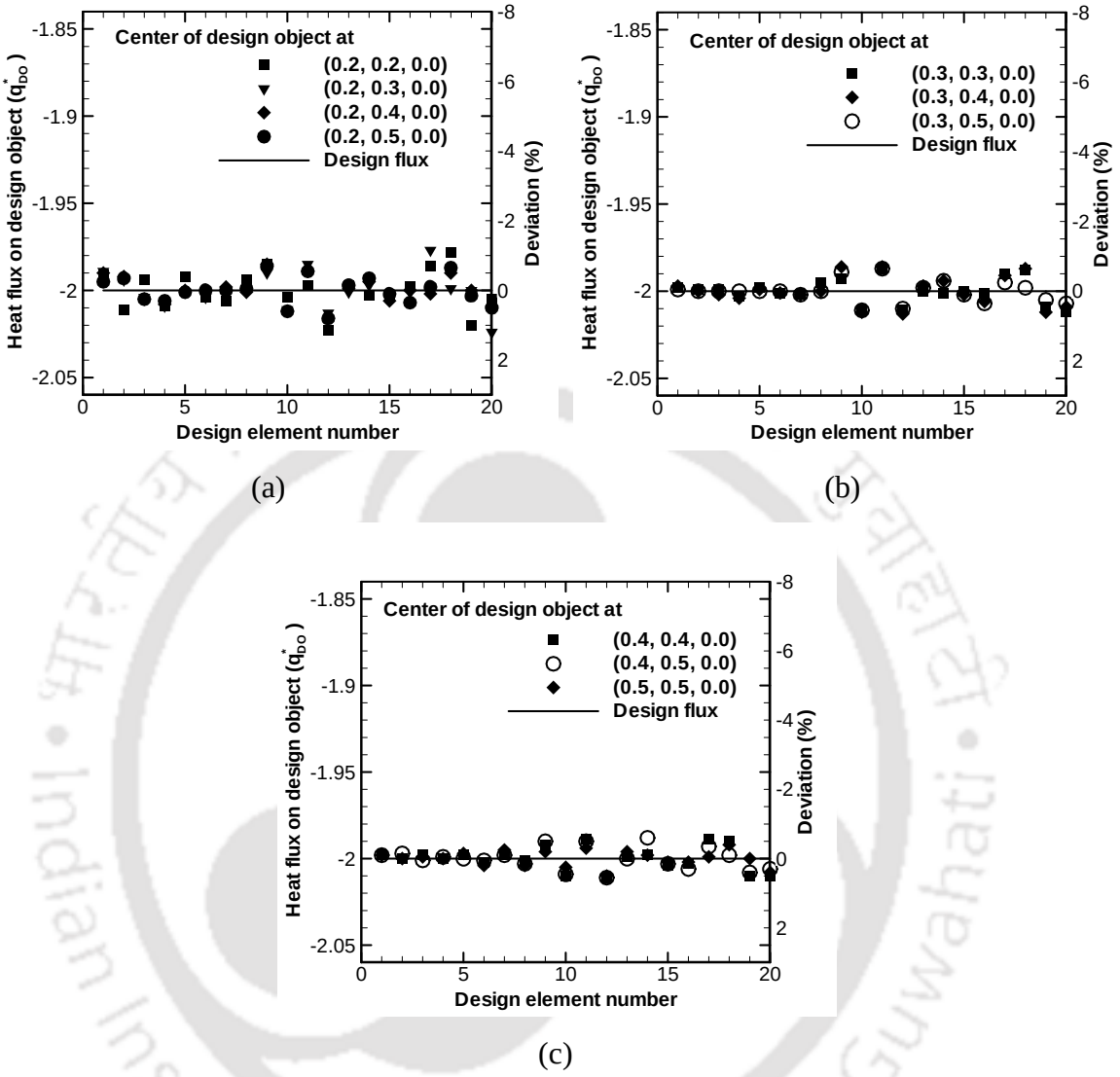

Figure 4.14. Estimated heat flux distribution on the surfaces of DO, (dimensions: $l = 0.2$ m, $w = 0.2$ m, $h = 0.2$ m) at 10 locations (Refer Fig. 4.12 a).

To have a better idea and to know how the 22 cases differ from one another, the coordinates of the 22 locations, (10 for model 1, 6 each for models 2 and 3) are given in Table 4.2 and their schematic locations on the bottom surface of furnace are shown in Figs. 4.12a-c. For the corresponding cases, Table 4.2 also contains the minimum value of objective function obtained after 1000 generations, and the maximum deviation in the estimated heat flux on either side. For a given DO, the suitability of a location is judged

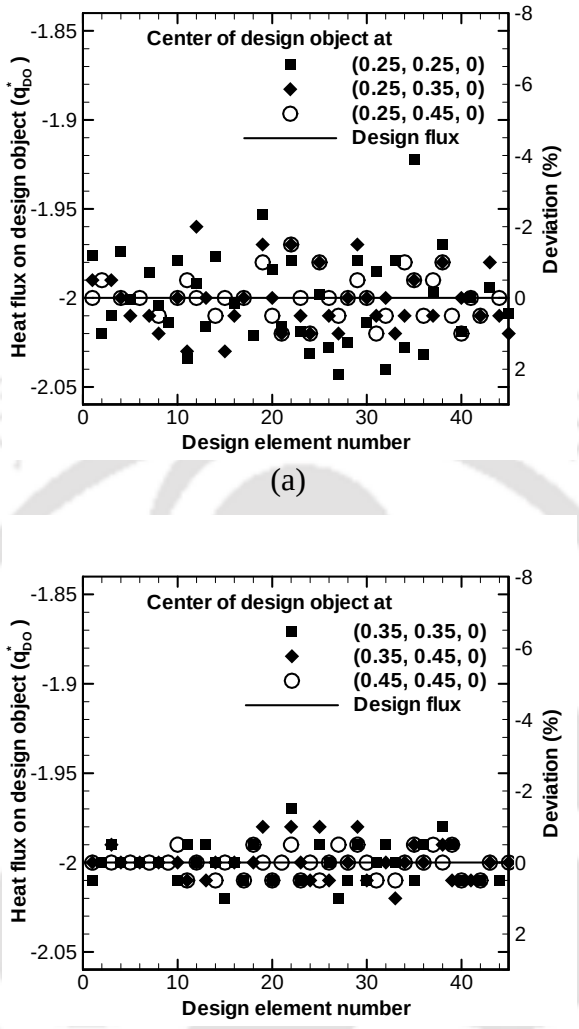

Figure 4.15. Estimated heat flux distribution on the surfaces of DO (dimensions: $l = 0.3$ m, $w = 0.3$ m, $h = 0.3$ m) at 6 locations (Fig. 4.12b).

by the amount of deviation in the estimated heat flux distribution from that of the desired one. Results for all the 22 cases given in Table 4.2 are shown in Figs. 4.14-4.16. Figs. 4.14a-c pertains to results of 10 possible locations of the DO model-1 $\left(\text{dimensions} = 0.2 \text{ m} \times 0.2 \text{ m} \times 0.2 \text{ m}\right)$, while Figs. 4.15a-b and 4.16a-b, deals with that of DO models-2 $\left(\text{dimensions} = 0.3 \text{ m} \times 0.3 \text{ m} \times 0.3 \text{ m}\right)$ and DO model-3 $\left(\text{dimensions} = 0.4 \text{ m} \times 0.4 \text{ m} \times 0.2 \text{ m}\right)$, respectively. For given size of the DOs and their

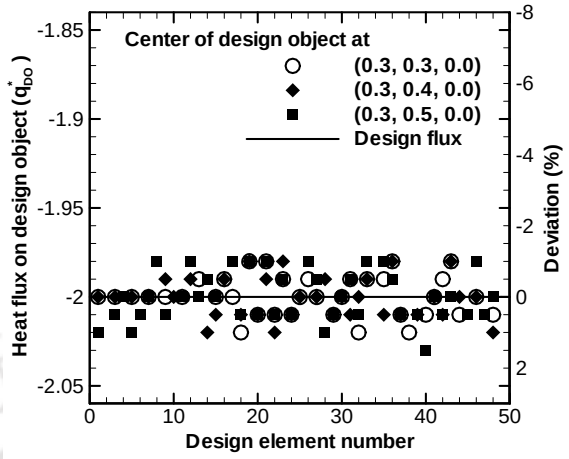

(a)

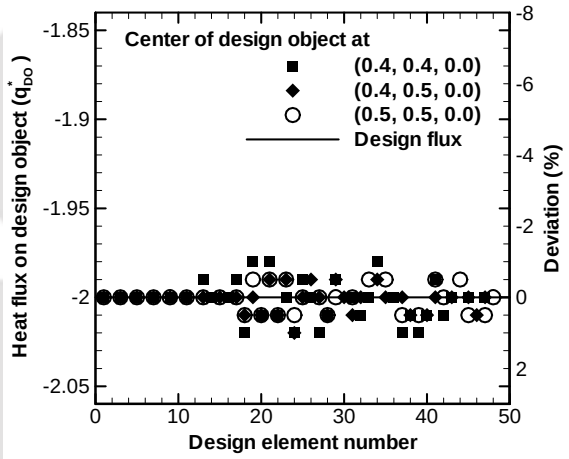

(b)

Figure 4.16. Estimated heat flux distribution on the surfaces of DO, (dimensions $l = 0.4$ m, $w = 0.4$ m, $h = 0.2$ m) at 6 locations (Fig. 4.12c).

22 chosen locations, for the sake of comparison, in Figs. 4.14 (for DO model-1), Figs. 4.15a-b (for DO model-2) and in Figs. 1.16a-b (for DO model-3) the ranges of ordinates are kept the same (-1.84 to 2.06). With dimensions of a surface element $(0.1\times 0.1\,\text{m})$, for DO model-1, the total number of surface elements is 20. Likewise, for DO models-2 $(\text{dimensions} = 0.3\,\text{m}\times 0.3\,\text{m}\times 0.3\,\text{m})$ and for DO model-3 $(\text{dimensions} = 0.4\ \text{m}\times 0.4\,\text{m}\times 0.2\,\text{m})$ the same are 45 and 48, respectively. Thus, for DO models 1, 2 and 3, abscissa ranges from 1 - 20, 1 - 45 and 1 - 48, respectively.

For DO model-1, results on suitability of 10 locations are shown in Figs. 4.14a-c. It is observed that the most accurate estimation of desired uniform heat flux (Fig. 4.14c) is obtained on the DO centered at (0.5, 0.5, 0.0) (Fig. 4.12a, location 10). However, for this DO model, at all 10 locations/cases, the maximum deviation is found less than 3%, and thus these locations are considered suitable for yielding uniform thermal conditions. For this DO model, for all 10 cases, the corresponding maximum deviations of estimated heat flux on the DO and the minimum value of the objective function are given in Table 4.2. It is to be noted that the 10 locations shown in Fig. 4.12a are in one quadrant. Thus, on the entire bottom area of the furnace enclosure, there are 30 other identical suitable locations.

Having found that for the DO model-1 $\left(\text{dimensions} = 0.2 \times 0.2 \times 0.2\,\text{m}\right)$, for uniform thermal conditions all the chosen locations are suitable, for next cases, we see the effect of changing the sizes of the DOs as DO model-2$\left(\text{dimensions} = 0.3 \times 0.3 \times 0.3\,\text{m}\right)$, and DO model-3$\left(\text{dimensions} = 0.4 \times 0.4 \times 0.2\,\text{m}\right)$. The results for DO model-2 and model-3 are shown in Figs. 4.15 and 4.16, respectively. Keeping the dimensions of the DOs and that of the furnace $\left(L = W = H = 1.0\ \text{m}\right)$ in mind, as mentioned before, in a quadrant for both the DOs the possible number of locations are 6. The same is shown in Figs. 4.12b and 4.12c.

From Figs. 4.15a and 4.15b, it is also observed that, as the height of the DO increases, compared to the results of the DO model-1 shown in Fig. 4.14a-c, the uniformity in the estimated heat flux deteriorates. The same can be quantitatively verified from the values of the deviations of estimated flux given in Table 4.2. For the DO model-2, considered in Figs. 4.15a and 4.15b, unlike model 1, in which all 10 locations are found suitable, in this case, only four (Fig. 4.12b, locations: 3-6) out of six locations are found suitable. For locations 1-2 in Fig. 4.12b, the deviation in the estimated heat flux distribution is found more than 3% and so assumed that not suitable for yielding the uniform thermal conditions. Since in case of DO model-3$\left(\text{dimensions} = 0.4\,\text{m} \times 0.4\,\text{m} \times 0.2\,\text{m}\right)$, even though the length and width are more than that of the model-2, since the height of the DO is less than that of the model-2, among all the six locations of DO model-3 (Fig. 4.12c),

the maximum deviation in the estimated heat flux distribution is found to be 2.85%. Therefore, all 6 locations (Fig. 4.12c) are found suitable for yielding the uniform thermal conditions.

From results given in Figs. 4.14- 4.16, it concludes that for uniform thermal conditions, all the locations are not suitable for a specific DO. With increase in height of the DO, constraints on their locations become more severe (model-2). This severity is comparatively less, when keeping the height fixed, the base dimensions of the DO are increased (model-3).

4.2.2.2 Optimal heater power setting for different locations of the DO

For a specific DO placed at a particular location suitable for the attainment of uniform thermal conditions, from the designer's point of view, it is important to know on what power which heaters will operate. This aspect is addressed through 3 diagonal locations for DO model-3 $\left(\text{dimensions: } 0.4\text{ m} \times 0.4\text{ m} \times 0.2\text{ m}\right)$. These 3 diverse locations are 1, 4 and 6 (Fig. 4.12c) having coordinates (0.3, 0.3, 0.0), (0.4, 0.4, 0.0) and (0.5, 0.5, 0.0), respectively.

For the chosen locations 1, 4, and 6, in Figs. 4.17-4.19, optimal power of the panel heaters have been shown along the 5 walls of the furnace. In these figures, sub-figures (a), (b), (c), (d) and (e), pertain to power of the heaters on top, east, west, back and front walls of the furnace. It is observed from Figs. 4.17-4.19 that the power of few panel heaters are comparable to the rated power and many of them require less than 1% of the rated power, in the practical applications these panel heaters can be neglected. The same trend is observed for all three selected locations of the DO. The effect of position of the DO does not appear significant in optimal heater power setting. Although for the purpose of design analysis, we have considered 500 panel heaters (100 on each wall), it is observed from Figs. 4.17-4.19 that for any of the three locations, not more than 30 heaters need to be placed. From these results, we can have the knowledge the numbers of

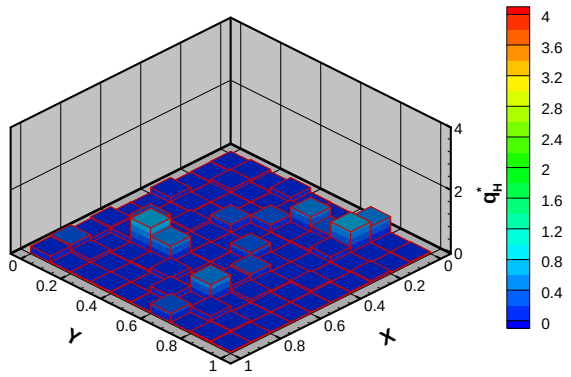

(a) Top wall

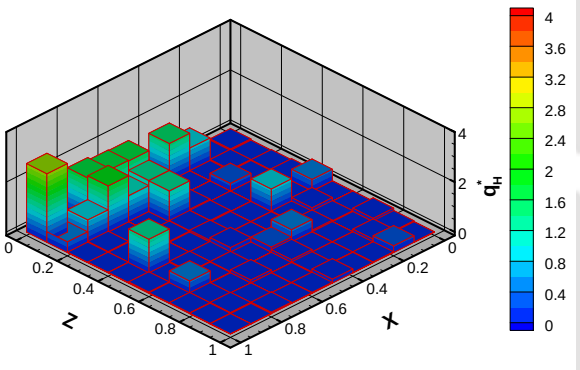

(b) East wall

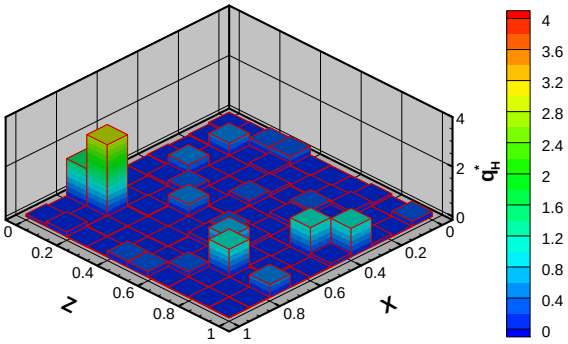

(c) West wall

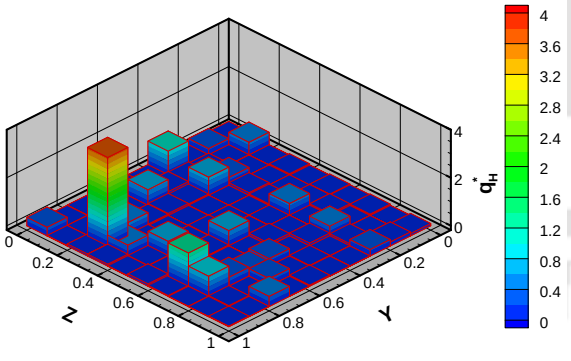

(d) Back wall

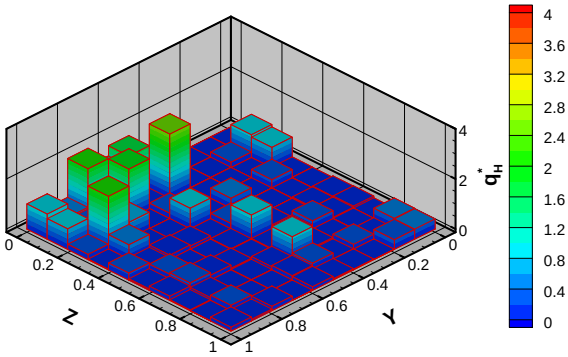

(e) Front wall

Figure 4.17. Optimal heater power distribution along the enclosure walls for a DO dimensions ($l = 0.4$ m, w=0.4 m, $h = 0.2$ m) located at (0.3,0.3,0.0).

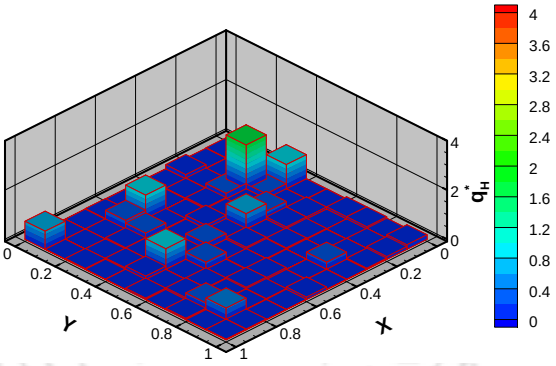

(a) Top wall

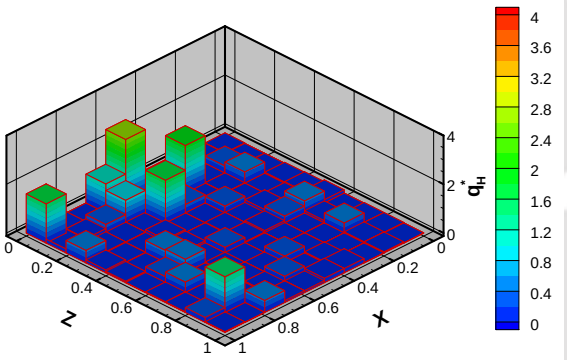

(b) East wall

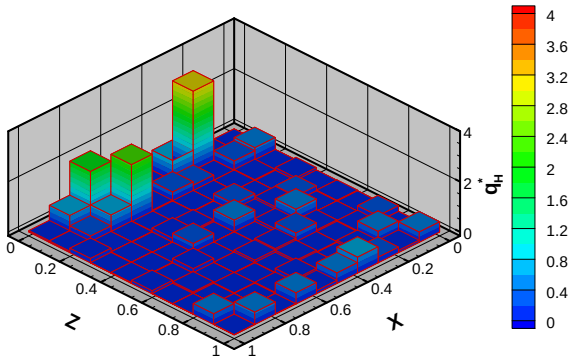

(c) West wall

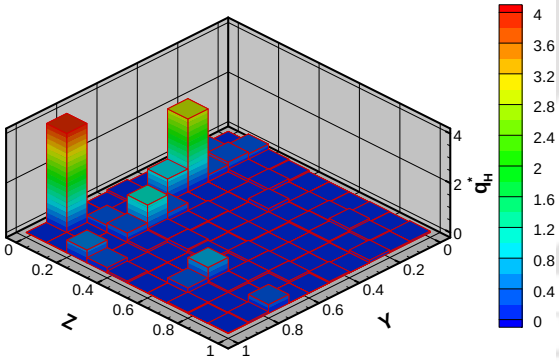

(d) Back wall

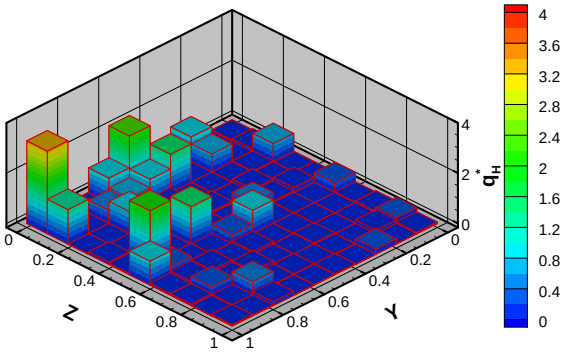

(e) Front wall

Figure 4.18. Optimal heater power distribution along the enclosure walls for a DO dimensions ($l = 0.4$ m, w=0.4 m, $h = 0.2$ m) located at (0.4,0.4,0.0).

.

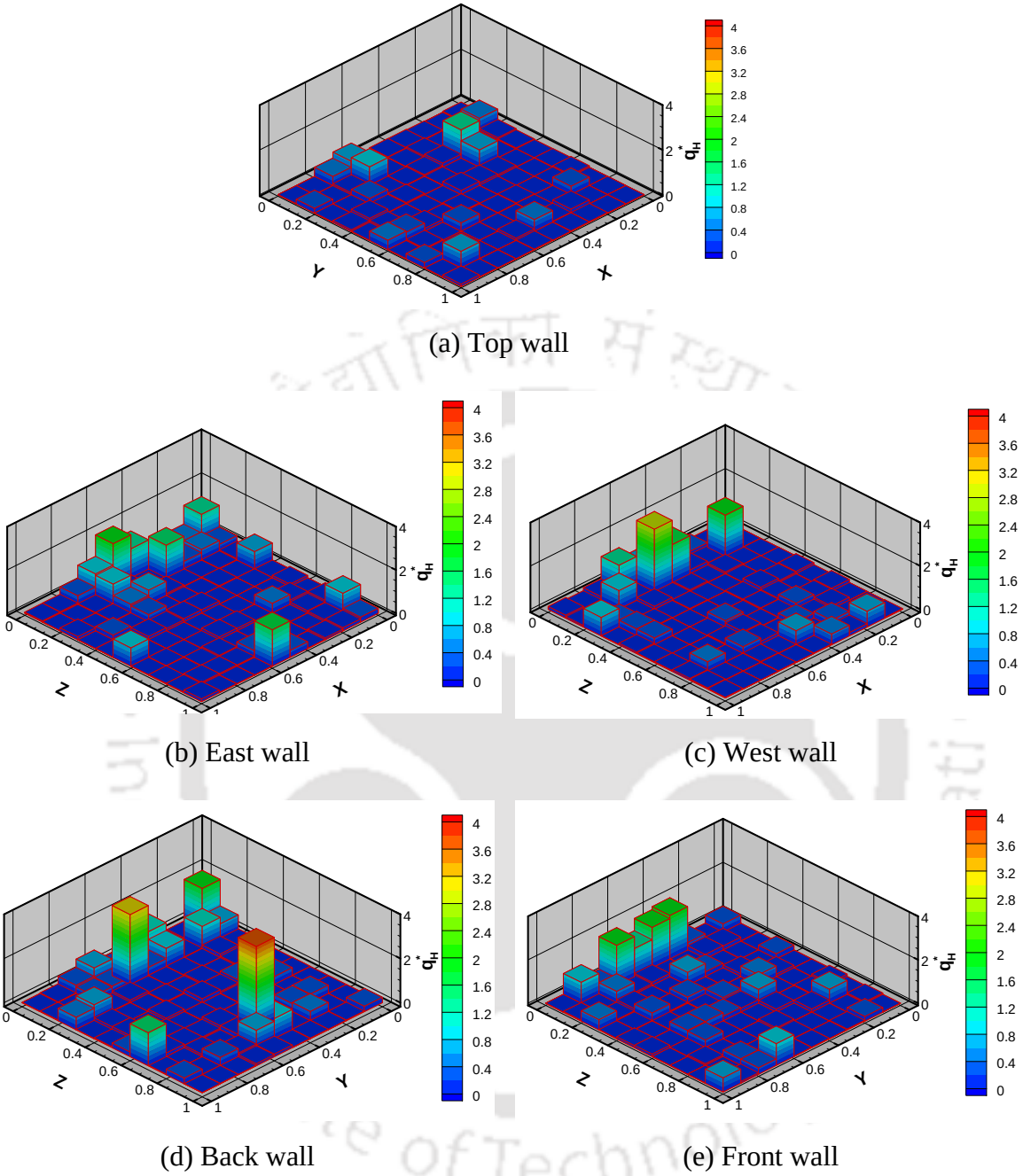

(a) Top wall

(b) East wall

(c) West wall

(d) Back wall

(e) Front wall

Figure 4.19. Optimal heater power distribution along the enclosure walls for a DO dimensions ($l = 0.4$ m, w=0.4 m, $h = 0.2$ m) located at (0.5,0.5,0.0).

heaters, their locations and the power on which they have to be operated to yield the uniform thermal conditions on the chosen DO, and for its particular location. This way

the manufacturers and the operators can know the required details a priori, for attainment of the uniform thermal conditions on the 3-D DO.

4.2.2.3 Effect of generations on objective function value

It is well known that, in the GA the accuracy of estimated parameters may improve with increase in number of generations [Das *et al.*, 2008]. In the present problem, this aspect has been demonstrated with the DO model-3 (dimensions: l= 0.4 m, w= 0.4 m, h = 0.2 m) placed at locations 1, 4 and 6 (Fig. 4.12c). These problems are studied for the different number of generation ranging from 1000 to 20000. The minimum objective function values after the chosen numbers of generations are shown in Fig. 4.20. It is observed that at all three locations, in initial 1000 generations decrease in objective function value is sharp, however, beyond that the rate of decrease (convergence) is so slow. Thus 1000 generations are appropriate. In the present work, all the runs were taken for 1000 generations. The linear relationship of CPU time and the numbers of generations is observed.

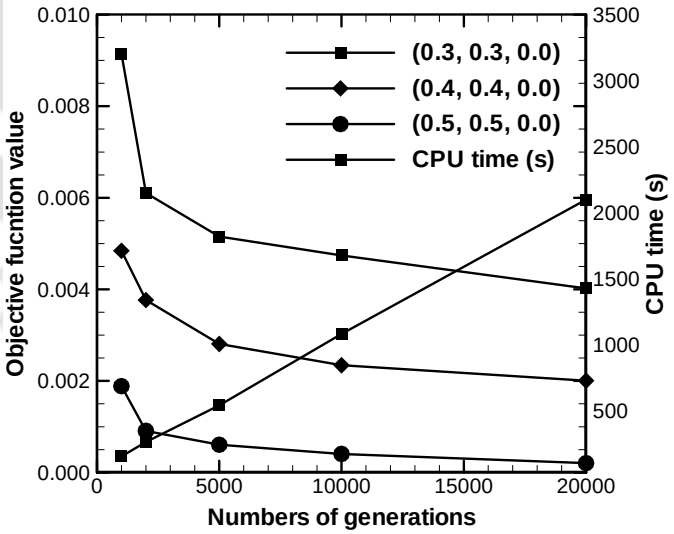

Figure 4.20. Effect of numbers of generations on the objective function value and CPU time for DO model-3 $(l = 0.4$ m, $w = 0.4$ m, $h = 0.2$ m$)$ at diagonal locations.

4.2.3 Study 3 - on configuration and numbers of multiple deign objects

In industrial heating processes, heating a single object/ product is not economically desirable. Towards this aspect this study aimed to design radiant furnaces that produce uniform thermal conditions on multiple 3-D DOs placed inside the furnace. For this, it becomes necessary to know, how many and with what configuration the DO should be located inside the enclosure. For uniform thermal conditions on the multiple 3-D DOs, in this study the suitable configurations (arrangements) of the DOs along the bottom of enclosure have been explored.

For the 3-D radiant furnace $\left(\text{dimensions: } L = W = H = 1 \text{ m}\right)$ and a DO $\left(\text{dimensions: } l = w = h = 0.2 \text{ m}\right)$, total 19 configurations with 2, 3, 4, 5, 6, 8 and 9 DOs are considered. The selected 19 cases are shown in Fig. 4.21a-s and their details are given in Table 4.3. The arrangement of the panel heaters along the walls of the furnace enclosure is same as shown in Fig. 4.1. For different cases, the numbers of surface elements on the DOs and the total surface elements are provided in Table 4.3. The adopted numerical designation of the surface elements on the DO for case 1 (Fig. 4.21a), is shown in Fig. 4.22. As the numbers of DOs changes, the number of surface elements of the DOs changes accordingly. Since, the dimensions of the furnace are fixed, except bottom surface (insulated area) the number of heater elements (500) on the five walls of the furnace remains constant.

In this study also the expected uniform thermal conditions on the surfaces of DOs are dimensionless temperature $\left(T^*_{DO} = 1.0\right)$ and heat flux distribution $\left(q^*_{DO} = -2.0\right)$. The optical properties of the heater surface, refractory wall and that of the DO are same as in previous two studies. From the section 4.2.1, it is understood that for desired uniform thermal conditions on a 3-D DO, for computation purpose, the panel heaters need to be considered along the five walls of the furnace, viz. top, back, front, west and east wall.

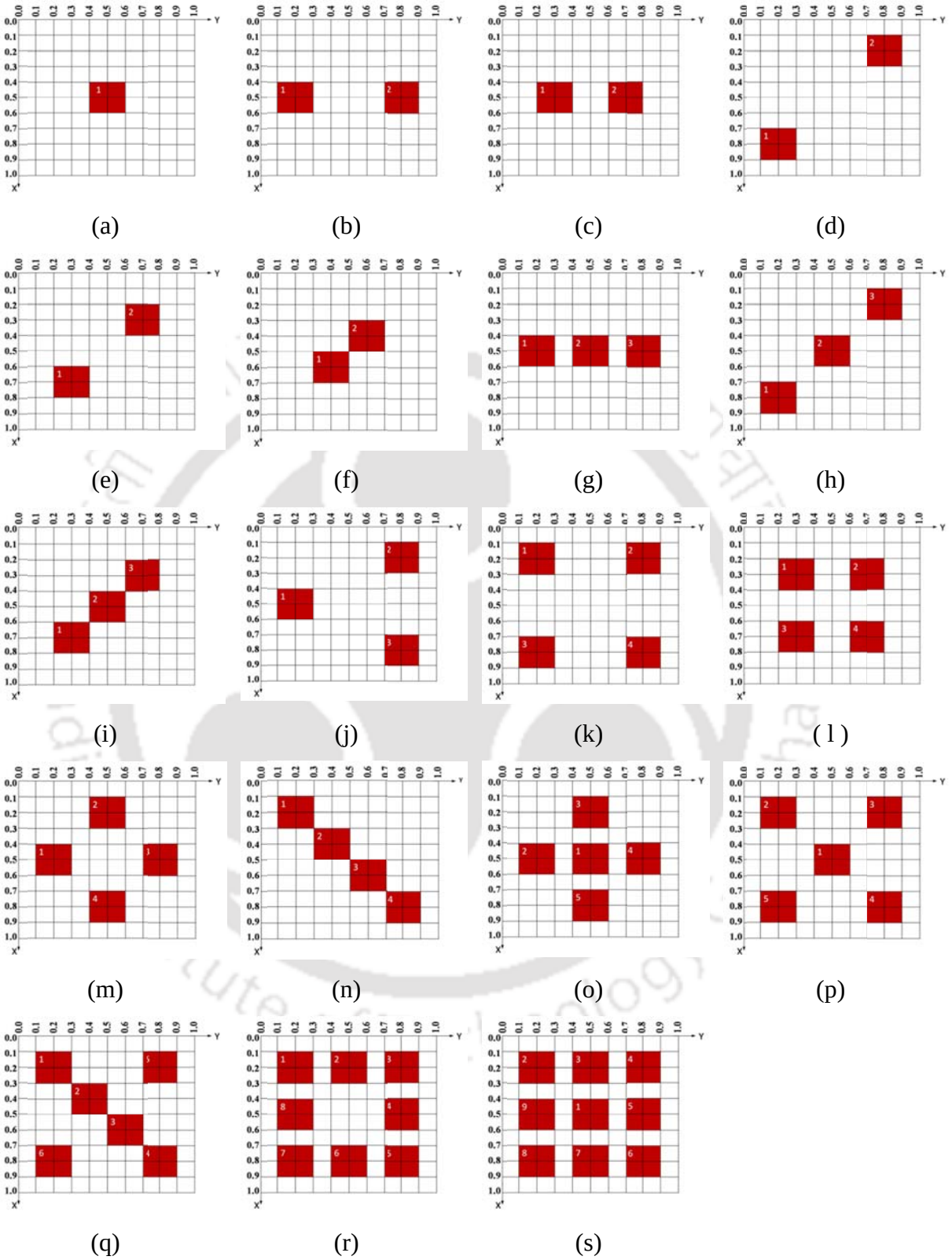

Figure 4.21. Configurations of 3-D design objects on the bottom of the radiant enclosure.

.

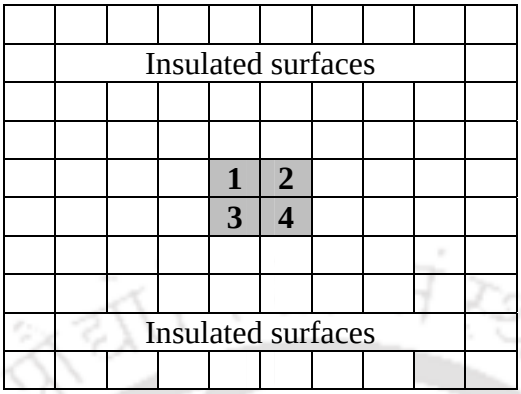

(a) bottom surface of the enclosure with top face of design object

6	**8**
5	**7**

(b) back face of design object

10	**12**
9	**11**

(c) front face of design object

16	**15**
14	**13**

(d) West face of design object

20	**19**
18	**17**

(e) East face of design object

Figure 4.22. Designation of surface elements on a centrally located DO ($l = w = h = 0.2$ m), on the bottom of radiant enclosure (Fig. 4.1).

4.2.3.1 Finding the suitable configuration of multiple DOs for uniform thermal conditions

Keeping the dimensions of the furnace enclosure fixed $\left(L = W = H = 1.0 \text{ m}\right)$ in the present study, for uniform thermal conditions the suitable configuration for different numbers of DOs are explored. The DOs are assumed to be irradiated from the heaters placed along the five walls of the radiant enclosure. The chosen possible arrangement of DOs shown in Figs. 4.21a-s, each case is treated as separate inverse boundary design problem. In every case the optimization is done using the MGA, with 10 population size 5000 generations are evaluated. In the computation, the constraints on the heater power $\left(q_H^*\right)$ was taken as 0.0001 – 4.0.

Table 4.3. Maximum deviation on estimated heat flux, minimum objective function value and CPU time for optimization for different configurations of the DOs.

Sr. No./ DO model number (Fig. 4.21)	No. of design objects	Number of surface elements		Maximum deviation in estimated heat flux on		Minimum objective function value	CPU time (sec)
		total	on design objects	lower side	higher side		
1/a	1	616	20	0.40	0.40	0.00024	521.32
2/b	2	632	40	2.85	4.25	0.0593	537.09
3/c	2	632	40	5.55	15.35	0.7346	535.34
4/d	2	632	40	0.75	1.30	0.0026	543.87
5/e	2	632	40	1.65	1.95	0.0104	542.46
6/f	2	632	40	5.70	14.10	0.5853	548.60
7/g	3	648	60	14.7	36.85	8.0170	553.93
8/h	3	648	60	34.6	54.975	15.9295	558.53
9/i	3	648	60	33.95	61.385	20.9119	558.87
10/j	3	648	60	2.70	2.80	0.0644	561.92
11/k	4	664	80	3.05	4.35	0.0739	578.00
12/l	4	664	80	14.10	16.20	3.5519	594.50
13/m	4	664	80	11.25	18.95	2.5278	581.37
14/n	4	664	80	9.45	12.10	1.3323	581.95
14/o	5	680	100	22.70	48.30	22.4009	617.10
16/p	5	680	100	7.40	5.45	0.3694	606.51
17/q	6	696	120	14.05	17.70	2.7901	620.34
18/r	8	728	160	30.70	39.05	32.5198	657.89
19/s	9	744	180	41.95	49.80	68.3119	698.43

In Table 4.3, the numbers of DOs $\left(\text{dimensions: } l = w = h = 0.2 \text{ m}\right)$, the surface elements on DOs and the total numbers of elements are listed corresponding to the configuration shown in Figs. 4.21a-s. The maximum deviation in estimated heat flux distribution on the

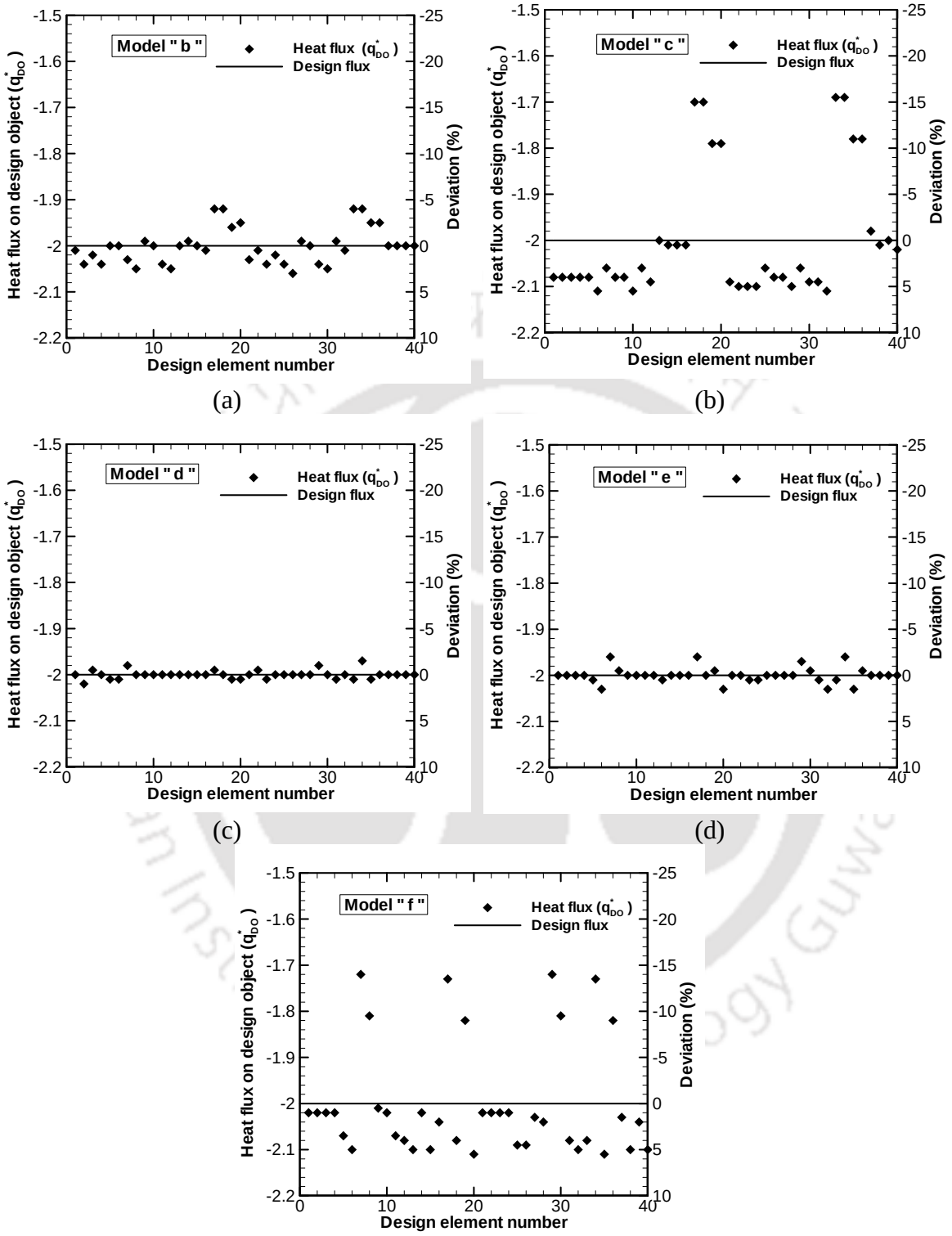

Figure 4.23. Estimated heat flux distribution on 2 DOs located with different configuration, (refer Fig. 4.21b-f).

DOs, minimum objective function value and the CPU time are given against the respective cases.

To have an in-depth analysis, for all the 19 cases, the element-wise distribution of estimated heat flux on surfaces of the DOs is shown in Figs. 4.23-4.27. The secondary Y-axis in each of the subfigures in Figs 4.23-4.27 shows the element-wise deviation of the estimated heat flux. In all the cases, the DOs are irradiated by heater elements located along the five walls of radiant furnace. The aim of this comparison is to show the variation in the estimated heat flux distribution and deviation from the desired uniform heat flux value $\left(q^{*}_{DO} = -2.0\right)$ for different configurations of the DOs. The alphabetical numbering of models/ cases is according to the configuration shown in Figs. 4.21a-s. For clarity and comparison, the range of ordinates is kept same, and for different models, plots have been shown separately.

With 2 DOs, the comparisons of estimated heat flux distributions for 5 different cases given Figs. 4.21b-f, are shown in Fig. 4.23a-e, respectively. It is observed from Figs. 4.23a-e that the estimation of heat flux distribution is the best (Fig. 4.23c) for the configuration of DOs shown in Fig. 4.21d. In this case (Fig. 4.23c), the maximum deviation is 2.05%. The next better estimated uniform heat flux distributions are found in Figs. 4.23a and 4.23d, which correspond to the configurations shown in Figs. 4.21b and 4.21e. For all 5 cases (Figs. 4.21b-f), the corresponding maximum deviations of estimated heat flux from the desired one, and the minimum values of the objective functions are given in Table 4.3. In the MGA, the minimum value of the objective function reflects the accuracy of estimated parameters. Smaller the value of the objective function, more accurate is the estimation. For the remaining two configurations, i.e., the cases shown in Fig. 4.21c and Fig. 4.21f, uniform thermal conditions are not obtained. For these two cases, the corresponding estimated heat flux distributions are shown in Figs. 4.23b and 4.23e. The deviations are observed to be much higher than the earlier three cases (configurations shown in Figs. 4.21b, 4.21d and 4.21e).

An observation of five configurations of 2 DOs shown in Figs. 4.21b-f, it is found that for the two cases (Figs. 4.21c and 4.21f), the distance between the DOs are less than that for the other three cases (Figs 4.21b, 4.21d and 4.21e). Further, among the three configurations (Figs 4.21b, 4.21d and 4.21e) in case of Fig. 4.21d in which the distances between the DOs are the maximum, the estimation of desired uniform heat flux is the best (Fig. 4.23c).

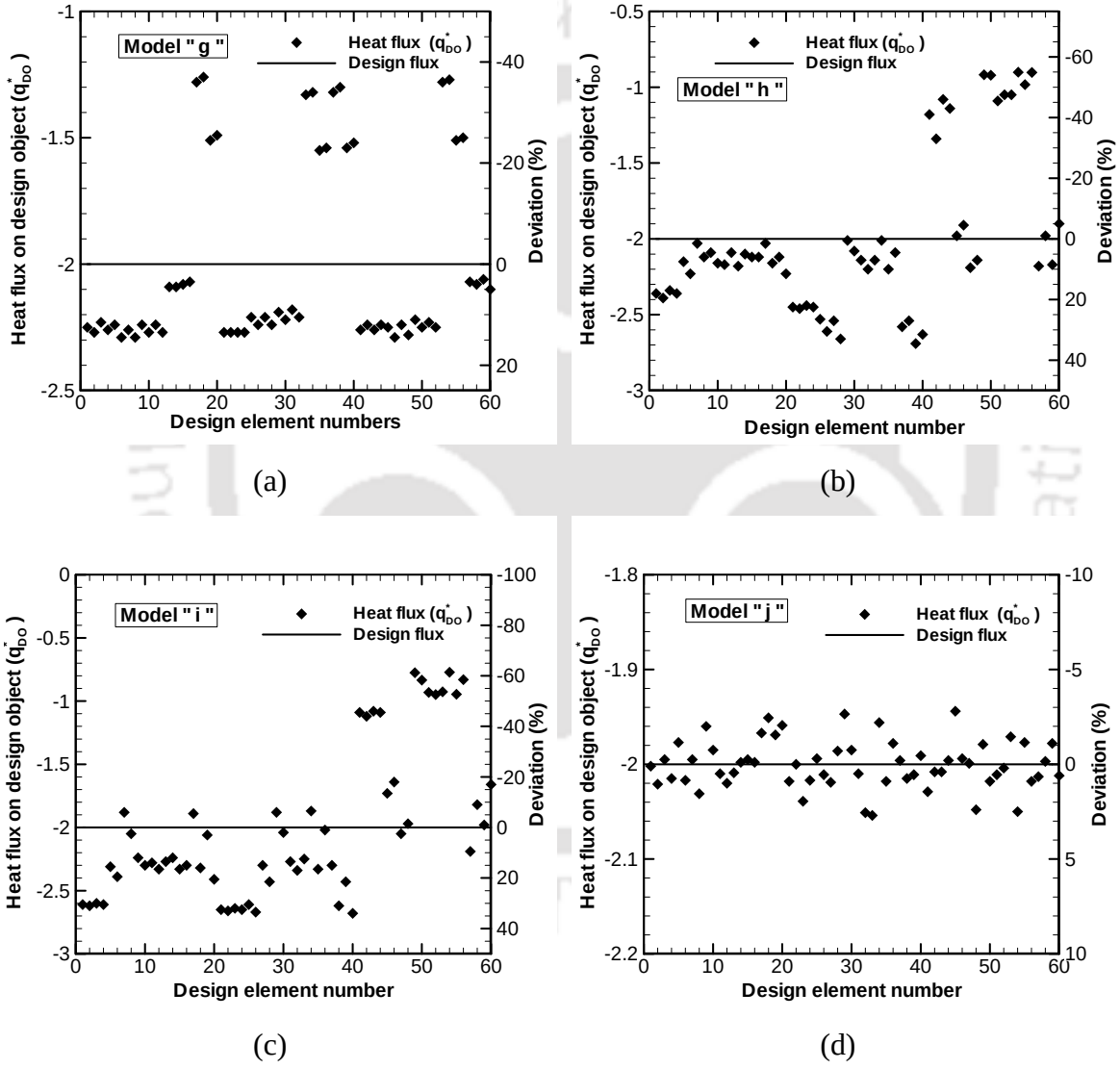

Figure 4.24. Estimated heat flux distribution on 3 DOs located with different configuration, (refer Fig. 4.21g-j).

Next, the cases with 3 DOs, the 4 chosen configurations are shown in Figs. 4.21g-j and their corresponding estimated heat flux distributions are shown in Figs. 4.24a-d, respectively. Among the 4 configurations (Figs. 4.21g-j), only one shown in Fig. 4.21j, estimated heat flux distributions is the best (Fig. 4.24d). It is to be noted that, in this case (Fig. 4.21j) the distances between the DOs are the maximum. In this case, the maximum deviation is 5.5%. For others, it is much more (Figs. 4.24a-c).

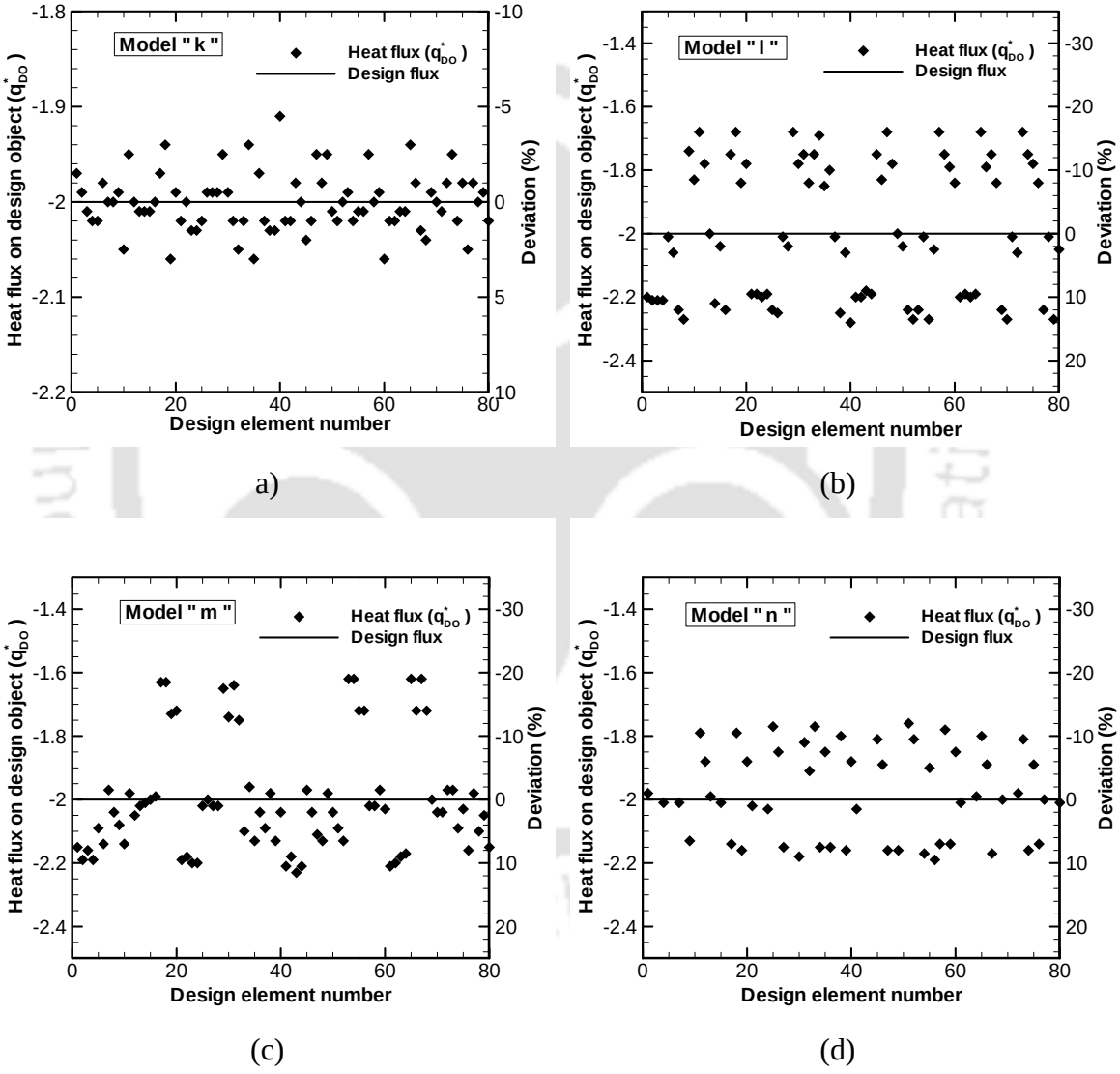

Figure 4.25. Estimated heat flux distribution on 4 DOs located with different configuration, (refer Fig. 4.21k-n).

Figures 4.25a-d show the estimated heat flux distribution for 4 cases given in Figs. 4.21k-n each with 4 DOs, respectively. Among the 4 cases, the configuration shown in Fig. 4.21k is found to provide the best estimation of heat flux distribution (Fig. 4.25a). In this case, the maximum deviation is 7.4%. Next, the two configurations with 5 DOs are considered (Fig. 4.2o-p). For these cases, estimated heat flux distributions are shown in Figs. 4.26a and 4.26b, respectively. Among these two, the configuration shown in Fig.4.21 gives relatively good result (Fig. 4.26b). The maximum deviations in the estimated heat fluxes for the cases shown in Figs. 4.21o and 4.21p are 71.0% and 12.85%, respectively.

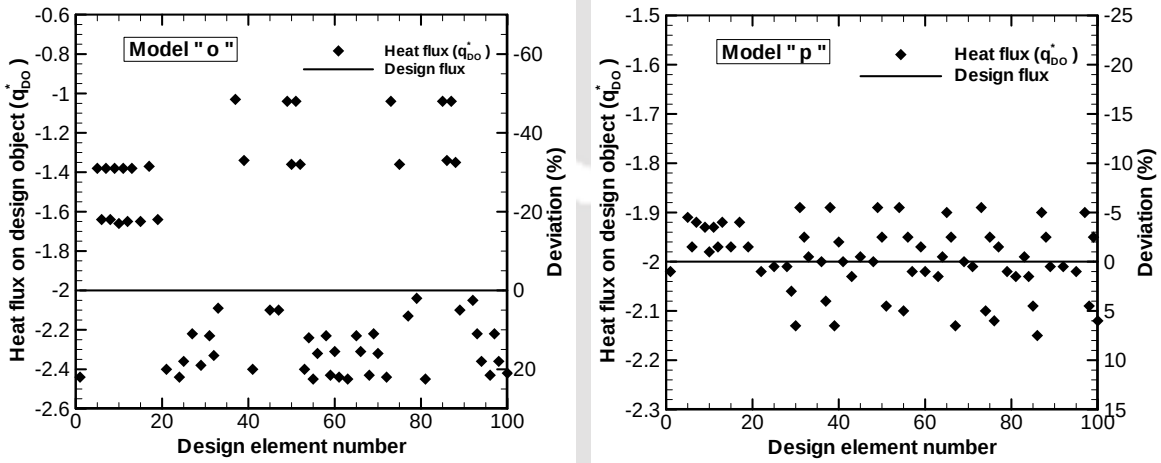

(a) (b)

Figure 4.26. Estimated heat flux distribution on 5 DOs located with different configuration, (refer Fig. 4.21o-p).

Similarly in Figs. 4.27a-c, the estimated heat flux distributions are shown for 6, 8, and 9 DOs, for which the configurations are shown in Fig 4.21q-s, respectively. The estimated heat flux distributions are found to go far off the desired one. The maximum deviations for configurations Fig. 4.21q-s are 31.75%, 69.75% and 91.75%, respectively.

An observations of Figs. 4.23-4.27 and Table 4.3 for the estimated heat flux distributions for 7 cases with case 1 with 2 DOs having 5 configurations (Figs. 4.21b-f) , case 2 with 3 DOs having 4 configurations (Figs. 4.21g-j), case 3 with 4 DOs having 4 configurations

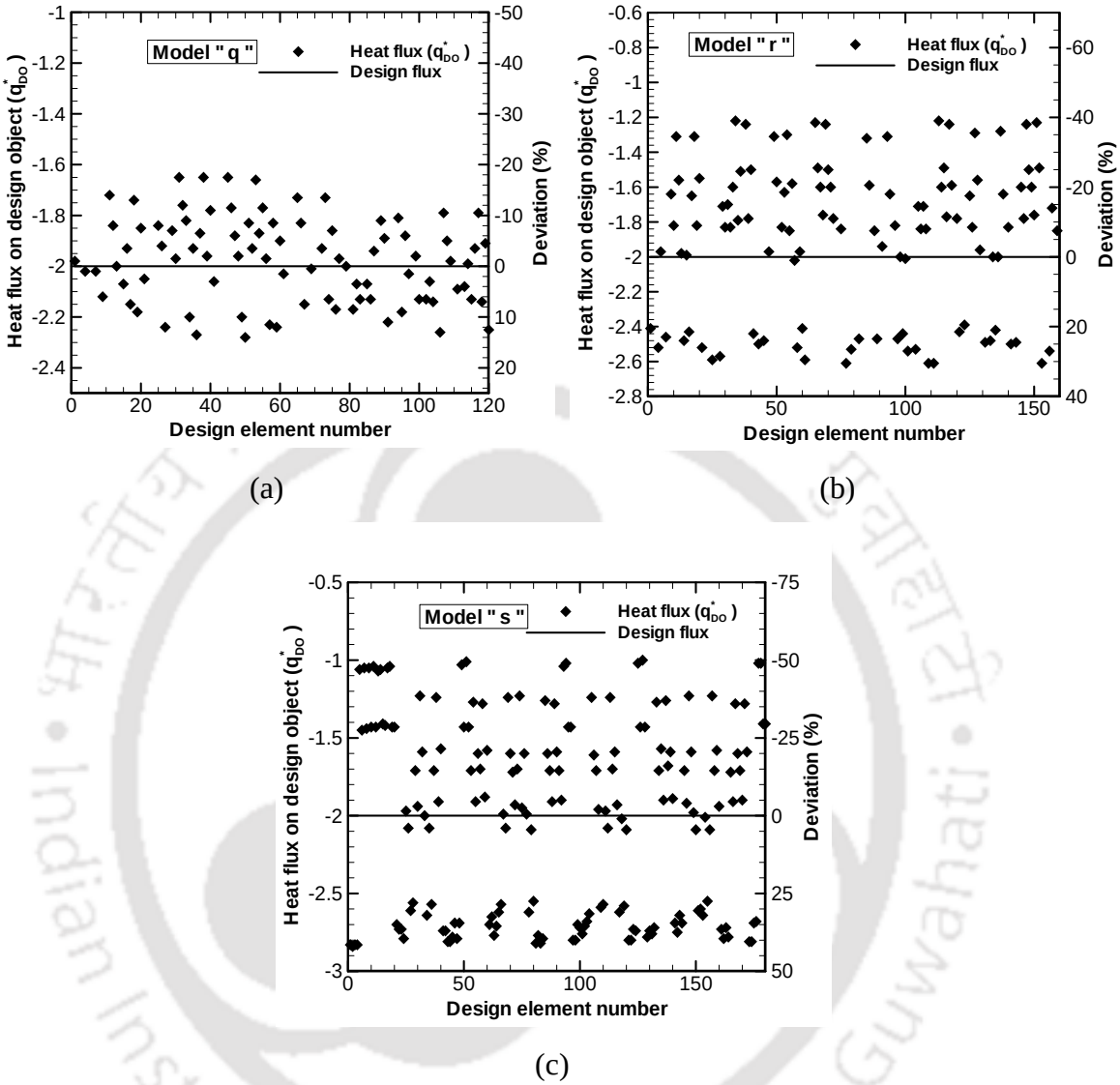

Figure 4.27. Estimated heat flux distribution on 6, 8 and 9 DOs located with configuration shown in Fig. 4.21q-s.

(Figs. 4.21k-n), case 4 with 5 DOs having 2 configurations (Fig. 4.21o and p) and cases 5-7 (Figs. 4.21q-s) with 6, 8 and 9 DOs, it is found that for a given number of DOs, all configurations do not yield the same results. The uniformity in the estimated heat flux distribution deteriorates as the numbers of DOs increases. For example, in case 1 with 2 DOs, the maximum deviation in the estimated heat flux was 2.05%, the same in case 2 with 3 DOs, case 3 with 4 DOs and case 4 with 5 DOs were 5.5%, 7.5% and 12.85,

respectively. For a given number of DOs, the higher the distance between the DOs, better the estimated heat flux distributions. A further observation of this study reveals that compared to the top surface of the DO, getting the uniform heat flux on the vertical surfaces of the DO is difficult, and in case of multiple DOs, as shown in the present work, the number of the DOs and the specific configuration further add to the limitations. It is seen that for more than 4 DOs (Figs. 4.21o-s) placed in the given radiant enclosure the uniform heat flux distributions (Figs. 4.26-4.27) are not obtained.

4.2.3.2 Effect of design constraints

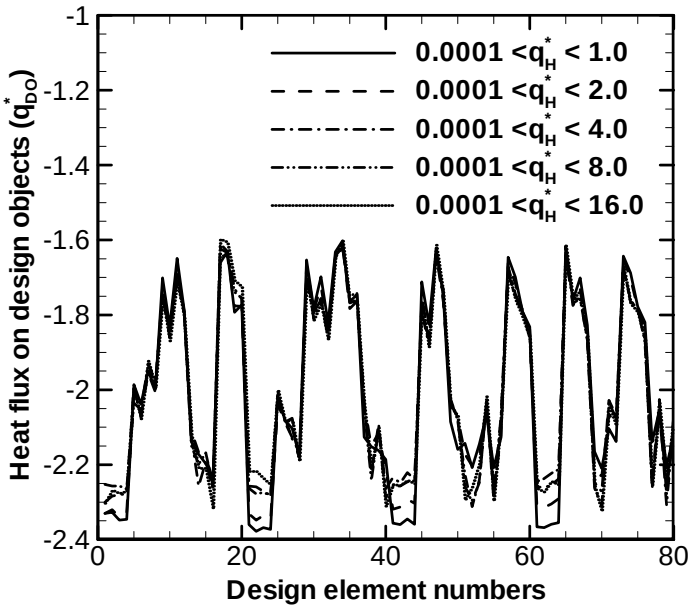

Figure 4.28. Comparison of estimated heat flux distributions on DO using different heater power ranges for the configuration shown in Fig. 4.21.

In all the 19 cases considered so far having different numbers of DOs and configurations, for the desired uniform thermal conditions, i.e. temperature $T^*_{DO} = 1.0$ and heat flux $q^*_{DO} = -2.0,$ the estimated heat flux distributions were obtained using the dimensionless power of panel heaters $\left(q^*_H\right)$ in the range 0.0001 to 4.0. To examine the effect of different design constraints (heater power ranges) on the uniformity of estimated uniform thermal conditions, a sample study has been made. The configuration with 4 DOs shown in Fig.

4.21*l* is considered. The comparison of estimated heat flux distribution on the DOs for five different heater power ranges, viz., 0.0001-1.0, 0.0001-2.0, 0.0001-4.0, 0.0001-8.0 and 0.0001-16.0 are shown in Fig. 4.28. It is observed from Fig. 4.28 that the deviations are the minimum for the heater power range 0.0001-4.0 that we have already considered. The results obtained with heater power range 0.0001-8.0 and 0.0001-16.0 are equally good. For the other two power ranges, i.e., 0.0001-1.0 and 0.0001-2.0, deviations in the estimated heat flux distributions are more. This finding is a typical characteristic of the optimization algorithms, relaxing the constraints on the unknown parameters gives the better estimation. This aspect is also been touched before.

4.2.3.3 Optimal heaters power distribution along the furnace walls

In the earlier study given in section 4.2.1, in which the estimated heat flux distributions were found for a centrally located single DO. It was found that for uniform thermal conditions, all panel heaters are not needed, and among those needed, all did not run on the same powers. With reference to the present problem, this aspect has been studied for a sample case of 2 DOs having configurations shown in Fig. 4.21d. It is to be noted that for this configurations, estimated heat flux distribution (Fig. 4.23c) was the best. For the configuration under consideration, the optimal heater power requirement along top, east, west, back and front walls are shown in Figs. 4.29a-e, respectively. In the analysis, we found that several heaters required very small power (< 1% of the rated power), and thus they can be neglected. In the computation, 100 heaters each along the five walls have been considered. However, it is found that total 30 panel heaters are sufficient to produce the desired uniform thermal conditions. For a given configuration of the DOs, a prior knowledge of heater power setting is the useful information in material heating applications.

This study can be a guideline for furnace designer and in heating operations to get the idea of suitable configuration and the maximum limit of the number of objects (DOs) to achieve uniform thermal conditions with the available size of the furnace enclosure. From the methodology presented in the present study, one can ensure the suitable

configurations of 3-D objects to achieve the uniform thermal conditions within the acceptable range of accuracy.

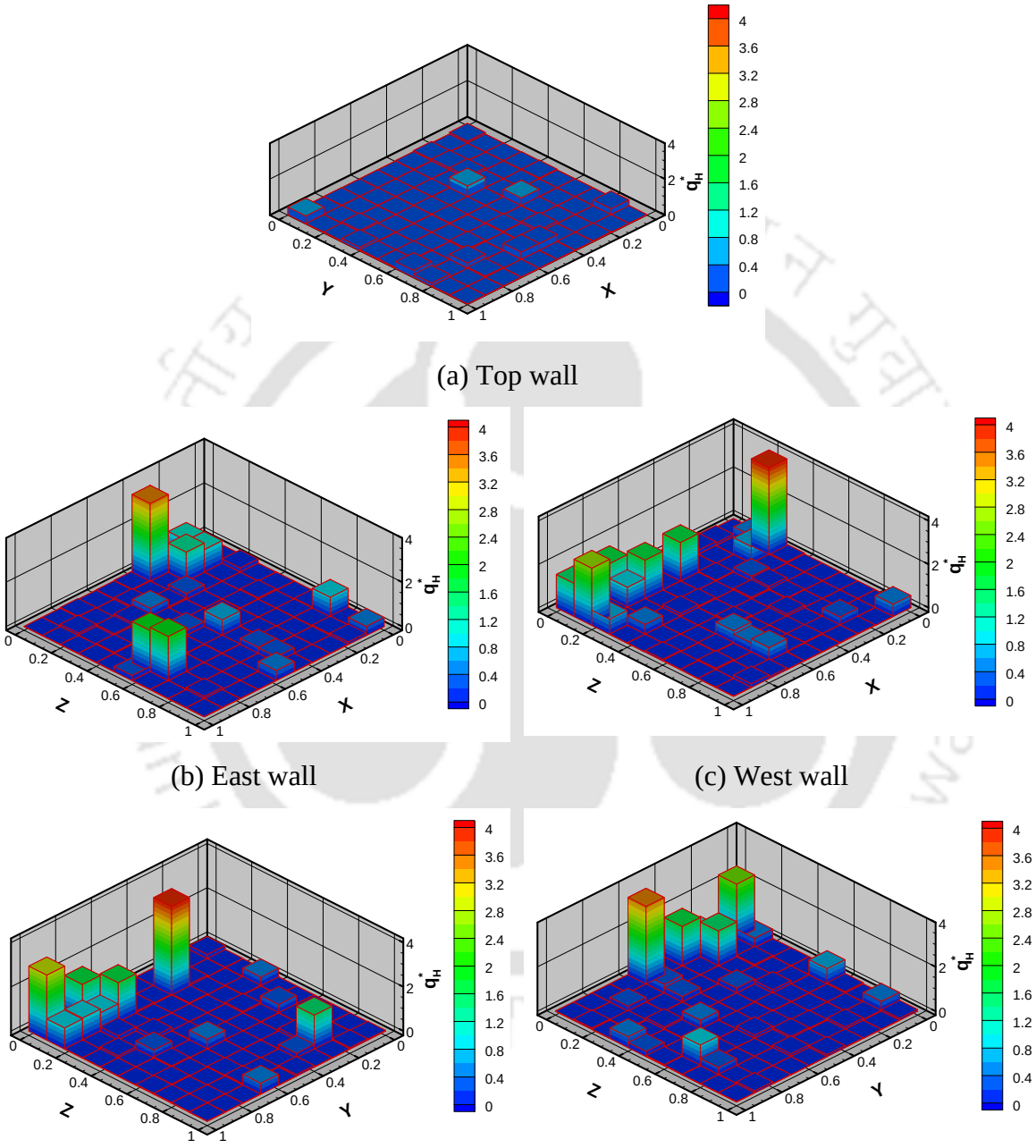

Figure 4.29. Optimal heater power distribution along the enclosure walls for the configuration shown in Fig 4.21d.

4.3 Summary

For uniform thermal conditions on a 3-D design object(s), to address various situations in the material heating, in this chapter results of three studies are given. In these three studies, for the inverse analysis in furnace boundaries design problems radiative information was computed using the REM^2 and the optimization was done using the MGA. In every case, the effect of specular reflections from the refractory walls and from the heater surfaces has been taken into account. The non-dimensional heater power ranges was taken as 0.0001 – 4.0. In the initial study, to have uniform thermal conditions on the surfaces of 3-D DO, for a given size of the radiant furnace, constraints on the size of a DO was investigated. 29 DO models covering a wide range of dimensions were considered. Out of the 29 DO models 16 were found suitable for yielding the uniform heat flux distribution. In these, the maximum $(\pm)$ deviation in the estimated heat flux distribution is $\leq 3.0\%$. For the DO models, a comparative study of 29 cases showed that the height of the 3-D DO puts more restrictions for yielding uniform thermal conditions than that of the length and the width.

In the second study, suitability and the significance of locations of 3-D DO placed along the bottom surface of 3-D radiant furnace was studied. For a radiant furnace of dimensions $L = W = H = 1\text{m}$ the study was done for three sizes of DOs, i.e, model-1 $(0.2\text{m} \times 0.2\text{m} \times 0.2\text{m})$ model-2 $(0.3\,\text{m} \times 0.3\,\text{m} \times 0.3\,\text{m})$ and model-3 $(0.4\,\text{m} \times 0.4\,\text{m} \times 0.2\,\text{m})$. The possible numbers of different locations of the DO models-1, 2 and 3 were 10, 6 and 6, respectively. For model-1, in which the height of the DO is 0.2 m, all locations were found suitable. Whereas, in model-2, in which the height is 0.3 m, only four out of six locations were found suitable, and in model-3, although the base dimensions of the DO $(0.4\,\text{m} \times 0.4\,\text{m})$ are more than the models-1 and 2, since the height is 0.2 m, unlike model-2, all 6 locations were found suitable. For models 1-3, a comparative study of 22 cases showed that the height of the 3-D DO puts more restrictions on suitable locations than that of the length and the width. For a suitable location, optimal power of the panel heaters has been estimated and the results are

analyzed. For model-3, for the 3 diagonal locations, it was shown that less than 50 heaters along the five walls of the furnace are adequate to yield the uniform thermal conditions.

In third study pertained to the suitability of configurations of the multiple DOs. A total of 19 different configurations with 2, 3, 4, 5, 6, 8 and 9 DOs were considered. For the desired uniform thermal conditions on the DOs, the inverse design was done to estimate the heat flux distributions on the DOs and thus to know the required optimal heater power settings. With all other parameters fixed, the distances among the DOs found to have a significant effect. More the distances, better the estimation of the uniform thermal conditions. For the present furnace dimensions, for particular configurations the maximum 4 numbers of DOs were found suitable to achieve the uniform thermal conditions. Further, it was shown that for any particular configuration all the heaters need not to be placed.

To have desired uniform thermal conditions on the 3-D DO(s), the studies presented in this chapter can be useful to handle the different situations in material heating applications.

CHAPTER 5

BOUNDARY DESIGN OF A RADIANT FURNACE FOR UNIFORM THERMAL CONDITIONS: A PRACTICAL APPROACH

5.1 Introduction

Estimation of optimal heater power settings for a 3-D radiant furnace that produce desired uniform thermal conditions on a 3-D design object (DO) is given in Chapter 3. In Chapter 4, various situations in material heating applications are addressed. In the practical applications, along with the desired and accurate output, the design should be feasible and suitable for fabrication, control, and operation. Towards this concept, the studies in this chapter focus on a new concept in furnace boundary design that will offer the easier thermal control, fabrication and operation. A step forward in boundary heater design problems, the heater grouping concept has been introduced. The basic motive of this concept is to reduce the numbers of heaters, and so ease in fabrication, control and operation. In this concept, instead of considering the discrete arrangement of panel heaters along the furnace walls, the heaters are grouped together in a feasible way before solving the furnace boundary design problem, and thus total numbers of heaters are reduced.

Using this concept, the boundary design studies of 3-D radiant furnace with 2-D and 3-D DO are presented. Through these studies, effects of grouping of heaters on the uniformity in estimated heat flux distribution and the optimal heater power settings along the furnace walls are discussed. In the former study, with a 3-D radiant furnace $(\text{dimensions}: 1.0\,\text{m} \times 1.0\,\text{m} \times 1.0\,\text{m})$, three cases of 2-D DOs $(\text{dimensions}: 0.4\,\text{m} \times 0.4\,\text{m}$, $0.6\,\text{m} \times 0.6\,\text{m}$ and $0.8\,\text{m} \times 0.8\,\text{m})$, are studied. In these three cases, the boundary design problems are studied with and without grouping the panel heaters. The later study is

carried out with a 3-D radiant furnace and a 3-D DO $(\text{dimensions}: 0.4\times0.4\times0.3\,\text{m})$ placed on the bottom of the enclosure. The radiative computation is done using the REM^2, and the MGA is used as an optimization tool. The results are presented in section 5.2. Summary of the results is given in the end of chapter, in section 5.4.

5.2 Heaters Grouping Concept for Boundary Design of Radiant Furnace

5.2.1 Boundary design of 3-D radiant furnace for 2-D design object

This study deals with the demonstration of a new approach in furnace boundary design problem that will be feasible for thermal control, fabrication and operation. In this concept, heaters along the furnace walls are grouped appropriately to reduce the numbers of heaters. Figs. 5.1a-b shows a schematic of radiant furnace enclosure (dimensions: $L=W=H=1.0$ m), with centrally located 2-D DO $(l\times w)$. In Fig. 5.1a, 100 panel heaters (dimensions: 0.1 m × 0.1 m) are accommodated along the top wall (dimensions: 1.0 m × 1.0 m). Using the proposed concept, 10 panel heaters $(0.1\text{m}\times0.1\text{m})$ are merged to form a single heater strip (dimensions: 1.0 m × 0.1 m). Fig. 5.1b shows the 10 heater strips along the top wall. The study also made with 20 heaters strips (dimensions: $0.5\text{ m}\times0.1\text{m})$, along the top walls (5 panel heaters are merged to single heater). In this way the numbers of heaters are reduced. Using this arrangement the optimal heater power settings have been estimated to yield uniform thermal conditions on the DO. For this study the expected uniform thermal conditions are, temperature $(T^*_{DO}=1.0)$ and heat flux $\left(q^*_{DO}=q_{DO}\big/\sigma T_R^4=-2.0\right)$. Using the heater grouping concept and the present algorithm (REM^2 + MGA), the optimal heaters power settings are estimated. To cover the wide range of the DO sizes, the present concept is demonstrated for three sizes of the 2-D DOs, (dimensions: 0.4 m × 0.4 m, 0.6 m × 0.6 m, and 0.8 m × 0.8 m).

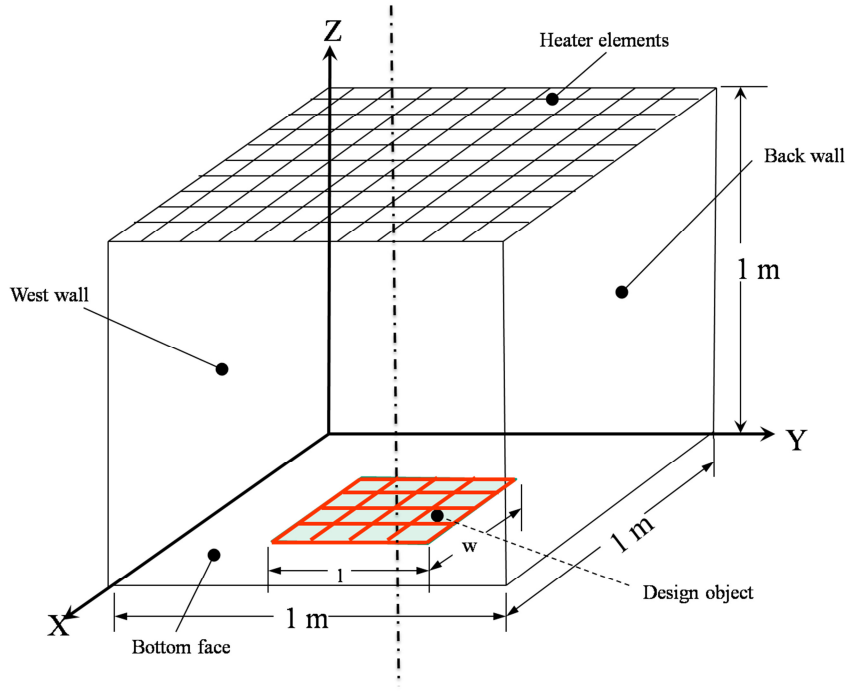

(a)

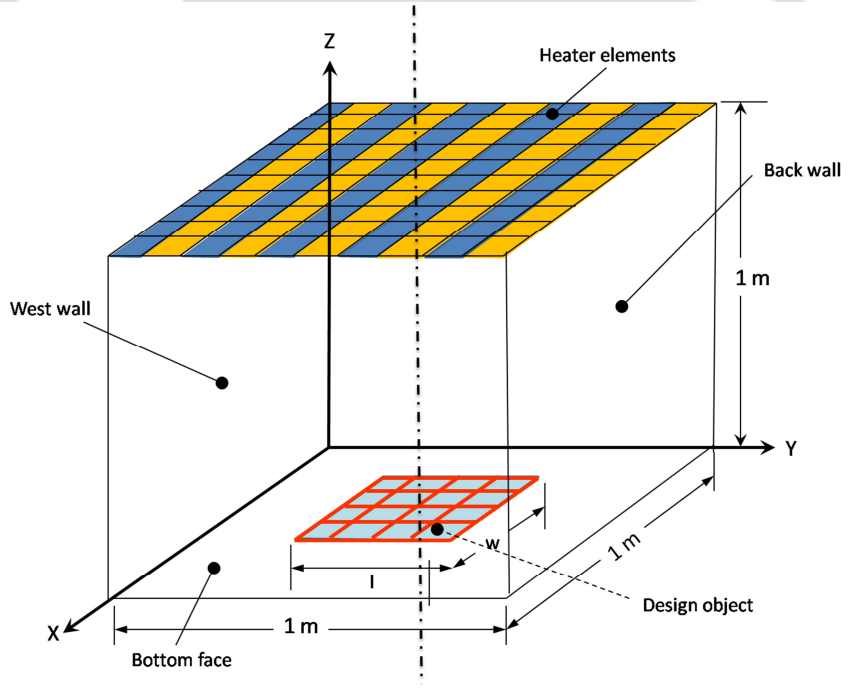

(b)

Figure 5.1. Schematic of the radiant furnace enclosure with centrally located 2-D DO showing (a) 100 heater elements, (b) 10 heater elements (strips), along top wall.

The heater elements along the top walls of radiant enclosure are considered good emitters having emissivity 0.9. The remaining surface elements on the vertical walls and on the bottom surface not covered by the DO are considered insulated and their emissivity is 0.3, while to that of the DO is taken as 0.5. Similar to the studies in Chapter 3 and Chapter 4, for radiative transfer calculation using the REM^2, whole domain is divided into the equal size surface element $0.1\ \text{m} \times 0.1\ \text{m}$. In both the cases (with and without grouping of heaters) the panel heaters can operate in a set power range $0.0001 \le q_H^* \le 4.0$. For optimization, using the MGA, with 10 population size 1000 generations are evaluated.

Figs. 5.2a-c shows the optimal heater power distribution along the top walls of a 3-D radiant furnace that produce uniform heat flux distribution on 2-D DO (0.4 m×0.4 m), using 100 heaters along top wall (Fig. 5.1a), using heater grouping concept, 10 heater strips (Fig. 5.1b), and using 20 heater strips, respectively. From Figs. 5a-c, it is observed that, using the heater grouping concept merely 4 heater strips (Fig. 5.2b) of a symmetric configuration are enough to produce the uniform thermal conditions on the chosen DO. This type of heater arrangement is feasible in practical furnace applications for easy thermal control, fabrication, and operation. Fig.5.2c shows the heater powers setting using 20 heater strips, five panel heaters grouped into one heater strip. The corresponding estimated heat flux distribution on the DO is given in Fig. 5.5a.

Next, using proposed heater grouping concept, the boundary design problem are investigated for two DO models of larger dimensions $(0.6\,\text{m}\times0.6\,\text{m}, \text{and } 0.8\,\text{m}\times0.8\,\text{m})$. All parameters in computations are kept unchanged. For the two DOs (dimensions: $0.6\,\text{m}\times0.6\,\text{m}$, and $0.8\,\text{m}\times0.8\,\text{m}$) results are shown in Figs. 5.3a-c and 5.4a-c, respectively. In both of the figures, sub-figures a-c shows optimal heater powers settings, without grouping of heaters, with heaters grouped in 10 strips, and with heaters grouped in 20 strips, respectively. The trends of results for these two cases are similar to that of DO model $(0.4\,\text{m}\times0.4\,\text{m})$, (Figs. 5.2a-c).

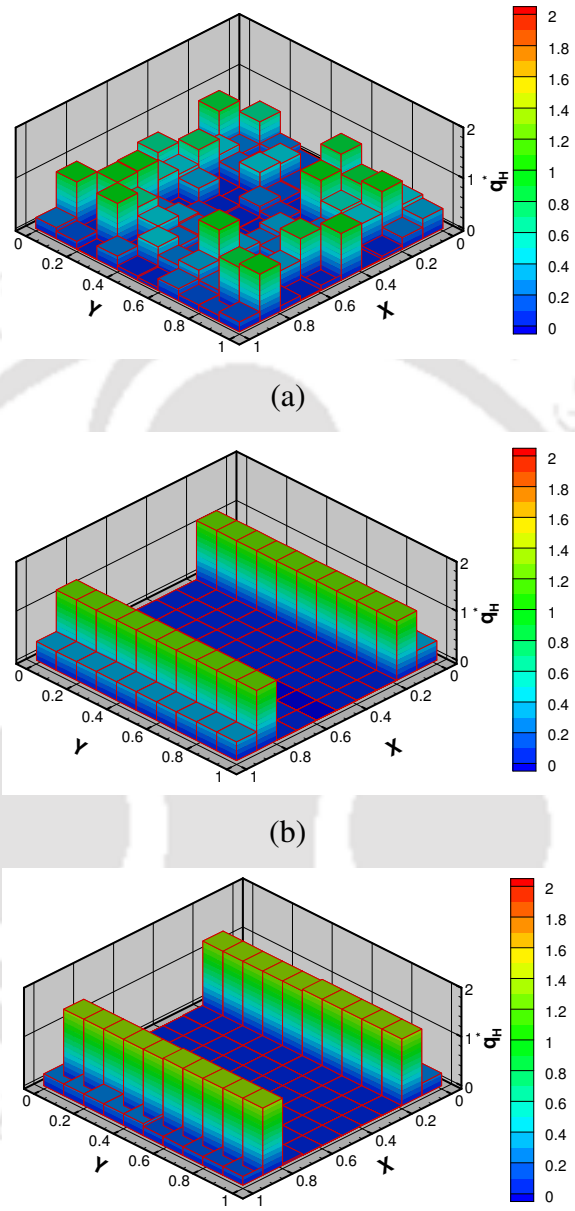

(a)

(b)

(c)

Figure 5.2. Optimal heater power distribution along the top walls of a 3-D radiant furnace that produce uniform heat flux distribution on 2-D DO $(0.4\,\mathrm{m}\times 0.4\,\mathrm{m})$ using (a) 100 heaters along top wall, (b) using heater grouping concept: 10 heater strips, (c) 20 heater strips.

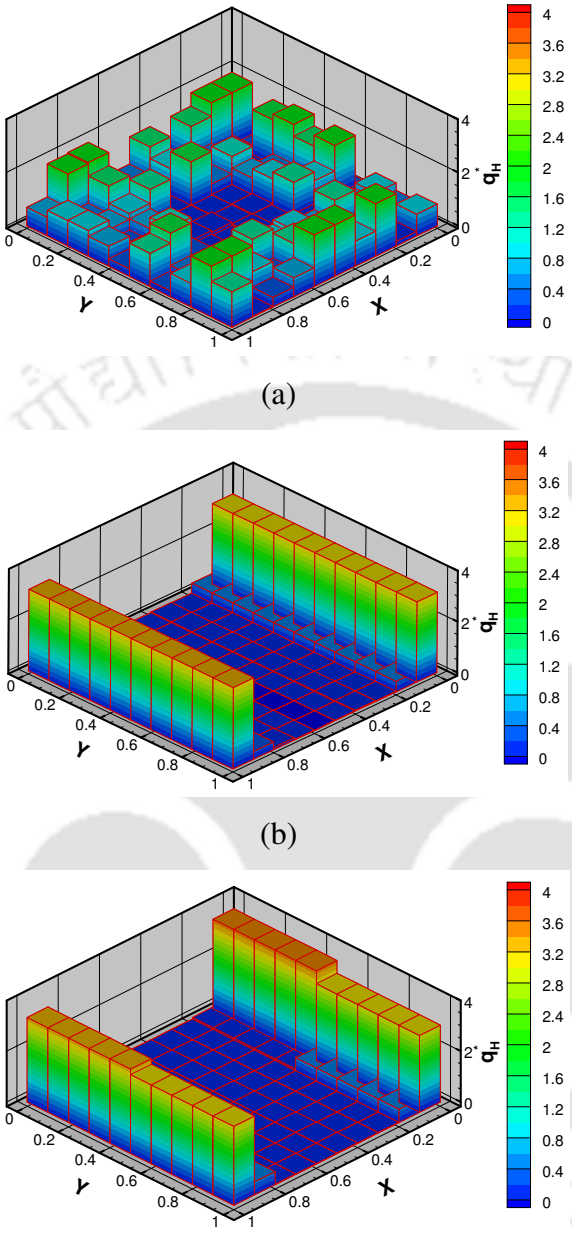

Figure 5.3. Optimal heater power distribution along the top walls of a 3-D radiant furnace that produce uniform heat flux distribution on 2-D DO $(0.6\,\mathrm{m}\times 0.6\,\mathrm{m})$ using (a) 100 heaters along top wall, (b) 10 heaters strips, (c) 20 heaters strips.

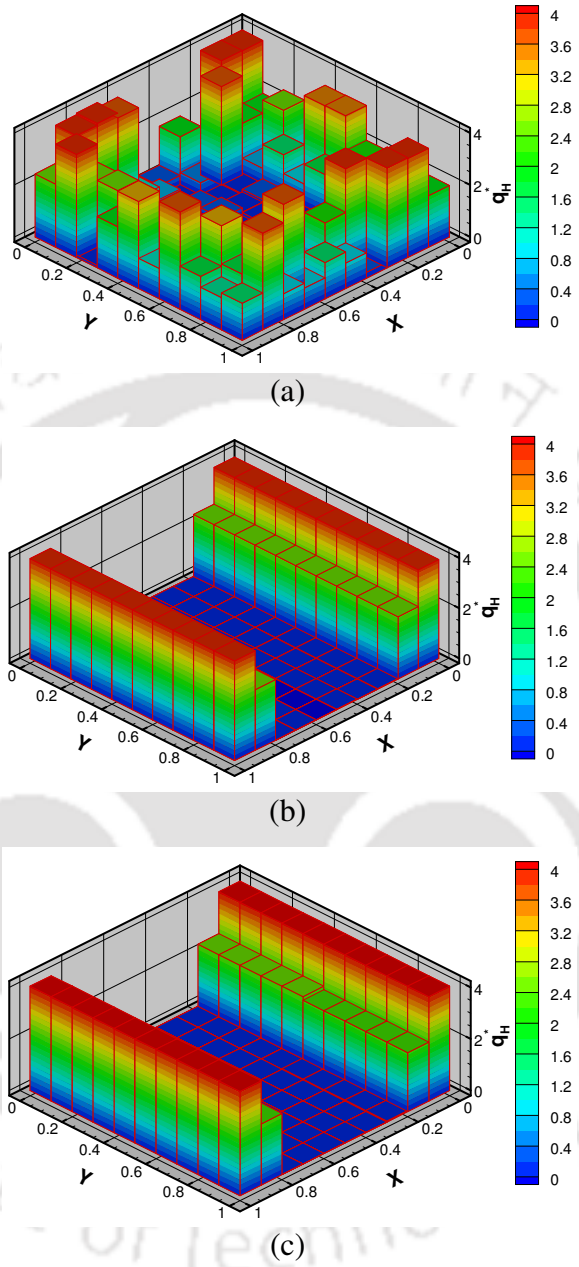

Figure 5.4. Optimal heater power distribution along the top walls of a 3-D radiant furnace that produce uniform heat flux distribution on 2-D DO $(0.8\,\mathrm{m}\times 0.8\,\mathrm{m})$ using (a) normal heater arrangement (100 heaters along top wall, (b) 10 heaters strips, (c) 20 heaters strips.

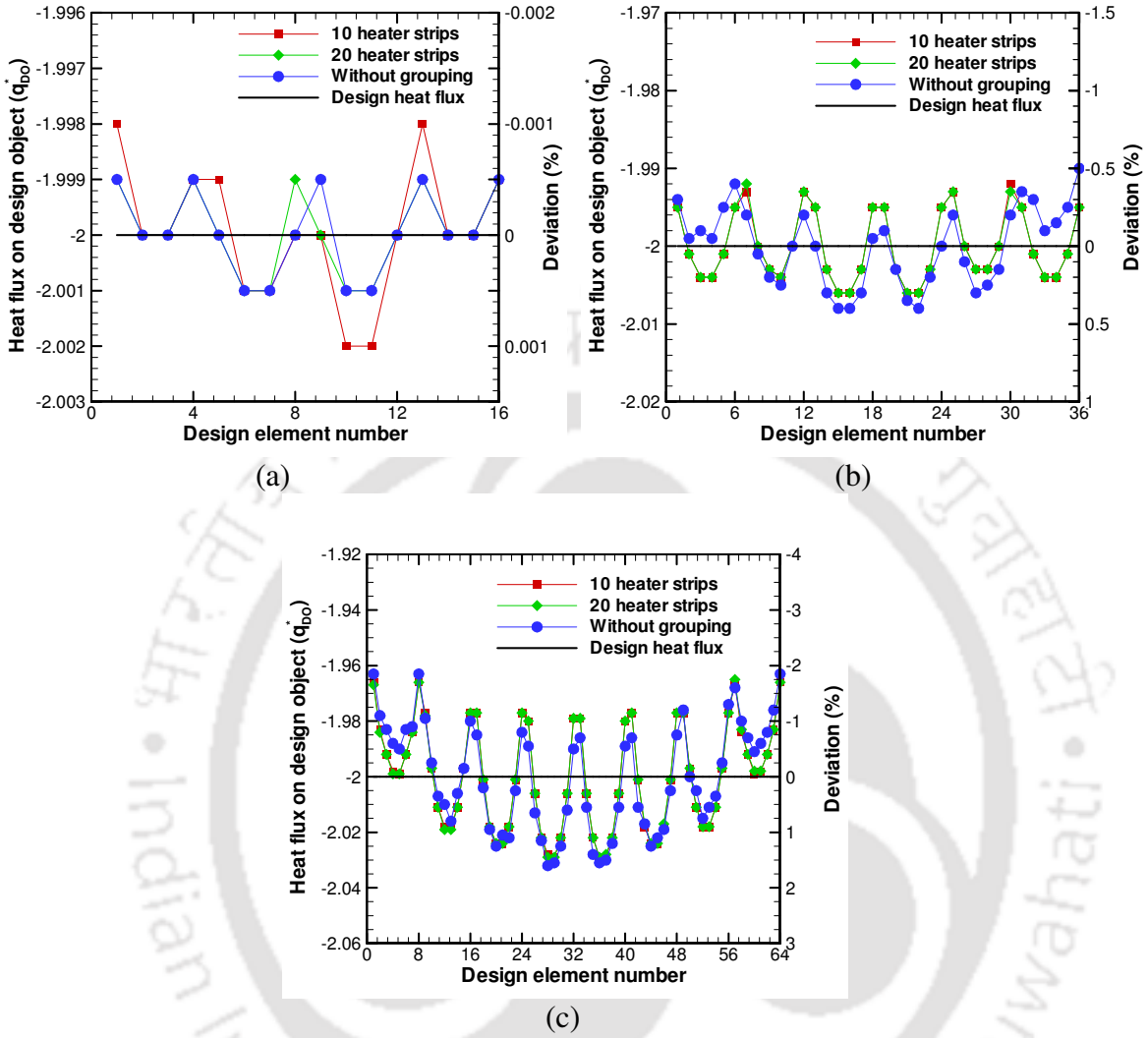

Figure 5.5. Comparisons of the estimated heat flux distribution on the DOs using grouped and ungrouped panel heaters. (a) 2-D DO $(\text{dimensions}: 0.4\times0.4\,\text{m})$., (b) 2-D DO $(\text{dimensions}: 0.6\times0.6\,\text{m})$., and (c) 2-D DO $(\text{dimensions}: 0.8\times0.8\,\text{m})$.

In these cases (Figs. 5.3a-c, Figs. 5.4a-c) also, with grouping the heaters into 10 strips, only 4 heater strips are found adequate for yielding the desired uniform thermal conditions, the corresponding estimated heat flux distributions on the DO are shown in Figs. 5.5b-c. From Figs. 5.5a-c, it is observed that using the heaters grouping concept, uniformity in estimated heat flux distribution get little bit distorted, however the uniformity is within ± 2.0%. This is attributed to, less availability for solution space in optimization process. This can be compensated by exact grouping the heaters having

virtually the same power requirement; this has been demonstrated in Chapter 6, section 6.3.5.

The computational time for these three cases is also recorded. For the chosen 3 DOs $(\text{dimensions}: 0.4\,\text{m}\times 0.4\,\text{m},\ 0.6\,\text{m}\times 0.6\,\text{m},\ 0.8\,\text{m}\times 0.8\,\text{m})$ using 100 heaters along the top walls the computational time was found same, 114.89 sec, while using the heaters grouping concept the computational time was 77.75 sec. This shows that using the present concept, the saving in computational time is 32.24%. This reduction in computation time is mainly from the optimizations algorithm. In next section the heater grouping concept is implemented to the boundary design problem of 3-D radiant furnace with 3-D DO.

5.2.2 Boundary design of 3-D radiant furnace for 3-D design object.

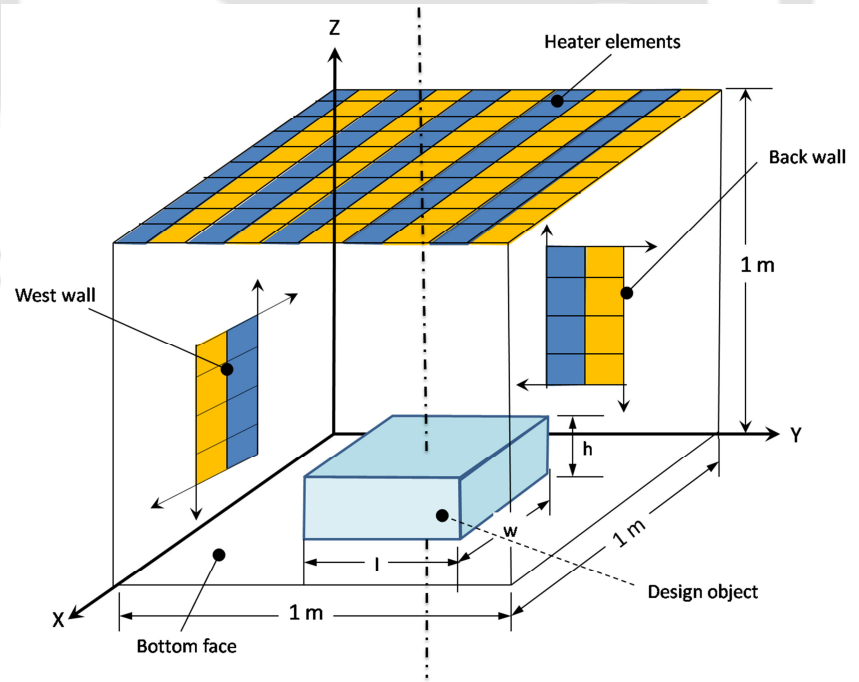

Figure 5.6. Schematic of the radiant furnace enclosure showing strip heaters along the 5 walls with centrally located 3-D design object on the bottom face.

Having demonstrated the heater grouping concept for boundary design of a 3-D radiant furnace with 2-D DO, the same concept is implemented to design a radiant furnace that produce the desired thermal conditions on the surfaces of 3-D DO. For this problem also, the same desired uniform thermal conditions are considered. The schematic of radiant furnace enclosure $\left(\text{dimensions}: L = W = H = 1.0\ \text{m}\right)$, with centrally located 3-D DO $\left(\text{dimensions}: l = 0.4\,\text{m},\ w = 0.4\,\text{m},\ h = 0.3\,\text{m}\right)$ is shown in Fig. 5.6.

Being understood from the results in Chapter 4, for the given 3-D radiant furnace, for yielding uniform thermal conditions on 3-D DO, for computations, heaters along the five walls of furnace are need to be considered. Discretizing the surfaces of five walls of furnace, viz. top, east, west, back and front wall, (refer Fig. 5.6) into equal size (0.1 m × 0.1 m) surface elements, thus the numbers of surface elements along the five walls becomes 500. For the problems in Chapter 3, and Chapter 4, 100 panel heaters along each wall of the furnace have been used. Using the heater grouping concept, in this problem, the heaters along the five walls are grouped into 50 heater strips, each formed by merging 10 heater elements together, as shown in Fig. 5.6.

The optimal heater power distribution along the five walls of furnace enclosure, using normal heaters arrangement and using the heaters grouping concept, are shown in Figs. 5.7a-e. From Figs. 5.7a-e it is observed that, the results of boundary design problem using the heater strips are more practical and feasible for fabrication, control and operation. The corresponding estimated heat flux distribution is shown in Fig. 5.8. Even the uniformity in estimated heat flux distribution is deteriorated using this concept, the maximum deviation (±) is less than 4%.

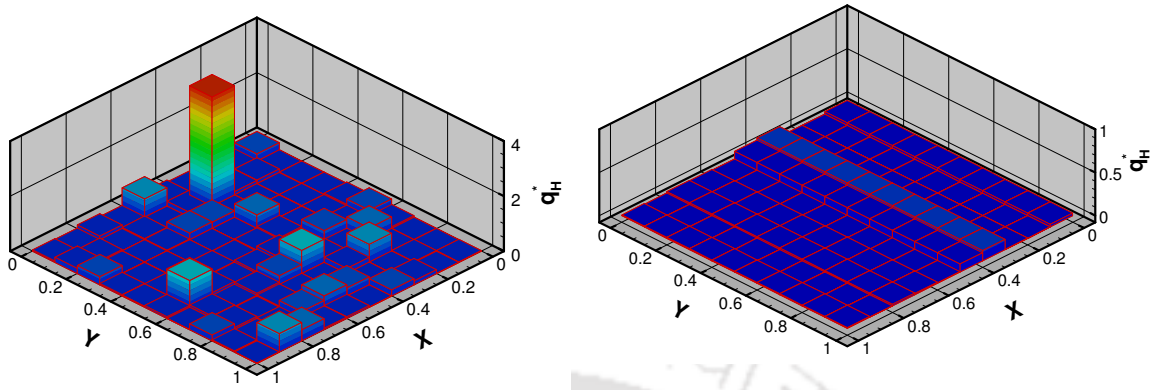

(a) Top wall

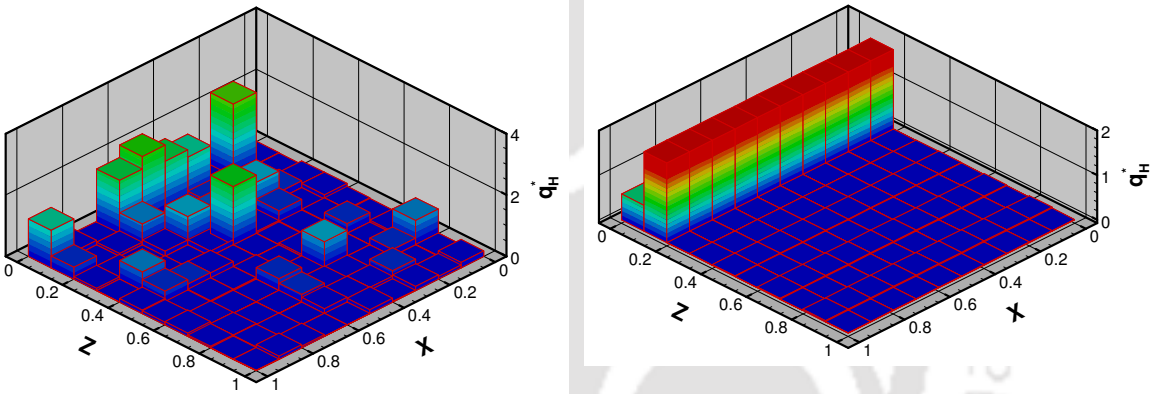

(b) East wall

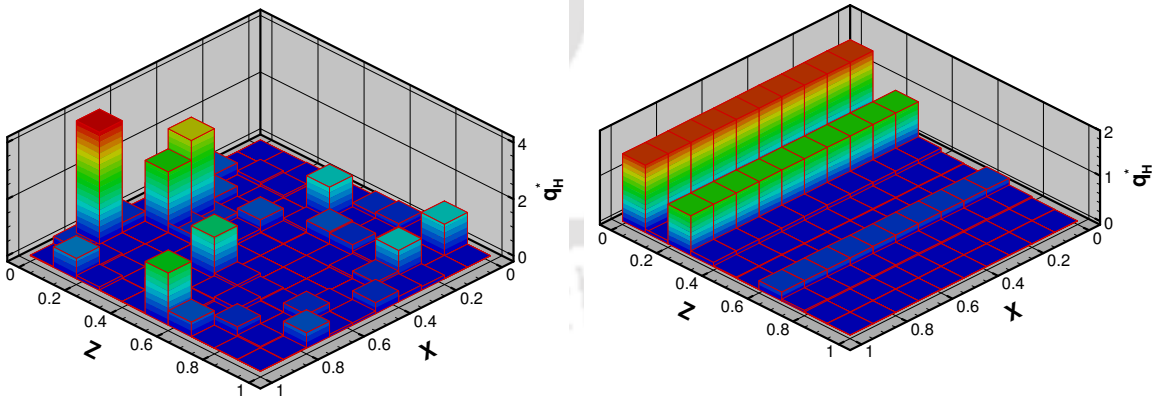

(c) West wall

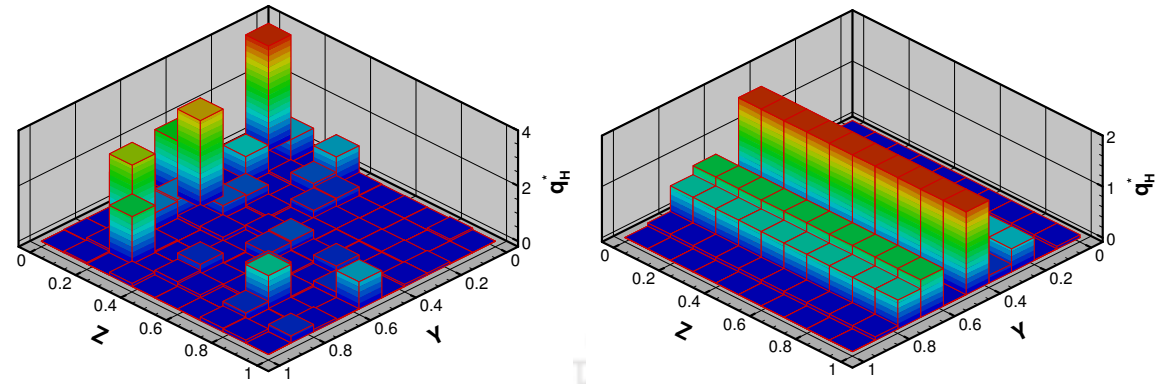

(d) Back wall

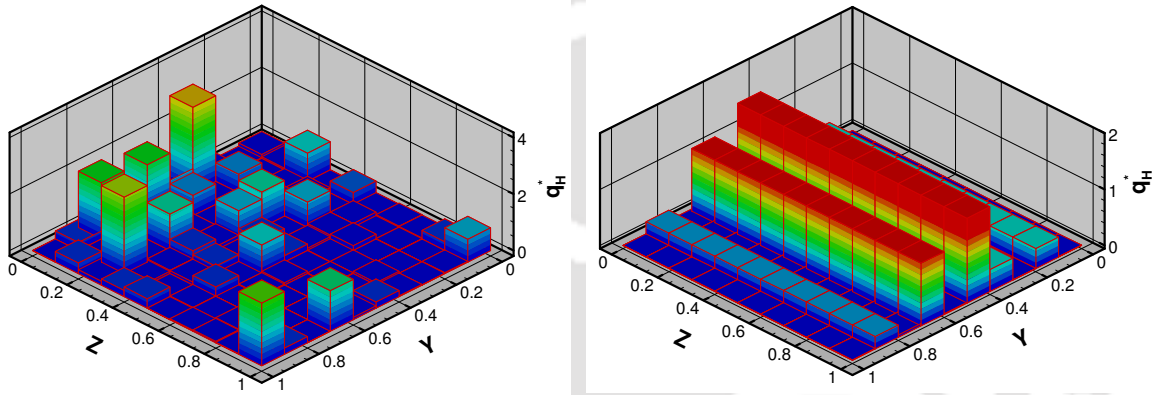

(e) Front wall

Figure 5.7. Optimal heater power distribution along the enclosure walls using normal heater arrangement and heaters grouping concept: boundary design for 3-D radiant furnace with 3-D DO $\left(\text{dimensions}: 0.4\,\text{m}\times 0.4\,\text{m}\times 0.3\,\text{m}\right)$.

The computational time for this problem is recorded using heater grouping concept and without the concept. With the chosen computational domain in which 500 heaters elements placed along the five walls, the computational time recorded as 558.68 sec., while using the heaters grouping concept (i.e. 50 heaters strips) the computational time recorded as 244.46 sec. This shows that using the present concept, saving in computational time is 56.24%. The results are summarized in Table 5.1. The present heater grouping concept is advantageous in designing the feasible and practical heater power setting to produce desired uniform thermal conditions on a 3-D DO.

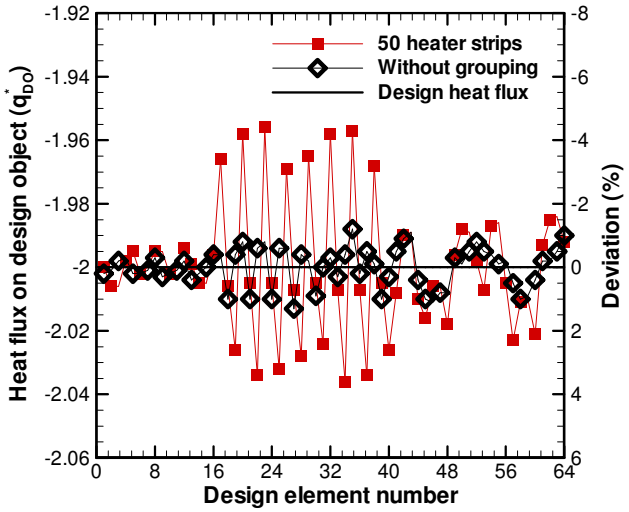

Figure 5.8. The estimated heat flux distribution on a DO (dimensions: $0.4\,\text{m}\times0.4\,\text{m}\times0.3\,\text{m}$) using grouped and ungrouped panel heaters.

.

Table 5.1. Computational CPU time using the proposed heater grouping concept.

DO model	Normal configuration		Proposed heaters grouping concept		Saving in computational time (%)
	Numbers of heater elements	CPU time (s)	Numbers of heater strips	CPU time (s)	
2-D DO	100	114.89	10	77.75	32.24
3-D DO	500	558.68	50	244.46	56.24

5.3 Summary

The studies in this chapter present the radiant boundary design problems towards the practical approach. A new approach in furnace boundary design problems has been introduced, which makes the furnace design feasible for fabrication, control and operation. In this the panel heaters are grouped together in a appropriate manner, and thus total numbers of heaters are reduced. Using this concept, the boundary design problems involving 3-D radiant furnace with 2-D and 3-D DOs are investigated. For these studies, REM^2 is used for radiative calculation and optimization is done using the MGA. From

the results, it is observed that the heater grouping concept is advantageous in boundary design problems, this make the design feasible for thermal control and fabrication. Moreover, using this concept, the computational cost reduced up to 53 %. With this solution approach, the uniform thermal conditions get slightly distorted; however, the estimated uniformity is within the 4% of deviation. This study is useful in radiant boundary design problems for estimating the feasible solutions.

CHAPTER 6

RADIANT BOUNDARY DESIGN FOR UNIFORM THERMAL CONDITIONS ON AN IRREGULAR SHAPED DESIGN OBJECTS

6.1 Introduction

To have desired post processing properties, several material heating processes require specific thermal conditions (temperature and/or heat flux distributions) on the desired region of the furnace enclosure. In Chapter 3, the radiant furnace design for a 3-D rectangular design object (DO) is given, and in Chapter 4, various situations in material heating processes have been addressed. In practical applications the DOs (products to be heated) can be of any shape and size. It is also understood the wide applications of the radiant furnaces such as material heating for various heat treatment processes, drying processes, rapid thermal processing of semiconductor wafers, etc. It has been established that to obtain the desired thermal conditions on the DO, the enclosure geometry, arrangement of heaters, power of heaters, location of the DO, etc., need to be properly accounted. From the literature given in Chapter 1 section 1.2, it is observed that most of the studies of radiant boundary design problems are limited to 2-D enclosures and so the 2-D design surfaces. The literature addressed the uniform thermal conditions on the planer irregular design surfaces are scanty and on 3-D irregular DO is not found.

A step forward towards the more generalized case, the studies in this chapter focus on estimation of optimal heaters power distribution that produce desired uniform thermal conditions on 2-D and 3-D irregular shaped DOs placed inside a 3-D radiant furnace. For calculation of radiative information in a 3-D enclosure, the REM^2 has been used. In inverse design, the objective function has been minimized using the MGA. In the following pages, the results of boundary design problems for 2-D and 3-D irregular

shaped DOs is given in section 6.2 and section 6.3, respectively. In these boundary design problems the effects of the size, shape of the radiant furnace and DO are also discussed. Next, results of a case study involving design of radiant furnace is given, when the DO is a replica of car body. In the end of the chapter, the results of these studies are summarized in section 6.4.

6.2 Radiant Boundary Design for 2-D Irregular Shaped Design Objects

For the desired uniform thermal conditions on 2-D irregular shaped DO placed on the bottom surface of a 3-D rectangular radiant furnace, in the present work, the optimal heater power settings along the walls of radiant enclosure have been estimated. The desired thermal conditions are $q^*_{DO} = -2.0$ and $T^*_{DO} = 1.0$. Figure 6.1a shows, schematic of the radiant enclosure $\left(\text{dimensions: } L = W = H = 1.0 \text{ m}\right)$ with centrally (0.5,0.5,0) located the circular shaped DO (diameter 0.5 m) on the bottom surface (X-Y plane). The DO is considered to be irradiated by panel heaters placed along one or more of walls of the enclosure. The bottom surface of the radiant enclosure not covered by the DO is insulated.

The aim of this work is to estimate the optimal power settings that produce the desired uniform thermal conditions on the irregular shaped DO. This is accomplished by first specifying the temperature distribution and then obtaining the heat flux on the surfaces of the DO using the REM^2 + MGA. The radiative information has been computed using the REM^2 and in the inverse analysis, for minimization of the objective function Eq. (3.24), the MGA has been used.

To obtain the radiative information using the REM^2, surfaces of the enclosure surfaces are divided into equal size (0.1 m×0.1 m) surface elements. Since the design surface is of irregular shape, it is divided into irregular triangular shaped surface elements. The total numbers of triangular elements, on a given design surface is 64 (Figs. 6.1a-b). Fig. 6.1b shows the surface element arrangement on the circular design surface and uncovered bottom surface of the radiant enclosure.

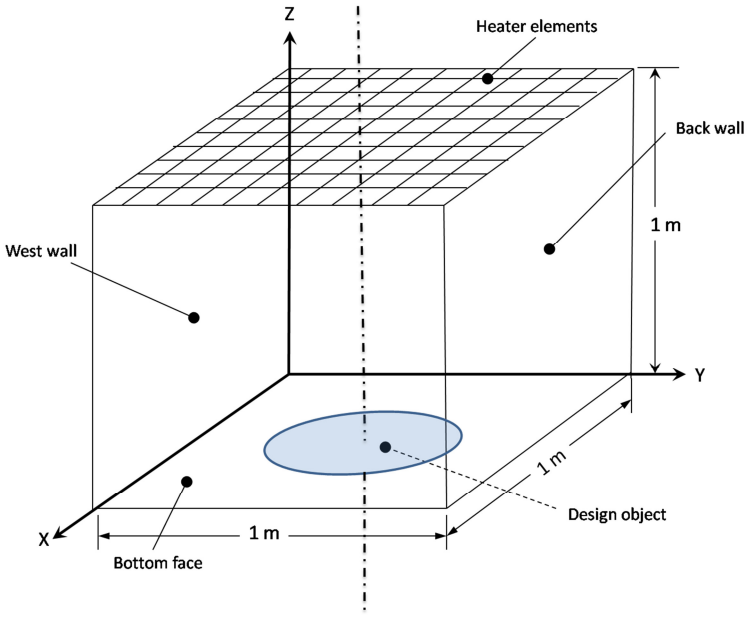

(a)

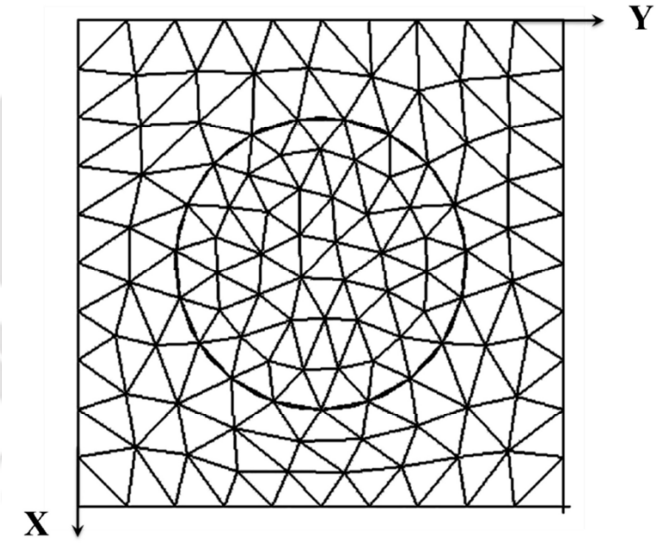

(b)

Figure 6.1. (a) Schematic of the 3-D radiant enclosure with circular DO, (b) irregular surface elements on DO and bottom of the radiant furnace.

For the studies in this chapter, the computational domains with the surface elements along the surfaces of furnace walls and the DO are modeled using PATRAN 2005 software (Computer Added Engineering, modeling and pre/post processing software). PATRAN is the world's widely used pre/post-processing software for finite element analysis, providing solid modeling, meshing, and analysis setup for MSC Nastran, Marc, Abaqus, and ANSYS. [http://www.mscsoftware.com/Products/CAE-Tools/Patran.aspx#]. This modeling is done at Institute of fluid sciences, Tohoku University Sendai, Japan. The role of this software is to get the coordinates of the nodes of surface elements. The emissivities of heater elements, refractory walls and the DO surfaces are 0.9, 0.3 and 0.6 respectively. Temperature and heat flux of a given surface elements are uniform over their area, and they are different for different surface elements.

Since in the present problems, DOs are of irregular shaped, in both the cases of 2-D and 3-D DOs, surface elements on the heater surface and on DO surfaces are not of same in size and shape. While computation, in every generation, the optimality of the heater power (q_H) have been maintained using the energy balance in the system. Mathematically this can be written as

$$\sum_{i=1}^{N_{DO}} A_{i,DO} \left| q_{i,DO} \right| = \sum_{j=1}^{N_H} A_{j,H} q_{j,H} \tag{6.1}$$

where $A_{i,DO}$ and $A_{j,H}$ is the area, and $q_{i,DO}$ and $q_{j,H}$ is the heat flux at i^{th} element on DO, and j^{th} element on the heater surface, respectively.

With the objective of having uniform heat flux $q^*_{DO} = -2.0$ on the surfaces of a circular design surface, in the following pages, estimation of power of the panel heaters are done. Initially, the panel heaters are considered on the five walls of the radiant enclosure viz. top, west, east, back and front wall, while the bottom surface on which the DO is located is assumed insulated. With the surface element size $0.1\text{m} \times 0.1\text{m}$, each wall has 100 panel heaters, and covers the entire surface area of a wall. With a population size of 10, crossover probability of 0.5, the MGA was allowed to run 1000 generations.

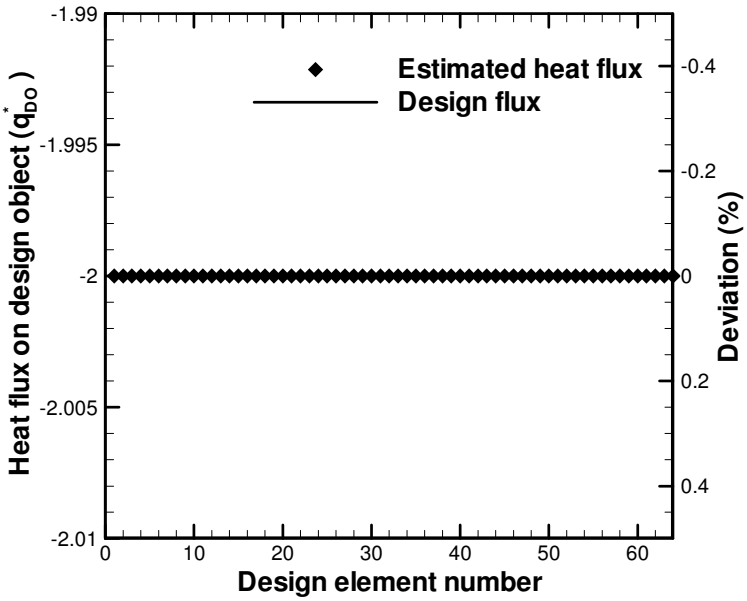

Figure 6.2. Estimated heat flux distribution on the DO (Fig. 6.1a), with panel heaters along the five walls of the furnace.

The estimated heat flux distribution on the DO and the optimal heater power distributions along the five walls of the furnace are given in Fig. 6.2 and Figs 6.3a-e, respectively. The deviation in the estimated heat flux distribution on the DO is found four digits accurate. In this case the minimum value of the objective function is obtained in the order of 10^{-07}. From Fig. 6.3a-e, it is observed that the heater power setting is uneven along the enclosure walls. Such kind of heater arrangement is difficult to fabricate and to control.

To have more realistic results, from the observations of literature, the present boundary design problem (Figs 6.1a-b) is solved with the panel heaters along the top wall only. Four vertical walls (west, east, back and front) and the bottom surface not covered by DO are kept insulated. For this case, Fig. 6.4a shows the estimated heat flux distribution and corresponding deviation on the DO, while Fig. 6.4b shows the optimal heater power distribution along the top wall of radiant enclosure. From Fig. 6.4a, it is observed that the uniformity in the estimated heat flux distribution is accurate, within 0.4% deviation. If we have a keen look on the Fig. 6.4b, it is observed that, not all but less than 15 heaters are

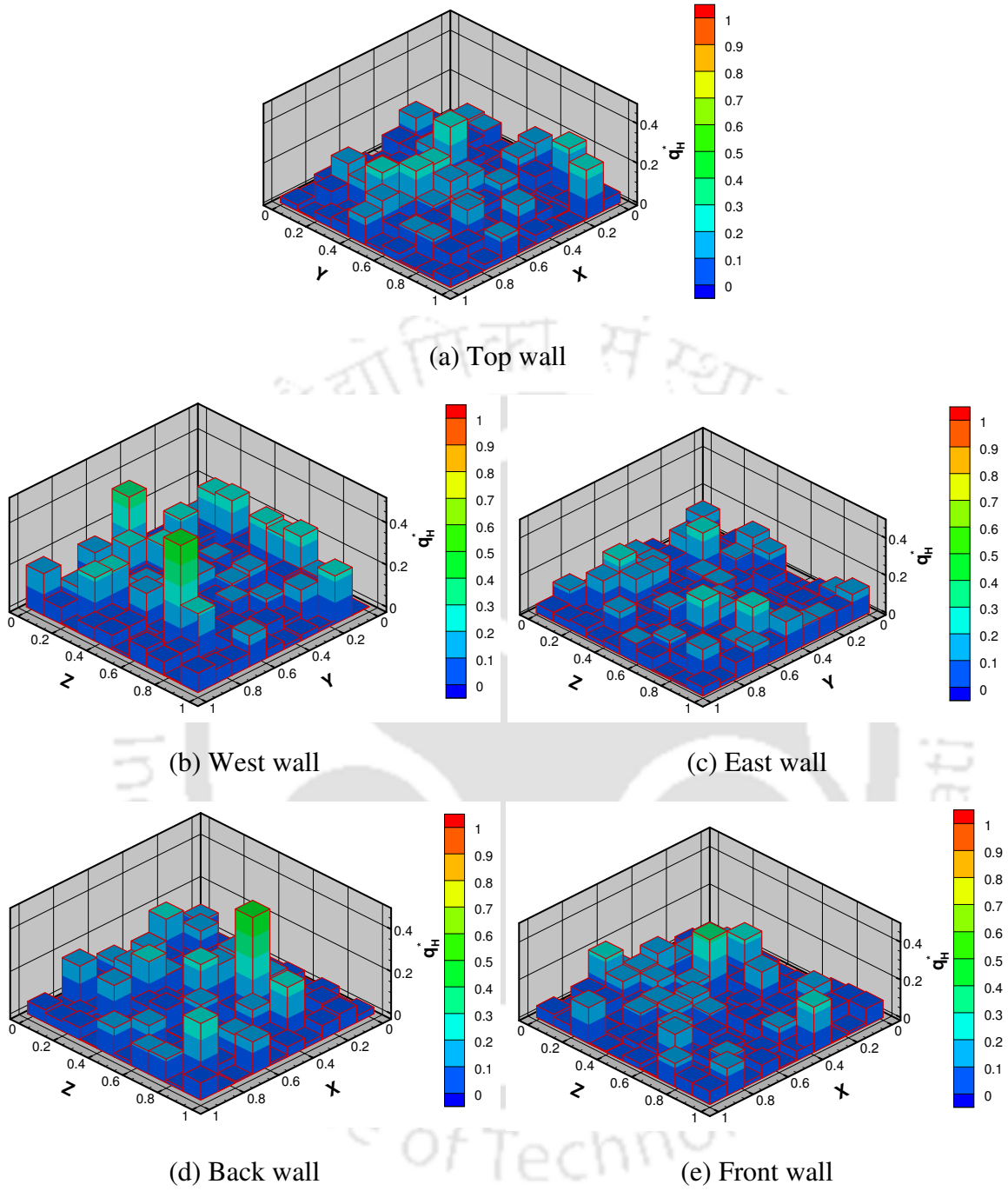

Figure 6.3. Optimal heater power distribution along the enclosure walls of radiant furnace.

enough to produce the desired effect. This type of heaters arrangement is feasible for fabrication and preferable in material heating processes.

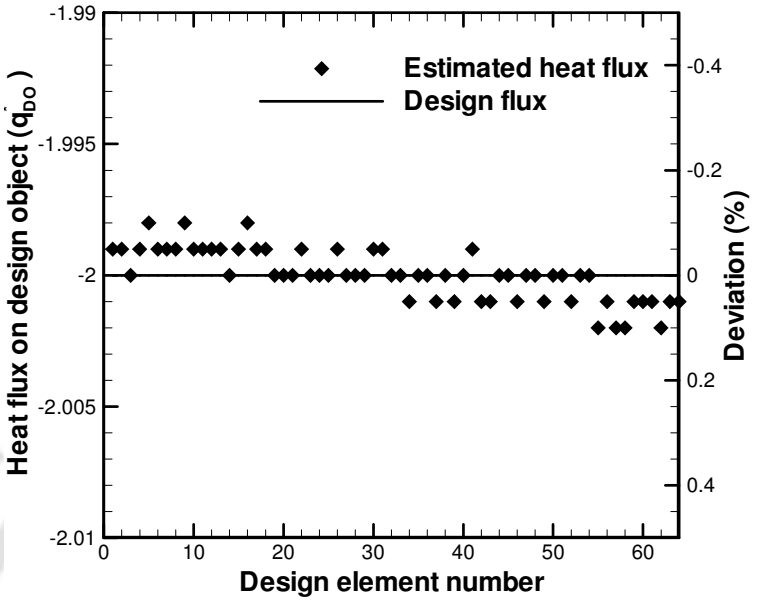

(a)

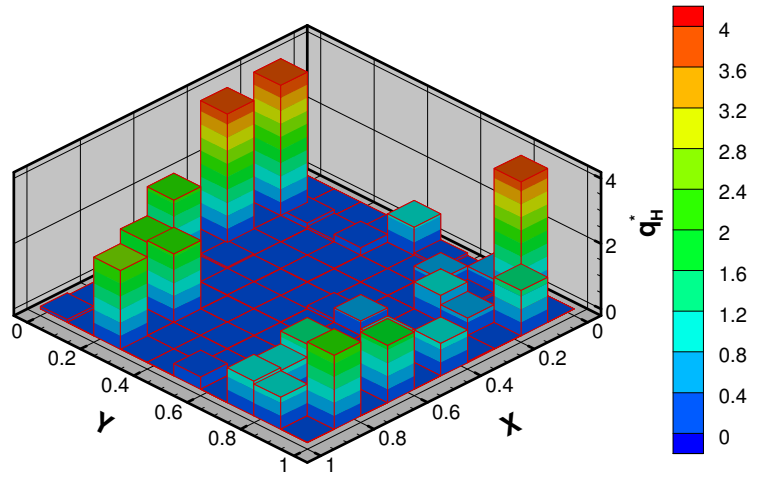

(b)

Figure 6.4. (a) Deviation in the estimated heat flux on the circular DO with panel heaters placed along the top wall only, (b) corresponding optimal heater power distribution along the top wall.

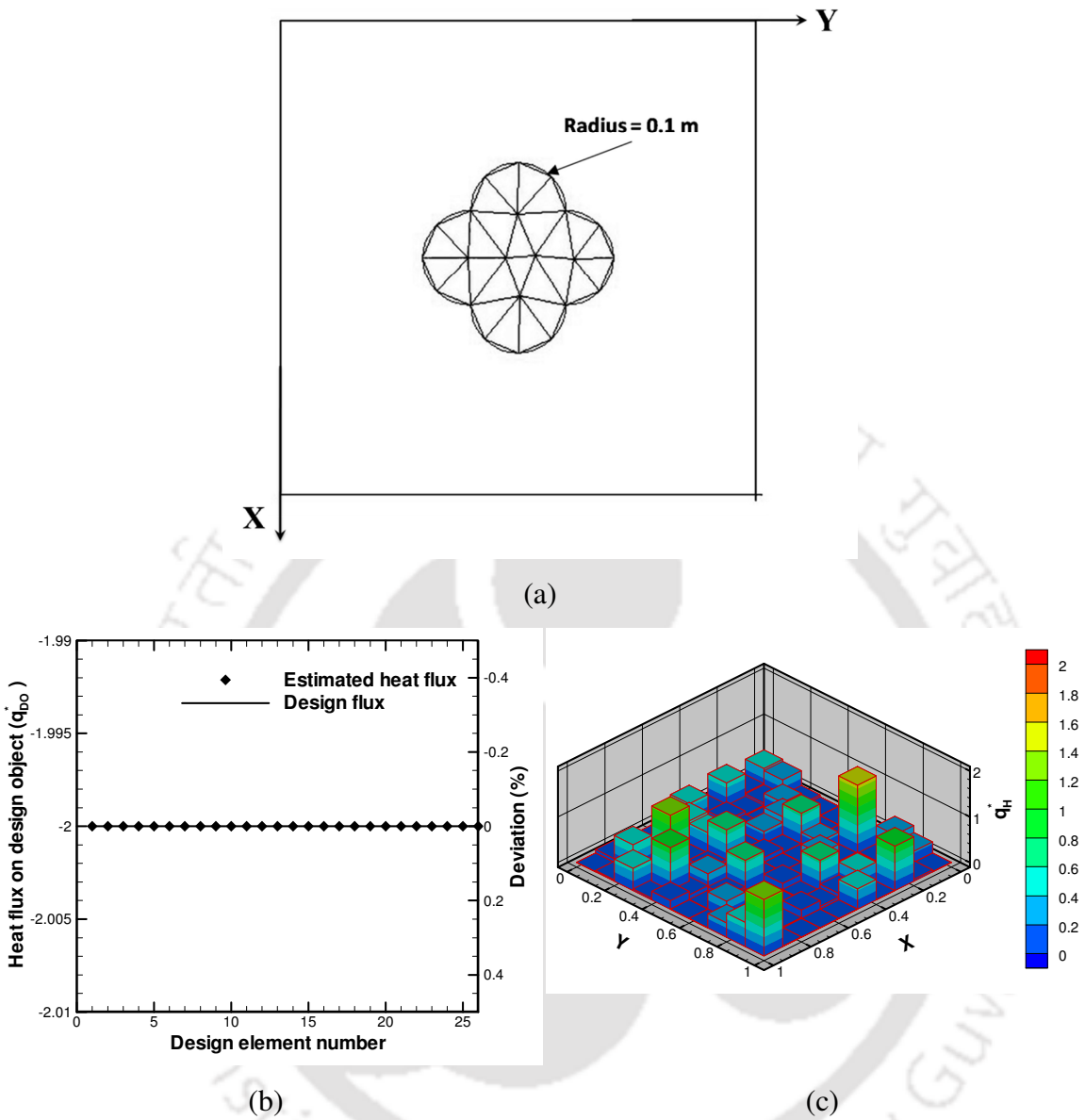

Figure 6.5. (a) Schematic of chosen irregular design surface placed on the bottom surface, (b) deviation in the estimated heat flux on the design surface, (c) optimal heater power distribution along the top wall.

The applicability of the present algorithm (REM^2 + MGA) is exemplified by considering another irregular design surface placed on the bottom of the furnace, shown in Fig. 6.5a. Fig. 6.5b and Fig. 6.5c shows the estimated heat flux distribution on DO and the optimal heater power requirement along the top wall of the furnace, respectively. In Fig. 6.5b, the estimated flux distribution on the DO is 4 digits accurate.

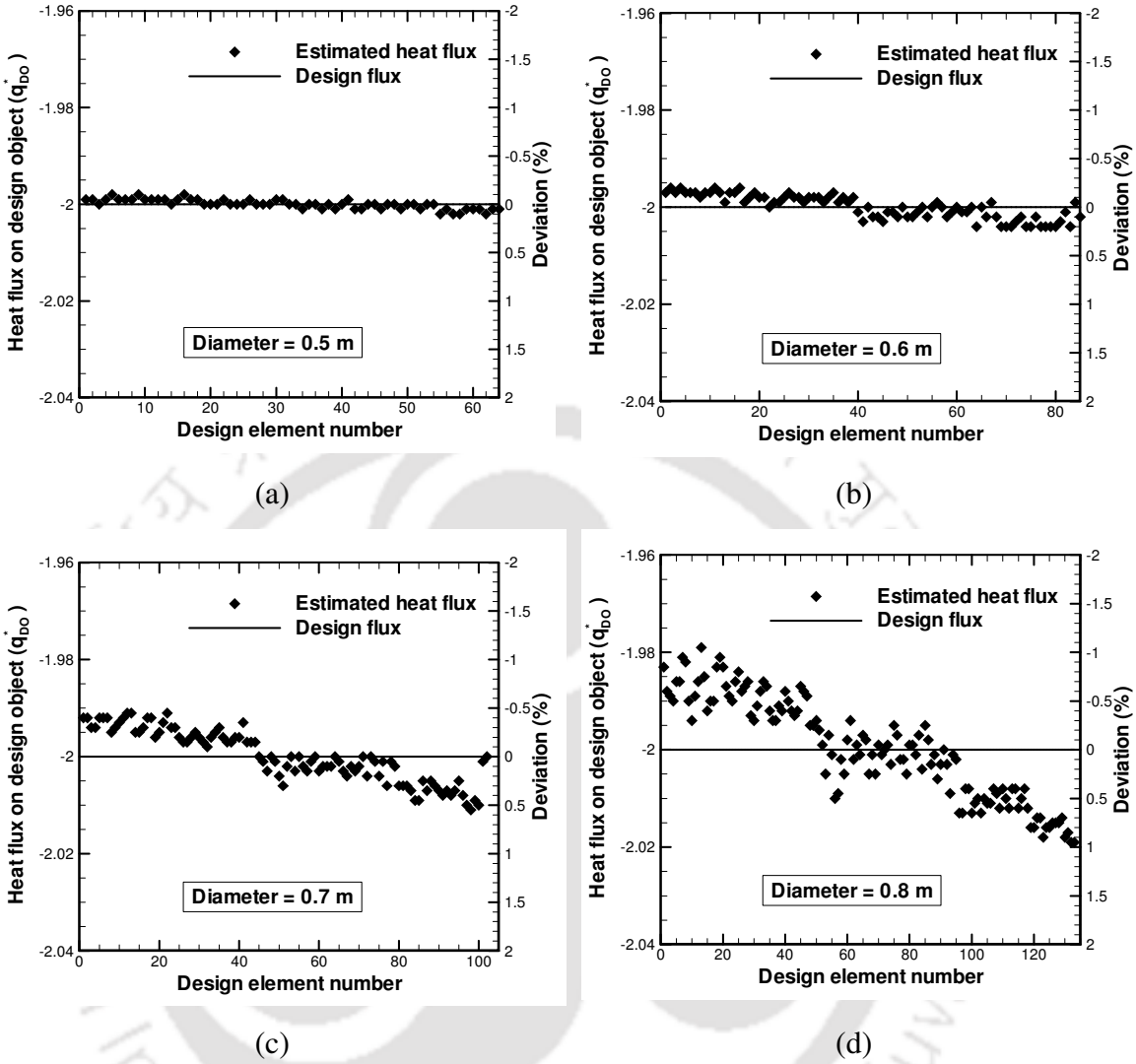

Figure 6.6. Estimated heat flux distribution on a circular design object of diameter (a) 0.5 m, (b) 0.6 m., (c) 0.7 m., (d) 0.8m.

Next for case 1, i.e. for circular design surface (Fig. 6.1a), the studies are conducted to analyze the effect the size of DO, and the aspect ratio of furnace enclosure. Fig. 6.6a-d shows the estimated flux distribution on the DO of four different sizes, with diameter 0.5 m., 0.6m., 0.7m., and 0.8 m., respectively. It is observed from Fig. 6.6a-d that the uniformity in heat flux distributions deteriorates with increase in the area of DO. The maximum deviation in estimated heat flux distribution on DO of diameter 0.5m, 0.6m.,

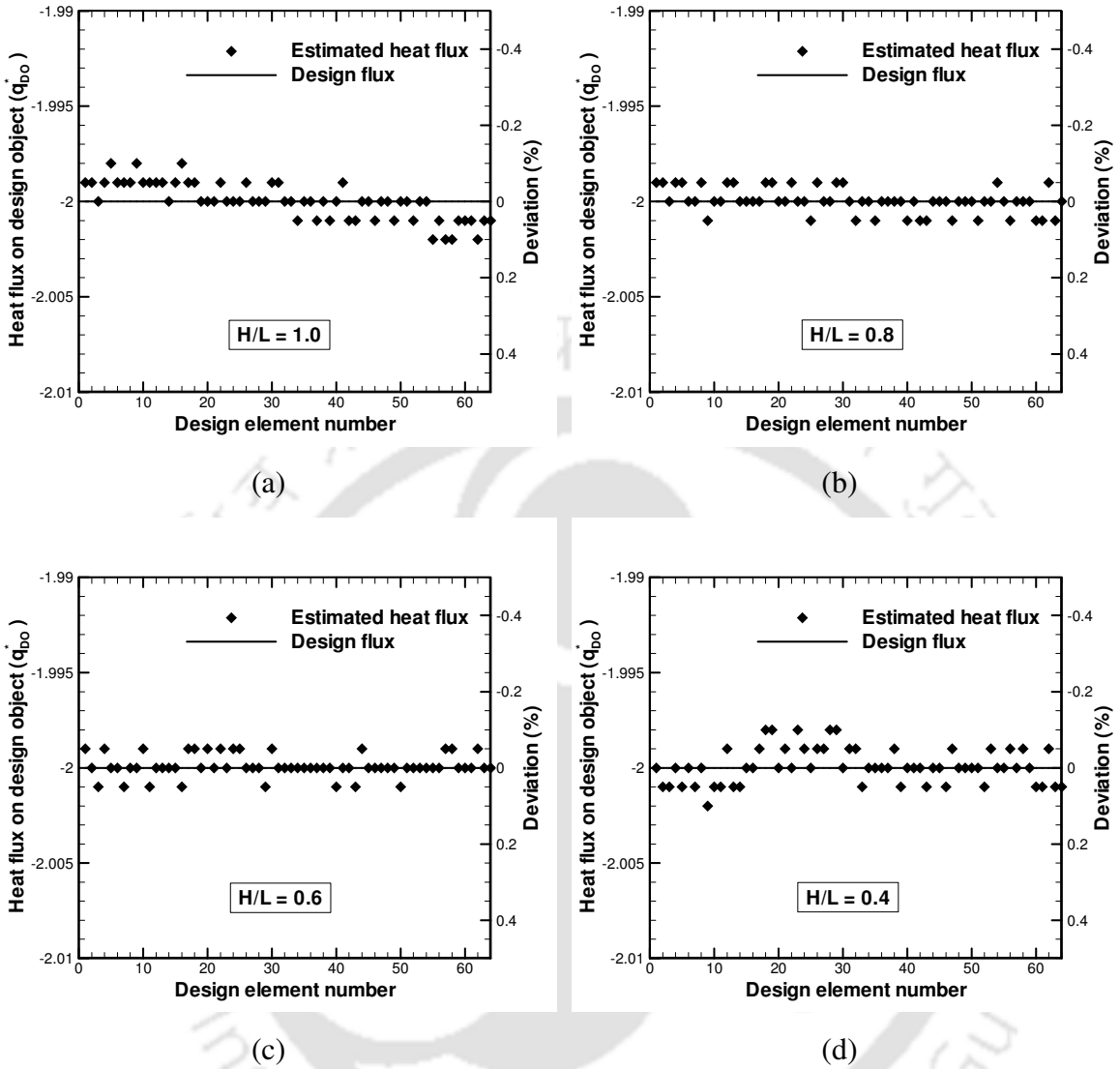

Figure 6.7. Estimated heat flux distribution on a circular design object (diameter 0.5 m), placed on the bottom of radiant enclosure (L=W= 1.0m) with different aspect ratio $\left(H/L\right)$= (a) 1.0, (b) 0.8, (c) 0.6, (d) 0.4.

0.7m., and 0.8 m. is found 0.199 %, 0.4%, 1.0%, and 2.0%, respectively. The results are also confirmed with Daun *et al.* (2006). Figs. 6.7a-d shows the estimated heat flux distribution on the DO (diameter 0.5 m) placed on the bottom of radiant furnace with four aspect ratios $\left(H/L\right)$, viz. 1.0, 0.8, 0.6 and 0.4, respectively. For these cases (Figs. 6.7a-d),

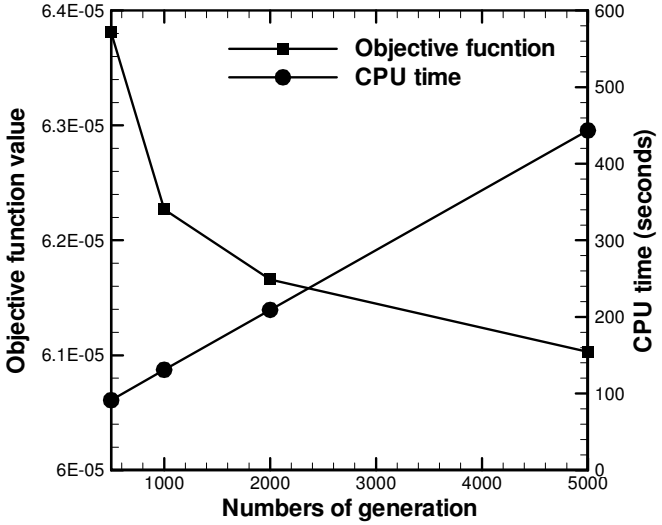

Figure 6.8. Effect of number of generations on the convergence of the objective function and the corresponding CPU time.

the maximum deviation of estimated heat flux is 0.199%, 0.10%, 0.10% and 0.2 %, respectively. The difference in the maximum deviation is attributed to the effect of specular vertical furnace walls. For particular material heating process, such kind of study is helpful in furnace design prior to the fabrication.

Having estimated the uniform thermal conditions accurately on the 2-D irregular shaped DOs, next, in the inverse analysis, the effect of numbers of generations and the CPU time has been studied. In present work, the MGA has been used as an optimization tool. The minimum value of the objective function reflects the accuracy in the solution. In the minimization problems such as the present one, as the objective function tends to minimum, simultaneously solution approaches to the global optimum. In this study, the algorithm studied for four numbers of generations, 500, 1000, 2000, and 5000. For these cases the CPU time is also recorded. Fig. 6.8 shows the variation in minimum value of the objective function with the numbers of generations, and the corresponding CPU time. The expected results are obtained; the trend is well matching with the literature (Das *et al.*, 2008a). With increasing number of generations, the convergence of objective

function is improved but the rate of convergence becomes slow. For the present study, 1000 generations are found adequate to get the accurate estimation. The CPU time has linearly increasing trend with the numbers of generations. In next section, the problem is extended to boundary design of 3-D radiant furnace for 3-D irregular shaped DOs.

6.3 Radiant Boundary Design for 3-D Irregular Shaped Design Object

The thermal uniformity is very important in several material heating processes like electronic components manufacturing, curing and drying of paints and many more. The importance of the uniform thermal conditions in material heating is well discussed in Chapter 1. In diverse applications of material heating processes, products of different shapes and sizes are needed to be processed. Shapes and sizes of the products are not regular all the times. It is seen that, in the literature (section 1.2), various boundary design problems involving different geometries and different modes of heat transfer have been analyzed. However, the boundary design problems involving the 3-D irregular shaped DO have not been found. The furnace boundary design problems for uniform thermal conditions on the 3-D irregular shaped DOs are of practical use.

The studies presented in this section deals with estimation of optimal heater power settings along the five walls of a 3-D radiant furnace that produce desired uniform thermal conditions on a 3-D irregular shaped DO placed inside the radiant furnace. The expected uniform thermal conditions are $\left(T^{*}=1.0 \text{ and } q_{DO}^{*}=-2.0\right)$. The present algorithm (REM^2 + MGA) is modified for 3-D irregular shaped DO using the energy balance given in Eq. 6.1. Different irregular shaped DOs, such as hemispherical, conical, cylindrical, and the DOs made of the combination of these shapes are considered. For sample DO models, the effects of DO size and aspect ratios of furnace enclosure, on the thermal uniformity are also studied. Suitability of the design parameters is decided on the basis of deviation in estimated heat flux distribution on DOs. Also, the furnace boundary design problem for more complex DO has been shown through the appropriate study.

6.3.1. Radiant boundary design for a hemispherical shaped design object

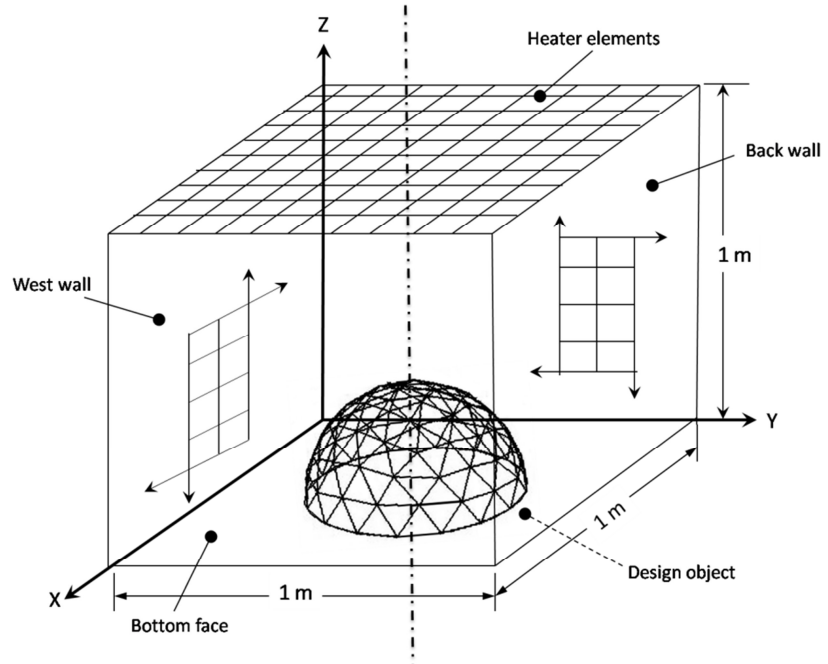

Figure 6.9. Schematic of the radiant furnace enclosure, and a hemispherical shaped DO (dia. 0.5 m) with irregular surface elements, placed on the bottom face of the furnace.

Fig. 6.9 shows the schematic of radiant furnace $\left(\text{dimensions: } L = W = H = 1.0 \text{ m}\right)$ with a centrally located hemispherical DO (diameter 0.5 m) on the bottom (X-Y plane) of the enclosure. Except the bottom surface, on which the DO is located, the DO is considered to be irradiated by the panel heaters placed along one or more of the remaining 5 walls of the furnace. The bottom surface of radiant furnace not covered by the DO is insulated. The five boundary walls (top, west, east, front and back) containing panel heaters can be diffuse or diffuse specular. To calculate the radiative information using REM^2, the inside surface areas of the radiant furnace are divided into equal size $\left(0.1\text{m}\times 0.1\text{m}\right)$. Since in the present section, the DOs are of irregular shapes, the surface areas of the DO are divided into irregular shaped triangular surface elements.

The panel heaters are set with the (non-dimensional) power range, $\left(q_H^*\right)$ of 0.0001 – 4.0. The lower bound for power of the panel heaters is intentionally taken very small, so that the heaters having very less power can be neglected. For all the cases in section 6.3, to minimize the objective function, in the MGA with population size 10, 5000 generations are performed. To maintain the optimality, in every generation the heater power have been regulated using Eq. (6.1). In this way in the present algorithm (MGA+REM^2), during every generation the power of heaters are varied within the given range.

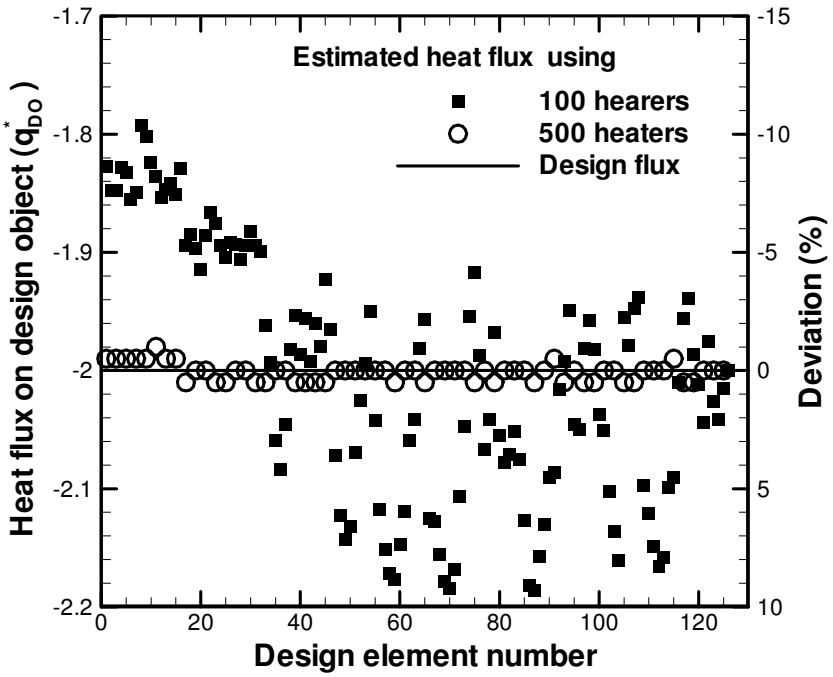

Figure 6.10. Estimated heat flux distribution using 100 heaters (along the top wall) and 500 (along the 5 walls) heaters on hemispherical DO (diameter 0.5 m).

For the case of hemispherical DO (Fig. 6.9), initially, heaters along the top wall are considered active for computation, while rest all surfaces are insulated. It is seen from Fig. 6.10 that considering 100 panel heaters along the top wall, even using optimization algorithm desired uniform thermal conditions are not achieved. Next, like the problems in Chapter 4, except the bottom wall on which the DO is located, 100 panel heaters along each of the 5 walls are considered. Fig. 6.10 shows the estimated heat flux distribution considering the heaters along each of the 5 walls of radiant enclosure. It is seen that the

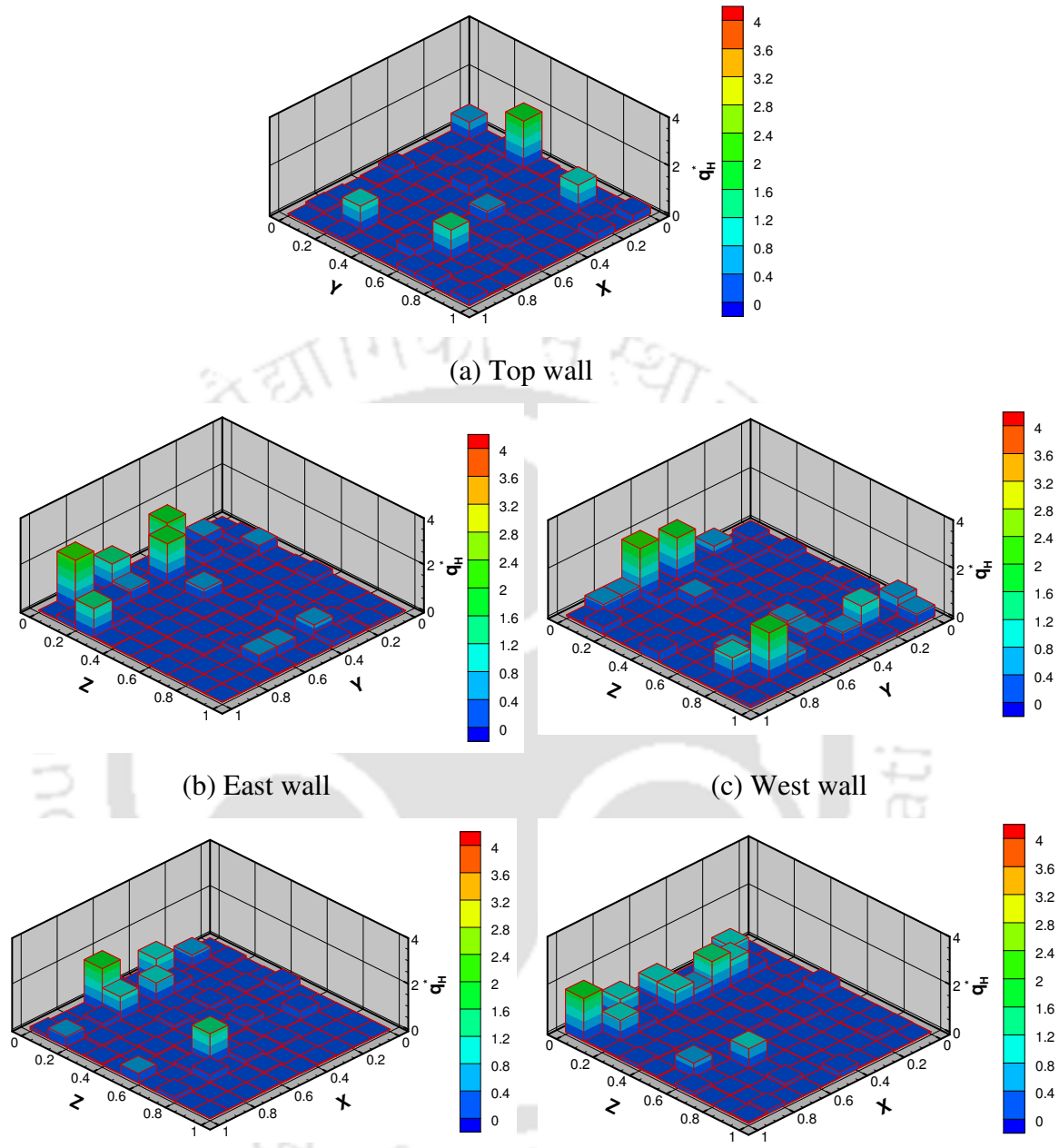

Figure 6.11. Optimal heater power distribution along the furnace walls for hemispherical DO model (dia. 0.5 m) (a) top wall (b) east wall (c) west wall, (d) back wall, (e) front wall.

desired uniform thermal conditions are achieved accurately, with maximum deviation $\pm 1.0\,\%$. Hence, in the present study all computations are done considering heaters along

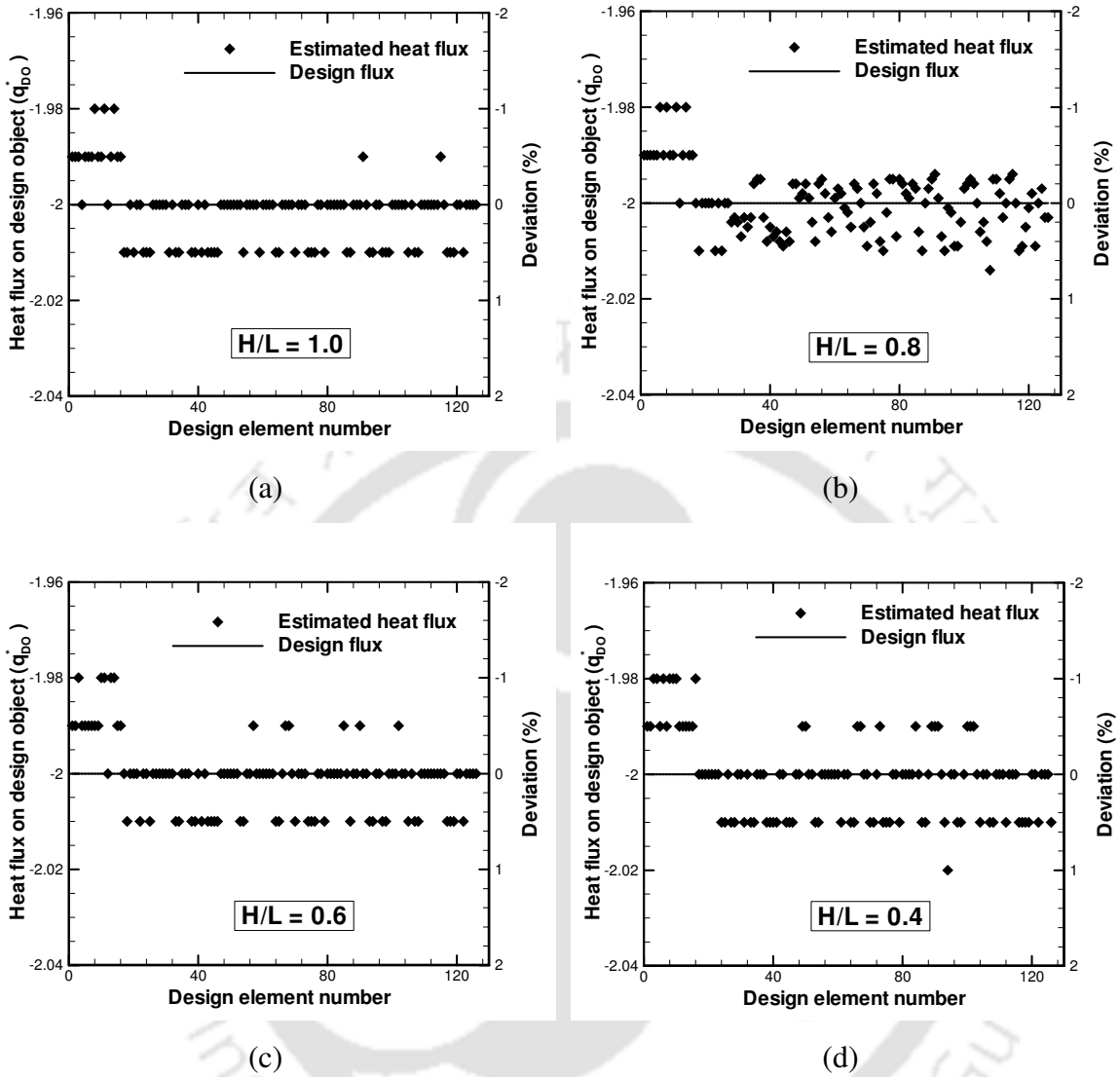

Figure 6.12. Effect of aspect ratio (*H/L*) of radiant enclosure on the uniformity of estimated heat flux distribution on the surface of hemispherical DO (dia. 0.5 m).

five walls of the radiant enclosure. Next, it is demonstrated that even 500 heater elements are used for computation, several of heater elements can be neglected according to the results and very few are required for the particular problem.

To have uniform thermal conditions, it becomes important to know the required heater configuration and optimal power distribution of the panel heaters along the furnace enclosure walls. It is also important to know that, is all the heaters to be placed and

activated? To ascertain these doubts, a sample study is done, in which the hemispherical DO (dia. 0.5 m), is centrally located (0.5, 0.5, 0.0) on the bottom surface of the radiant enclosure, $(L=W=H=1.0\text{m})$, as shown in Fig. 6.9a. The optimal power requirement for the heaters placed along top, east, west, back and front wall is shown in Fig. 6.13a-e, respectively. From Fig. 6.11a-e, it is observed that some of the heater elements require very less power, so they can be neglected. Such policy can work well for practical applications to save the fabrication cost. It is evident from the results, even though for the numerical experiments, 500 heater elements are needed, but for a specific DO, this does not mean that all the heaters are actually to be placed. In the present case it is observed that less than 30 heater elements are enough to produce the desired effect.

After accurate estimation of desired thermal conditions on a hemispherical shaped DO, next, keeping dimensions of the DO fixed (dia. 0.5 m), the effect of aspect ratios on estimation of heat flux distribution have been studied. The boundary design problems have been studied with length and width of furnace enclosure L = 1.0 m and W = 1.0 m and four aspect ratio values viz. $H/L = 0.4$, 0.6, 0.8 and 1.0. As mentioned before, the surface of hemispherical DO (dia.=0.5 m) is divided into 126 irregular triangular surface elements. The estimated heat flux distribution on the surface of DO and deviation (%) in estimated flux, for different aspect ratios of the radiant enclosure, is shown in Figs. 6.12a-d. It is seen that, with all the four aspect ratios, viz. $H/L = 0.4, 0.6, 0.8 \text{ and } 1.0,$ the desired uniform heat flux $q^*_{DO} = -2.0$ on the surface of a DO is achievable. The maximum deviation in four cases i.e. $H/L = 0.4, 0.6, 0.8$ and 1.0, is found as 1.9%, 1.8 %, 1.7%, and 1.45%, respectively.

From the study given in Chapter 4, section 4.2, it is learnt that for a given dimensions of the furnace, all the sizes of DOs are not equally suitable for yielding uniform thermal conditions, it is interesting to know how the estimation behaves with different dimensions of present DO. Having understood, the effect of aspect ratios of the furnace enclosure, next keeping the dimensions of furnace enclosure $(L = W = H = 1.0\text{ m})$, heater power

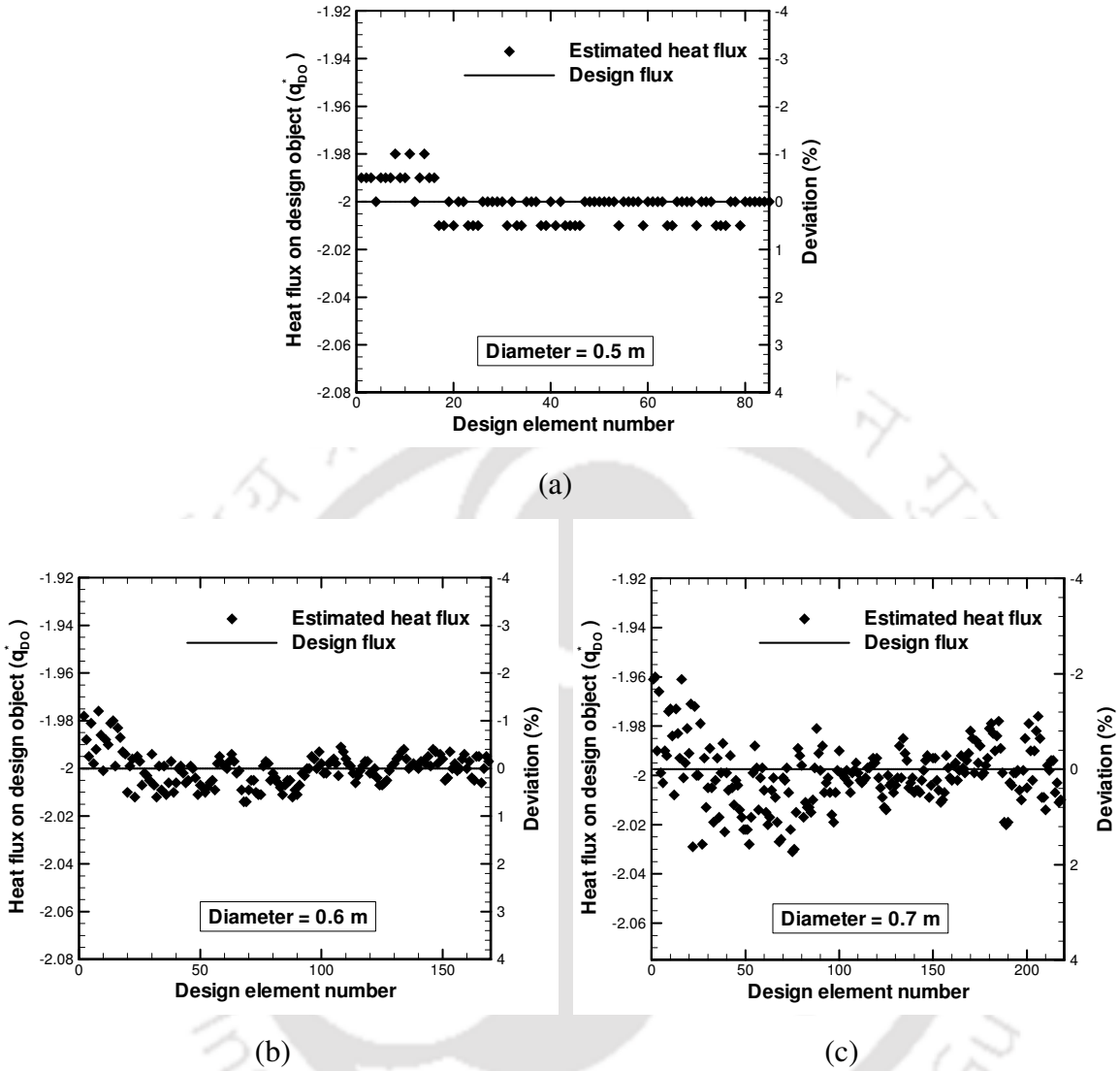

Figure 6.13. Effect of size (diameter) of hemispherical design object on the uniformity of estimated heat flux distribution, Furnace enclosure size $(L = W = H = 1.0\,\mathrm{m})$.

range and the other parameters of algorithm fixed, uniformity in estimated heat flux distribution is studied for different sizes of hemispherical shaped DOs, viz. diameter 0.5m, 0.6m, and 0.7m. The estimated heat flux distribution and the corresponding deviation (%) on the hemispherical DO of dia. 0.5m, 0.6m and 0.7 m. is shown in Figs.6.13a-c, respectively. The maximum deviation in estimated heat flux distribution for hemispherical DO of dia. 0.5m, 0.6m and 0.7 m is found to be 1.45%, 1.90% and 3.55%,

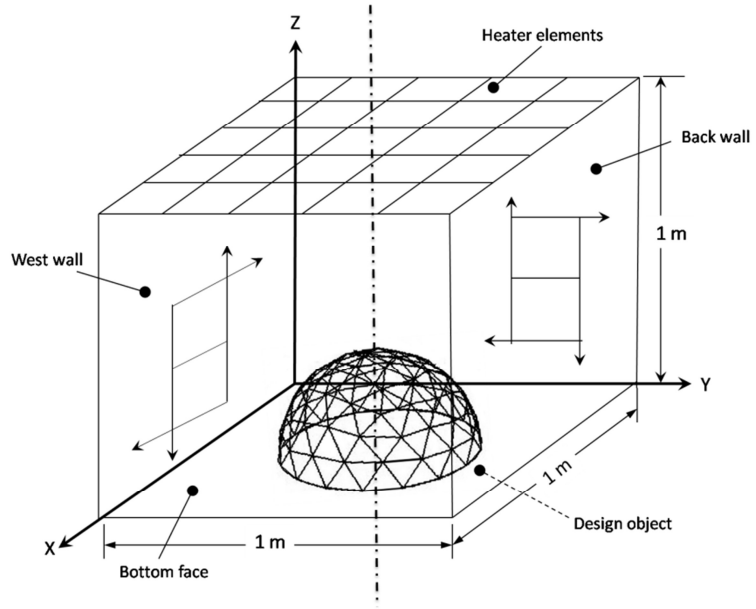

(a)

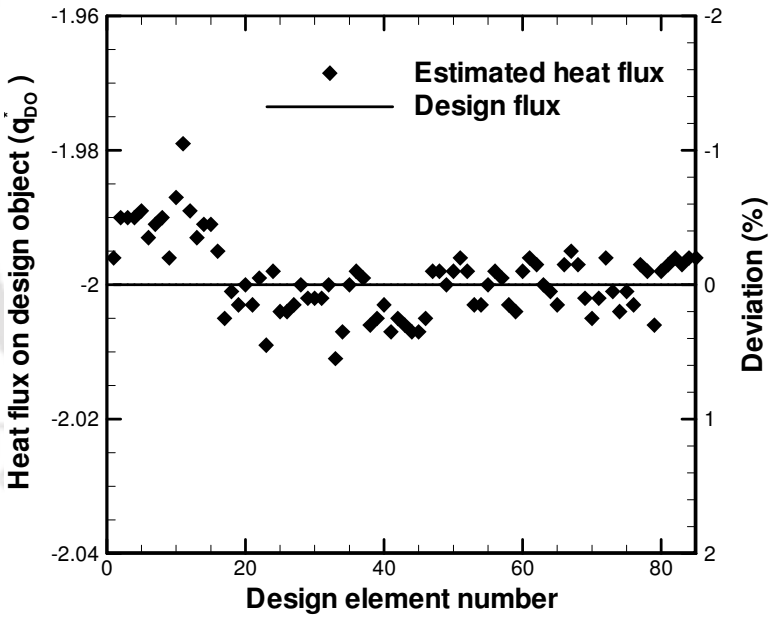

(b)

Figure 6.14. Estimated heat flux distribution on hemispherical DO (dia. 0.5 m) with 25 heater $(\text{dimension: } 0.2\,\text{m}\times 0.2\,\text{m})$ elements on each of the five furnace walls.

respectively. It is observed from the Figs.6.13a-c, the uniformity on the smaller size DO is more accurate.

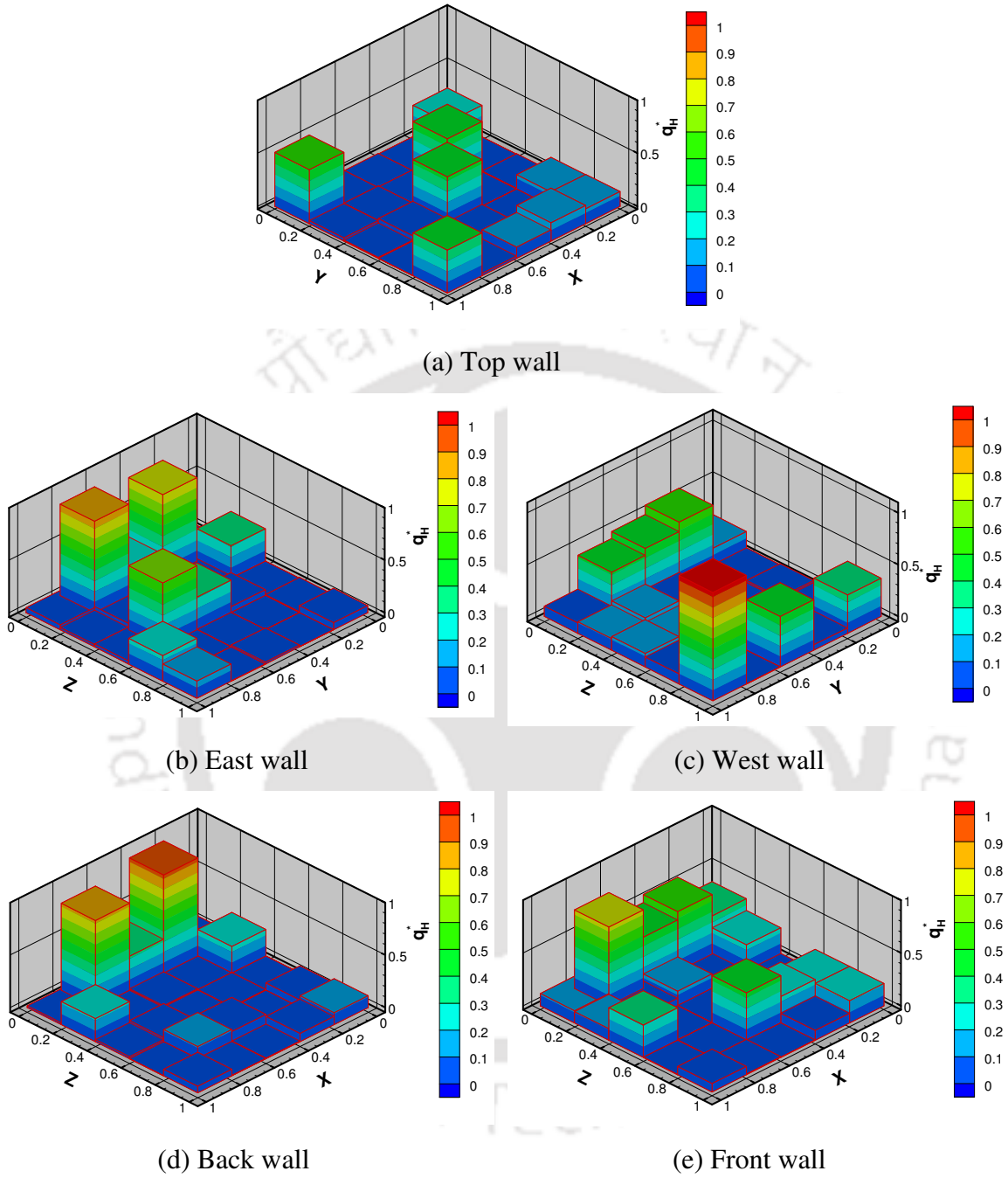

Figure 6.15. Optimal heater power distribution (125 heaters) along the enclosure walls for hemispherical DO (dia. = 0.5 m) (a) top wall (b) east wall (c) west wall, (d) back wall, (e) front wall.

In practical applications, the furnace design should be feasible for fabrication and control. Towards the efforts to reduce numbers of heaters, with same problem (Fig. 6.9), keeping all parameters unchanged except the size of panel heaters, the same design problem is investigated with panel heaters of size $(0.2\,\mathrm{m}\times 0.2\,\mathrm{m})$, the schematic is shown in Fig. 6.14a. It is to be noted that in Fig. 6.9, the dimensions of the panel heaters was $(0.1\,\mathrm{m}\times 0.1\,\mathrm{m})$ i.e. half of the present dimensions. So with the dimensions of the furnace enclosure $(L = W = H = 1.0\,\mathrm{m})$, each wall can accommodate 25 heater elements, thus on five walls total 125 heater elements. The estimated heat flux distribution on the DO is shown in Fig. 6.14b, and the corresponding heater power settings along the five walls (top, east west, back and front) of the furnace in shown in Fig. 6.15a-e, respectively. From the comparison of the results given in Fig. 6.11a-e and Figs. 6.15a-e, it is observed that the heater power setting shown in Figs. 6.15a-e is more feasible for implementation, and that too without much loss in the uniformity of thermal conditions (refer Fig. 6.14). the deviation in the estimated heat flux distribution is less than 2%. It is shown in section 5.2, less number of unknown parameters (here the heaters power) are relatively easy for calculations in optimization algorithms. In the following sections, the results of furnace boundary design problems for deferent irregular shaped DOs are presented.

6.3.2. Radiant boundary design for a conical shaped design object

In this section, to have desired uniform thermal conditions on a conical DO, the heater power settings along five walls of furnace are estimated. Fig. 6.16 shows the schematic of radiant furnace $(\text{dimensions: } L = W = H = 1.0\,\mathrm{m})$, with centrally located conical DO (base dia. 0.5m, height 0.5m) on the bottom of enclosure. For this study, four sizes of a conical DO models have been considered, viz. model (1) dia. 0.5 m, height 0.20 m, (2) dia. 0.5 m, height 0.25 m, (3) dia. 0.5 m, height 0.50 m, and (4) dia. 0.8 m, height 0.8 m. The estimated heat flux distribution for chosen conical DO model 1- 4 is shown in Figs. 6.17a-d, respectively.

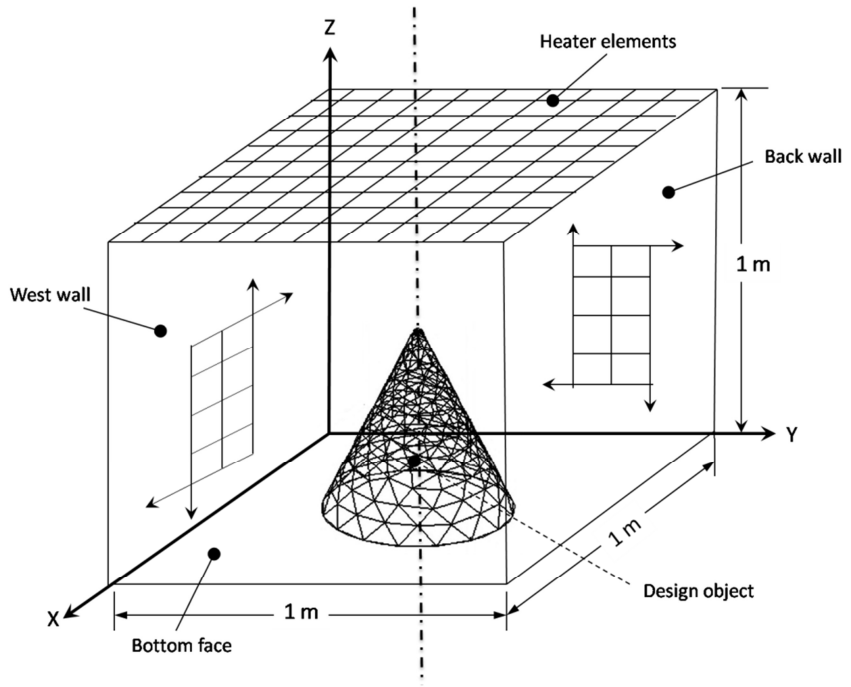

Figure 6.16. Schematic of the radiant furnace enclosure, and a conical shaped DO (dia. 0.5 m. and height 0.5 m) with irregular surface elements placed on the bottom face of the furnace.

Form Fig. 6.17a-d it is observed that the deviation in estimated flux distribution is more for larger size of the DOs. The maximum deviation in estimated heat flux on the surface of the conical DO model 1- 4 is 0.30%, 0.40%, 1.30% and 11.50%, respectively. Among them first three are of same base diameter (0.5 m) and of different height, (0.2 m, 0.25 m, and 0.5 m. The maximum deviation in case of DO model 4 (dia. 0.8 m, height 0.80 m) is found much more than the other three. This is attributed to the larger size of DO model; this size is considerably big with respect to the furnace size.

Next, with a conical DO model-3 (dia. 0.5 m, height 0.50 m) the change in uniformity of heat flux distribution with the aspect ratios (*H/L*) of the furnace enclosure is analyzed.

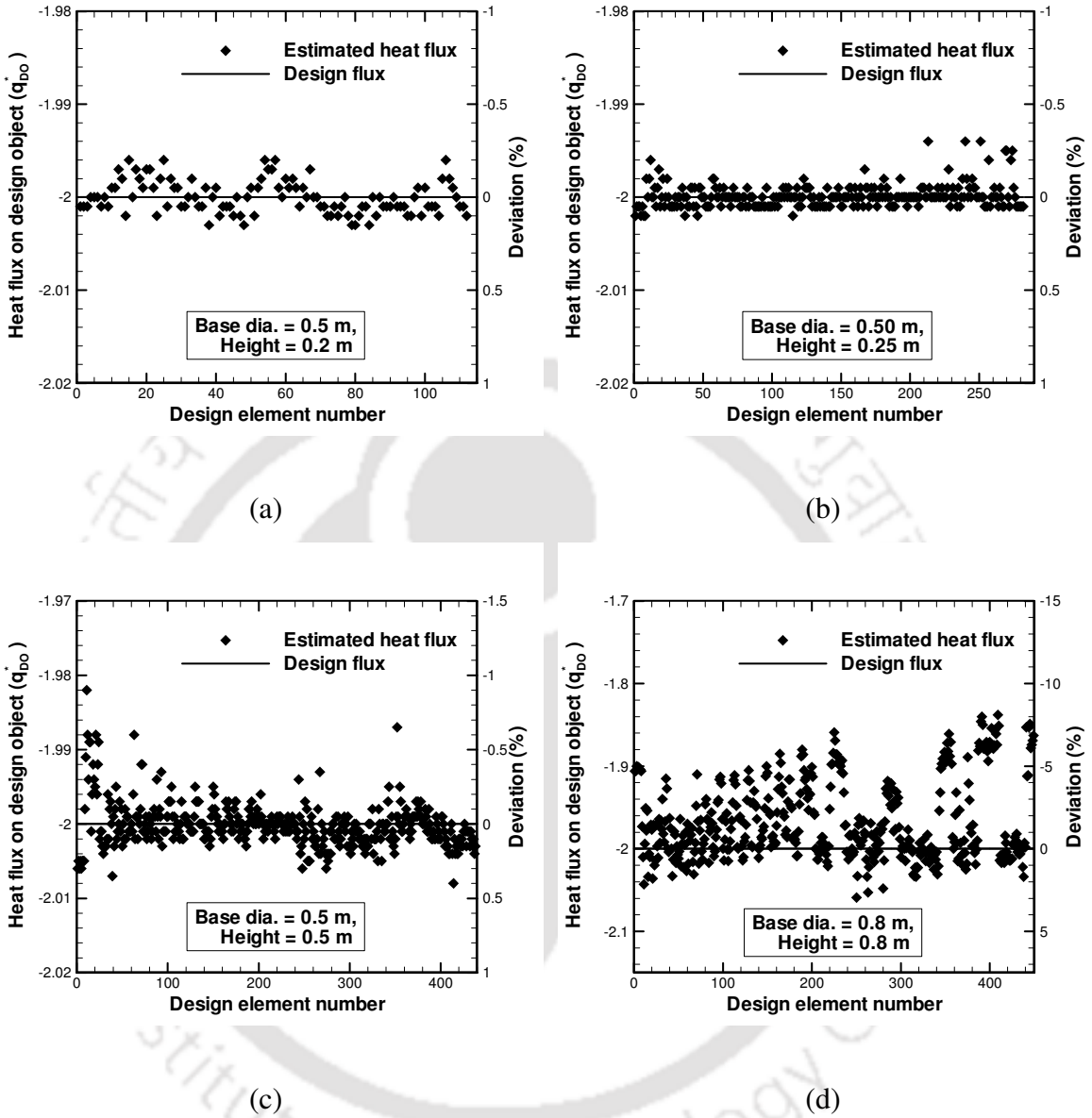

Figure 6.17. Estimated heat flux distribution on conical DOs of different sizes placed inside a fixed dimensions furnace enclosure $(1\,\text{m} \times 1\,\text{m} \times 1\,\text{m})$.

The estimated heat flux distribution on surfaces of the DOs using four aspect ratios, $H/L = 0.4$, 0.6, 0.8 and 1.0 is shown in Figs. 8.18a-d. From Figs. 6.18a-d, it is observed that with all the four aspect ratios, viz. *H/L* = 0.4, 0.6, 0.8, and 1.0, the desired uniform heat flux of $q^*_{DO} = -2.0$ on the surface of a DO is achieved. Among the four cases, better

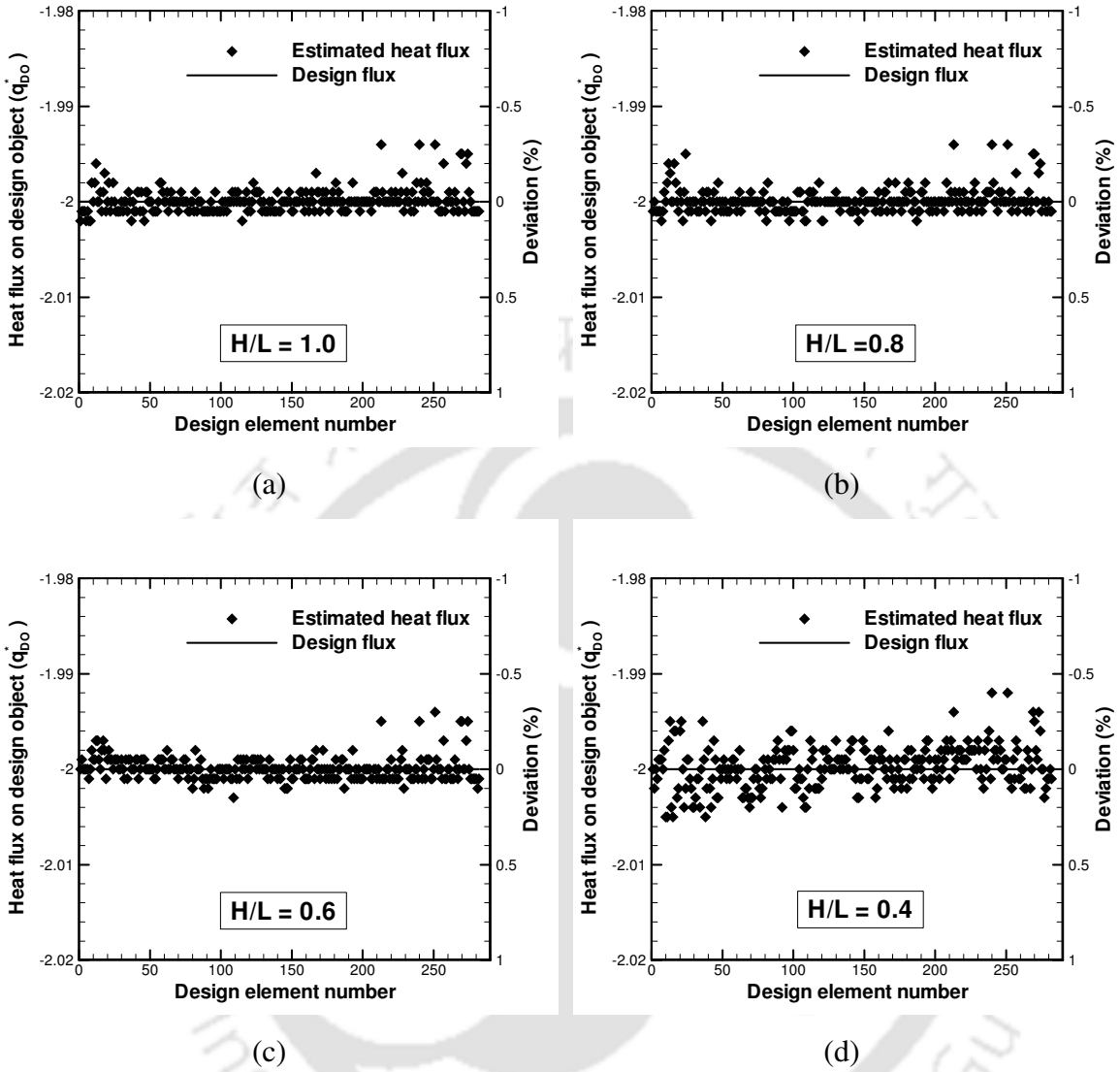

Figure 6.18. Estimated heat flux distribution on a conical DO (dia. 0.5 m, height 0.25 m) placed inside the enclosure of different aspect ratio (*H/L*) (a) 1.0, (b) 0.8, (c) 0.6, (d) 0.4.

uniformity in estimated heat flux distribution on the surfaces of a DO is observed with the aspect ratios 1.0 (Fig. 6.18a) and 0.8 (Fig. 6.11d). The maximum deviation in estimated heat flux distribution in these four cases i.e. *H/L* = 0.4, 0.6, 0.8, and 1.0 is found as 0.65%, 0.45 %, 0.40%, and 0.40%, respectively.

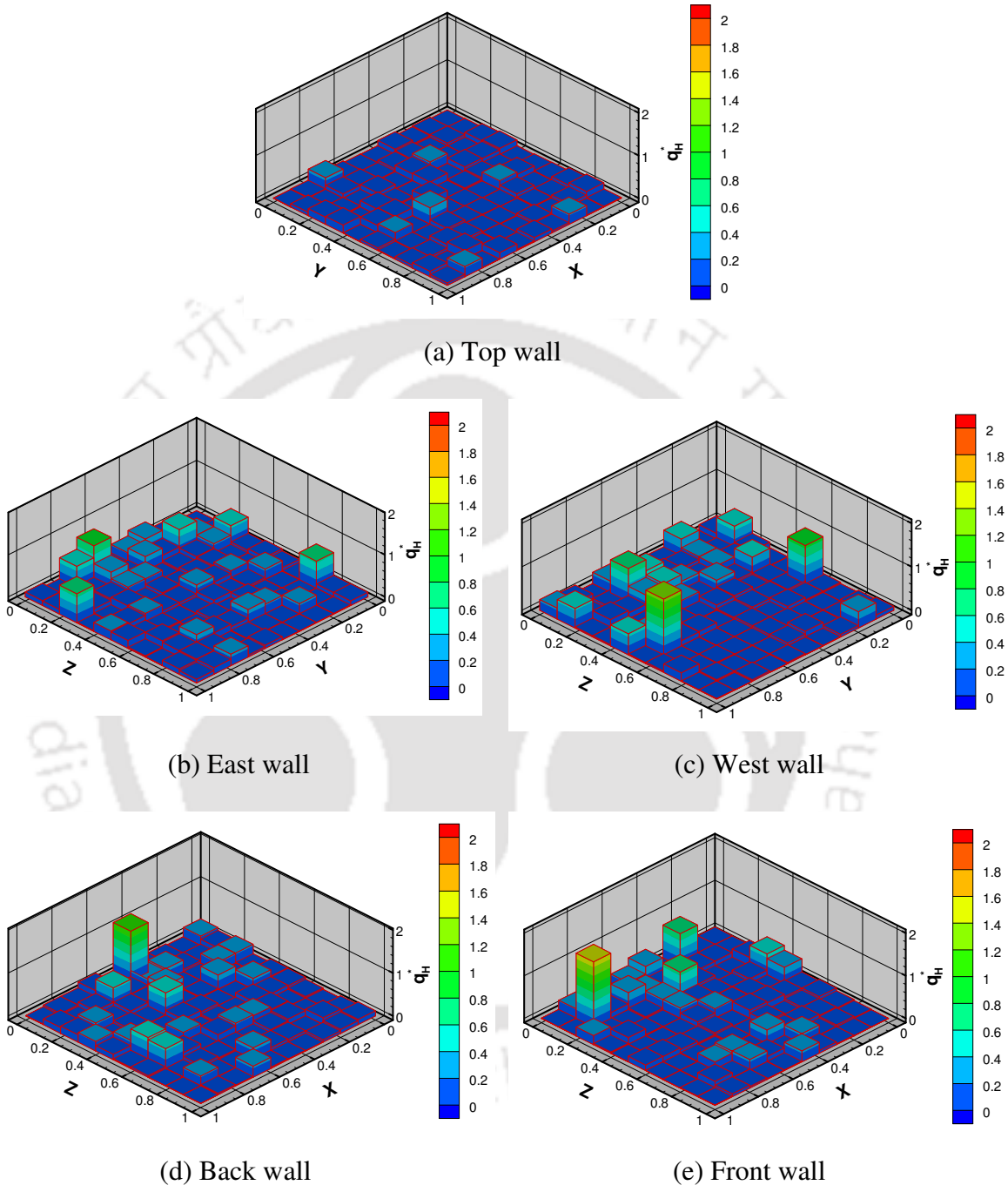

(a) Top wall

(b) East wall

(c) West wall

(d) Back wall

(e) Front wall

Figure 6.19. Optimal heater power distribution (500 heaters) along the enclosure walls for conical DO model, (dia. 0.5 m, height 0.25m), (a) top wall (b) east wall (c) west wall, (d) back wall, (e) front wall.

Like for the hemispherical DOs (section 6.3.1), similar trends of results have been observed for conical DOs. The optimal heater power setting along the five walls of furnace enclosure for conical DO model-2 (dia. 0.5 m, height 0.50 m) is shown in Fig. 6.19a-e. In this heater power settings also, very few heaters are needed for producing uniform thermal conditions.

6.3.3. Radiant boundary design for a cylindrical shaped design object

In several products/components cylindrical shape is very common. Casing of missiles and similar kind of structures, wheel drums of heavy automobile, food processing containers, and several automobile and industrial products are some of the examples. In this section, for uniform thermal conditions on a cylindrical DO, the optimal heater power settings have been determined.

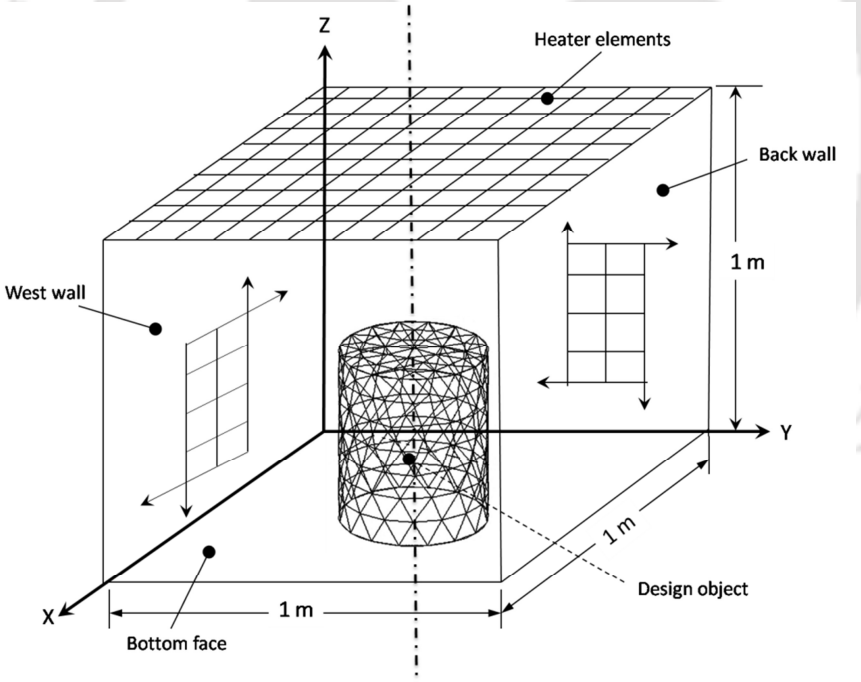

Figure 6.20. Schematic of the radiant furnace enclosure, and a cylindrical shaped DO (dia. 0.5 m. and height 0.6 m) with irregular surface elements, placed on the bottom of the $(1\,\mathrm{m}\times 1\,\mathrm{m}\times 1\,\mathrm{m})$.

.

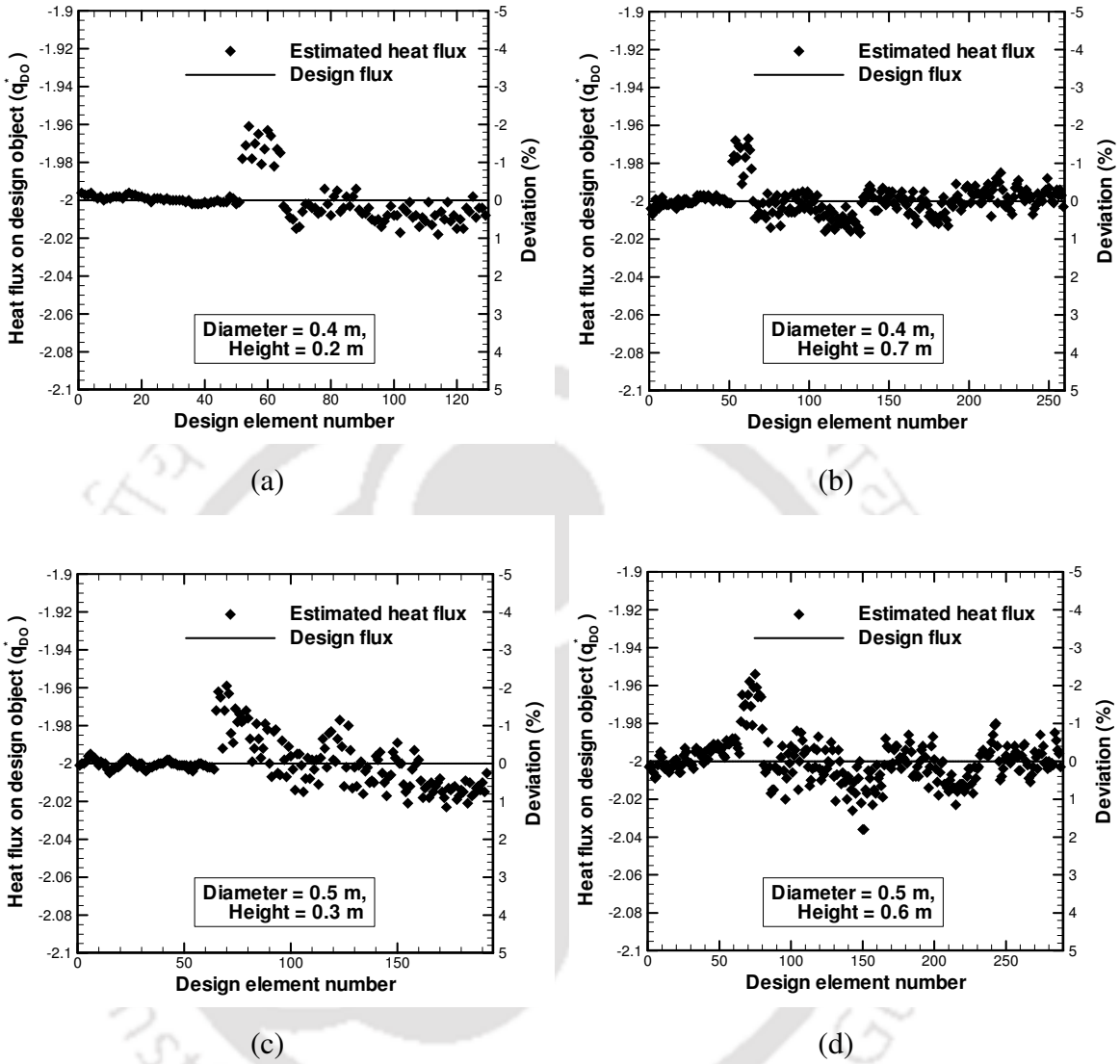

Figure 6.21. Estimated heat flux distribution on cylindrical DOs of different sizes placed inside a fixed dimensions furnace enclosure $(1\text{m}\times1\text{m}\times1\text{m})$.

Schematic of the problem involving a furnace enclosure $(\text{dimensions: } L = W = H = 1.0 \text{ m})$ and a centrally placed cylindrical DO (dia. 0.5m, height 0.6m) is shown in Fig. 6.20. Same as the previous case (section 6.3.2), the inside wall surfaces are divided into equal size $(0.1\text{m}\times0.1\text{m})$ surface elements, so the 100 panel heaters along each of the five walls of furnace. Cylindrical DO is divided into irregular

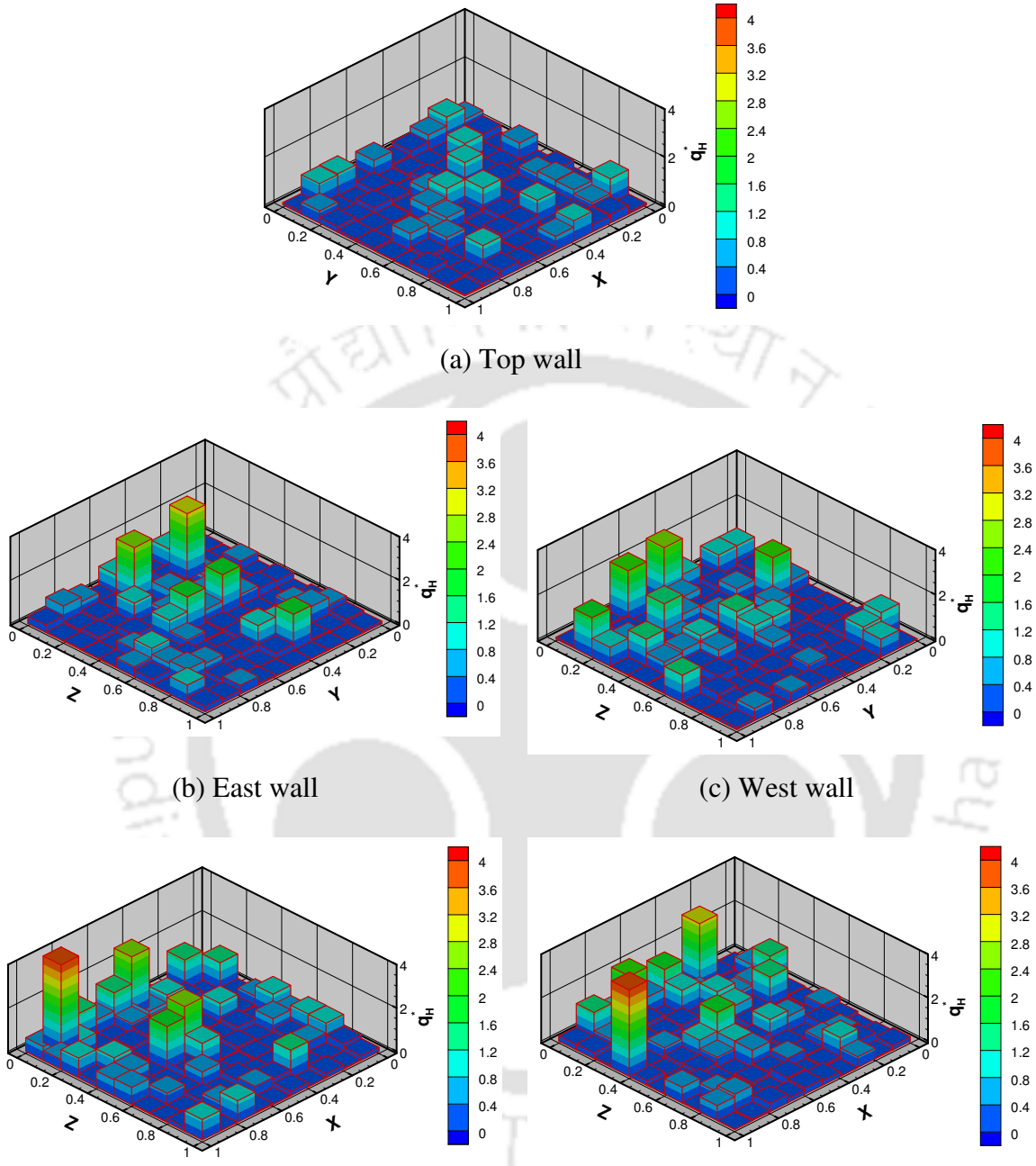

Figure 6.22. Optimal heater power distribution along the enclosure walls for cylindrical DO (dia. 0.4; height 0.7 m), (a) top wall (b) east wall (c) west wall, (d) back wall, (e) front wall.

shaped triangular surface elements. For this study, four cylindrical shaped DO models having different diameters and heights have been considered, viz. model-(1) dia. 0.4 m, height 0.2 m, (2) dia. 0.4 m, height 0.7 m, (3) dia. 0.5 m, height 0.30 m, and (4) dia. 0.5 m, height 0.6 m. Figs. 6.21a-d shows the estimated heat flux distribution on the surfaces of four cylindrical DO model 1- 4, respectively.

The maximum deviation in estimated heat flux on the surface of the cylindrical DO models 1- 4 is found to be 2.5%, 2.85%, 3.20% and 4.10%, respectively. Form Figs. 6.21a-d it is observed that heat flux uniformity on few initial surface elements is relatively accurate than the latter one. The surface elements having more uniform heat flux are the elements along top circular surface. The surface elements showing more deviation are the surface elements very near to the bottom on the furnace. The variation in estimated heat flux deviations is owing to the difference in radiative visibility among the DO surface elements and the heaters located along furnace walls. From the results shown in Fig. 6.17a-d and Fig. 6.21a-d, it is observed that to produce uniform thermal conditions on the cylindrical objects (6.21a-d) is relatively difficult than that of the conical DO (Fig. 6.17a-d). The optimal heater power distribution along the five walls of the furnace enclosure, which produce the uniform heat flux distribution on the cylindrical DO model-2 (dia. 0.4 m, height 0.70 m) is shown in Fig. 6.22a-e. Compare to the previous cases of heater power settings i.e. of spherical DO (Fig. 6.13a-e) and conical DO (Figs. 6.19a-e), in the present case of cylindrical DO (Figs.6.22) heaters power are relatively more dispersed along the furnace walls. From the experience it is observed that the heater power get more dispersed where the solution is relatively difficult.

6.3.4. Radiant boundary design for a 3-D irregular shaped design object: combinations of cylindrical and conical shape.

In this section, application of the present algorithm is extended for finding the optimal power of the panel heaters to produce desired uniform thermal conditions on more complex shaped DO, which is the combination of conical and cylindrical shapes. Applications of such problems are mainly in fabrication of testing facility for the missile casing components. Fig. 6.23 shows the schematic of computational domain, consist of

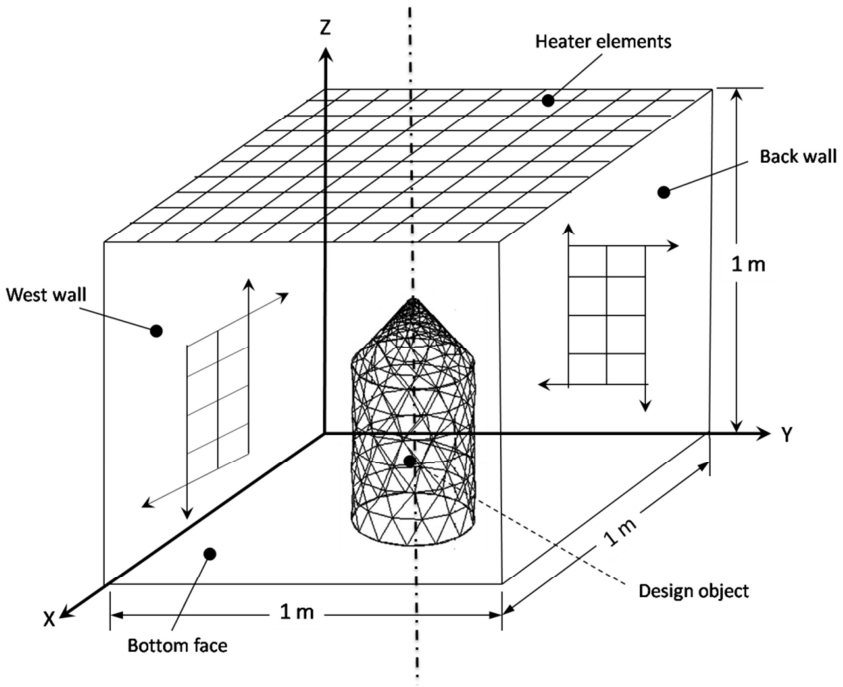

Figure 6.23. Schematic of the radiant furnace enclosure and a DO (combination of cylinder dia. 0.4 m. and height 0.5 m and cone dia. 0.4 m. and height 0.2 m) with irregular surface elements, placed on the bottom face of the furnace $(1\,\mathrm{m}\times 1\,\mathrm{m}\times 1\,\mathrm{m})$.

.

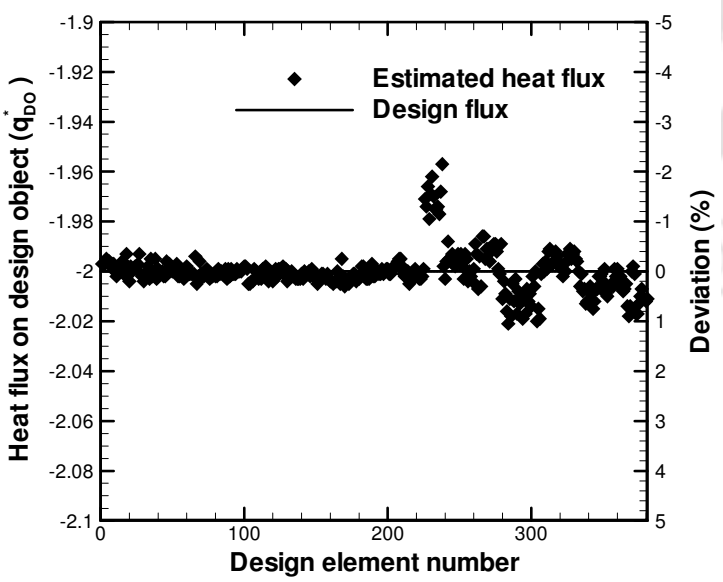

Figure 6.24. Estimated heat flux distribution on design object shown in Fig. 6.23.

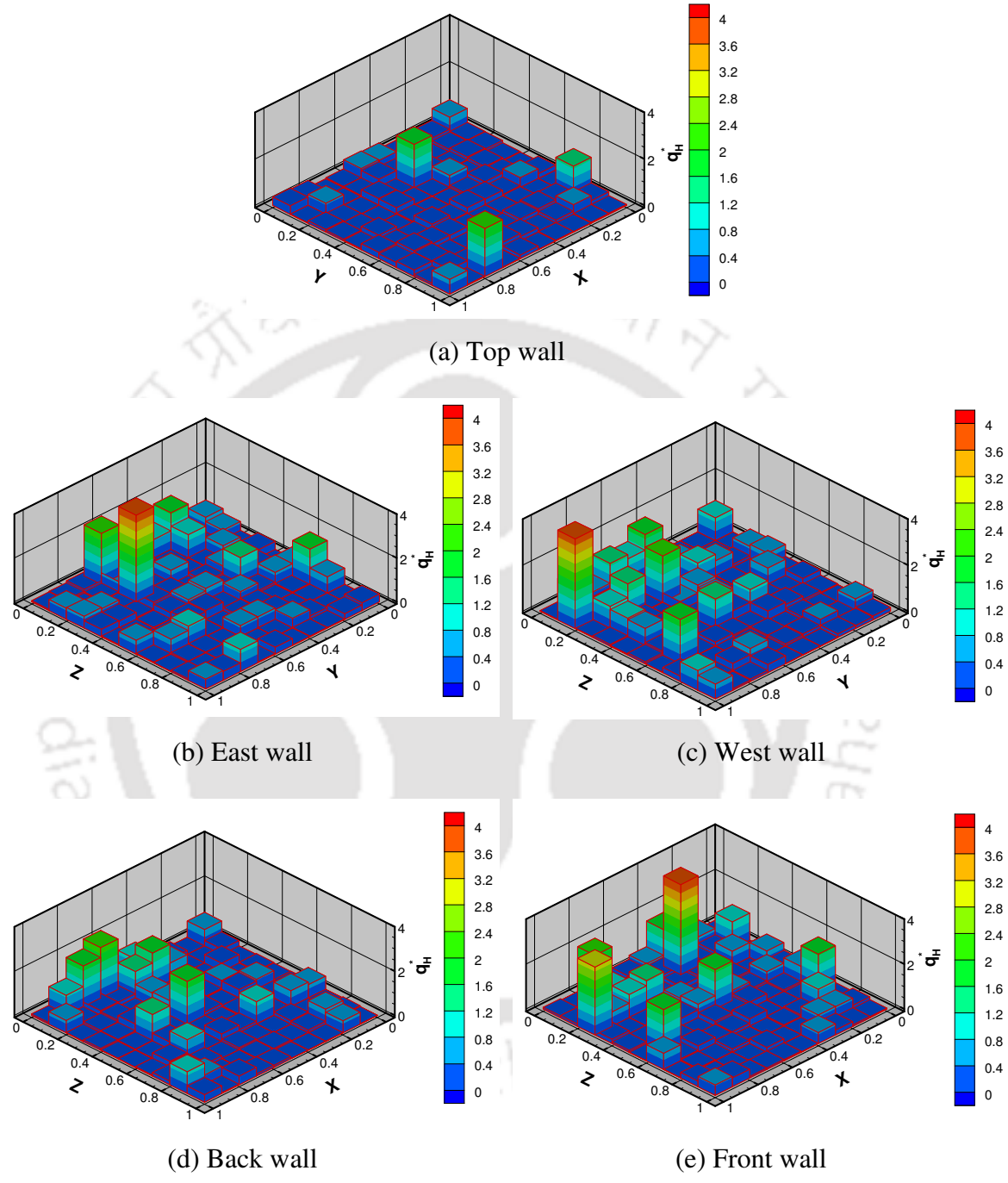

Figure 6.25. Optimal heater power distribution along the five walls of the furnace for the DO shown in Fig 6.23 (a) top wall (b) east wall (c) west wall, (d) back wall, (e) front wall.

radiant furnace dimensions: $L = W = H = 1.0$ m, with a centrally located DO (cylinder: dia. 0.4m, height 0.5m; + cone: base dia. 0.4m, height 0.2m). The DO is assumed to be irradiated by 100 panel heaters along each of the five walls of the furnace, while the bottom surface not covered by the DO is insulated.

The estimated heat flux distribution and corresponding deviation on the chosen DO (Fig. 6.23) is shown in Figs. 6.24. It can be seen that the results shown in Fig. 6.24 is like the combinations of estimated heat flux distribution on conical and the cylindrical DO. The maximum deviation in the estimated heat flux distribution is 3.15%. The maximum deviation is the sum of the deviations on the either side (±) of the design heat flux $\left(q^*_{DO} = -2.0\right)$. The optimal heater power distribution along the five walls of the furnace enclosure for the chosen DO (Fig. 6.23) is shown in Fig. 6.25a-e. As in case of spherical and conical DO, similar trend in heaters power distribution is obtained. In this heater power setting also, only few heaters is need the substantial power and rest of other very less, so they can be neglected.

6.3.5. Radiant furnace design for more complex design object

After successful demonstration of the design of optimal heater power settings for desired uniform thermal conditions on the 2-D and the 3-D DOs irregular shaped objects, in this section, the boundary heater design for an industrial relevant application is given through a sample study. In this study, more complex case has been considered; a car body model is taken as a DO (Fig. 6.26a). The chosen DO model is a sheet metal body of any car, and the aim is to design the boundary heaters of radiant furnace that produce uniform thermal conditions on the whole car body. This kind of study can be very useful in the paint drying operation in the automobile industries that can save considerable cost of heating. It is to be noted that the DO considered in present study is not an exact simulation of any particular car body model; it is a representation of application based complex shaped DO. The schematic of the radiant furnace enclosure with the design model placed on the bottom of furnace is as shown in Fig. 6.26a, while the magnified view of the design model with irregular surface elements is shown in Fig. 6.26b.

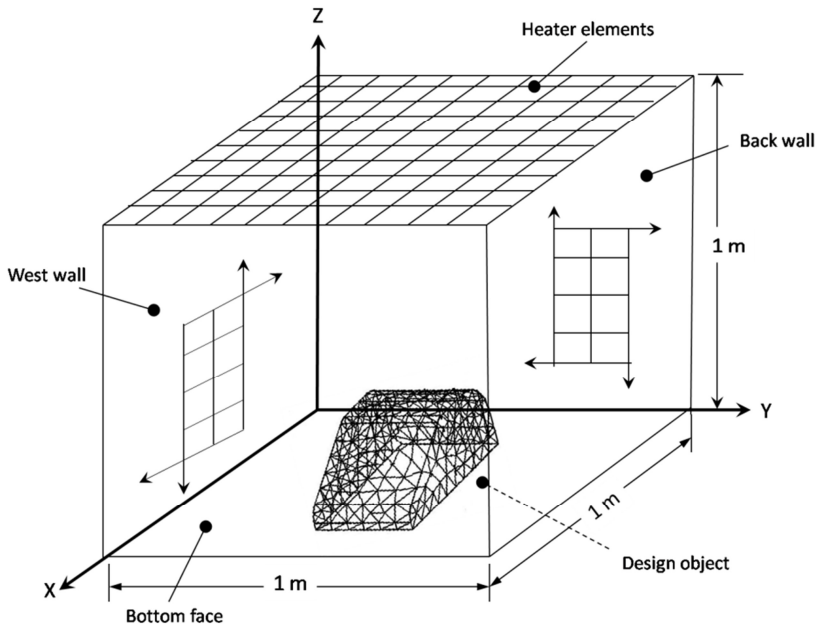

(a)

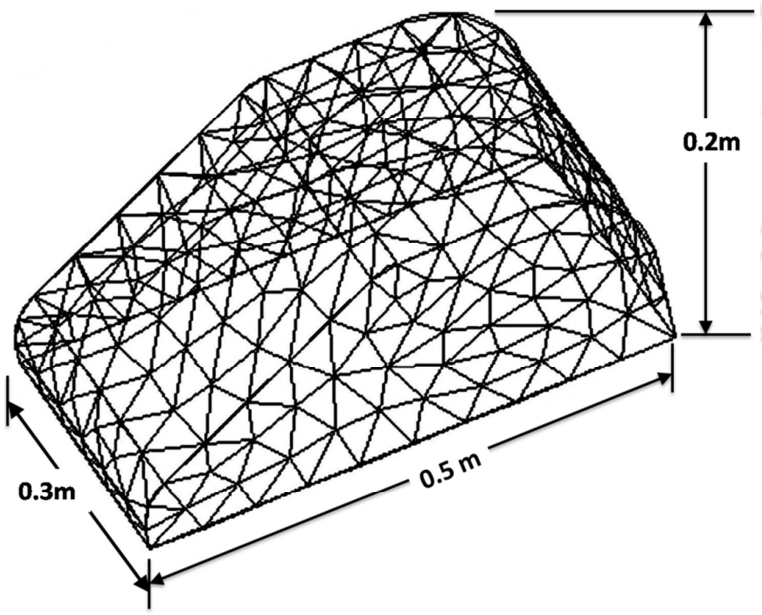

(b)

Figure 6.26. (a) Schematic of the radiant furnace enclosure and a car body model (DO) $(l = 0.5\,\text{m},\ w = 0.3\,\text{m},\ h = 0.2\,\text{m})$ with irregular surface elements placed on the bottom of furnace, (b) the DO with irregular triangular surface elements.

.

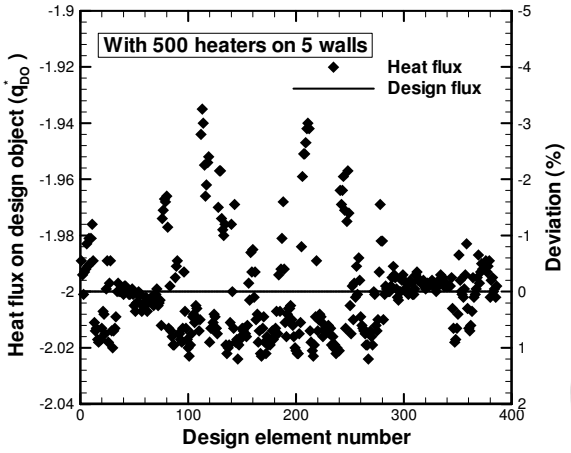

(a)

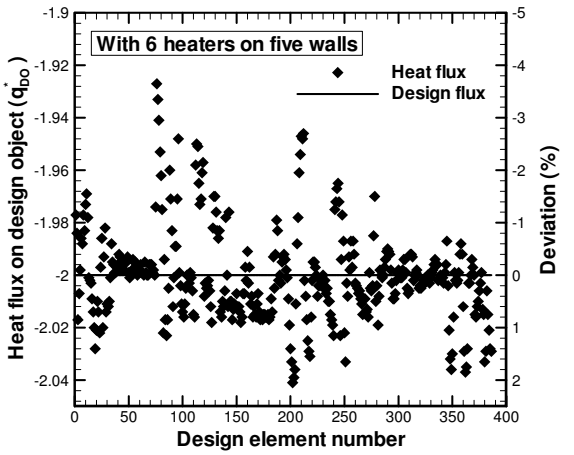

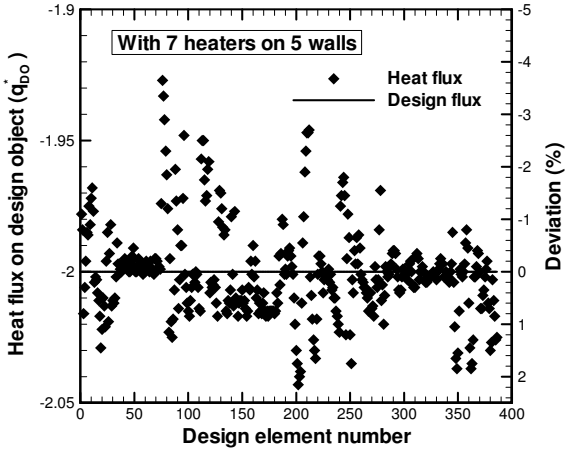

(b) (c)

Figure 6.27. Estimated heat flux distribution for (a) general case (refer Fig.6.26), (b) using 6 heaters, and (c) using 7 heaters.

The computational model including the furnace enclosure is built using modeling software PATRAN 2005. All enclosure walls are divided into equal size 0.1 m × 0.1 m of square elements, 100 surface elements on each of five walls while the car body model is divided into 386 irregular shaped triangular surface elements.

The desired uniform thermal conditions on a chosen DO are $T^* = 1.0$ and $q^*_{DO} = -2.0$. For finding the optimal heater power settings, in first part of this study, 100 heaters are

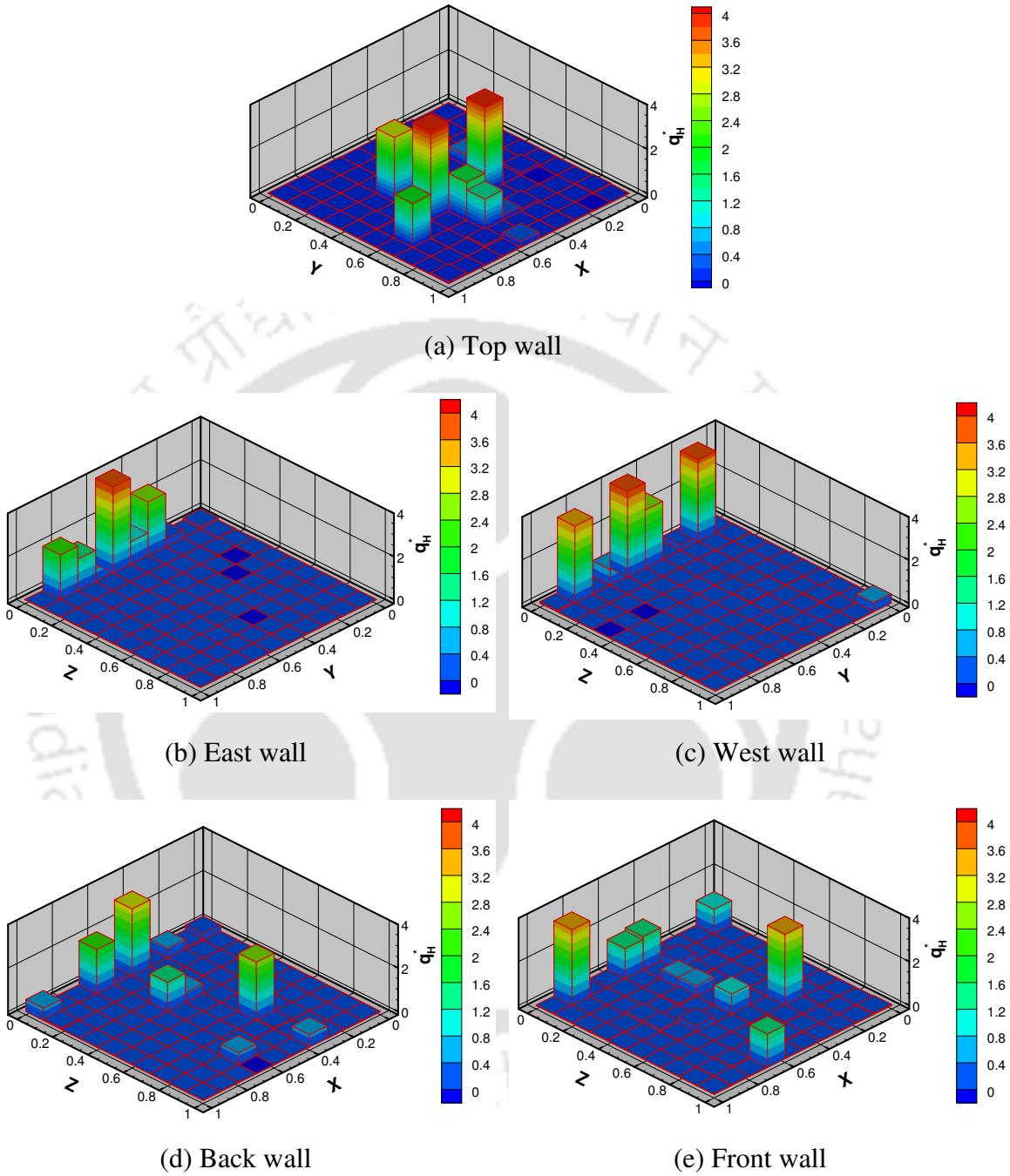

(a) Top wall

(b) East wall

(c) West wall

(d) Back wall

(e) Front wall

Figure 6.28. Optimal heater power distribution along the enclosure walls for car body model (a) top wall (b) east wall (c) west wall, (d) back wall, (e) front wall.

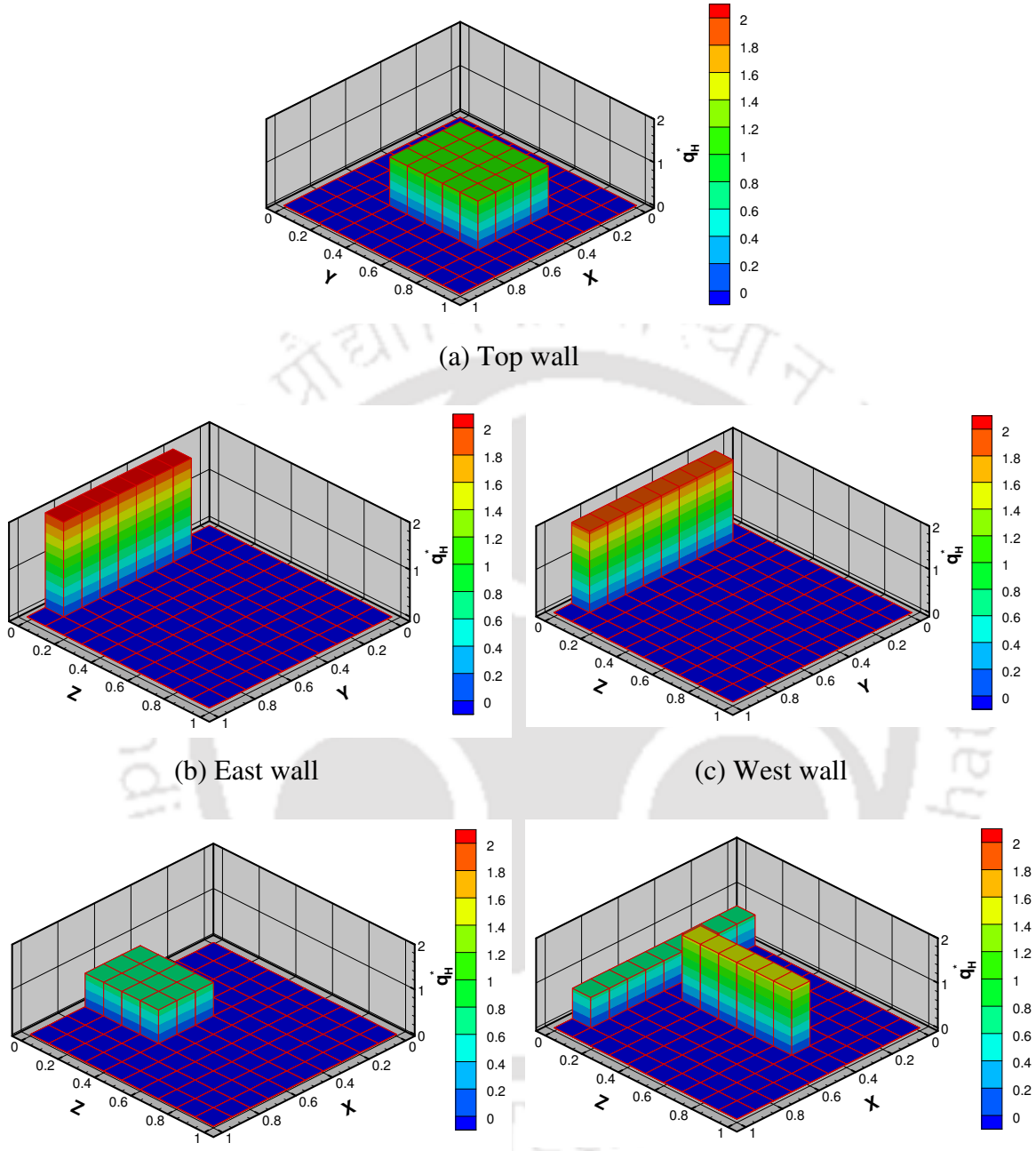

Figure 6.29. Modified optimal heater power distribution (6 heaters) along the enclosure walls for car model (a) top wall (b) east wall (c) west wall, (d) back wall, (e) front wall.

considered along each of the five walls of furnace enclosure. So this computation is done with 500 heater elements and the objective is to produce the desired uniform thermal conditions on the chosen DO. Using the present optimization algorithm (REM^2 + MGA), the optimal heater power distribution along the furnace wall are determined. In the MGA with population size 10, 5000 generations are performed. Fig. 6.27a shows the estimated heat flux distribution on surfaces of the chosen DO (Fig. 6.26b). The maximum deviation in the estimated flux is found to be 4.5% and the average deviation is 0.0282%. Fig. 6.28a-e shows the corresponding optimal heater power distribution along the five walls of furnace. From Figs. 6.28a-e, it is observed that even 500 panel heaters have been used for computation, merely about 25 panel heaters are sufficient to produce the desired uniform thermal conditions.

For practical applications, the heater power setting can be more interesting if the numbers of heaters reduced to the possible minimum. Towards this aspect, for the same problem (Fig. 6.26a), a general solution for feasible design of radiant furnace has been developed. The panel heaters having considerable power requirement have been grouped into a single heater on each wall except the front wall, the panel heaters from front wall grouped into two, thus now only six heaters are along the five walls of enclosure. The inverse boundary design problem is solved. Now there are only six unknown parameters. In this way the computational load of optimization algorithm is reduced drastically. In this study, the algorithm parameter kept unchanged. Fig. 6.27b shows the estimated heat flux distribution on the DO (Figs. 6.26b). It is observed from Fig. 6.27b that, the maximum and average deviation is 5.70 % and 0.0242%, respectively. Even with only 6 heaters along the five walls of enclosure, the deviation is acceptable. This suggest that the location of the heaters is very much important in the boundary design problems, and that can be found using the proper optimization procedure. It is to be noted that, the grouping of heaters is done on the basis of results shown in Figs. 6.28a-e. The optimal heater power distribution with 6 heaters along the five walls is shown in Figs.6.29a-e. Unless the optimization algorithm is used, to decide the location and the power requirement of heaters is difficult.

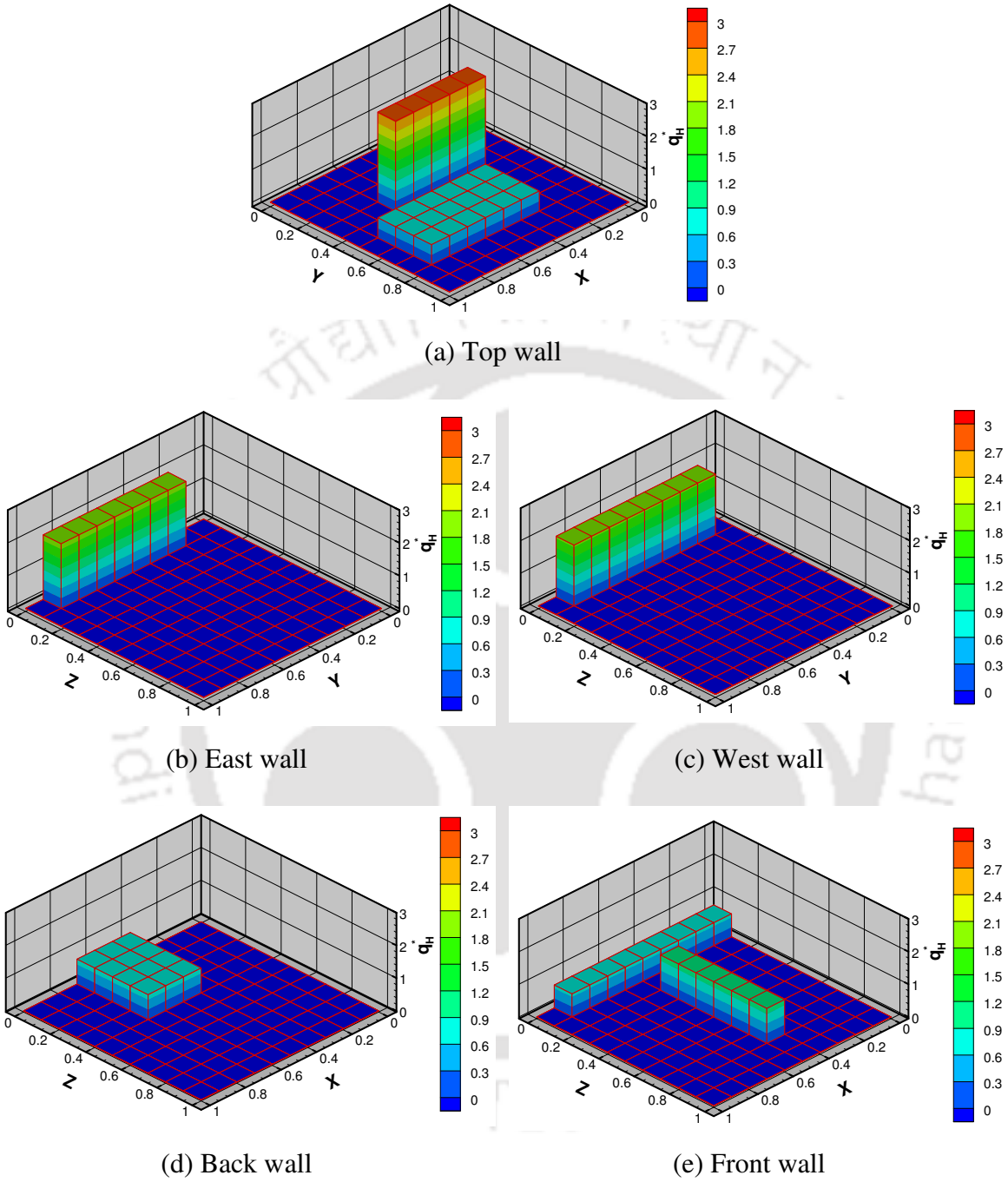

Figure 6.30. Modified optimal heater power distribution (7 heaters) along the enclosure walls for car model (a) top wall (b) east wall (c) west wall, (d) back wall, (e) front wall.

As shown in Fig. 6.27b, the deviation in the estimated heat flux is more than that of the case shown in Fig. 6.27a. Next, with the aim to reduce the deviation in estimated heat flux distribution, the same problem has been studied using the more number of heaters. In this case, from the results shown in Figs. 6.28a-e, seven regions along the five walls have been selected for grouping of heaters, and evaluated the problem with 7 heater elements. It is obvious that more is the number of heaters higher will be chances of solution and so further accurate estimation. The basic intension is to cover more possible heaters from Figs 6.28a-e. The estimated heat flux distribution is shown in Fig. 6.27c, while the corresponding heater power requirement is shown in Figs. 6.30a-e. In this case, the maximum deviation is 5.80% and the average deviation is 0.02358%. From the Fig. 6.27b and Fig. 6.27c, it is observed that with increasing the heaters from 6 to 7 there is no considerable improvement in the uniformity of thermal conditions. In this way, using the present algorithm one can find the required locations, power and number of the heaters to produce the desired uniform thermal conditions within the required range of accuracy.

For the given size of radiant furnace and for the chosen DO model (irregular or regular shaped), to have a precise control of uniform thermal conditions on the DO, this study can prove helpful to find the locations, size and the optimal power requirement for heaters.

6.4. Summary

The studies given in this chapter dealt with finding the optimal heater power distribution that produce desired uniform thermal conditions on the surfaces of a 2-D and a 3-D irregular shaped DO placed inside the 3-D radiant furnace. The present algorithm has been (REM^2 +MGA) modified, and its applicability is demonstrated. For the problems of 2-D DO, two irregular shaped DO are considered. Considering the heaters along the top wall of the enclosure, the desired uniform heat flux distribution on the DO is obtained accurately, within the deviation of 0.4%. For the planer design surface, the location of the heaters on all five walls is not necessary. For the present 2-D DO problems, in the MGA, 500 generations are found adequate to yield the uniform thermal conditions accurately.

For the problems involving the 3-D irregular shaped DOs placed inside the 3-D radiant furnace, the heater power distribution and the estimated uniform heat flux distribution are determined. The hemispherical, conical, cylindrical, and combinations of such irregular shaped objects are considered as the DOs. Accurate uniform thermal conditions are obtained. The effect of size of the DOs and the effect of aspect ratios of the furnace enclosure has been discussed. The sizes of the DOs with respect to the size of the furnace enclosure have found significant effect on the estimation of the thermal conditions. Even though 500 heaters are used for computation, few are found enough to produce desired thermal conditions.

Towards the more complex case, a replica of car body is considered as a DO, and for this case the optimal heater power distribution is estimated. Considering 100 panel heaters on each of the five walls of radiant furnace, the maximum and average deviation in the estimated flux is found to be 4.5% and 0.0282%, respectively. On the basis of earlier optimal heater power settings, to reduce the number of heaters, the grouping of particular heaters into a single or two along each of the five walls is successfully demonstrated. Using six heaters along the 5 walls of furnace, the maximum and average deviation is found to be 5.80 % and 0.0242%, respectively. Using seven heaters, the maximum and average deviation in this case is found as 5.70 % and 0.02358%, respectively. With the present optimization algorithm one can develop the better final design for uniform thermal conditions on any 2-D or 3-D irregular shaped DOs. This study can be a guideline for furnace designers to get an idea of the locations, size and the heaters power requirement. Also the present work establishes the feasibility of the usage of the REM^2 and the MGA for further complex problems.

CHAPTER 7

CONCLUSIONS AND SCOPE FOR FUTURE WORK

7.1 Conclusions

Several material heating operations in manufacturing and processing industries require specific uniform thermal conditions (temperature and/or heat flux) over the part of the system. Material heating for precision heat treatment, hot working processes, drying of paints, drying of powder coatings, manufacturing of electronic components, and material heating in laboratory experiments, etc., are some of the examples where the uniform thermal conditions are needed. For the desired thermal conditions, in the design of radiant furnace, configuration and powers of the heaters, geometry of the furnace, properties of the furnace material, and location of the objects are some of the important aspects.

This thesis dealt with the design of optimal heaters power settings along the walls of 3-D radiant furnaces that yield uniform thermal conditions on the 3-D design objects (DOs). Studies covered the solution and analysis of boundary design problems for different situations in material heating applications. Radiation element method by ray emission model (REM^2) was used to calculate the radiative information. The objective function was minimized using the micro-genetic algorithm (MGA). In the following pages conclusions of the studies carried out in this thesis are given. The scope for future work is enumerated in section 7.2.

Chapter 1 entitled "Introduction" started with the motivation of the present work. Applications and importance of furnaces in industries, and problems associated with its operations were briefly discussed. The basic requirement of the furnaces, importance of thermal uniformity in material heating and the factors affecting the thermal uniformity were elaborated. Having understood the importance of present furnace boundary design,

the literature review has been given. The literature review included the discussion on previous studies dealing with furnace boundary design problems for uniform thermal conditions and the various methodologies used for them. Based on the literature review the objectives of the present work were outlined.

For desired uniform thermal conditions, the problems of finding the optimal heater power settings along the furnace walls falls in the category of inverse problems, and such problems are ill posed. In Chapter 2, solution methods for inverse problems in heat transfer were discussed. Taking a note from the literature review that in the inverse methods, especially for furnace boundary design problems, it is difficult to impose the design constraints, on the other hand the optimization methods handle it very well. Among the optimization techniques, the evolutionary methods like the GAs have some added advantages. Since in the boundary design problems considered in this thesis, the number of unknown parameters (powers of the panel heaters) are large (300 to 500), hence this aspect is handled by the MGA, which is an improved form of the genetic algorithm. The advantages of the MGA in the present furnace design problems were elaborated.

In Chapter 3, the algorithm to determine the optimal heater power settings that produce a desired uniform heat flux distribution over the surfaces of a centrally located 3-D object on the bottom surface of a 3-D rectangular radiant enclosure was proposed. In this, radiative information was computed using the REM^2 and the MGA was used to minimize the objective function. Effect of specular reflections from the heater surfaces and walls was accounted. Formulation of the direct and the inverse radiative transfer problems were given. In both direct and inverse problems, radiative information was computed using the REM^2. To minimize the objective function in inverse analysis, the MGA was used as an optimization tool. Before going for actual computation, the solution methodologies of REM^2 for the direct problem and REM^2 + MGA for the inverse problem were validated. The good agreement was found between the computed results and that of calculated using the analytical approach. For the direct problem, the results of grid and ray independence tests were given.

The proposed algorithm (REM^2 + MGA) was implemented for basic furnace boundary design problem. For the desired uniform thermal conditions on the 3-D DO, the optimal configurations and powers of the panel heaters along the walls of the 3-D radiant furnace was estimated. The uniformity in the estimated heat flux distribution on the surfaces of the 3-D DO was found accurate within the maximum deviation < 2%. It was found that the mere placement of panel heaters along the top wall did not provide uniform thermal conditions on the surface of the 3-D DO. This necessitated the consideration of panel heaters along the four vertical walls of the furnace too. Next, the effects of aspect ratios of the furnace enclosure and the design constraints (heater power ranges) on the estimated heat flux distribution on the DO were studied. The best results were found for aspect ratio 0.5, also for higher aspect ratios the results were found acceptable. In the last section of this chapter, for every case, the optimal heater power distributions along the five walls of the furnace were plotted and results were analyzed. It was found that for the uniform thermal conditions, all the heaters along furnace walls need not to be considered.

For the desired uniform thermal conditions on a 3-D DO, after demonstrating the optimal design of heater power setting for a basic model of the radiant furnace in Chapter 3, in Chapter 4, three different situations in material heating applications were addressed. First study dealt with finding the constraints on the size of a centrally located 3-D DO. To cover a wide range of dimensions, 29 DO models were considered. The suitability of the DO models was decided on the basis of the maximum deviation in the estimated heat flux distribution. Out of 29 DO models, only 16 were found suitable to yield the uniform heat flux distribution, with the maximum deviation < 3%. In this study, it was found that the height of the DOs had a prominent effect on the estimation of uniform heat flux distribution. For a particular model 333, 4 different desired uniform heat fluxes viz. $q^*_{DO} = -2.0, -3.0, -4.0$ and -6.0 were estimated. In all cases, the estimated values were found close to the desired one. For one of the 29 cases with $q^*_{DO} = -2.0,$ in which the estimated heat flux was acceptable, the optimal heater power distribution along the five walls of the furnace enclosure was also given. It was found that for the uniform thermal

condition, all the heaters along the five walls of the furnace are not needed. In heat processing applications, this study can be a guideline for furnace designer/user to get the idea of the limitation on size of the DO that can have uniform thermal conditions.

To have an idea of implementation of the present numerical results in practical application, the simple experiments have been conducted using two model of 3-D radiant furnace with 3-D DO. The difference between the numerically computed heat flux distribution and that of from calculated from experimental results have been analyzed. Due to the differences in the numerical and experimental parameters such as, the material properties, working environment and energy losses, the experimental results were found deviating from the numerical results. The average difference was found 30%. On the positive side the trends of experimental values were matching with the numerical results. Since the experimental study is not the main aim of the thesis, it goes as additional information in annexure. The detail of the experiments, fabrication of experimental setup, experiment procedure, and the results analysis is given in annexure.

In the second study, in furnace boundary design problems, suitability and significance of location of the 3-D DO on the bottom surface of 3-D radiant furnace was studied. For a radiant furnace of dimensions $1\,\mathrm{m}\times 1\,\mathrm{m}\times 1\mathrm{m}$, the study was done for three sizes of DOs, i.e, model-1: $(0.2\mathrm{m}\times 0.2\mathrm{m}\times 0.2\mathrm{m})$, model-2: $(0.3\ \mathrm{m}\times 0.3\ \mathrm{m}\times 0.3\,\mathrm{m})$ and model-3: $(0.4\ \mathrm{m}\times 0.4\ \mathrm{m}\times 0.2\,\mathrm{m})$. For these DO models, 22 possible locations were evaluated. For DO models 1, 2 and 3, the possible numbers of locations were 10, 6 and 6, respectively. For the DO model-1, in which the height was 0.2 m, all locations were found suitable. Whereas, in the DO model-2, in which the height was 0.3 m, only four out of six locations were found suitable, and in the DO model-3, although the base dimensions $(0.4\ \mathrm{m}\times 0.4\,\mathrm{m})$ were more than the models-1 and 2, since the height was 0.2 m, unlike DO model-2, all 6 locations were found suitable. From a comparative study of the 22 cases, it was found that the height of 3-D DO imposed more restrictions on suitable locations than that of the length and the width. In this study, like before, the criteria of suitability was the maximum deviation < 3%. For DO model-3, for the 3 diagonal

locations, optimal powers of the panel heaters were estimated and analyzed. In all three cases, it was found that less than 50 heaters along the five walls were adequate to yield the uniform thermal conditions. This study is useful to have prior knowledge about the suitable location for a particular size of product to be heated.

Towards the furnace design for mass production, the third study dealt with the furnace boundary design problems in which multiple DOs could be accommodated. A total of 19 different configurations with 2, 3, 4, 5, 6, 8 and 9 DOs were considered. For the desired uniform thermal conditions, the inverse design was done to estimate the heat flux distributions on the DOs and thus the suitable configurations of the DOs were decided. In every case, the estimated heat flux distributions on the surfaces of the 3-D DO(s), and for a sample cases, the optimal heater power settings along the walls of the furnace enclosure were estimated. With other parameters fixed, the distances among the DOs were found to have a significant effect. With increase in distances among the DOs, the estimation of the uniform thermal conditions was found better. For the present furnace dimensions, for particular configurations, maximum 4 numbers of DOs were found suitable to achieve the desired uniform thermal conditions. For treating the more numbers of DOs simultaneously, the proportionate increase in furnace dimensions is needed. This study will be useful for furnace design and operation to find the suitable configuration with given numbers of DOs that can be treated within the required limit of accuracy. In all three studies, REM^2 was used to calculate the radiative information while the MGA was used as an optimization tool.

Towards the ease in implementation and control of the heater power settings in furnace boundary design problems in Chapter 5, the concept of grouping of discrete heaters was presented. The basic motive of the concept was to reduce the numbers of heaters that would make the fabrication and the control easy. The applicability and the efficacy of this concept were exemplified through the implementation for 3-D furnace design problem with 2-D and 3-D DOs. With this approach, the uniform thermal conditions found little distorted, but the uniformity was within the 4% of deviation. For 2-D and 3-D DO problems, the saving in the CPU times were 32.24 and 52.24 %, respectively. This study

showed that with the grouping approach, without sacrificing much, the numbers of heaters can be reduced, and thereby fabricate and control of radiant furnaces could be made easier.

Having analyzed several situations of regular 3-D DOs, in Chapter 6, results were presented for the estimation of optimal heater power settings in a 3-D radiant furnace that yield desired uniform thermal conditions on the 2-D and 3-D irregular shaped DOs. For these studies, the present algorithm (REM^2 + MGA) was modified. Since the surface elements on the DOs were irregular in shape, the optimality among the heater and design surfaces was maintained using complete energy balance in the system in every generation. Considering the panel heaters along the top wall of the enclosure, the desired uniform heat flux distribution was obtained within the deviation of 0.4%. It was also observed that, for 2-D design surface the location of the heaters along all the five walls was not necessary. For the present problem with 2-D DOs, in the MGA 500 generations were found adequate.

Next, for uniform thermal conditions on 3-D irregular shaped DOs, optimal heater power settings along the walls of 3-D radiant furnace were estimated. The hemispherical, conical, cylindrical and combinations of these irregular shaped objects were considered as the DOs. In every case, the estimated heat flux distributions on the DO and the deviation in the estimated flux were given. In all these cases, deviation in estimated heat flux was found within $\pm 1\%$. The effects of size of the DOs and the aspect ratios of the furnace enclosure were discussed. The sizes of the DOs with respect to the size of furnace enclosure were found of significant. From the results of heater power setting, it was found that out of 500 panel heaters less than 25 heaters were found enough to produce the desired thermal conditions.

Towards the more complex case of 3-D irregular shaped DO, a replica of the car body was modeled as a DO. Considering 100 panel heaters on each of the five walls of the furnace, the maximum and average deviation in the estimated fluxes were 4.5% and 0.0282%, respectively. To reduce the number of heater elements, on the basis of earlier

optimal heater power settings, the grouping of particular heaters into a single or two along each of the walls was successfully demonstrated. Using six heaters along the 5 walls of furnace, the maximum and average deviations were 5.80 % and 0.0242%, respectively. Using seven heaters, the maximum and average deviations in this case were found as 5.70 % and 0.02358%, respectively. For uniform thermal conditions, with the present optimization algorithm, one can have a better thermal design of the radiant furnace needed for precision material heating processes for any 2-D or 3-D regular or irregular shaped DOs. This study can be a helpful for furnace designers to estimate the heater power settings for 2-D and 3-D irregular shaped DOs. Also the present work establishes the feasibility of the usage of the REM^2 and the MGA for different types of boundary design problems.

There are several applications in the material heating processes where the analysis presented in Chapter 3 can be found useful. For uniform thermal conditions, various problems considered in Chapters 4 and 5, and their analysis of the results, provide a wealth of information regarding the effects and the limitations in terms of size, shape, and the configurations of the DOs in the furnace applications. In Chapter 6, a general case of furnace boundary design with 2-D or 3-D irregular shaped DOs was presented, Overall, the results presented in this thesis will prove helpful in thermal design and operation of a radiant furnace that needs to provide uniform thermal conditions on different types of regular and irregular shaped 3-D DOs.

7.2 Scope for Future Work

The problems discussed in this thesis dealt with boundary design problems in 3-D radiant furnaces that produce the uniform thermal conditions on 3-D DOs, and their analysis for different situations in material heating. After accurate estimation of the desired uniform thermal conditions on 3-D DO, various combinations of different cases and several application based problems were addressed. Furthermore, the radiant furnace design for 3-D irregular shaped DOs was also given. The work presented in this thesis is a valuable addition to know-how about the resulting thermal conditions with particular combination of DO and the furnace dimensions, location of DOs and the limitations for yielding uniform thermal conditions over a 3-D DOs. Several new observations are found which will help in further advancement to research in this field. As an extension of the present work, some studies that can be taken up, are the following:

(1) In the present work, thermal design of furnace has been done to produce the uniform heat flux distributions on a 3-D DO(s). The aspect of the heat load time pertaining to the particular applications using the present algorithm will be helpful in dealing with real-time analysis.
(2) Energy transfer in problems considered in this work has been through the transparent media. This study can be extended for participating medium, or specifically for particular applications in the material heating such as carburizing, nitriding, carbo-nitriding, etc.
(3) For the present boundary design problems, the MGA was used as an optimization tool. Other metaheuristic/ evolutionary techniques can be explored to improve the accuracy of the design, and to handle more complex situations in the material heating such as drying of paints, material heating in chemical industries which involve the mass transfer also. Simultaneously, faster algorithms are on demand always.
(4) To simulate the computational design parameters and their corresponding results, different situations can be simulated experimentally.
(5) In commercial CFD applications, analysis software packages are available widely like FLUENT, ANSYS, etc. It will be interesting to use such software along with

the available optimization techniques for dealing the various and complex situations in material heating. This may add significant contribution in terms of the accuracy and the efficiency of computation in the field of furnace boundary design problems.

(6) Considering the other modes of heat transfer, viz. conduction and convection, the furnace design problems can be focused to capture the effect of conduction and the convection heat transfer through the medium.

(7) The problems of design of heater power settings for desired thermal conditions should not be limited for solid material heating but can be explored for heating of fluids for particular applications, or to produce specific thermal conditions and the flow pattern within the domain. This will be of great importance not only in academics but also in numerous industrial applications.

REFERENCES

Abraham J.P. and Sparrow E.M., (2003), Three-Dimensional Laminar and Turbulent Natural Convection in a Continuously/Discretely Wall-Heated Enclosure Containing a Thermal Load, *Numerical. Heat Transfer, Part A*, Vol. 44, pp. 105–125.

Asllani A., and Lari A., (2007), Decision Support Using Genetic Algorithm for Dynamic and Multiple Criteria Web-Site Optimizations, *European Journal of Operational Research*, Vol. 176, pp. 1767–1777.

Banan M., Gray R.T. and Wilcox W.R., (1991), An Experimental Approach to Determine the Heat Transfer Coefficient in Directional Solidification Furnaces, *Journal of Crystal Growth*, Vol. 113, pp. 557-565.

Barichello L.B., Garcia R.D.M., and Siewert C.E., (1997), On Inverse Boundary-Condition Problems in Radiative Transfer, *Journal of Quantitative Spectroscopy and Radiative Transfer*, Vol. 57, pp. 405-410.

Bayat N., Mehraban S., and Sarvari S.M.H., (2010), Inverse Boundary Design of a Radiant Furnace With Diffuse-Spectral Design Surface, *International Communications in Heat and Mass Transfer*, Vol. 37, pp. 103–110.

Bechwith T.G., Marangoni R. D., Lienhard J.H., (2004), Mechanical Measurement, 5th ed., Pearson Education, Singapore, pp. 58-83.

Carroll D.L., (1996a), Genetic Algorithms and Optimizing Chemical Oxygen-Iodine Lasers, Developments in Theoretical and Applied Mechanics, Vol. XVIII, eds. H. Wilson, R. Batra, C. Bert, A. Davis R. Schapery, D. Stewart, and F. Swinson, School of Engineering, The University of Alabama, pp. 411-424.

Carroll, D.L., (1996b), Chemical Laser Modeling with Genetic Algorithms, *AIAA*

Journal, Vol. 34(2), pp. 338-346.

Chelouah R., and Siarry P., (2000), Tabu Search Applied to Global Optimization, *European Journal of Operation Research*, Vol. 123, pp. 256-70.

Chopade R.P., Agnihotri E., Singh A.K., Kumar A., Uppaluri R., Mishra S.C., and Mahanta P., (2011a), Application of a Particle Swarm Algorithm for Parameter Retrieval in a Transient Conduction-Radiation Problem, *Numerical Heat Transfer, Part A*, Vol. 59(9), pp. 672 – 692.

Chopade R.P., Mishra S.C., Mahanta P., Maruyama S., (2011b), Numerical Analysis of an Inverse Boundary Design Problem of 3-D Radiant Furnace with a 3-D Design Object, *Numerical heat Transfer, Part A*, Vol. 60, 2011, pp. 25–49.

Christophe L.N. and Frederic L., (2004), A Parameter Estimation Approach to Solve the Inverse Problem of Point Heat Sources Identification, *International Journal of Heat and Mass Transfer*, Vol. 47, pp. 827-841.

Colaco M.J., and Orlande H.R.B., (2004), Inverse Natural Convection Problem of Simultaneous Estimation of Two Boundary Heat Fluxes in Irregular Cavities, *International Journal of J. Heat and Mass Transfer*, Vol. 47, pp. 1201-1215.

Das R., Mishra S.C., Ajith M., and Uppaluri R., (2008a), An Inverse Analysis of a Transient 2-D Conduction–Radiation Problem Using the Lattice Boltzmann Method and the Finite Volume Method Coupled with the Genetic Algorithm, *Journal of Quantitative Spectroscopy and Radiative Transfer* , Vol. 109, pp. 2060–2077.

Das R., Mishra S.C., and Uppaluri R., (2008b), Multi-parameter Estimation in a Transient Conduction-Radiation Problem using the Lattice Boltzmann Method and the Finite Volume Method Coupled with the Genetic Algorithms, *Numerical Heat Transfer, Part A*, Vol. 53, pp. 1321–1338.

Daun K.J. and Howell J.R., (2005), Inverse Design Methods for Radiative Transfer Systems, *Journal of Quantitative Spectroscopy and Radiative Transfer*, Vol. 93, pp. 43–60.

Daun K.J., Franca F., Larsen M., Leduc G., and Howell J. R., (2006), Comparison of Inverse Design of Radiant Enclosures, *Journal of Heat Transfer*, Vol.128, pp. 269-282.

Daun K.J., Morton D.P., and Howell J.R., (2003a), Geometric Optimization of Radiant Enclosures Containing Specular Surfaces, *Journal of Heat Transfer*, Vol. 125, pp. 845-851.

Daun K.J., Howell J.R., and Morton D.P., (2004), Optimization of Transient Heater Setting to Provide Spatially Uniform Heating in Manufacturing Processes Involving Radiant Heating, *Numerical Heat Transfer Part A*, Vol. 46, pp. 651-667.

Daun, K.J., Howell, J.R., and Morton, D.P., (2003b), Geometric Optimization of Radiant Enclosures through Nonlinear Programming, *Numerical Heat transfer, part B*, Vol. 43(3), pp. 203-219.

Deep K., Singh K.P., Kansal M.L. and Mohan C., (2009), A Real Coded Genetic Algorithm for Solving Integer and Mixed Integer Optimization Problems, *Applied Mathematics and Computation*, Vol. 212, pp. 505–518.

Deiveegan M., Balaji C. and Venkateshan S.P., (2006), Comparison of Various Methods for Simultaneous Retrieval of Surface Emissivities and Gas Properties in Gray Participating Media, *Journal of Heat Transfer*, Vol. 128, pp. 829-837.

Dias T. Jr., and Milanez L.F., (2006), Optimal Location of Heat Sources on a Vertical Wall with Natural Convection through Genetic Algorithms, International *Journal of Heat and Mass Transfer*, Vol. 49, pp. 2090–2096

Dorigo M., and Maria G., (1997), Ant Colony System: A Cooperative Learning Approach to the Travelling Salesman Problem, *IEEE Transaction on Evolutionary Computation*, Vol. 1, pp. 53–66.

Eric G.J., and Abushagur M.A.G., (1997), Image Deconvolution using a Micro Genetic Algorithm, *Optics Communications*, Vol. 140, pp. 6-10.

Erturk H., Ezekoye O.A., and Howell J.R., (2002a), The Application of an Inverse Formulation in the Design of Boundary Conditions for Transient Radiating Enclosures, *Journal of Heat Transfer*, Vol. 124, pp. 1095-1102.

Erturk H., Ezekoye O.A., and Howell J.R., (2002b), Comparison of Three Regularized Solution Techniques in a Three-Dimensional Inverse Radiation Problem, *Journal of Quantitative Spectroscopy and Radiative Transfer*, Vol. 73, pp. 307–316.

Erturk H., Ezekoye O.A., and Howell J.R., (2004), Boundary Condition Design to Heat a Moving Object at Uniform Transient Temperature using Inverse Formulation, *Journal of Manufacturing Science and Engineering*, Vol. 126, pp. 619-626.

Erturk H., Gamba M., Ezekoye O.A., and Howell J.R., (2008), Validation of Inverse Boundary Condition Design in a Thermometry Test Bed, *Journal of Quantitative Spectroscopy and Radiative Transfer*, Vol. 109, pp. 317-326.

Fan H., Li B., Yang L., and Wang R., (2002), Solution of the Inverse Radiative Load Problem in a Two-Dimensional System, *Journal of Quantitative Spectroscopy and Radiative Transfer*, Vol. 74, pp. 85–95.

Fan J.R., Sun P., Zheng Y.Q., Ma Y.L. and Cen K.F., (1999), Numerical and Experimental Investigation on the Reduction of NO_x Emission in a 600 MW Utility Furnace by Using OFA, *Fuel*, Vol. 78, pp. 1387-1394.

Fedorov A.G., Lee K.H., and Viskanta R., (1998), Inverse Optimal Design of the Radiant Heating in Materials Processing and Manufacturing, *Journal of Material Engineering and Performance*, Vol. 7, pp. 719-726.

Fiveland W.A., (1988), Three-Dimensional Radiative Heat-Transfer Solutions by the Discrete-Ordinates Method, *Journal of Thermophysics and Heat Transfer*, Vol. 2, pp. 309-316.

Fleck J.A., (1961), The Calculation of Nonlinear Radiation Transport by a Monte Carlo Method: Statistical Physics, *Methods in Computational Physics*, Vol. 1, pp. 43-65.

Franca F.H.R., Ezekoye O.A., and Howell J.R., (2001), Inverse Boundary Design Combining Radiation and Convection Heat Transfer, *Journal of Heat Transfer*, Vol.123, pp. 884-891.

Garcia S., and Scott E. P., (1998a), Use of Genetic Algorithms in Thermal Property Estimation: Part I - Experimental Design Optimization, *Numerical Heat Transfer, Part A*, Vol. 33, pp. 135-147.

Garcia S., Guynn J., and Scott E. P., (1998b), Use of Genetic Algorithms in Thermal Property Estimation: Part II - Simultaneous Estimation of Thermal Properties, *Numerical Heat Transfer, Part A,* Vol. 33, pp. 149-168.

Glover, F., (1986), Future Paths for Integer Programming and Links to Artificial Intelligence, *Computers and Operation Research*, Vol. 13(5), pp. 533–549.

Goldberg D.E., (1989), Genetic Algorithms in Search, Optimization and Machine Learning, Addison-Wesley, Massachusetts.

Goldberg D.E., (1989), Sizing Populations for Serial and Parallel Genetic Algorithms,

Proceeding of 3rd Int. Conf. on Genetic Algorithms and their Applications, pp. 70–79.

Golovkin I.E., Mancini R.C., Louis S.J., Lee R.W., and Klein L., (2002), Analysis of X-Ray Spectral Data with Genetic Algorithms, *Journal of Quantitative Spectroscopy and Radiative Transfer*, Vol. 75, pp. 625–636.

Guo Z. and Maruyama S., (2001), Prediction of Radiative Heat Transfer in Industrial Equipment Using the Radiation Element Method, *Journal of Heat Transfer*, Vol. 123, pp. 530-536.

Guo Z., Maruyama S., and Tsukada T., (1997), Radiative Heat Transfer in Curved Specular Surfaces in Czochralski Crystal Growth Furnace, *Numerical Heat Transfer, Part A*, Vol. 32:6, pp. 595-611.

Hansen, P.C., (1992), Numerical Tools for Analysis and Solution of Fredholm Integral Equations of the First Kind, *Inverse Problems*, Vol. 8, pp. 849-872.

Ho C.-H. and Ozisik M.N., (1988), Inverse Radiation Problems In Inhomogeneous Media, *Journal of Quantitative Spectroscopy and Radiative Transfer*, Vol. 40(5), pp. 553-560.

Hodul D., and Morda D., (1991), RTP Temperature Uniformity Mapping, *Nuclear Instruments and Methods in Physics Research*, Vol. I355, pp. 269-274.

Hoffmann R.S., Seewald A., Schneider P.S., and Franca F.H.R., (2010), Inverse Design of Thermal Systems with Spectrally Dependent Emissivities, *International Journal of Heat and Mass Transfer*, Vol. 53, pp. 931-939.

Holland J.H., (1975), Adaption in Natural and Artificial Systems, University of Michigan Press, Michigan, Ann Arbor.

Homaifar A., Lai H.Y. and McCormick E., (1994), System Optimization of Turbo Fan Engines using Genetic Algorithm, *Applied Mathematical Modeling*, Vol. 18, pp. 72-83.

Hosseini S.M., Mansouri S.H., Howell J.R, (2003), Inverse Boundary Design Radiation Problem in Absorbing Emitting Media with Irregular Geometry, *Numerical Heat Transfer, Part A*, Vol. 43, pp. 565-584.

Hottel H.C. and Cohen E.S., (1958), Radiant Heat Exchange in a Gas-Filled Enclosure: Allowance for Non-Uniformity of Gas Temperature, *AIChE Journal*, Vol. 4, pp. 3-14.

Howell J.R., Ezekoye O.A., and Morales J.C., (2000), Inverse Design Model for Radiative Heat Transfer, *Journal of Heat Transfer*, Vol. 122, pp. 492- 502.

Huang C.H. and Ozisik M.N., (1991), A Direct Integration Approach for Simultaneously Estimating Temperature Dependent thermal Conductivity and Heat Capacity, *Numerical Heat Transfer, Part A*, Vol. 20, pp. 95-110.

Huang C. –H., and Hsiung T.-Y., (1999), An Inverse Design Problem of Estimating Optimal Shape of Cooling Passages in Turbine Blades, *International Journal of Heat and Mass Transfer*, Vol. 42, pp. 4307-4319.

Huang C.H. and Yan, J.Y., (1995), An Inverse Problem in Simultaneously Measuring Temperature Dependent thermal Conductivity and Heat Capacity, *International Journal of Heat and Mass Transfer*, Vol. 38, pp. 3433-3441.

Jaluria Y., (2009), Simulation Based Optimization of Thermal Systems, *Applied Thermal Engineering*, Vol. 29, pp. 1346-1355.

Ji C.-C., Tuan P.-C., and Jang H.-Y., (1997), A Recursive Least-Squares Algorithm for on-Line 1-D Inverse Heat Conduction Estimation, *International Journal of Heat and Mass Transfer*, Vol. 40, pp. 2081-2096.

Kang J. and Rong Y., (2006), Modeling and Simulation of Load Heating in Heat Treatment Furnaces, *Journal of Materials Processing Technology*, Vol. 174, pp. 109–114.

Karim M.M., Suzuki K. and Kai H., (2004), Optimal Design of Hydrofoil and Marine Propeller using Micro-Genetic Algorithm μGA, *Journal of Naval Architecture Marine Engineering*, Vol. 1, pp. 47-61.

Kaya N., (2006), Machining Fixture Locating and Clamping Position Optimization using Genetic Algorithms, *Computers in Industries*, Vol. 57, pp. 112–120.

Kazarlis S.A., Papadakis S.E., Theocharis J.B., and Petridis V., (2001), Micro Genetic Algorithms as Generalized Hill – Climbing Operators for Optimization, *IEEE Transaction on Evolutionary Computation*, Vol. 5, pp. 204–217.

Kennedy J., and Eberhart R., (1995), Particle Swarm Optimization, *Proceeding of IEEE International Conference on Neural Networks IV*, pp. 1942–1948.

Khlevnoy B., Sakharov M., Ogarev S., Sapritsky V., Yamada Y., and Anhalt K., (2008), Investigation of Furnace Uniformity and its Effect on High-Temperature Fixed-Point Performance, *International Journal of Thermophysics*, Vol. 29, pp. 271–284.

Khouja M., Michalewicz Z., and Wilmot M., (1998), The use of Genetic Algorithms to Solve the Economic Lot Size Scheduling Problem, *European Journal of Operation Research*, Vol. 110, pp. 509-524.

Kim K.W., and Baek S.W., (2007), Efficient Inverse Radiation Analysis in a Cylindrical Geometry using a Combined Method of Hybrid Genetic Algorithm and Finite-Difference Newton Method, *Journal of Quantitative Spectroscopy and Radiative Transfer*, Vol. 108, pp. 423-439.

Kim K.W., Baek S.W., Kim M.Y., and Ryou H.S., (2004), Estimation of Emissivities in a Two-Dimensional Irregular Geometry by Inverse Radiation Analysis using Hybrid Genetic Algorithm, *Journal of Quantitative Spectroscopy and Radiative Transfer*, Vol. 87, pp. 1-14.

Kirkpatrick C.D., Gelatt Jr., and Veechi M.P., (1983), Optimization by Simulated Annealing, *Science*, Vol. 220, pp. 671- 680.

Kline, S.J., and McClintock F.A., (1953), Describing Uncertainties in Single-Sample Experiments, *Mechanical Engineering*, Vol. 75(1), pp. 3-8.

Knutson K.L., Campbell S.A., and Dunn F., (1994), Modeling of Three-Dimensional Effects on Temperature Uniformity in Rapid thermal Processing of Eight Inch Wafers, *IEEE Transaction on Semiconductor Manufacturing*, Vol. 71, pp. 68-72.

Krishnakumar K., (1989), Micro Genetic Algorithms for Stationary and Non-Stationary Function Optimization, SPIE conference on Intelligent Control and Adaptive Systems, 119632.

Kudo K., Kuroda A., Eid A., Saito T. and Oguma, M., (1995), Solution of the Inverse Radiative Load Problems by the Singular Value Decomposition, *Proceeding of ICHMT First International Conference on Radiative Transfer*, Kusadasi, Turkey, P. Menguc, ed., pp.568-578.

Kurpisz K. and Nowak A.J, (1995), Inverse Thermal Problems, 1st ed. Computational Mechanics Publications, Southampton, UK.

Lee K.H., Baek S.W., and Kim K.W., (2008), Inverse Radiation Analysis using Repulsive Particle Swarm Optimization Algorithm, *International Journal of Heat and Mass Transfer*, Vol. 51, pp. 2772–2783.

Levenberg K., (1944), A Method for the Solution of Certain Non-Linear Problems in

Least Squares, *The Quarterly of Applied Mathematics*, Vol. 2, pp. 164–168.

Levine D., (1996), Application of a Hybrid Genetic Algorithm to Airline Crew Scheduling, *Computers in Operation Research*, Vol. 23(6), pp. 547-558.

Li H.Y. and Ozisik M.N., (1992), Identification of the Temperature Profile in an Absorbing, Emitting and Isotropically Scattering Medium by Inverse Analysis, *Journal of Heat Transfer*, Vol. 114, pp. 1060-1063.

Li H.Y., (1994), Estimation of the Temperature Profile in a Cylindrical Medium by Inverse Analysis, *Journal of Quantitative Spectroscopy and Radiative Transfer*, Vol. 52, pp. 755-764.

Li H. Y., (1997), A Genetic Algorithm for Inverse Radiation Problems, *International Journal of Heat and Mass Transfer*, Vol. 40(7), pp. 1545-1549.

Li H.Y., (2001), A Two-Dimensional Cylindrical Inverse Source Problem in Radiative Transfer, *Journal of Quantitative Spectroscopy and Radiative Transfer*, Vol. 69, pp. 403-414.

Lin S., and Chu H.-S., (2002), Application of Inverse Problem Algorithm for Temperature Uniformity in Rapid Thermal Processing, *Thin Solid Films*, Vol. 402, pp. 280–289.

Linhua L., Heping T., and Qizheng Y., (1999), Inverse Radiation Problem of Temperature Field in Three-Dimensional Rectangular Furnaces, *International Communications in Heat and Mass Transfer*, Vol. 26(2), pp. 239-248.

Liu L.H., (2000), Simultaneous Identification of Temperature Profile and Absorption Coefficient in One-Dimensional Semitransparent Medium by Inverse Radiation Analysis, *International Communications in Heat and Mass Transfer*, Vol. 27(5), pp. 635-643.

Madadi R.R., and Balaji C., (2008), Optimization of the Location of Multiple Discrete Heat Sources in a Ventilated Cavity using Artificial Neural Networks and Micro Genetic Algorithm, *International Journal of Heat and Mass Transfer*, Vol. 51, pp. 2299–2312.

Mahanta P. and Mishra S.C., (2002), Collapsed Dimension Method Applied to Radiative Transfer Problems in Complex Enclosures with Participating Medium, *Numerical Heat Transfer, part B*, Vol. 42, pp. 367-38.

Malhotra C.P., Mahajan R.L., Sampath W.S., Barth K.L., and Enzenroth R.A., (2006), Control of Temperature Uniformity During the Manufacture of Stable Thin-Film Photovoltaic Devices, *International Journal of Heat and Mass Transfer*, Vol. 49, pp. 2840–2850.

Maruyama S., (1993), Radiation Heat Transfer Between Arbitrary Three-Dimensional Bodies With Specular and Diffuse Surfaces, *Numerical Heat Transfer, Part A*, Vol. 24, pp. 181-196.

Maruyama S., (2004), Light Energy, Yogendo Ltd, Tokyo, Japan.

Maruyama S., and Aihara T., (1997), Radiation Heat Transfer of Arbitrary Three–Dimensional Absorbing, Emitting and Scattering Media and Specular and Diffuse Surfaces, *Journal of Heat Transfer*, Vol. 119, pp. 129-136.

Maruyama S., Takeuchi Y., Sakai S., and Guo Z., (2002), Improvement of Computational Time in Radiative Heat Transfer of Three-Dimensional Participating Media using the Radiation Element Method, *Journal of Quantitative Spectroscopy and Radiative Transfer*, Vol. 73, pp. 239-248.

Mataga P.A., Hutchinson J.W., Chalmers B., Bell R.O. and Kalejs J.P., (1987), Effects

of Transverse Temperature Field Non-Uniformity on Stress in Silicon Sheet Growth, *Journal of Crystal Growth*, Vol. 82, pp. 60-64.

McCormick N. J., (1984), Recent Developments in Inverse Scattering Transport Methods, *Transport Theory and Statistical Physics*, Vol. 13(1), pp. 15-56.

McCormick N. J., (1992), Inverse Radiative Transfer Problems: A Review, *Nuclear Science and Engineering*, Vol. 112, pp. 185-198.

McCormick. N.J., (1986), Methods For Solving Inverse Problems For Radiation Transport-An Update, *Transport Theory Statistical Physics*, Vol. 15, pp. 759-772.

Mishra S.C., and Prasad M., (2002), Radiative Heat Transfer in Absorbing-Emitting-Scattering Gray Media inside 1-D Cartesian Enclosure using the Collapsed Dimension Method, *International Journal of Heat and Mass Transfer*, Vol. 45, pp. 697-700.

Modest M. F., (2003), Radiative Heat Transfer. 2nd ed., Academic Press, New York.

Mossi A.C., Vielmo H.A., Franca F.H.R., and Howell J.R., (2008), Inverse Design Involving Combined Radiative and Turbulent Convective Heat Transfer, *International Journal of Heat and Mass Transfer*, Vol. 51, pp. 3217–3226.

Nelder J.A., and Mead R., (1965), A Simplex Method for Function Minimization, *The Computer Journal*, Vol. 7, pp. 308–313.

Neto A.J.S. and Ozisik M.N., (1995), An Inverse Problem of Simultaneous Estimation of Radiation Phase Function, Albedo and Optical Thickness, *Journal of Quantitative Spectroscopy and Radiative Transfer*, Vol. 53, pp. 397-409.

Norman S.A., (1992), Optimization of Transient Temperature Uniformity in RTP Systems, *IEEE Transaction on Electron Devices*, Vol. 39, pp. 205 – 207.

Onwubolu G.C. and Babu B.V., (2004), New Optimization Techniques in Engineering, 1st ed. Springer-Verlag, Berlin Heidelberg, New York.

Osman M.S., Abo –S.M.A., and Mousa A.A., (2004), A Solution to the Optimal Power Flow using Genetic Algorithm, *Applied Mathematics and Computation*, Vol. 155, pp. 391-405.

Ozcan S.E., Cangar O., Vranken E., and Berckmans D., (2005), Predicting 3-D Spatial Temperature Uniformity in Food Storage Systems from Inlet Temperature Distribution, *Postharvest Biology and Technology*, Vol. 37, pp. 186–194.

Ozisik M.N, and Orlande H.R.B., (2000), Inverse Heat Transfer: Fundamentals and Applications, Taylor and Francis, New York, NY.

Park H.M. and Yoo D.H., (2001), A Multidimensional Inverse Radiation Problem of Estimating the Strength of Heat Source in Participating Media, *International Journal of Heat and Mass Transfer*, Vol. 44, pp. 2949-2956.

Park H.M. and Chung O.Y., (1999), An Inverse Natural Convection Problem of Estimating the Strength of a Heat Source, *International Journal of Heat and Mass Transfer*, Vol. 42, pp. 4259 - 4273.

Park H.M. and Jung W.S., (2001a), The Karhunen -Loeve Galerkin Method for the Inverse Natural Convection Problems, *International Journal of Heat and Mass Transfer*, Vol. 44, pp. 155 - 167.

Park, H.M. and Jung, W.S., (2001b), Recursive Solution of an Inverse Heat Transfer Problem in Rapid Thermal Processing Systems, *International Journal of Heat and Mass Transfer*, Vol. 44, pp. 2053-2065.

Payan S., Sarvari S.M.H., and Ajam H., (2009), Inverse Boundary Design of Square Enclosures with Natural Convection, *International Journal of Thermal Sciences*, Vol. 48, pp. 682–690.

Porter J.M., Larsen M.E., Barnes J.W., and Howell J.R., (2006), Metaheuristic Optimization of a Discrete Array of Radiant Heaters, *Journal of Heat Transfer*, Vol. 128, pp. 1031-1040.

Pourshaghaghy A., Pooladvand K., Kowsary F., and Karimi-Z. K., (2006), An Inverse Radiation Boundary Design Problem for an Enclosure Filled with an Emitting, Absorbing, and Scattering Media, *International Communications in Heat and Mass Transfer*, Vol. 33, pp. 381-390.

Prudhomme M., and Nguyen T. H., (2001), Solution of Inverse Free Convection Problems by Conjugate Gradient Method: Effects of Rayleigh Number, *International Journal of Heat and Mass Transfer*, Vol. 44, pp. 2011-2027.

Rahmani R.K., Molavi H., Ayasoufi A., Koomullil R.P., and Cheng G., (2010), Solution of Radiative Boundary Design Problems using a Combined Optimization Technique, *Numerical Heat Transfer, Part B*, Vol. 57(5), pp. 348-371.

Raithby G.D. and Chui E.H., (1990), A Finite Volume Method for Predicting Radiant Heat Transfer in Enclosures with Participating Media. *Journal of Heat Transfer*, Vol. 112, pp. 415-423.

Rao S.S., (1990), Optimization theory and Applications, Wiley Eastern Ltd., Second edition.

Roy S., Ghosh S., and Shvpuri R., (1997), A New Approach to Optimal Design of Multi-Stage Metal Forming Processes with Micro Genetic Algorithms, *International Journal of Machine Tools and Manufacture*, Vol. 37, pp. 29-44.

Rukolaine S.A., (2007), Regularization of Inverse Boundary Design Radiative Heat Transfer Problems, *Journal of Quantitative Spectroscopy and Radiative Transfer*, Vol. 104, pp. 171–195.

Safavinejad A., Mansouri S.H., Sakurai A., and Maruyama S., (2009), Optimal Number and Location of Heaters in 2-D Radiant Enclosures Composed of Specular and Diffuse Surfaces Using Micro-Genetic Algorithm, *Applied Thermal Engineering*, Vol. 29, , pp. 1075 -1085.

Safavinejad A., Maruyama S., Mansouri S.H., and Sakurai A., (2008), Optimal Boundary Design of Radiant Enclosure using Mirco-Genetic Algorithm, *Journal of Thermal Science and Technology*, Vol. 3, pp. 179-194.

Sarvari S.M.H., (2005), Inverse Determination of Heat Source Distribution in Conductive-Radiative Media with Irregular Geometry, *Journal of Quantitative Spectroscopy and Radiative Transfer*, Vol. 93, pp. 383-395.

Sarvari S.M.H., (2007), Optimal Geometry Design of Radiative Enclosures using the Genetic Algorithm, *Numerical Heat Transfer, Part A*, Vol. 52, pp. 127-143.

Sarvari S.M.H., Howell J.R., and Mansouri S.H., (2003a), A General Method for Estimation of Boundary Conditions over the Surface of Shields Surrounded by Radiating Enclosures, *Numerical Heat Transfer, Part B*, Vol. 44, pp. 25–43.

Sarvari S.M.H., Howell J.R., and Mansouri S.H., (2003b), Inverse Boundary Design Conduction-Radiation Problem in Irregular Two-Dimensional Domains, *Numerical Heat Transfer, Part B*, Vol. 44, pp. 209–224.

Siegel R. and Howell J., (2002), Thermal Radiation Heat Transfer, 4th ed., Taylor & Francis, New York.

Siewert C.E., (1993), An Inverse Source Problem In Radiative Transfer, *Journal of Quantitative Spectroscopy and Radiative Transfer*, Vol. 50, pp. 603-609,

Siewert, C.E., (1994), A Radiative-Transfer Inverse-Source Problem For a Sphere, *Journal of Quantitative Spectroscopy and Radiative Transfer*, Vol. 52, pp. 157-160

Sivanandam S.N. and Deepa S.N., (2008), Introduction to Genetic Algorithms, Springer-Verlag Berlin Heidelberg New York.

Storn R., and Price K., (1997), Differential Evolution - A Simple and Efficient Heuristic for Global Optimization over Continuous Spaces, *Journal of Global Optimization*, Vol. 11, pp. 341–359.

Su C.-R., and Chen C.-K., (2007), Geometry Estimation of the Furnace Inner Wall by an Inverse Approach, *International Journal of Heat and Mass Transfer*, Vol. 50, pp. 3767–3773.

Suda T., Takafuji M., Hirata T., Yoshino M. and Sato J., (2002), A Study of Combustion Behavior of Pulverized Coal in High-Temperature Air, *Proceeding of the Combustion Institute*, Vol. 29, pp. 503-509.

Szollos A., Smid M., and Hajek J., 2009, Aerodynamic Optimization via Multi-Objective Micro-Genetic Algorithm with Range Adaptation, Knowledge-Based Re-initialization, Crowding and e-Dominance, *Advances in Engineering Software*, Vol. 40, pp. 419–430.

Taberlet E. and Fautrelle Y., (1985), Turbulent Stirring in an Experimental Induction Furnace, *Journal of Fluid Mechanics*, Vol. 159, pp. 409 - 431.

Tan J. Y. and Liu L. H., (2009), Inverse Geometry Design of Radiating Enclosure

Filled with Participating Media Using Meshless Method, *Numerical Heat Transfer, Part A*, Vol. 56, pp. 132 - 152.

Theodoropoulou A., Adomaitis R.A., and Zafiriou E., (1998), Model Reduction for Optimization of Rapid Thermal Chemical Vapor Deposition Systems, *IEEE Transaction on Semiconductor Manufacturing*, Vol. 11, pp. 85–98.

Theodoropoulou A., Zafiriou E., and Adomaitis R. A., (1999), Inverse Model-Based Real-Time Control for Temperature Uniformity of RTCVD, *IEEE Transaction on Semiconductor Manufacturing*, Vol. 12, pp. 87-101.

Tikhonov, A.N., (1975), Inverse Problems in Heat Conduction, *Journal of Engineering Physics*, Vol. 29, pp. 816-820.

Tiwari S., and Chakraborti N., (2006), Multi-Objective Optimization of a Two-Dimensional Cutting Problem using Genetic Algorithms, *Journal of Material Processing and Technology*, Vol. 173, pp.384-393.

Trinks W., Mawhinney M.H., Shannon R.A., Reed R.J. and Garvey J.R., (2004), Industrial Furnaces, 6th Ed., John Wiley & Sons, Inc., Hoboken, New Jersey.

Tse D.C.M. and Chan L.Y.Y., (1999), Application of Micro Genetic Algorithms and Neural Networks for Airfoil Design Optimization, *RTO AVT Symposium on Aerodynamic Design and Optimization of Flight Vehicles in a Concurrent Multi-Disciplinary Environment*, Ottawa, Canada.

Verboven P., Scheerlinck N., Baerdemaeker J.D., and Nicola B.M., (2000), Computational Fluid Dynamics Modeling and Validation of the Isothermal Air Flow in a Forced Convection Oven, *Journal of Food Engineering*, Vol. 43, pp. 41-53.

Verma S. and Balaji C., (2007), Multi-Parameter Estimation in Combined Conduction–

Radiation From a Plane Parallel Participating Medium Using Genetic Algorithms, *International Journal of Heat and Mass Transfer*, Vol. 50, pp. 1706–1714.

Wang F., Liu D., Cen K.-F., Yan J.-H., Huang Q.-X., and Chi Y., (2008), Efficient Inverse Radiation Analysis of Temperature Distribution in Participating Medium Based on Backward Monte Carlo Method, *Journal of Quantitative Spectroscopy and Radiative Transfer*, Vol. 109, pp. 2171-2181.

White M.K., and Probert D., (1991), Heat Transfers in Treatment Furnaces, *Applied Energy*, Vol.38, pp. 293-323.

Wu C.Y. and Wu S.H., (1999), A New Application of Successive Approximation to Radiative Exchange Among Surfaces: Direct and Inverse Problems, *International Journal of Heat and Mass Transfer*, Vol. 42, pp. 2255-2267.

Yang G., Reinstein L. E., Pai S., Xu Z., and Carroll D.L., (1998), A New Genetic Algorithm Technique in Optimization of Permanent 125-I Prostate Implants, *Medical Physics*, Vol. 25(12), pp. 2308-2315.

Yang T. and Nishi M., (1980), Inverse Design of Optimal Diffusers with Experimental Corroboration, *Journal of Fluids Engineering*, Vol. 102, pp. 121-124.

Yong M., Falzon B.G., and Iannucci L., (2008), On the Application of Genetic Algorithms for Optimizing Composites Against Impact Loading, *International Journal of Impact Engineering*, Vol. 35, pp. 1293-1302.

Zashkova L., (2008), Mathematical Modeling of the Heat Behavior in the Ceramic Chamber Furnaces at Different Temperature Baking Curves, *Simulation Modeling Practice and Theory*, Vol. 16, pp. 1640–1658.

Zhou H.-C. , Hou Y.-B., Chen D.-L., and Zheng C.-G., (2002), An Inverse Radiative

Transfer Problem of Simultaneously Estimating Profiles of Temperature and Radiative Parameters From Boundary Intensity and Temperature Measurements, *Journal of Quantitative Spectroscopy and Radiative Transfer*, Vol. 74, pp. 605 - 620.

Zhou H.-C., Loua C., Cheng Q., Jiang Z., He J., Huang B., Pei Z., and Lu C., (2005), Experimental Investigations on Visualization of Three-Dimensional Temperature Distributions in a Large-Scale Pulverized-Coal-Fired Boiler Furnace, *Proceeding of the. Combustion Institute*, Vol. 30, pp. 1699-1706.

ANNEXTURE - I

Experimental Study of Radiant Furnace Boundary Design

1. Introduction

For uniform thermal conditions on a 3-D DO, the numerical results for basic problem are given and discussed in Chapter 3. The methodologies used (REM^2 + MGA) for the furnace boundary design problems is numerically validated in section 3.3.3, boundary design problems for various situations in material heating applications are discussed in Chapter 4, such as with different sizes of the DO models, their locations and with different configurations. In the present experimental work, two boundary design problems with DO models, 553 ($\text{dimensions}: 0.5\,\text{m} \times 0.5\,\text{m} \times 0.3\,\text{m}$), and 333 ($\text{dimensions}: 0.3\,\text{m} \times 0.3\,\text{m} \times 0.3\,\text{m}$), are studied, separately. The designations and the element wise details are given in Chapter 4 (section 4.2). In the following sections, fabrication of experimental setup and working procedure for the experiment are given. The heat flux at selected locations along the surfaces of the DO, computed using numerical design, and that of calculated from the experimental observations are then analysed.

In this study, for a 3-D DO the optimal powers of 500 panel heaters (100 panel heaters along each of the five walls) are estimated. It is seen that for uniform thermal conditions on a particular DO model, not all but about 50 heaters are need to be placed, and activated with the given power (Figs. 4.11a-e). The requirement of number of heaters and their powers is different for different DO model and different cases. This is well discussed in Chapter 4.

The prime aim of present experimental study is to check the implementation of numerical results in practical situation. To fabricate the experimental setup with about 50 heater elements at a specific location along the furnace walls is indeed a difficult task, and also

the most difficult is to control them individually with different powers. Without given off the objective of the study, to make the experimental task comparatively feasible, same boundary design problem has been solved with grouping the heaters along the five walls. In this computation, 100 panel heaters (dimensions: $0.1\text{m}\times0.1\text{m}$) along each wall are grouped into single panel heater (dimensions: $1\text{m}\times1\text{m}$) and thus only the power of five heaters are unknown parameters in the present design problem. This is done to make the heater powers control feasible in the experiments. Obviously grouping all the heaters along a wall into a single heater does not produce uniform thermal conditions on 3-D DO. This is attributed to less availability of solution combinations for the optimization algorithm. As given above the aim of this experimental study is to see the relationship of the numerical results (estimated heat flux on the DO) with the experimental one. Even with five heaters along the five walls of furnace, and the estimated heat flux on the DO is not uniform, if the same arrangement simulated experimentally, the numerical and the experimental results can be compared.

In this study the actual dimensions of the furnace enclosure is $L=W=H=$ 1.0 m, and the two DO models are 553 and 333. For the experiment, the computational domain is geometrically scaled down to 20% of the computational domain. The radiative heat transfer is computed using the REM^2. In the REM^2, absorption configuration factors and the diffuse reflection configuration factors are basically responsible for radiative exchange among the surface elements along the furnace walls and the DO. The proportionate change in size of furnace enclosure and DO does not affect the results. In the following sections, first the numerical results are presented, next to this, fabrication of experimental setup, experimental procedure and comparison of the numerical and the experimental results are given.

2. Numerical results for experiments

In this study, the present furnace boundary design problem simulated experimentally. Two 3-D rectangular DO models 553 $(\text{dimensions}: 0.4\text{m}\times0.4\text{m}\times0.3\text{m})$, and 333 $(\text{dimensions}: 0.4\text{m}\times0.4\text{m}\times0.3\text{m})$ are considered. The designation of DO models and

the numerical designations of surface elements on the DO are given in chapter 4 (section 4.2). It is discussed in previous subsection the basic aim of the experiments is to analyze

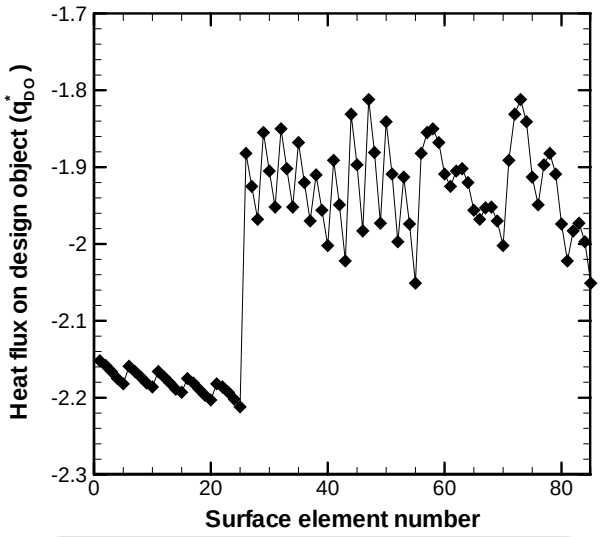

(a)

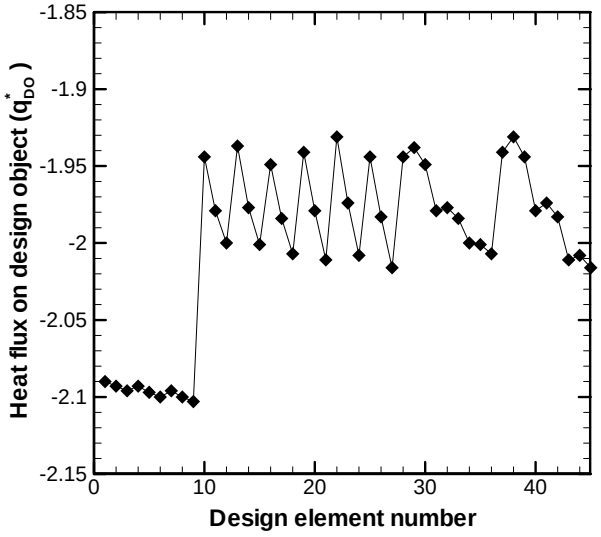

(b)

Figure 1. Numerically estimated heat flux distribution on the surfaces of the DO using 5 heaters along the furnace walls (a) DO model 553 (b) DO model 333 (refer Figs. 4.2).

.

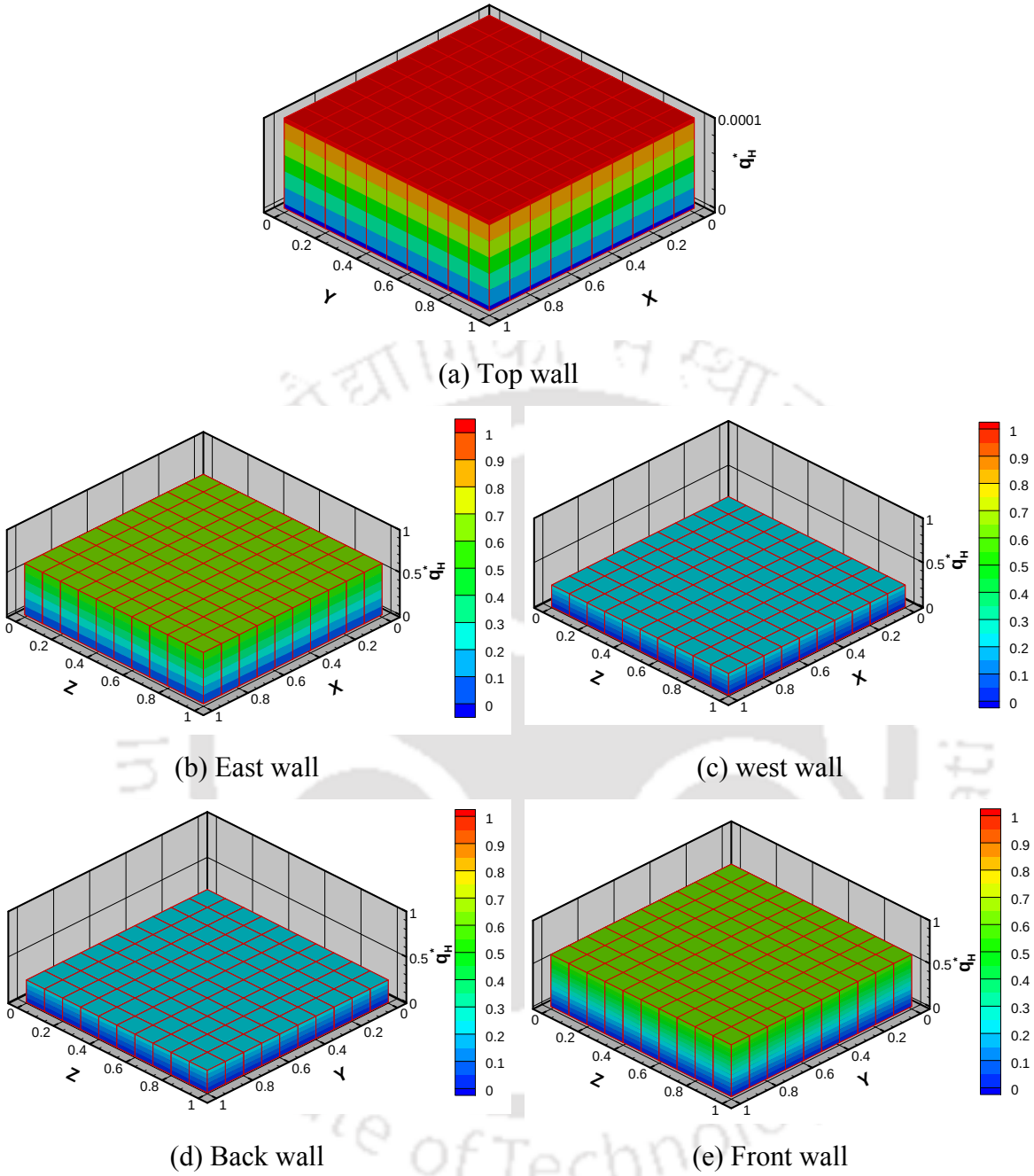

Figure 2. Optimal heater power distribution along the enclosure walls using DO model 553, (a) top wall (b) east wall (c) west wall, (d) back wall, (e) front wall.

the difference between the numerical and experimental results of radiant boundary design problem with 3-D DO. In the following paragraphs the numerical results of boundary design problem considering 5 panel heaters along the five furnace walls (five walls of furnace represent the group of 100 panel heaters) are given.

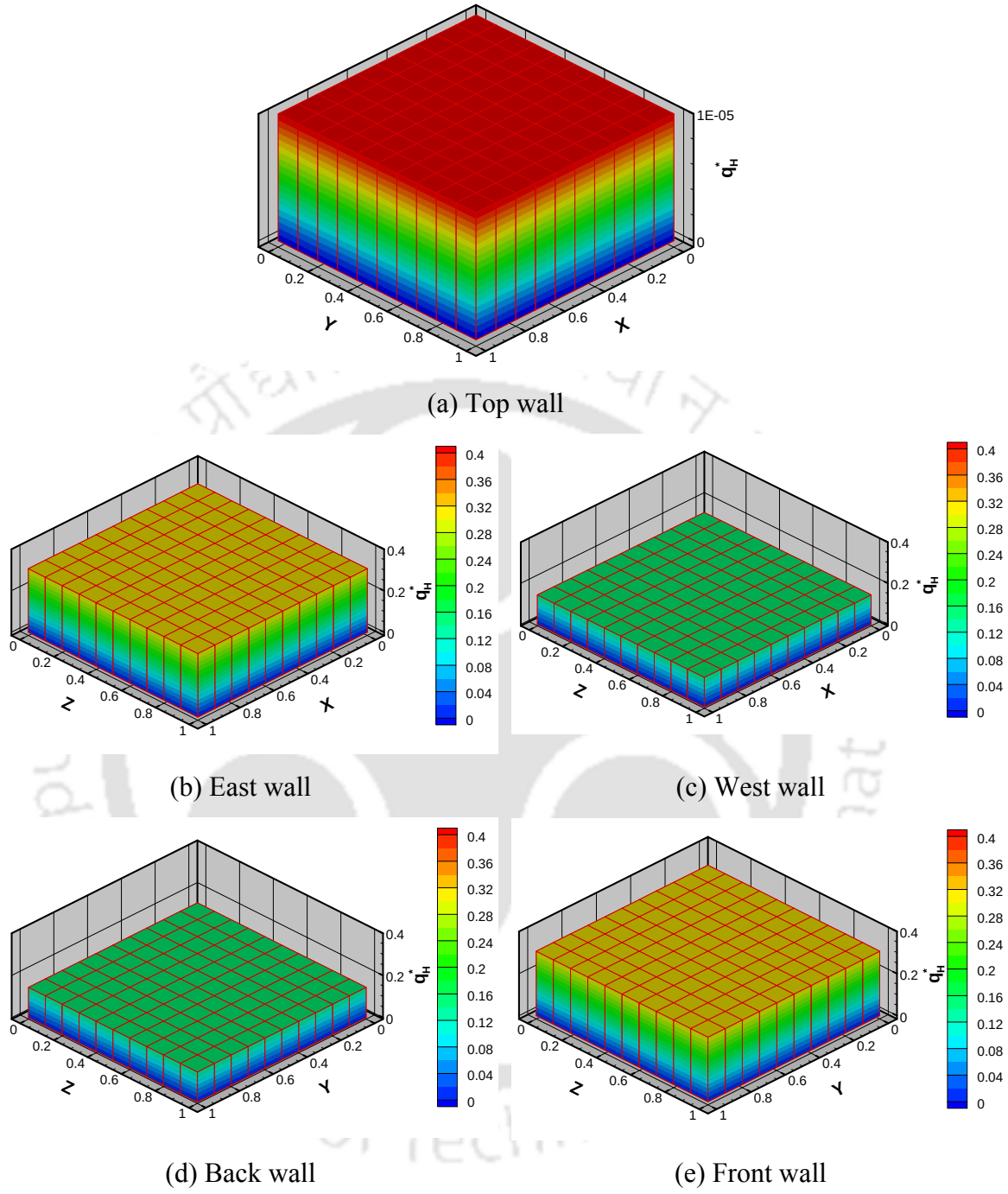

(a) Top wall

(b) East wall

(c) West wall

(d) Back wall

(e) Front wall

Figure 3. Optimal heater power distribution along the enclosure walls using DO model 333, (a) top wall (b) east wall (c) west wall, (d) back wall, (e) front wall.

For the present experimental study, a cubical furnace enclosure (dimensions : $L = W = H = 1.0\,\text{m}$) with the DO model 553 and 333, placed on bottom of

the enclosure (Fig. 4.1) is considered separately. The emissivity of the heater elements are taken as 0.95 and that of DO surface is 0.17. Radiative information is computed using REM^2 and in optimization, objective function (Eq. 3.24) is minimized using the MGA. With population size 10, 1000 generations are evaluated. The estimated heat flux distribution on the surfaces of DO model 555 and DO model 333 is shown in Fig. 1a and Fig. 1b, respectively, while the corresponding heaters power distribution along the five walls of the furnace is shown in Fig. 2a-e and Fig. 3a-e, respectively. It is to be noted that all the results shown here are in dimensionless form. It is expected that, using 5 heaters along the 5 walls of the furnace uniform thermal conditions are not expected. In the experiments, the given powers of the heaters will be imposed on the furnace boundaries and the net heat flux on the surfaces of the DOs will be calculated from the temperature measurement. In next section, the fabrication of experimental setup is given. The experimental work is done at the heat transfer laboratory, Institute of Fluid Sciences, Tohoku University, Sendai, Japan.

3. Fabrication of the experimental setup

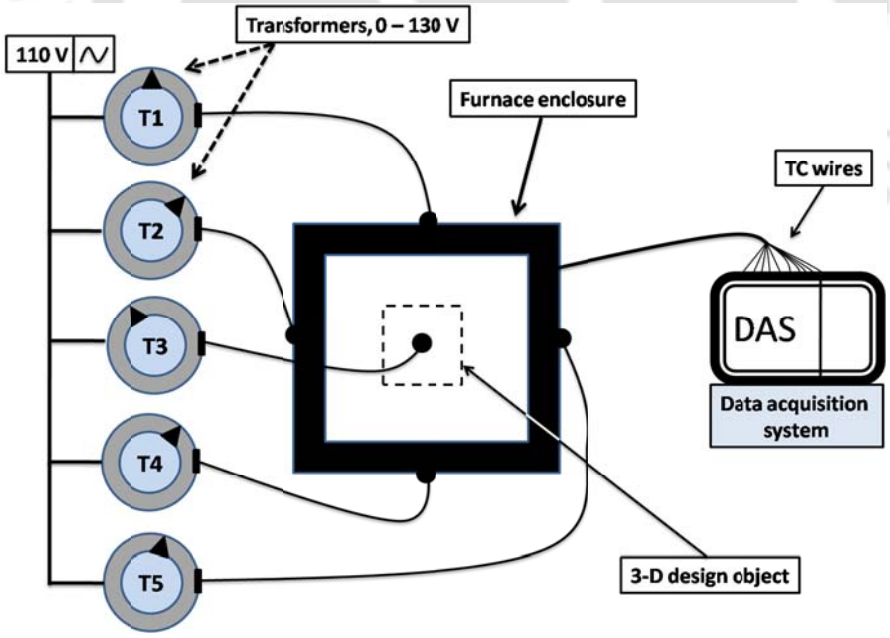

Figure 4. Schematic of the experimental setup (Top view).

Fig. 4 shows the schematic of experimental setup. For the experiment computational domain dimensions: $L = W = H = 1.0\,\text{m}$ is geometrically scaled down to 1/5th (20%) of the original dimensions. Thus, dimensions of the radiant enclosure become $L = W = H = 0.2\,\text{m}$, and the proportionate dimensions of the DO models 553 and 333 becomes $L = 0.1\,\text{m}$, $W = 0.1\,\text{m}$, $H = 0.06\,\text{m}$, and $L = W = H = 0.06\,\text{m}$, respectively. Similarly, the surface elements size becomes $0.02\,\text{m} \times 0.02\,\text{m}$, which is 20% of the

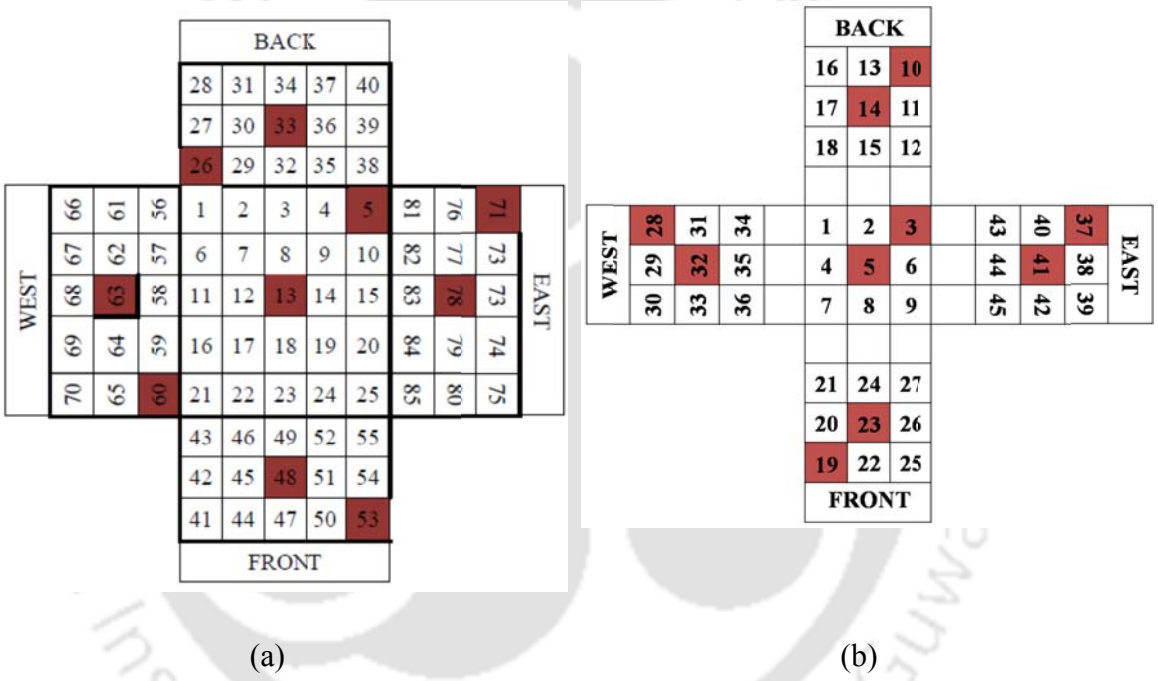

Figure 5. Locations of the thermocouples along the surface elements of (a) DO model 553, and (b) DO model 333.

original size $(0.1\,\text{m} \times 0.1\,\text{m})$. So the numbers of surface elements on five faces of the DO remain unchanged, by number these are 85 and 27on the DO model 553 and 333, respectively. The selected locations for temperature measurements on the surfaces of the DO model 555 and DO model 333 are shown in Fig. 5a and Fig. 5b, respectively. For temperature measurements 10 locations are selected, two locations along the each of the 5 surfaces of the DO, one is the central surface element and another is the corner element.

It is known from the computational results that on the particular face of the DO, the difference between estimated flux at the central surface element and at corner is the maximum, so the locations are chosen likewise. Table 1 shows the chosen surface elements and thermocouple location numbers.

Table 1. Chosen location numbers and corresponding surface elements numbers on the surfaces of the DO for temperature measurement.

DO model	Thermocouple location Number							
	1	2	3	4	5	6	7	8
	Surface element number							
553	13	5	71	78	33	26	63	60
333	5	3	14	10	23	19	32	28

The experimental setup is fabricated in the heat transfer laboratory, Institute of Fluid Sciences, Tohoku University, Sendai, Japan. The fabrication procedure in sequence is given below.

- For fabrication of furnace enclosure of dimensions $L = W = H = 0.2\,\text{m}$, the Styrofoam (a kind of expanded polystyrene foam, k = 0.03W/m.K) of 5 cm thickness is used for enclosure walls. The walls are made of total 10 mm thickness. The Styrofoam is cut accurately to form five walls of furnace; squareness on all the cut surfaces is maintained. Non-flammable, non reactive adhesive is used during assembly of Styrofoam wall panels. Thus the furnace enclosure of size $0.2\,\text{m} \times 0.2\,\text{m} \times 0.2\,\text{m}$ is fabricated. All the joints are ensured for any air gap.
- 5 band heaters dimensions: $0.2\,\text{m} \times 0.2\,\text{m}$, are used for the experiment. The maximum wattage of the heater was 6000 W/m^2, so the total wattage of the present heater (area 0.04m^2) is 240 W. Before installation of the heaters on internal surface of the furnace walls, heater characteristic (current vs. voltage) has been cheeked and is shown in Fig. 6a. This is done for controlling the power

of heaters; it is the relationship between the voltage and current. With the known area of heaters surface, from this characteristic plot, the required voltage for producing particular heat energy, i.e. heat flux on the surface of heater (W/m^2), can be decided. The heaters input can be regulated using the corresponding voltage to get the particular wattage (power) of panel heater.

- In the present numerical analysis the emissivity of heater surface is taken as 0.95, to simulate the situation, the black body paint (emissivity 0.95) has been applied on one side of the heater surface.
- Heaters then fixed with (nonflammable, nonreactive) adhesive on the internal surface of the furnace wall, black surface of the heaters facing the DO, which is centrally located on bottom surface of furnace enclosure. Thus the furnace enclosure with heaters is ready.
- Next, the DO models 553 $\left(\text{dimensions}: l = 0.1\text{m}, w = 0.1\text{m}, h = 0.06\text{m}\right)$ and 333 $\left(\text{dimensions}: l = w = h = 0.06\text{m}\right)$ are cut to the size, the material used for DO model is a high insulation type themocole (k = 0.028-0.031 Kcal/hr. m.°C).
- According to the dimensions of the DOs the surface elements (dimensions: $0.02\text{m} \times 0.02\text{m}$) have been marked along the five faces, as shown in Figs. 5a-b. The numbers of surface elements of the DO model 553 and 333 are 85 and 27 respectively.
- Calibrated thermocouples (T-type) are fixed at 8 chosen locations along the five faces of the DO. Other end of thermocouples is connected to the data acquisition system (refer Fig. 4). All the thermocouples have been fabricated in-house. Fabrication and calibration and uncertainty of thermocouples are elaborated in Appendix I.
- After fixing the thermocouples at chosen locations, the chromium sheet of thickness 200 micron (emissivity 0.17, k = 11 $W \cdot m^{-1} \cdot K^{-1}$) wrapped on the DO accurately. This is done to simulate the surface properties of the metals.

- DO is fixed at the center of base of the furnace and then the fabricated enclosure fixed firmly on the base plate.
- To control the input power of 5 heaters placed along the 5 walls of furnace, the AC supply provided through 5 transformers (refer Fig. 4).

In this way complete setup of furnace enclosure with a particular DO model is ready for experiment. The list and the specifications of the instruments used during the experiment are given in Appendix III.

4. Experiment procedure

After fabrication of the experimental setup (Fig. 4), experiments are carried out using the following procedure.

- All the electrical connections and data acquisition system connections are checked; the room temperature reading has been recorded as 288K (15 °C). In non-dimensionalization of heat flux, the room temperature has been used as reference temperature, so this reading in important.
- According to the numerical results (refer Figs. 2-3) the transformers have set to supply the particular voltages to the heaters that produce required heat fluxes. The voltage supplied to the heaters has been confirmed with clamp type multi-meter.
- At selected surface elements along the surfaces of DO, the steady state temperatures have been recorded through data acquisition system.
- The same procedure is repeated for another DO model.

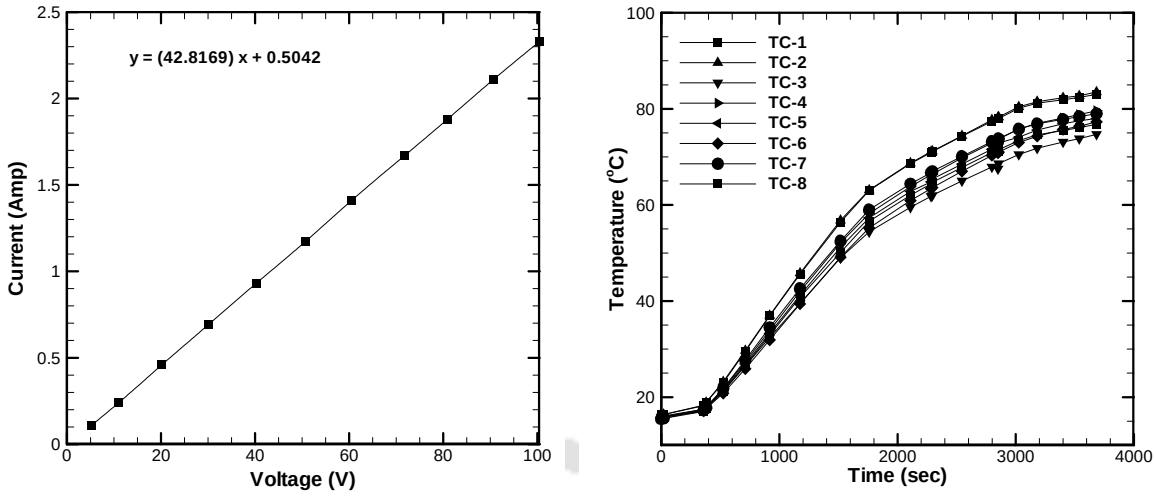

(a) (b)

Figure 6. (a) Heater characteristic, (b) heating history at 8 locations along the surface of a DO.

5. Numerical results analysis

After connecting the power to the heaters, at 8 chosen locations (Figs. 5) the steady state temperatures have been recorded. The present numerical results are based on the steady state temperature. It is observed that to reach the steady state temperatures, the system takes about 60 minutes. The sample temperature history is shown in Fig. 6. The net radiative heat flux received on the chosen surface elements (Table 1) is calculated using Stefan-Boltzmann equation.

$$q_R = \sigma\left(T_f^4 - T_i^4\right) \quad \text{W/m}^2 \tag{1}$$

where $\sigma = 5.6703\times10^{-8}$ $\text{W/m}^2.\text{K}^4$

T_f and T_i = *final and initial steady state temperature*,

In the calculation of estimated heat flux received on chosen surface elements of the DOs, few assumptions are made, that include, the heat transfer is only by radiative transfer

mode, all the walls are perfectly insulated, and distribution of uniform heat flux along the entire area of the heater surface.

In error analysis, the estimated error in the radiative heat flux calculation (Eq. 1) is calculated using Kline and McClintock (1953) procedure, and the detail is given in Appendix II. The maximum uncertainty in heat flux calculations is found to be 0.23%.

Figs. 7 and Figs. 8 shows the comparison of estimated heat flux values at 8 chosen surface elements computed numerically and that of calculated from the experimental observations, for the DO model 553 and DO model 333, respectively. In Fig. 7a, the results are given in dimensional form while Fig. 7b shows the same results in non-dimensional form. The estimated heat flux distribution for DO model 333 is shown in Figs. 8a-b. From the comparison of numerical and experimental estimated heat flux distribution (Figs. 7-8), it is found that the estimated heat fluxes calculated from experiments are average 30% less than that of from numerical values, however the trends of the results are matching very well.

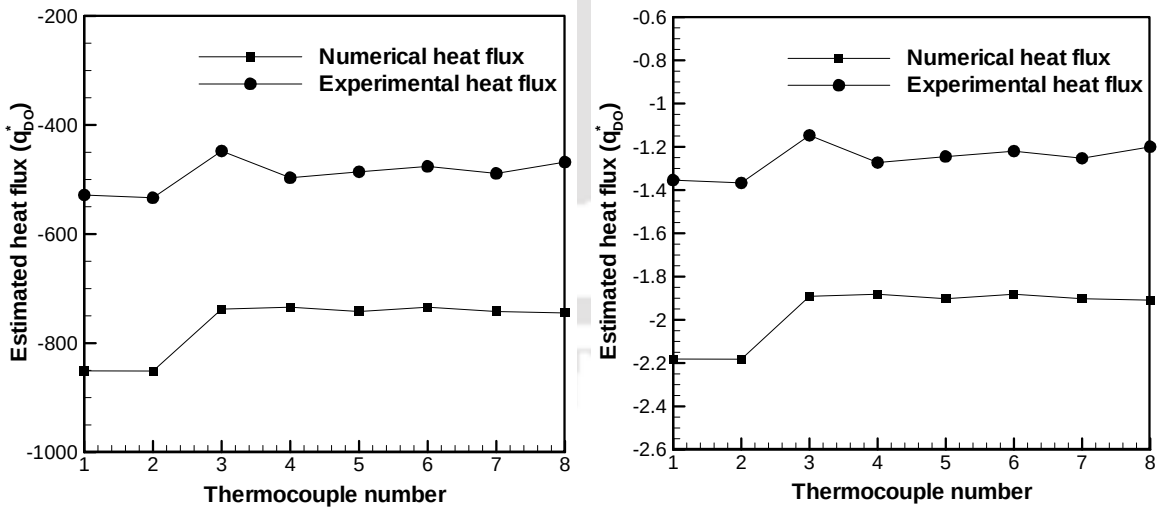

(a) (b)

Figure 7. Estimated heat flux obtained at 8 chosen surface elements of the DO 553, (a) dimensional form, (b) non-dimensional form.

.

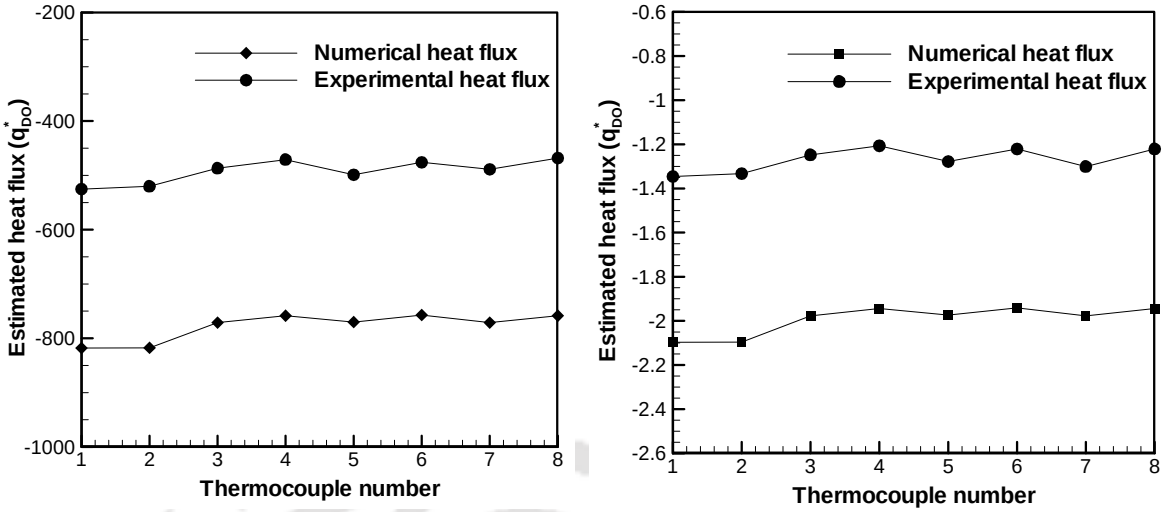

(a) (b)

Figure 8. Estimated heat flux obtained at 8 chosen surface elements of the DO 333, (a) dimensional form, (b) non-dimensional form.

This difference is attributed to (a) conduction losses, about 22.5 W/m^2 energy loss from each of the furnace walls (outside actual temperature was recorded 7°C), this contribute 16% of the total heat supplied, (b) unlike in the computational problems, entire heater surface do not attain the uniform temperature and so the heat flux, mainly along the edges of the heaters, (c) loss of energy through leakage. On the positive side, the trends of experimental results are well matching with that of from numerical computations. If we consider the above said energy losses during the experiment, the obtained experimental results are acceptable. The matching trends of numerical and experimental results implies that, using all heaters with the given power from numerical solution, and simulating the numerical conditions exactly, uniform heat flux distribution can be produce on a chosen 3-D object.

6. Summary

The numerical results of present radiant furnace design problems are compared with the experimental results. For this study, simple experimental simulations of radiant furnace with two 3-D DO models are carried out separately. Experimental setup is fabricated in-house and the temperature at the chosen surface elements is recorded. In both of the cases

studied (of two DO model), it is found that, the estimated heat fluxes on chosen locations calculated from experimental measurements, are average 30% less than that of from computed values. This variation is attributed to (a) the conduction loss through the six walls of furnace enclosure that contribute about 16% of the total heat supplied, (b) unlike in the computational problems, the entire heater surface do not attain the uniform temperature and so the heat flux, specifically along the edges of the heaters, (c) loss of energy through leakage. However, the trends in experimental results are well matching with that of from numerical computations. If we consider the above said energy losses, the experimental results are acceptable. These matching trends of the results implies that using all the heaters with the given power from the numerical solution, exact desired uniform heat flux distribution can be produce on a 3-D object.

Appendix – I

Fabrication and Calibration of Thermocouples

1. Introduction

For the study given in Annexure-I, for temperature measurement T-type [copper (+) – constantan (-)] thermocouples (TCs) are used. The operating range of the T-type thermocouples is -200 to 350 °C. In the following sections fabrication, calibration of thermocouples and uncertainty analysis is given.

2. Fabrication of Thermocouples

TCs can be made by simply mechanical tying, soldering or spot welding the ends of two metal wires. In the present work, spot welding machine (specially made for thermocouple manufacturing) is used to form the junction of a TC wires. In the present work, copper, and constantan, wires of AWG 39 (dia. 0.08mm; made: Omega, USA) were used. For fabrication of the TCs following procedure has been adopted.

- Approximately 3-5 mm of copper and constantan wires are bared using the wire stripper.
- The bare ends are flattened.
- The bare ends of wires are polished to shine bright using 400 grit carbide paper. The polished ends are cleaned with 70% isopropyl alcohol.
- The wire ends are overlapped and twisted to 2-3 turns.
- The spot weld machine set to medium power and time.
- The junction is fixed on welding plate using clamps. Carefully the electrode end pressed to the junction until the alarm beeps. One may repeat the attempt, varying the power and time until a good weld is achieved.
- The junction formation is inspected using the magnifying lens.

3. Calibration of Thermocouples

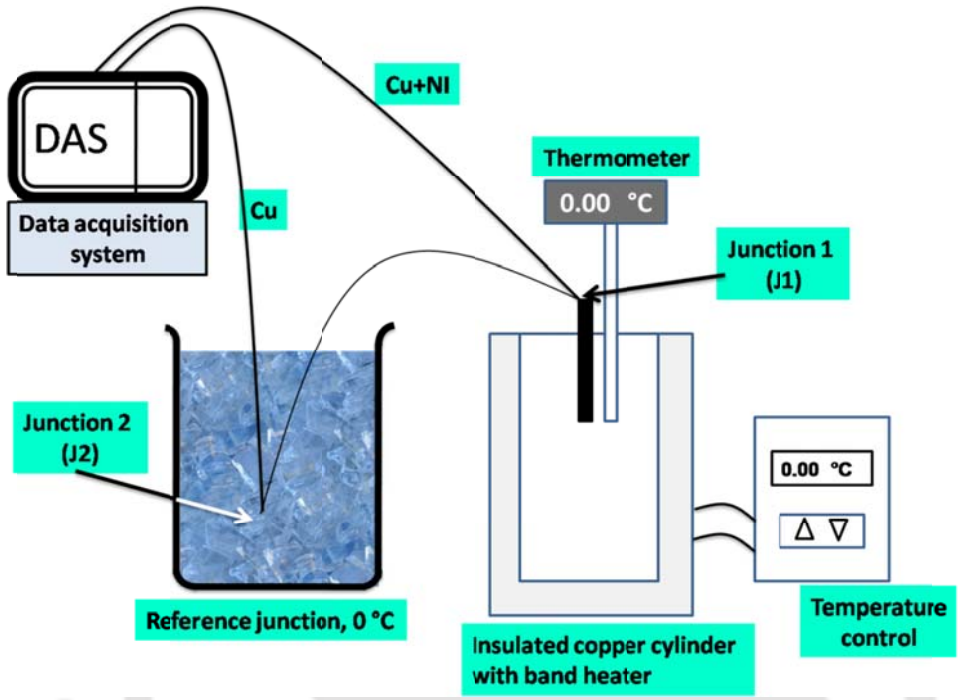

Figure A1: Schematic of TC calibration setup.

The TCs are fabricated using the procedure given in previous section. The schematic of the calibration setup is shown in Figure A1. For the calibration of thermocouple we need constant temperature bath. In the present study, the insulated pure copper cylinder of 50 mm diameter and 150 mm height, with circumferentially wrapped band heater has been used as a constant temperature bath. The reference junction has been maintained at 0°C is a small container with mixture of ice and water. The following procedure is adopted for TC calibration.

- Insert one junction (J1) into the constant temperature bath and the other (J2) into the reference temperature which is maintained at 0°C (Mixture of solid ice and pure water).
- Connect the other two ends of the TC to a data acquisition system (DAS) as shown in Fig. A1 to measure the generated emf.

- Set the constant temperature bath at 20° C. Wait till the constant bath temperature reaches steady state temperature, monitor the temperature indicator on the temperature bath.
- Record the precise thermometer reading of temperature bath.
- Record the emf generated using the multi-meter in mV.
- Increase the constant bath temperature by 10 °C and repeat the procedure.
- Repeat the procedure for all 10 TCs.

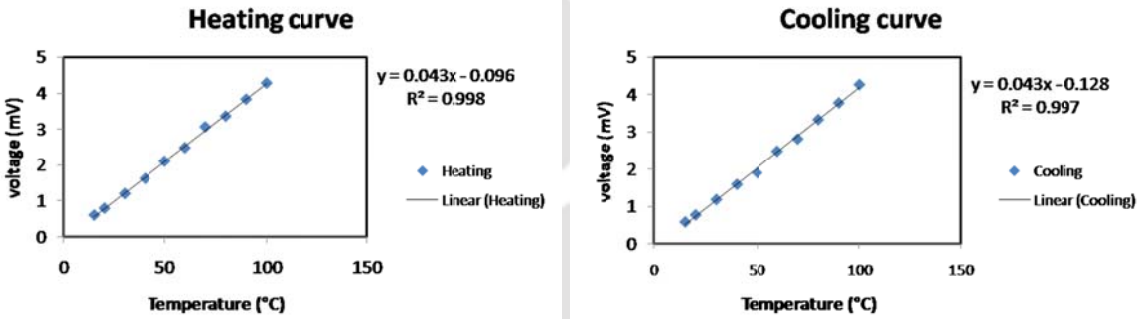

(a) (b)

Figure A2: Calibration curves for sample thermocouple.

A sample calibration curve is shown in Fig. A2, in both heating and cooling curves R-squared value (R^2) is quite close to 1. So the calibration is assumed to be correct. R^2 is the coefficient of determination ($0 < R^2 < 1$). It denotes the strength of the linear association between x and y and so the accuracy of the linear relationship. Calibration uncertainty is calculated using the population based theory (Bechwith *et al.*, 2004), the maximum uncertainty is found ±0.089 mV, with 95% confidence level, which is acceptable for laboratory experiments.

Next, with sample thermocouple, the uncertainty analysis in temperature measurement has been carried out. In metrology, measurement uncertainty is a non-negative parameter characterizing the dispersion of the values attributed to a measured quantity. All measurements are subject to uncertainty and a measured value is only complete if it is

accompanied by a statement of the associated uncertainty and confidence level. Fractional uncertainty is the measurement uncertainty divided by the measured value.

Total 5 sets of readings are taken for the temperature range 15 to 100 °C. Among all the measurements values, maximum deviation is found to be 0.4 °C, and the measured temperature range is 85 °C (100-85). It is observed that, the occurrence of the maximum error is 30%, so this uncertainty is with 68.3% confidence level, and thus with 95 % confidence level the uncertainty in temperature measurement becomes ±0.784 °C [Bechwith *et al.*, 2004].

Appendix – II

Error analysis

Kline and McClintock (1953) proposed a procedure for estimating the uncertainty of measured quantity in experimental studies. If an estimated quantity R, depend on the independent variable say $x_{1,}x_{2,}x_{3,}.....,x_n$ then

$$R = R\left(x_{1,}x_{2,}x_{3,}.....,x_n\right) \tag{A-1}$$

Then the maximum value of uncertainty is given by

$$\Delta R = \sqrt{\left(\frac{\partial R}{\partial x_1}\Delta x_1\right)^2 + \left(\frac{\partial R}{\partial x_2}\Delta x_2\right)^2 + ...+ \left(\frac{\partial R}{\partial x_n}\Delta x_n\right)^2} \tag{A-2}$$

In the present case, the heat flux on the surface elements of the design object is calculated using

$$q_R^{"} = \sigma\left(T_f^4 - T_i^4\right)\ {W}/{m^2}$$
$$where\ \ \sigma = 5.6703\times10^{-8}\ {W}/{m^2.K^4} \tag{A-3}$$

Where T_f and T_i are the final and initial absolute temperatures.

Hence the estimated uncertainty calculation formula becomes

$$\Delta q_R = \sqrt{\left(\frac{\partial q_R}{\partial T_f}\left(\Delta T_f\right)\right)^2 + \left(\frac{\partial q_R}{\partial T_i}\left(\Delta T_i\right)\right)^2} \tag{A-4}$$

$$\Delta q_R = \sqrt{\left(\frac{4\left(\Delta T_f\right)}{T_f}\right)^2 + \left(\frac{4\left(\Delta T_i\right)}{T_i}\right)^2} \tag{A-5}$$

Where $\Delta T = \pm 0.784\,°C$, and maximum temperature range=(100-15) = 85 °C

Hence

$$\Delta q_R = \sqrt{16 \times \left(\frac{0.784}{85}\right)^2 + 16 \times \left(\frac{0.784}{85}\right)^2} \qquad \text{(A-6)}$$

$$= 0.002722$$

$$\Delta q_R = 0.27\%$$

Therefore the maximum uncertainty in heat flux calculation is 0.27%.

Appendix – III

Technical specifications of the instruments used in the experiments

1. Thermocouples (TC1-TC10)

Type: T-type, Copper (+) constantan (-).

Make: fabricated in-house, TC wires: Omega Instruments, USA.

Junction : Spot welded

Range : -200ºC to 350 ºC

2. Data Acquisition Unit

Make : GRAPHTEC corporation, USA

Model : midi LOGGER GL 200

Channels : 10

Communication Port : USB

Voltage range: –22.000 to +22.000 mV, resolution 0.001mV

Temperature range: for T-type TC: -200-400 °C

Ref. contact compensation accuracy: ±0.5 °C, Measurement Accuracy: ±0.5 °C

3. DCM-22AD, Sanwa Clamp multi-meter

SANWA electric instruments Co. LTD Tokyo Japan (http://overseas.sanwa-meter.co.jp/index.php?dcm-22ad)